APPLICATION OF POLYMER GELS AS CONFORMANCE CONTROL AGENTS FOR CARBON DIOXIDE EOR FLOODS IN CARBONATE RESERVOIRS

A Thesis

by

ALI HUSSEIN A. AL-ALI

Submitted to the Office of Graduate Studies of
Texas A&M University
in partial fulfillment of the requirements for the degree of

MASTER OF SCIENCE

Approved by:

Chair of Committee,	David S. Schechter
Committee Members,	Robert H. Lane
	Yuefeng Sun
Head of Department,	Dan Hill

December 2012

Major Subject: Petroleum Engineering

ABSTRACT

With the production from mature oil fields declining, the increasing demand of oil urges towards more effective recovery of the available resources. Currently, the CO_2 Floods are the second most applied EOR processes in the world behind steam injection. With more than 30 years of experience gained from CO_2 flooding, successful projects have showed incremental oil recovery ranging from 7 to 15 % of the oil initially in place. Despite all of the anticipated success of CO_2 floods, its viscosity nature is in heterogeneous and naturally fractured reservoirs is challenging;CO_2 will flow preferentially through the easiest paths resulting in early breakthrough and extraction ineffectiveness leaving zones of oil intact. This research aims at investigating gel treatments and viscosified water-alternating-gas CO_2 mobility control techniques. A set of experiments have been conducted to verify the effectiveness and practicality of the proposed mobility control approaches.

Our research employed an imaging technique integrating an X-Ray CT scanner with a CT friendly aluminum coreflood cell. With the integrated systems, we were able to obtain real time images when processed provide qualitative and qualitative evaluations to the coreflood. The research studies included preliminary studies of CO_2 and water injection performance in fractured and unfractured cores. These experiments provided a base performance to which the performances of the mobility control attempts were compared. We have applied the same methodology in evaluation of the experimental results to both conformance control gel treatments and viscosified water-

alternating-gas CO_2 mobility control. The gel conformance control studies showed encouraging results in minimizing the effect of heterogeneities directing the injected CO_2 to extract more oil from the low permeability zones; the gel strength was evaluated in terms of breakdown and leakoff utilizing the production data aided with CT imaging analysis. The viscosified water coupled with CO_2 investigations showed great promising results proving the superiority over neat CO_2 injection. This research serves as a preliminary understanding to the applicability of tested mobility control approaches providing a base to future studies in this category of research.

DEDICATION

I lovingly dedicate this thesis to:

My Mother Layla, to whom I owe everything in my life;

My father Hussein, for believing in me throughout my whole life

Exceptional dedication to beloved sisters and brothers: Fatimah, Maryam, Mohammed, Hassan, Abdullah, AlZahra'a, Wala'a and Abdulmohsen for the love and support they have given me.

Finally,

To my beloved fiancé, Bshayer, for her patience and support;

And to my dear friends Abduljalil Al-Ali and Mohammed Al-Momatin.

ACKNOWLEDGEMENTS

I would like to thank my committee chair, Dr. Schechter, and my committee members, Dr. Lane, and Dr. Sun for their guidance and support throughout the course of this research.

Special thanks also to my friends Zuhair Al-Yousef and Hussain Al-Jeshi for making my time at Texas A&M University and College Station such a great experience. I also want to extend my gratitude to the department faculty and staff.

Finally, thanks to my mother and father for their encouragement and to my fiancé for her patience and love.

TABLE OF CONTENTS

Page

LIST OF FIGURES

FIGURE Page

LIST OF TABLES

TABLE Page

CHAPTER I

INTRODUCTION

1.1 Introduction

Even with the recent advances in alternative energy sources, oil remains and expected to remain the major energy source in the world. See **Fig.1.1.** With the production from mature oil fields declining, the increasing demand of oil urges towards more effective recovery of the available resources. Currently, the CO_2 Floods are the second most applied EOR processes in the world behind steam injection. See **Fig.1.2.** (Espie 2005)

With more than 30 years of experience gained from CO_2 flooding, successful projects have showed incremental oil recovery ranging from 7 to 15 % of the oil initially in place. The pricing of $CO_{2,}$ effectiveness of enhancing the recovery and the environmental issues all play major role in making CO_2 EOR a hot prospect in the future years. Carbon dioxide is effective in improving oil recovery due to reasons: density and viscosity.(Espie 2005)

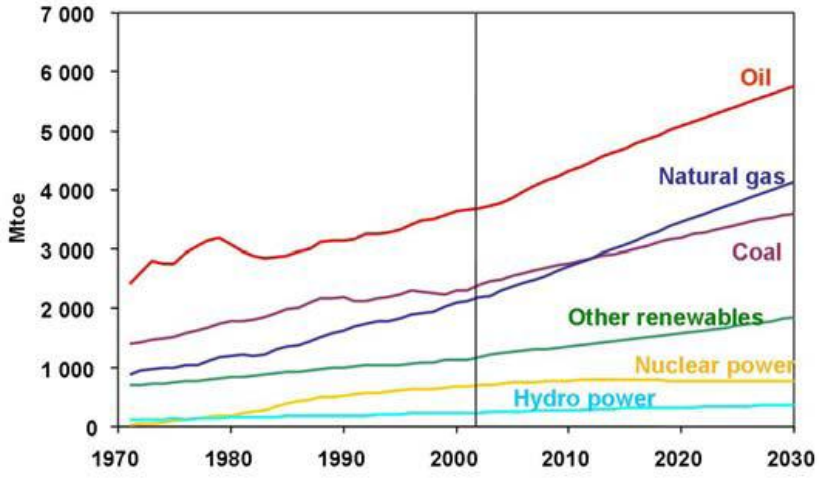

Fig.1.1 – Global Energy Sources Since 1970(Espie 2005)

Fig.1.2 – Utilization of EOR Processes in US in 2004(Espie 2005)

At high pressure, CO_2 forms a phase whose density is close the density of liquids. The dense CO_2 has better performance in extracting hydrocarbon components

from oil than if it was lower in density, i.e. lower pressure. However, even at these conditions CO_2 remains having low viscosity and density relative to liquids.

The quantity of oil recovered by CO_2 injection is influenced by several features of the reservoir including the reservoir rock properties, reservoir pressure and temperature and fluid composition and properties. However, the most influential parameter is the heterogeneity of the reservoir.

Despite all of the anticipated success of CO_2 floods, its viscosity nature is in heterogeneous and naturally fractured reservoirs is challenging;CO_2 will flow preferentially through the easiest paths resulting in early breakthrough and extraction ineffectiveness leaving zones of oil intact.(Jarrell 2002)

The designing, application and performance are still under ongoing research. Primarily, the focus is on studies of increasing the sweep efficiency. For successful and economically attractive CO_2 application in heterogeneous reservoirs, it is crucial to develop, propose and verify mobility control techniques.

Four major approaches have been proposed to enhance the CO_2 flood efficiency: water alternating gas (WAG), cross-linked gel treatments, CO_2 viscosifier and CO_2 foaming agents.

Conformance control approach employs gel treatments to act as a blocking agents reducing channeling through fractures or high-permeability zones of oil reservoir without significantly damaging hydrocarbon productivity and improve the overall oil recovery from the flooding process. Accordingly, the goal of the gel is to maximize gel penetration and permeability reduction in high permeable zone while minimizing gel

penetration and permeability reduction in less permeable zones of the reservoir. A successful treatment will direct the CO_2 away from the high permeability zones towards the lower permeability intact regions.

Thickening agents or viscosifiers approach is one of the two direct approaches, in addition to gel application. The tactic is to add and dissolve polymers in CO_2 phase increasing its viscosity. At reservoir at reservoir pressure and temperature, CO_2 is a dense fluid-its density is near that of oil. Polymers combined with cosolvents such as toluene are added in low concentrations dissolving in the CO_2 resulting in increased CO_2 solution viscosity by a factor of 10-20. However, this approach remains the less developed and investigated compared to WAG, foams and gel application. The most challenging problems of viscosifying agents are the solubility of these of polymers into the CO_2 phase and to what extent the viscosity of the CO_2 phase will increase.

Foaming mechanism employs the principle of having CO_2 as a dispersed phase which has a lower mobility than CO_2 alone. Surfactants are injected in the porous medium and CO_2 gas disperses into the liquid phase forming foam. The foam bubbles are separated by thin films called lamellae that resist flow. The resistance to flow is caused by the viscous shear stresses of the films and the forces required for pushing the lamellae through the pore throats. The confirmation of CO_2-foam effectiveness has been a research topic of interest for years; several experimental and field evaluations have been reported but it has not been of attraction in the recent years due to the lack of understanding and prediction of performance.

Our research employs an imaging technique integrating an X-Ray CT scanner with a CT friendly aluminum coreflood cell. With the integrated systems, we were able to obtain real time images when processed provide qualitative and qualitative evaluations to the coreflood. The research studies include preliminary studies of CO_2 and water injection performance in fractured and unfractured cores, evaluation of gel treatments in fractured carbonate rocks and viscosified water coupled with CO_2 floods.

1.2 Objectives

This research aims at investigating and proposing CO_2 mobility control techniques. The first stage, base coreflood experiments were conducted to fractured and unfractured core towards better understanding of the main factors controlling the success of the floods in fractured reservoirs simulated with the experimental setup. The second stage of the research addresses the application of conformance control gels taking into account the factors affecting the performance of polymer gels such as: pressure, temperature, age and chemical composition. The third stage inspects the performance of viscosified waters alternating with CO_2 utilizing the CT scanner in comparison with performance of the cross-linked gels. Data collected from the experiments and processed from the CT images will be combined to assess the overall sweep efficiency of all experiments.

1.3 Theoretical Background

In this section, CO_2 phases and properties under different conditions of pressure and temperature will be discussed. The displacement mechanisms will be reviewed briefly followed by an introduction to MMP estimations using correlations. Moreover, the basic mobility control approaches will be stated and discussed concisely. More comprehensive review of the mobility control approaches will be addressed in the next chapter with emphasis on gel applications.

1.3.1 CO_2 Phases and Properties

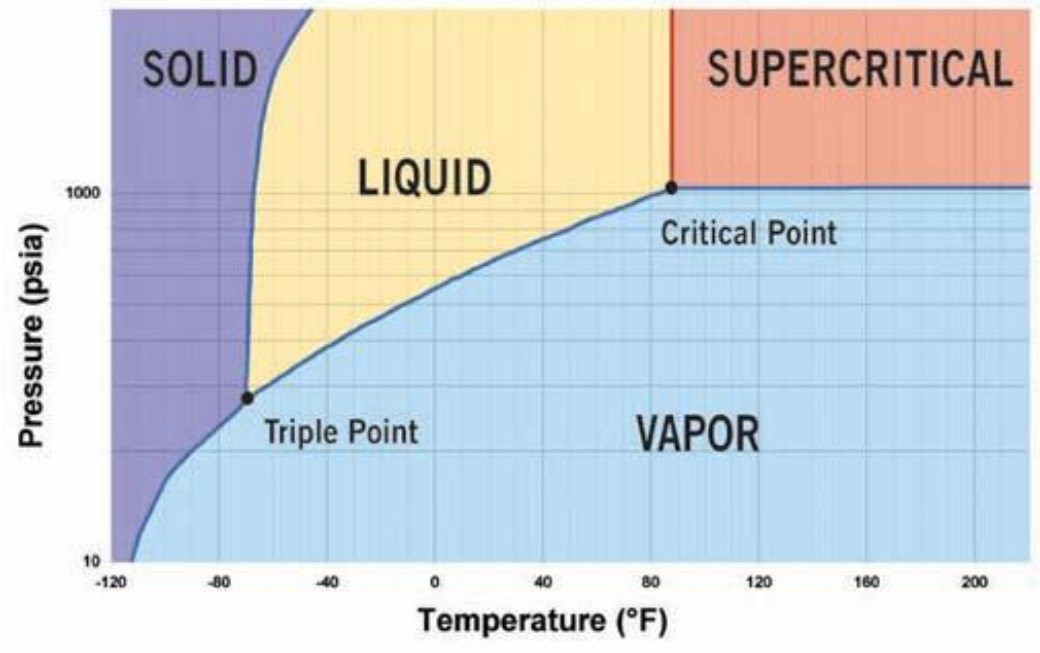

Fig.1.3 – CO_2 Phase Diagram

CO_2 properties vary greatly with changes in pressure and temperature. Understanding how the different properties change is essential in designing effective CO_2 floods. The CO_2 phase diagram, **Fig.1.3**, shows that CO_2 reaches supercritical state at 89 ^oF(32 ^oC) and 1070 psi (73 atm).Supercritical CO_2 at typical reservoir conditions has density in the range of 0.7-0.9 g/cc (44-56 lb/ft^3). In its supercritical state, CO_2 adopts properties both gas-like and liquid-like expanding to fill volumes like a gas while maintain a density close to that of liquids. The dual characteristics of supercritical CO_2 have shown great results acting as a solvent in extracting chemical compounds in addition to its low toxicity and environmental impact. Also, it is a key parameter to fully understand how solubility, capillary forces and interfacial tension properties act at supercritical condition.(Jarrell 2002)

Carbon dioxide is effective in removing oil from porous rock due the nature of its viscosity, density and acidity. CO_2 acts on oil in three ways: it causes swelling – reduces viscosity and increases density. At high pressure, CO_2 forms a phase whose density is close the density of liquids. The dense CO_2 has better performance in extracting hydrocarbon components from oil than if it was lower in density, i.e. lower pressure. However, CO_2 remains having low viscosity relative to liquids. As the pressure increases, more CO_2 goes in the oil causing the viscosity to drop and the density to rise; however, when CO_2 goes into water, the mixture density decreases. Moreover, carbonate rocks get affected by the acidity nature of the CO_2 resulting in increases in the injectivity of water. (Jarrell 2002)

1.3.2 CO_2 Displacement Mechanisms

In porous medium, Carbon dioxide displaces oil in in different mechanisms summarized as follows: (Jarrell 2002)

1. Solution Gas Drive: This mechanism occurs at relatively low reservoir pressure. As the pressure gets higher, more CO_2 gets into oil and when pressure decreases CO_2 comes out of the solution. Few fields have utilized this mechanism of pressurizing-depleting approach. One of the few examples is the Mead-Strawn project where this approach was used for 5 years after stopping the CO_2-waterflood project due to excessive water production. About 25% of the total oil in place was produced at low WOR.
2. Immiscible Displacement: The mechanism acts as a liquid-liquid displacement. The immiscible CO_2 floods aids in lowering the oil viscosity and causing oil to swell, thus, releasing more of the trapped oil. This approach has been applied in several cases of heavy oils where viscosity reduction effects dominate. At these conditions, high pressures are required to start miscibility which makes it unattractive option.
3. Hydrocarbon – CO_2 Miscible Displacement: Light hydrocarbons like Methane and Ethane are can be completely miscible with CO_2 at low pressure. The approach uses a slug of low-molecular-weight hydrocarbon mixture ahead of the CO_2 slug. Very few applications of this mechanism have been reported and no encouraging results were observed.
4. Hydrocarbon Vaporization: As an alternative to FCM, this approach requires lower pressures to start the miscibility. The Process starts with injection of lean gas

contacting the reservoir oil and extracting light to intermediate components creating a miscible transition zone. As the gas moves in the reservoir, it gets enriched with hydrocarbons.

5. Multiple Contact Miscibility (MCM): This miscibility mechanism between the two phases requires multiple contacts in which oil and CO_2 continue to exchange components back and forth. The miscibility between oil and CO_2 requires a pressure greater than a minimum which is named as the minimum miscibility pressure (MMP). The process includes acts of vaporizing, condensing, and vaporizing-condensing drive mechanisms. The process starts with CO_2 condensing in the oil and driving the methane out. The light oil components then vaporize into the gaseous phase CO_2, making it denser and thus more soluble in oil. See **Fig.1.4.** This process continues until the two phases become indistinguishable in terms of fluid properties.CO_2 dissolving in the crude oil causes the oil to swell reaching a lower density, which causes the recovery factor to increase since for a fixed volume in the reservoir there is less oil compared to pre CO_2 dissolving.

Fig.1.4 – Oil and CO_2 Miscibility(Webinar 2011)

6. First Contact Miscibility (FCM): Under this condition the injected CO_2 and the in-situ hydrocarbons form a single phase mixture regardless of the mixing proportions. This approach requires relatively high pressure to attain the complete miscibility of the two fluids. This condition is hard to achieve with practicality.

1.3.3 Prediction of CO_2 MMP

Prediction of minimum miscibility pressure (MMP) is essential step in successful design and application of a CO_2 injection EOR project. The most common accurate experimental method is the slim tube test; though, this method is both expensive and time consuming.

Quick analysis can be used to estimate MMP utilizing correlations; these correlation give direct and important information about the pressure required to reach miscibility and accordingly know whether the displacement mechanism in the reservoir is miscible or immiscible.

Glaso proposed a correlation that predicts minimum miscibility pressure MMP for dynamic miscibility of reservoir fluids by hydrocarbon gases, N_2 and CO_2. His equations were based on previous work of Benham *et al*. (Benham et al. 1960; Glaso 1980) The input parameters for his correlation were: reservoir temperature, molecular weight of C_{7+}, mole percent of C_2-C_6 intermediate content. The proposed equations by Glaso were:

$$(MMP)_{x=34} = 6{,}329 - 25.410\,y - (46.475 - 0.185\,y)z + \left(1.127x10^{-12}\ \text{x}\ y^{5.258}\ \text{x}\ e^{319.8zy^{-1.708}}\right)T \quad \text{....(1.1)}$$

$$(MMP)_{x=44} = 5{,}503 - 19.238\,y - (80.913 - 0.273\,y)z + \left(1.17x10^{-9}\ \text{x}\ y^{3.73}\ \text{x}\ e^{13.567zy^{-1.508}}\right)T \quad \text{...(1.2)}$$

$$(MMP)_{x=54} = 7{,}437 - 25.703\,y - (73.515 - 0.214\,y)z + \left(4.92x10^{-14}\ \text{x}\ y^{5.52}\ \text{x}\ e^{21.706zy^{-1.109}}\right)T \quad \text{..(1.3)}$$

$$y = \left(\frac{2.622}{\gamma_{C_{7+}}^{-0.846}}\right)^{6.558} \quad \text{.....(1.4)}$$

Where:

x= is the molecular weight of C_2 through C_6 components in injection gas, in lbm/mol

y= is corrected molecular weight of C_{7+} in the stock-tank oil in lbm/mol

γ_{C7+} = specific gravity of heptane-plus fraction, and

z= mole percent methane in injection gas

MMP values can be interpolated between theses equations if x is different from those specified in the equations. The corrected molecular weight of the stock tank oil is indicative to how paraffinic the crude is.

Fairoozabadi *et al* proposed a correlation that predicts MMP under the effect of dynamic miscibility as a function of mole percent of intermediates in oil, molecular weight of heptane plus and temperature. The equation serves in predicting MMP for lean gas or N_2 injection; intermediate contents of the reservoir fluid accounts for the presence of $C_2 - C_6$, CO_2, and H_2S. The study concluded that exclusion of C_6 from intermediates improves the correlation estimate of the MMP. The heptane plus molecular weight is an indication of how volatile the oil is.(Firoozabadi and Aziz 1986)

Where:

$$x_{int} = x_{CO2} + \sum_{i=2}^{i=5} x_i = mole\ percent\ of\ intermediates \quad \text{.....(1.5)}$$

$M_{C7+} = molecular\ weight\ of\ heptane\ plus$

T= temperature in ^{o}F

Eakin and Mitch have suggested a correlation based on their work with Rising Bubble Apparatus (RBA). RBA is a much quicker apparatus to predict MMP with compared to slim-tube tests, though, it predicts higher MMP. The input variables were: solvent composition, C_{7+} molecular weight, and the pseudoreduced temperature of the reservoir fluid. The solvents used for this work were nitrogen, flue gas, carbon dioxide, and rich and lean natural gases. The equation has high accuracy of MMP prediction with crudes closer to the quality of that used in the experiments with API 36.8 and 25.4, at 180 and 240°F.(Eakin and Mitch 1988) The general proposed correlation by Eakin and Mitch is:

$$\ln p_{pr} = \ln(MMP / p_{pc}) = (0.1697 - 0.06912/T_{pr}) \times y_{C1} \times M_{C7+}^{0.5} + (2.3865 - 0.005955\frac{M_{C7+}}{T_{pr}}) \times y_{C2+} + (0.01221 M_{C7+} - 0.0005899\frac{M_{C7+}^{1.5}}{T_{pr}}) \times y_{CO2} \quad \text{.....(1.6)}$$

y= mole fraction of certain molecular weight range hydrocarbon in the reservoir fluid

P_{pr}= pseudo reduced pressure of the reservoir fluid

P_{pc}= pseudo critical pressure of the reservoir fluid

T_{pr}= pseudo reduced temperature of the reservoir fluid

T_{pc}= pseudo critical temperature of the reservoir fluid

Cronquist proposed a simple correlation that takes into account reservoir temperature and molecular weight of C5+.The work done covered a wide range of API gravities and temperatures.(Aleidan and Mamora 2011)

$$MMP = 15.988T^{(0.744206+0.0011038MwC5+)} \quad \text{.....(1.7)}$$

T: Temperature in ^{o}F

Mw_{C5+}: The molecular weight of pentane and heavier fractions in the reservoir oil.

Emera and Lu developed new correlation to predict MMP of oil and CO_2 or flue gas using GA modeling technique. The new correlation takes into consideration the following parameters: reservoir temperature, molecular weight of C_{5+}, oil volatiles (C_1 and N_2) and oil intermediates (C_2-C_4, H_2S, and CO_2).(Emera and Lu 2005) The correlations take the following forms:

1-For oil with bubble point pressure P_b > 0.345 MPa (50 psi):

$$MMP = 7.43497x\,10^{-5}\,x(1.8\,T+32)^{1.1669}\,(MW_{C5+})^{1.201}\left(\frac{Volatiles}{Interm.}\right)^{0.109} \quad \text{.....(1.8)}$$

2- For oil with bubble point pressure P_b < 0.345 MPa (50 psi) for oil with zero volatiles fraction and non-zero intermediates fraction:

$$MMP = 7.43497x\,10^{-5}\,x(1.8\,T+32)^{1.1669}\,(MW_{C5+})^{1.201}\left(\frac{Volatiles}{Interm.}\right)^{0.109}\left(\frac{1}{Interm.}\right)^{0.023} \quad \text{.....(1.9)}$$

3- For oil with bubble point pressure P_b < 0.345 MPa (50 psi) for oil with zero volatiles fraction and intermediates fraction:

$$MMP = 7.43497x\,10^{-5}\,x(1.8\,T+32)^{1.1669}\,(MW_{C5+})^{1.201} \quad \text{.....(1.10)}$$

If the predicted MMP <P_b, P_b=MMP.

For our coreflood experiments we decided to use the Cronquist correlation from DOE reports because of the limited fluid data.

1.3.4 CO_2 Mobility Control

At reservoir conditions CO_2 remains having low viscosity relative to liquids. Its viscosity nature is challenging in heterogeneous and naturally fractured reservoirs; CO_2 will flow preferentially through the easiest paths resulting in early breakthrough and extraction ineffectiveness leaving behind zones of oil intact. For successful and economically attractive CO_2 application in heterogeneous reservoirs, it is crucial to develop, propose and verify mobility control techniques.

The high mobility in fractures and uneven flow in heterogeneities is not as attractive or efficient as in homogenous rocks. See **Fig.1.5.** The unfavorable CO_2 high mobility in porous medium urges the search for mobility control solutions increasing the CO_2 viscosity or blocking the permeable zones directing it to flow through the less permeable zones.

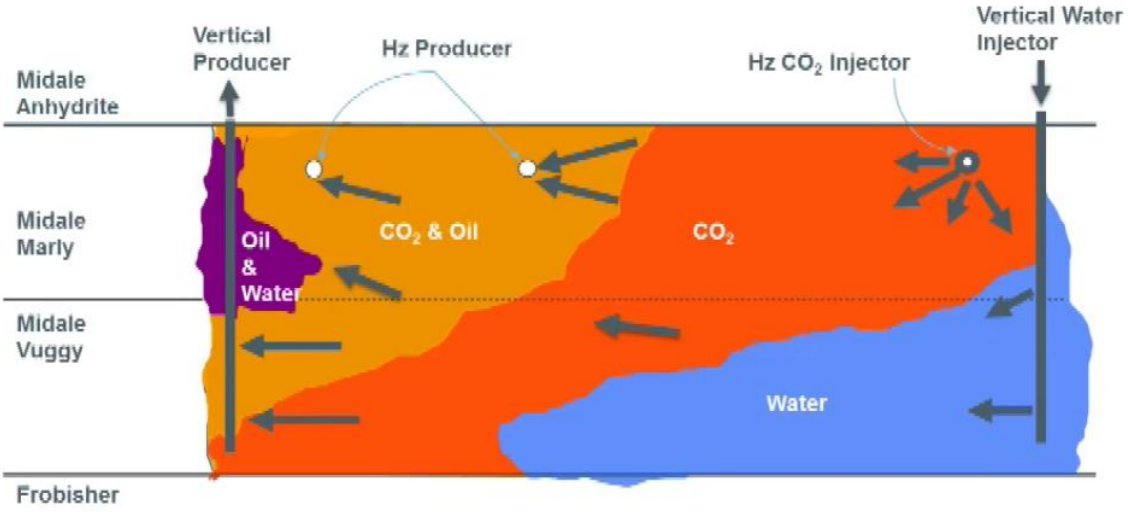

Fig.1.5 – Schematic of CO_2 Flood Performance in a Heterogeneous Reservoir(Webinar 2011)

Four major approaches have been proposed to enhance the CO_2 flood efficiency: water alternating gas (WAG), cross-linked gel treatments, CO_2 viscosifier and CO_2 foaming agents. In the following sections, the main mobility control approaches will be reviewed with emphasis on gel treatments and water alternating gas (WAG) since these two approaches will be evaluated and discussed experimentally. Some of the most applied techniques and approaches are:

1. **Water alternating gas (WAG):** water and CO_2 are injected in a cyclic manner with the objective of decreasing the viscous fingering due to the low viscosity of the CO_2,thus lowering the mobility ratio of the injected gas to the oil.
2. **Thickening agents:** At reservoir at reservoir pressure and temperature, CO_2 is a dense fluid-its density is near that of oil. Polymers are added in low

concentrations dissolving in the CO_2 resulting in increased CO_2 solution viscosity by a factor of 10-20.

3. **Foaming agents:** The mechanism employs the principle of having CO_2 as a dispersed phase which has a lower mobility than CO_2 alone. Surfactants are to be injected in the porous medium and CO_2 gas disperses into the liquid phase forming foam.
4. **Gel application:** The objective of gel placement as to act as a blocking agent reducing channeling through fractures or high-permeability zones of oil reservoir without significantly damaging hydrocarbon productivity and improve the overall oil recovery from the flooding process. So, the goal of the gel is to maximize gel penetration and permeability reduction in high permeable zone while minimizing gel penetration and permeability reduction in less permeable zones of the reservoir.

1.3.4.1 Water Alternating Gas

The WAG scheme combines two traditional recovery techniques: waterflooding and CO_2 injection. Inherent in all CO_2 injection is the lack of mobility and gravity control. The scheme aims at controlling the CO_2 mobility by injection in alternating cycles with the less mobile and cheaper chase water. This design combines the better microscopic displacement of CO_2 with the water's overall better macroscopic sweep. The first reported WAG application goes back to 1957 to the North Pembina field in Alberta, Canada. A common plan is to inject with WAG ratios of 0.5:4 in cycles of 0.1 to 2% PV slugs of each of the two fluids. (Rogers and Grigg 2000)

Numerous factors affect the WAG performance have been studied such as: heterogeneity, permeability, initial water saturation, wettability, fluid properties, miscibility conditions, injection techniques and flow geometry. Several studies suggested that the flood efficiency is lowered as the rock permeability decreases, the initial water saturation and the degree of heterogeneity both increase. In fairly homogenous reservoirs the injected water enters the zones previously invaded by gas diverting the chasing gas into the other zones. But the presence of fractures alters the performance greatly and the challenge becomes to utilize conformance control agent to direct the injected gas into the matrix, reducing oil bypass. Several experimental studies and field applications have been reported in the recent years as EOR processes gained increased interest.(Rogers and Grigg 2000)

In 2006, Schechter *et al* reported using viscosified water to decelerate the CO_2 even more; Xanthan was picked to viscosify the water. The objective was that the injected water acts like a fluid healing the fracture preceding the injected slug of CO_2.They have found that large amount of the injected liquid leaked-off into the matrix leaving the fracture plane open for CO_2 flow. Although the application resulted in incremental recovery over plain CGI, the leak-off was excessive that it needed to be assuaged. The authors suggested that more work should be used to minimize the leak-off ; one of the approaches is to add effective amounts of cross-linkers helping the viscosified water in keeping its viscosity better.(Chakravarthy et al. 2006)

1.3.4.2 Thickening Agents

Thickening or viscosifying CO_2 is one of the two direct approaches, in addition to gel application. The tactic is to add dissolve polymers in CO_2 phase increasing the viscosity. At reservoir at reservoir pressure and temperature, CO_2 is a dense fluid-its density is near that of oil. Polymers combined with cosolvents such as toluene are added in low concentrations dissolving in the CO_2 resulting in increased CO_2 solution viscosity by a factor of 10-20.However, this approach remains the less developed and investigated compared to WAGs, foams and gel application. The most challenging problem of viscosifying agents is the solubility of these of polymers into CO_2 and to what extent the viscosity of CO_2 will increase.(Chakravarthy et al. 2006)

Heller *et al*. research focused on testing different polymers as viscosifying agents in supercritical CO_2.They main properties in the evaluation process were: solubility and viscosity increase. The solubility increases with increase in CO_2 density. Also, they studied how solubility is affected by polymer properties such as: structure, stereochemistry (spatial arrangement of atoms inside molecules) and molecular weight. Although the work done did not show great increase in viscosity of CO_2 by any of the tested polymers , the study gave starting guidelines to those interested in designing thickening agents as which practice on a property yields higher thickening ability. (Heller et al. 1985)

Terry *et al*. tested olefin monomers and benzoyl peroxide as an initiator for thickening supercritical CO_2.They were successful in dissolving the polymers but no appreciable increases in viscosity was observed. (Terry et al. 1987)

Enick *et al*. made great research efforts during 2000 to 2003.In their earlier work they designed different thickeners and tested them against solubility in CO_2 without cosolvents. Fluoroacrylate-styrene copolymers were found to be the most effective thickeners. As an example bulk polymerized, 29-30% Styrene – 71-70% Fluoroacrylate random copolymers resulted in an increase of the viscosity by 2-400 fold. The tested mixture showed very high solubility performance. Higher velocities and lower concentration were verified to result in lower mobility reduction. However, the successfully designed thickener had two disadvantages: unpractical cost and harm to the environment. They concluded their work with suggesting the design of nonfluorous thickeners composed just of carbon, hydrogen, oxygen, and nitrogen. Acetate based polymers would be a good candidate. As an example, poly (vinyl Acetate) PVAc should great solubility with reasonable cost. However, the pressure required to initiate dissolution of PVAc was 6000-9000 psia, which is impractical field choice. The objective is to find a better cosolvent to enhance PVAc solubility in CO_2 at lower pressure.(Enick et al. 2000; Xu et al. 2003)

Bae and Irani conducted a series of studies using siloxane polymers and toluene as cosolvent. Later in the research, different cosolvents were tried but the results were merely similar to the first one and no significant improvement has been made in terms of cost. The suggested thickeners with cosolvents showed successful performance in lowering the required miscibility pressure. Also, the polymers in the effluent did not correlate with the viscosity of the oil. The researchers recommended research more

research to be made on cost saving to make economical viable thickeners.(Bae 1995; Bae and Irani 1993)

1.3.4.3 CO_2 Foam

The unfavorable CO_2 high mobility in porous medium urged the search for increasing the CO_2 viscosity and thus reducing the mobility. One of the methods to achieve that is to use CO_2-foam. The confirmation of CO_2-foam effectiveness has been a research topic of interest in the recent years, and several experimental and field evaluations have been reported.

The mechanism employs the principle of having CO_2 as a dispersed phase which has a lower mobility than CO_2 alone. Surfactants are to be injected in the porous medium and CO_2 gas disperses into the liquid phase forming foam. The foam bubbles are separated by thin films called lamellae that resist flow. The resistance to flow is caused by the viscous shear stresses of the films and the forces required for pushing the lamellae through the pore throats. Usually, foam is generated by surfactant solution-alternating-gas (SAG) injection or co-injection of gas and surfactant solution.(Masalmeh et al. 2011; Nguyen et al. 2000)

The applicability of this approach requires technical and economical verification and screening under different conditions. Some of the main parameters affecting CO_2 foaming process are: surfactant type and concentration, surfactant retention, rheology pH, oil presence and rock properties.

Foaming applications have many challenges especially in terms of foam stability, placement near theft zones and surfactant adsorption in carbonate reservoirs. Due to

technical and scope purposes ,foam processes will not be tested in the experiments, but a brief review of some of the previous work done in this topic will be presented.(Du et al. 2008)

Nguyen *et al* reviewed the relative permeabilities and mobilities behavior with description of the microscopic mechanisms associated with foaming. They also reviewed different models of foam flow through porous media highlighting the advantages and the disadvantages of each model. They found that foam flow through porous media exhibits two flow regimes: high quality and low quality regimes, and that in some cases behavior approaching the behavior of Newtonian fluids. Also, the foam quality was found to increase with increasing the total flow rate. They concluded with some recommendations and observations on how models can be improved.(Nguyen et al. 2000)

Liu *et al*. work was to study the effects of studied Salinity, pH, and Surfactant Concentration Effects on CO_2-Foam stability and performance at reservoir conditions. They found that foam stability is not highly sensitive to surfactant (CD) concentration. Also, they found that above a critical surfactant concentration, foam solubility is insensitive to salinity. The concluded that adsorption increases with increase in salinity and it also increases with decrease in PH due to the decreases in surface charge.(Liu et al. 2005)

Viet Q. *et al* proposed a novel approach of dissolving the surfactant directly in the CO_2.Two different methods were studied on carbonate cores: continuous CO_2-dissolved-surfactant injection and water-alternating-gas with CO_2-dissolved-surfactant injection. This approach was found to lower injection costs, reduce loss of surfactant due

to adsorption onto matrix and improve foam generation. Three injection strategies were experimented: conventional SAG (surfactant within water- alternated-CO_2), WAGS (water-alternating – gas with surfactant dissolved) and novel CO_2 (continuous injection of CO_2 with dissolved surfactant).Simulation studies were done utilizing CMG/STARS software to emphasize the microscopic buoyancy and heterogeneity effects. They found that the CO_2 injection with dissolved surfactant, in comparison to WAGs and SAG, yielded higher recovery without injected water. It also required lower injection pressure and improved well injectivity.(Le et al. 2008)

Dong *et al* studied the effect of water solubility on carbon dioxide foam flow in porous media. Two types of gases with contrast in solubility, CO_2 and N_2, were tested with the aid of X-ray computed tomography (CT) to visualize the dynamic flow process inside the core. The two gases were compared for pressure drops, liquid production rates and in-situ water saturation profiles to better understand the effect of water solubility on foam rheology. They found that CO_2 ,having higher solubility in water than N2 ,lowers surfactant solubility in water and lowers surface tension leading to decreases in foam viscosity. The CT images revealed lower sweep efficiency of CO_2 foam compared to N_2, confirmed by calculations showing higher remaining liquid after CO_2 foam sweep.(Du et al. 2008)

Fjelde *et al*. performed experiments to study the effect of CO_2-foaming agents on oil recovery and the transport of CO_2 in fractured carbonate oil reservoirs. The effect of foaming agents on CO_2 diffusion at reservoir conditions was determined. They

concluded their work with comparison of bulk diffusion coefficients of CO_2 in synthetic seawater and in aqueous solution.(Fjelde et al. 2008)

Zuta *et al* performed modeling and analytical studies accompanied with simulation to study the transport of CO_2-foaming agents in two different types of fractures. They investigated the transport rate of foam and studied the concentration distribution in the matrix. The simulation work utilized CMG to match the experimental results in order to deeply identify the main mechanisms controlling the CO_2-foam which showed that flow from fractures into matrix depends on: time- concentration of the CO_2-foaming-agent solutions, and the presence of oil. They concluded that the transport of CO_2-foaming agents in the fractures is diffusion-controlled.(Zuta and Fjelde 2010)

Alireza *et al* performed visualization experiments to investigate the performance of subcritical CO_2 and CO_2-foam injection in heavy oil and study the micro mechanisms of displacement and recovery of oil by foam. They reported three models of how foam interacts with medium-heavy crude oil. They concluded that injecting surfactants prior to foam flood speeds up the foam formation, but does not improve the ultimate increment of oil recovery. The models also revealed that, foaming agents not only improve sweep efficiency but also increase the micro scale efficiency of displacement. Oil displacement by foams was found to be more effective than double drainage displacement process during CO_2 flood.(Emadi et al. 2011)

1.3.4.4 Gel Applications

The most applied gel system in the oil industry has been hydrolyzed Polyacrylamide (HPAM) with Cr (III) Acetate as cross-linkers. See **Fig.1.6.** The

objective of the cross-linkers is to strengthen the gel against solubility and erosion by forming covalent chemical bonds and a permanent polymer network.

The main parameters to be considered in gel applications:

- Availability and cost of used gel: survey is needed.
- Concentration of gel in solvent (ppm): both economic and engineering decision.
- Cross-linker to Gel ratio: Generally, increasing the cross-linker concentration will yield a stronger gel. However, exaggeration in increasing the concentration means more cost and even, causes gel syneresis (water expulsion and gel shrinkage).
- Additives to gel systems: Sodium Lactate is one of the most used additives to the gel system for gel stability control of gelation time (how viscosity of gel changes with time).

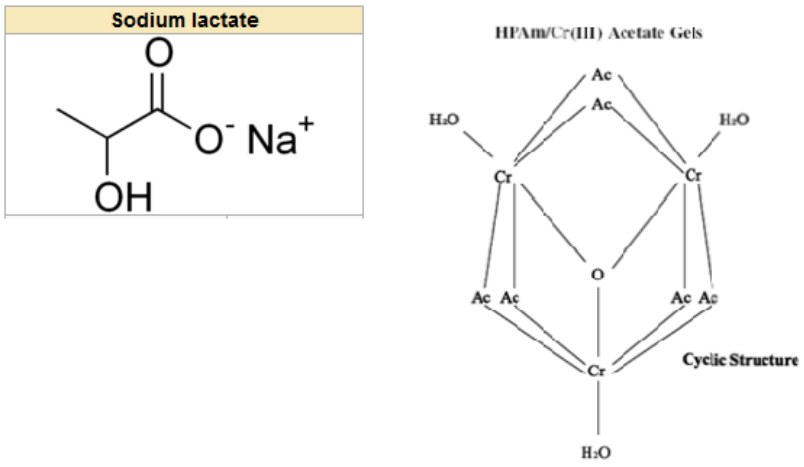

Fig.1.6 – Sodium Lactate and HPAM-Cr (III) Acetate System

1.3.5 Flooding Visualization

The universal System HD 350 X-ray CT scanner (computed tomography) was used to obtain cross-sectional scans enabling visualization of flood throughout the core. See **Fig.1.7.** The X-ray CT imaging technique was first invented by Sir Godfrey Hounsfield in 1972. (Wellington and Vinegar 1987) It was first used in medical applications such as brain-scanning but its application in petroleum studies gained popularity in the next years.(Withjack et al. 2003)

Fig.1.7 – Universal Systems® CT Scanner

The CT-scanners generate cross sectional images through a desired objective by revolving the X-ray tube around the object to acquire projections at different angles at every single slice.3-D images then, can be constructed taking combining 2-D images taken in small intervals over a constant axis. The real-time images can be utilized in CO_2 EOR floods to evaluate some phenomenon and features as the sweep efficiency, viscous fingering, and gravity segregation.

The basic principles of CT images data processing and its applications in petroleum industry will be discussed.

1.3.5.1 CT Scan Principles

CT scanning is based on analyzing and quantifying the attenuation of X-ray beams penetrating an object at different angles as the X-ray emission device rotates around the object. Several detectors record the intensity day of the transmitted X-ray, from which, a cross sectional slice is generated by the computer. 3-D images then can be constructed taking combining 2-D images taken in across the sample small intervals over a constant axis.(F. Mees 2003; Wellington and Vinegar 1987)

The attenuation is represented as flows:

$$\frac{I}{I_o} = exp^{-\mu h} \quad \text{.....(1.11)}$$

Where:

μ :is the linear attenuation coefficient

I:is the intensity of emitted X-ray

I_o: is the intensity of the X-ray after passing through the sample.

h:is the thickness of the sample.

The relationship between the atomic number and X-ray energy is represented as:

$$\mu = \rho\left[\sigma(E) + b\frac{Z_e^{3.8}}{E^{3.2}}\right] \quad \text{.....(1.12)}$$

Where:

ρ: is the electron density

σ (E): is the Klein-Nishina coefficient

Z: is the effective atomic number of the object

E:is the X-ray photon energy in keV

B: constant (9.8×10^{24})

The CT number is usually expressed in Hounsfield units (HU):

$$\psi = 1000\times\left(\frac{\mu}{\mu_w}-1\right) \quad \text{.....(1.13)}$$

Where:

ψ: is the attenuation coefficient (CT number) in HU

μ_w : the attenuation coefficient of water in m^{-1}

μ: is the local linear attenuation coefficient averaged over a voxel in m^{-1}.

1.3.5.2 CT Scan Applications

The CT imaging gained popularity in petroleum research due its relative low cost, ease of use and wide range of applications. The calculated CT numbers are used for calculations of porosity, fluid saturations and recovery efficiency. Moreover, researcher used the CT images for qualitative studies the effects of recovery mechanisms, gravity and viscous forces, trapping and heterogeneity.(F. Mees 2003; Wellington and Vinegar 1987)

In enhanced oil recovery (EOR) and flow efficiency studies, researchers have found that the usage of dopants enhances the contrast between oil and water in two phase flow floods enabling clearer qualitative distinction in the images and calculation of saturation distribution.

Withjack *et al*.(2003) reviewed the applications of CT imaging in petroleum industry. They listed many useful applications such as core description, recovery mechanisms evaluation and saturation profiling. Also, they briefly described some of the uses in formation damage and well stimulation studies such as evaluation how deep the damage affected the wellbore and how effective the acids in doing stimulation jobs. In EOR studies, CT imaging was used in many objectives such as polymer gel propagation monitoring throughout fractures.(Withjack et al. 2003)

Schechter *et al.* have used CT imaging technique in a series of CO_2 EOR studies. Their work focused mainly on CO_2 floods performance in the presence of fractures and heterogeneities. The tendency of CO_2 to flow through the lowest resistance paths and its low viscosity both represent a challenge to its application in terms of sweep efficiency and how much trapped oil can be recovered. See **Fig.1.8.** The studies utilized CT images to quantify the recovery rates and evaluate the porosity distributions during CO_2 floods. During their work they studied different mechanisms of CO_2 mobility control such as: WAGs (Water alternating gas), thickening agents and polymer gels. An example of their work is shown in the next figure. Their work provided the base for this research in studies of mobility control agents.(Chakravarthy et al. 2006)

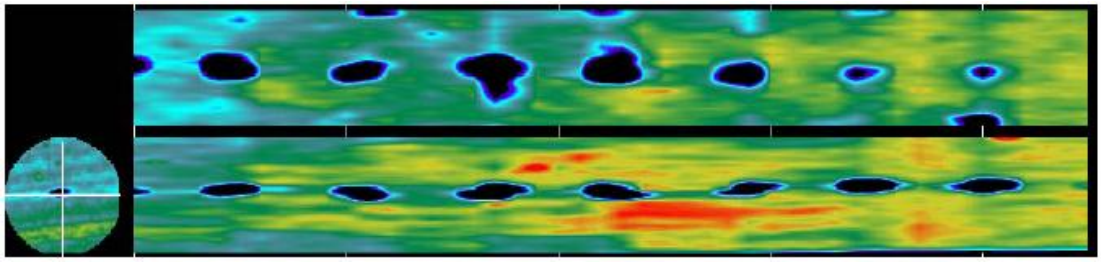

Fig.1.8 – Visualization of CO_2 Flood With Gel Treatment

Wellington and Vinegar have conducted pioneering studies in the application of CT imaging in their studies. They have used this technique to study rock compressibility and mud invasion evaluations. Also, they presented the use of CT images to correlate with well logs. They have studied different CO_2 flood schemes studying: immiscible floods, first contact miscibility (FCM) and multiple contact miscibility(MCM).In their CO_2 floods they evaluated different factors affecting the success of these applications: capillary forces, viscous forces , gravitational forces.(Wellington and Vinegar 1987)

Bataweel *et al*. utilized CT imaging to study the performance of several chemical EOR flooding schemes: polymer, surfactant, surfactant-polymer (SP), and alkali-surfactant-polymer (ASP).In their work , they evaluated and quantified the oil distribution in the sandstone core and the recovery rates.(Bataweel et al. 2011)

1.3.6 Methodology

Our research employs an imaging technique integrating an X-Ray CT scanner with a CT friendly aluminum coreflood cell. With the integrated systems, we were able to obtain real time images when processed provide qualitative and qualitative evaluations to the coreflood.

The research studies include preliminary studies of CO_2 and water injection performance in fractured and unfractured cores, evaluation of gel treatments in fractured carbonate rocks and viscosified water coupled with CO_2 floods. In the first stage, base coreflood experiments were conducted to fractured and unfractured core towards better understanding of the main factors controlling the success of the floods in fractured reservoirs simulated with the experimental setup. The second stage of the research addressed the application of conformance control gels taking into account the factors affecting the performance of polymer gels such as: pressure, temperature, age and chemical composition. The third stage inspected the performance of viscosified waters alternating with CO_2 utilizing the CT scanner in comparison with performance of the cross-linked gels.

CHAPTER II

LITERATURE REVIEW

2.1 Introduction

Gel application is considered the most aggressive type of conformance control. The objective of gel placement is to improve the overall sweep efficiency and oil recovery from the flooding process. The challenge is, however, to act as a blocking agent reducing channeling through fractures or high-permeability zones of oil reservoir without significantly damaging hydrocarbon productivity. See **Fig.2.1.** This is especially effective in naturally fractured carbonates were the high-perm zones are in the form of network rather than a particular zone. The design should maximize gel penetration and permeability reduction in more permeable zones while minimizing gel penetration and permeability reduction in less permeable zones of the reservoir.(Vargas-Vasquez and Romero-Zerón 2008)

The gel technology has been applied for more than twenty years. However, most of the work has been applied for water shutoff purposes in injection wells in sandstone environment and there is lack of information on applications of gels as mobility control agents for CO_2 EOR purposes and also in carbonates. Injection wells treatments will require higher volumes of gels deep into the target zones filling the conductive channels between injectors and producers.(Vargas-Vasquez and Romero-Zerón 2008)

Gels are injected as a solution of polymer and crosslinker into the desired zones. Later in time, the two components will react forming gel. When the well is put back into production or injection the reservoir fluids will behave differently and will differ in their flow ability in the presence of gels. The required time between the mixing of the chemicals and the formation of the gel is termed “Gelation Time”. A brief literature review of the chemistry and the physical properties of the gels will be presented.(Vargas-Vasquez and Romero-Zerón 2008)

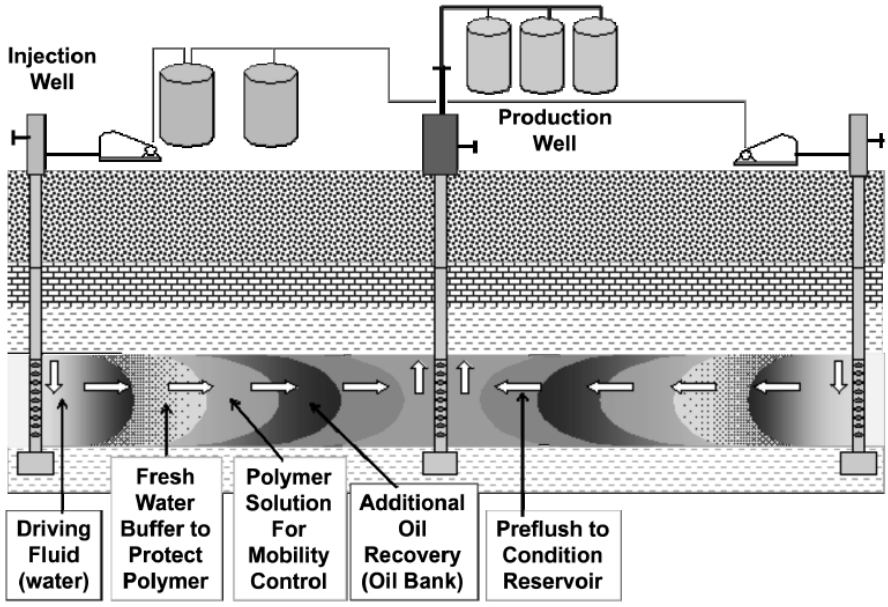

Fig.2.1 – Injection of Polymer Gel for Mobility Control

The main parameters to be considered in gel applications:

- Availability and cost of used gel: survey is needed.
- Concentration of gel in solvent (ppm): both economic and engineering decision.
- Cross-linker to Gel ratio: Generally, increasing the cross-linker concentration will yield a stronger gel. However, exaggeration in increasing the concentration means more cost and even, causes gel syneresis (water expulsion and gel shrinkage).
- Additives to gel systems: Sodium Lactate, shown in **Fig.2.2.** , is one of the most used additives to gel systems for gel stability and control of gelation time (how viscosity of gel changes with time).

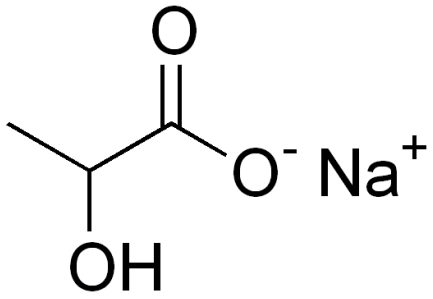

Fig.2.2 – Sodium Lactate (Wikipedia/ chemblink.com)

2.2 Gels Chemistry

A polymer gel is a matter that has solid and liquid-like properties formed of polymer molecules are further cross-linked by chemical bonds (typically covalent). The term “Cross-linker” refers to a substance that strengthen the gel against solubility and erosion by forming chemical bonds linking one polymer chain to another forming a permanent polymer network. The cross-linked polymers are insoluble in all solvents that do not destroy the chemical network. Hydrogels (sometimes called responsive gel) are made when gels swell in water and reach an equilibrium volume.(Vargas-Vasquez and Romero-Zerón 2008; Vargas-Vasquez et al. 2009)

Polyacrylamide (PAM) is a water-soluble polymer from acrylamide subunits. See **Fig.2.3.** It is mostly used as flocculants and in water filtration applications. In the petroleum industry, this polymer gained popularity both from technical and economical point of view. PAM solutions have been found to show both shear thinning / thickening (also called dilatancy and viscoelastic behavior) behavior in porous medium. At high rates of injection, usually experienced in EOR applications, the shear thickening behavior dominates. That is, the viscosity of the polymer solution increases with increased shear i.e. increased flux for the fluid. (Seright et al. 2011)

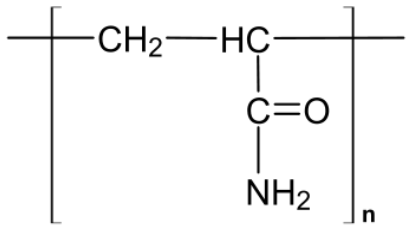

Fig.2.3 – Structure of Polyacrylamide

Cr (III) Acetate is commonly used in forming hydrolyzed polyacrylamide (HPAM) polymer gels with high water concentrations (up to 99.7 wt. %). It comes in two common forms: Cr (III) Acetate hydroxide (Cr3 (OH) 2(OOCCH3)7) and Cr (III) Ac (Cr(OOCCH3)3). See **Fig.2.4.** (Vargas-Vasquez et al. 2009)

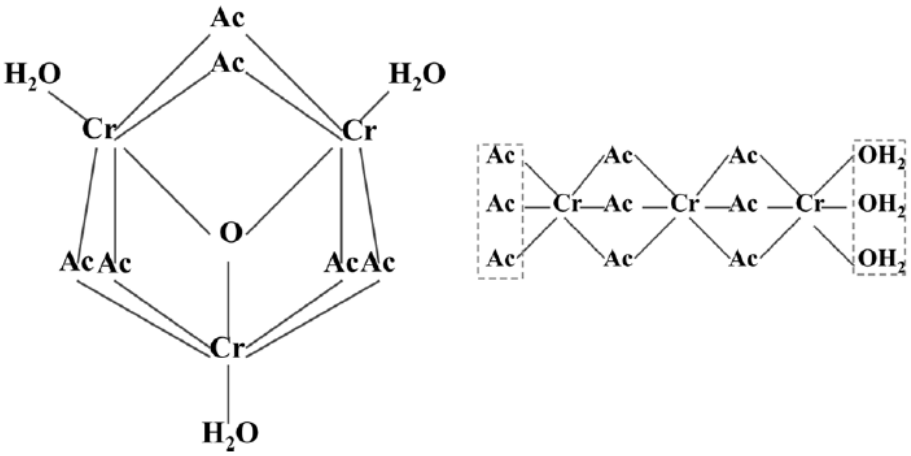

Fig.2.4 – Cr (III) Ac Cyclic Structure (Left) and Linear Structure (Right)

Natarajan *et al* performed a set of experiments to study the effects of varying Cr(III)/Acetate ratio on crosslinking HPAM. They showed that using excess Acetate ion(as sodium Acetate) will reduce the rate of crosslinking the polymer insuring deeper penetration of the gelant solution in the fractures network before the development of flow resistance. Their work confirmed that the reaction between Chromium Acetate and partially HPAM is too rapid such that a flowing gel can be designed that do not penetrate the adjacent matrix. The increase of Acetate/Cr(III) was able to change the gel time from few hours to several days. Also, they concluded that gel solutions made from aged Chromium stock had much shorter gel times than fresh stock, which suggests that the linear Chromium Acetate is more reactive than the cyclic structure.(Natarajan et al. 1998)

H. Jin *et al* conducted a series of experiments to study how Cr(III) Acetates in the absence of polymer react with carbonates. They used Chromium (III) Acetate with Chromium (III) concentration of 200 ppm and an Ac/Cr mole ratio of 3 with 19- to 25-md dolomite. The rock-fluid interactions lead to loss of Chromium and may limit the penetration of a gel treatment. A model was proposed to model the rate of Chromium retention by precipitation in dolomite cores that was consistent with the experimental results. The precipitation of Chromium in dolomite rock is a rate-dependent process and long residence time will result in large amounts of Chromium retention. Moreover, the precipitation is increased by the increase in the degree of salinity.(Jin et al. 2002)

Van der Hoek *et al* studied the effects of gel composition, permeability, temperature and treatment volume on the behavior of two cross-linked gel systems in the

temperature range of 80^{o}C to 120^{o}C.The in-situ gel strength was determined and a mathematical model was proposed describing the compression and displacement of gel. The gel yielding behavior was descried by three mechanisms: gel compressibility, micro flow and two-phase flow. Compression occurs due to the flexible membrane in the pressure transducer. The undamaged gel network exhibits micro flow owing to the intrinsic permeability of the gel. Experiments confirmed the permeability increase reduces the required pressure drop to yield the gel. This effect of the variation in permeability is more pronounced in low permeability range, while in high permeable ones, it becomes more a function of gel bulk strength. For the tested gels, the ultimate gel strength was not a function of temperature. The temperature effects were found to delay reaching the final gel strength at lower temperatures. The authors recommended more research to be conducted on modeling the behaviors although the proposed model showed good agreement with the experimental results.(Hoek et al. 2001)

In 2003, Vasquez *et al* evaluated the effectiveness of novel, organically cross-linked, conformance polymer gel in providing long-term blockage to water flow at elevated temperatures up to 350°F. The gel system was verified, also, for providing adequate gel time for placement. Further tests were conducted to examine how permeability reduction changes over time as a function of temperature. Due to the limitations of polyacrylamides (PAMs) having short and unpredictable gelation times at high temperature, the authors used two polymer systems suitable for the purpose of the experiments: A) Copolymer of acrylamide and t-butylacrylate with organic low-toxicity cross-linker polyethyleneimine (PEI). B) Mixture of acrylamide and acrylamido-2-

ethylpropane sulfonic acid (AMPS) with longer gel times than Polymer System A. Both gel systems showed effectiveness in reducing water permeability, proving thermal stability at high temperatures but system B was preferred for showing longer gelation times.(Vasquez et al. 2003)

2.3 PAM Chromium Mixtures

The most applied gel system in the oil industry has been hydrolyzed polyacrylamide (HPAM) with Cr(III) Acetate as a cross-linker. It has been widely used in injection well treatments for conformance control, water shut-off in in naturally fractured reservoirs, vugular or high-permeability channels, and near-well treatment for squeeze treatments and sealing of open hole wellbores. HPAM based gels have been found to be more resistant to acidic conditions than other competitors like borate cross-linked guar which is limited to certain pH conditions. See **Fig.2.5.** In fact, several parameters made them highly desirable such as: high molecular weight, high solution viscosities at low polymer concentrations, low toxicity and hydrophilicity (Having affinity for water; absorbing or dissolving in water).(Vargas-Vasquez and Romero-Zerón 2008; Vargas-Vasquez et al. 2009)

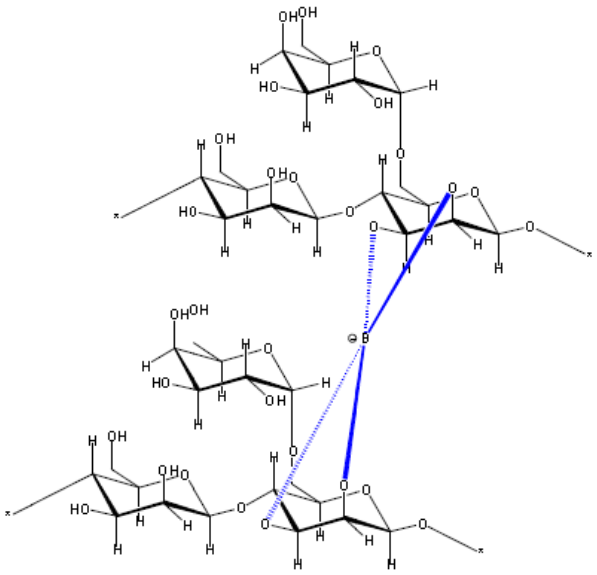

Fig.2.5 – Borate Cross-Linked Guar Gel System

2.3.1 Background

The cross-linked acrylamide gels were reported in oil industry studies as early as late 1950s. The earlier studies focused on studying the swelling nature of the gel. White showed that swelling degree decreases with increasing crosslinking density while Hirokawa *et al.* (1984) showed that non-ionic N-isopropylacrylamide gels shrink with increased temperature. In 1988, Sydansk developed HPAM/Chromium (III) aqueous gel using polyacrylamide or partly hydrolyzed polyacrylamide. Cr(III) Acetate was the preferred Cr(III)-carboxylate complex because it is very stable at various reservoir conditions and has long gelation times. Chromium III are used as cross-linking ions; these cations react with the occasional carboxylate groups along the Polyacrylamide

polymer chain as shown in **Fig.2.6.** (DiGiacomo and Schramm 1983; Sydansk 1989; Vargas-Vasquez et al. 2009)

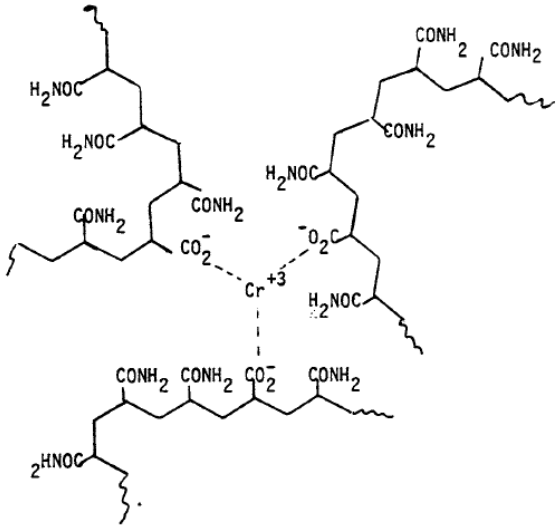

Fig.2.6 – PAM Cross-Linking Through the Occasional Carboxylate Groups

One of the important characteristics of HPAM/Cr(III) Acetate gels is the growth of pre-gel aggregates. The aggregates are soluble molecules formed from numerous HPAM molecules that were present in the HPAM solution. When pre-gel aggregates form and grow during injection, the reservoir rock acts as filter which might block the flow paths and hinder gel propagation.(Vargas-Vasquez et al. 2009)

HPAM / $Cr(OAc)_3$ polymer gels are injected into the formation in two approaches depending on the reservoir conditions and the treatment requirements: pre-formed and in-situ formed gels.(McCool et al. 2009)

The first approach is preparing the cross-linked polymer and allowing it to form the gel prior to injection. This is called “preformed gel” referring to a gel state that does not flow into the matrix of the porous rock. Of course, preformed gel can extrude through fractures. The PAM is dissolved in water and then Cr(III) Acetate is added. The whole mixture is allowed to hydrate and left for a day or more depending on the gelation time and the desired gel state. The advantage of this approach is that it minimizes formation wall damage during gel thrust through fractures. The preformed gel exhibits low intrinsic permeability and very high viscosity. When water or gas is injected after gel placement, preformed gels are typically highly resistant to washout. In the entrance section, the gel shows high flow resistance where the gel structure is partially damaged, followed by steady flow and low resistance values downstream. The limitation is how far pre-formed gels can advance in the fractures.

The second approach is to inject the chemicals directly after mixing before the gelation process is completed. At that stage, the polymer is not cross-linked yet. Before the cross-linking completes, some of the polymer and the cross-linker components might enter the matrix eliminating heterogeneities in the matrix. During injection, the gel is exhibits relatively low flow resistance. Then, the composition is left for some time to form the gel. The composition will start as aggregates until it reaches the state of fully developed cross-linked gel; the gel will then experience higher steady flow resistance.

Unlike the preformed gel, in-situ gels flow resistance increases reaching the front. Preformed gel exhibit higher resistance at the entrance and lower at the front where the gel suffers some degree of breakdown. Gels at reservoir conditions will require longer time for the gel cross-linking process to ensue. Only after the gel reaches the desired condition, CO_2 flood should be set back into action. The gel formed by this approach results in more structured gel than in the preformed gel case where the gel is disturbed by flow. This means higher flow resistance than for the preformed gels. Some researchers recommend this approach for heterogeneous but unfractured rocks.

2.3.2 Gelation Kinetics

Gelation time and gel consistency are the main two issues to be considered by engineers and operators performing gel injection deep into the formation. For instance, the injection time cannot exceed gelation time. The maximum pressure sustainable by gel is function of the gel consistency (measured usually in terms of yield stress). Both parameters are function of temperature, polymer concentration and structure (molecular weight, hydrolysis degree) and cross-linker concentration. Vasquez *et al* (2003) made a comprehensive review of HPAM/Cr(III) Acetate gelation kinetics. The major points will be summarized:(Vargas-Vasquez and Romero-Zerón 2008; Vargas-Vasquez et al. 2009)

- Temperature, pH, solvent salinity, cross-linker concentration, reservoir minerals, polymer hydrolysis, polymer molecular weight, shear environment, and polymer concentration all affect the gelation kinetics.
- Temperature is most influential parameter affecting gelation time.

- HPAM- Cr(III) Acetate gels are kinetically stable rather than thermodynamically stable. Kinetic stability, in contrary to thermodynamic stability, requires energy to convert the reactants to products; that is, it prefers to be in the reactants state.(CHEMWIKI 2010)
- Gel times decrease with increased pH and temperature.
- HPAM/Cr(III) Acetate polymer gel is stable for years at temperatures ranging from 13 ^{o}C to 124 ^{o}C.
- HPAM/Cr(III) Acetate gels can have solutions of pH ranging from 3.3 to 12.5.
- The gelation time is a strong function of polymer concentration and relatively a weak function of cross-linker concentration. That is, gelation time and gel strength increases with increasing polymer concentration and decreasing polymer / cross-linker ratio.
- High salinity brines are practical for HPAM/Cr(III) Acetate. In low salinity solutions, polymer molecules have higher association degree. However, the effects of salts on nonionic polymers are not well understood.
- Some formations have tendency to adsorb PAM. e.g. montmorillonite and quartz. The interactions with the formation must be taken into consideration to avoid failures in designing gel treatments in inaccurate estimation of gelation time and gel strength.

D. Broseta *et al* confirmed that polymer concentration has higher effect on cross-linking kinetics than cross-linker concentration. To slow down gelation in high temperature reservoirs, they suggested using systems with less cross-linker

(Cr(III)Acetate) or less acrylate monomers (by lowering the PAM concentration or hydrolysis degree). It is important to study the temperature profile surrounding the wellbore because the during gel injection, the wellbore wall gets lower in temperature compared to reservoir temperature. Relations can be used to represent gelation time as a function of temperature.(Liu and Seright 2000)

$$t_g = A\,exp(-\Delta H/RT) \quad \text{.....(2.1)}$$

$$t_g(T) = t_g(T_0)exp\left[-\Delta H(1/RT - 1/RT_0)\right] \quad \text{.....(2.2)}$$

Where:

t_g = gelation time, sec.

A = prefactor of Arrhenius law.

ΔH = apparent activation energy, J/mol.

R = gas constant (=8.3144 Joule/K).

T = temperature, °C or °K

T_0 = reference temperature

ΔH (in J/mol) an apparent activation energy that reflects the energy involved in the crosslinking reaction.

2.3.3 Gel Rheology

HPAM/Cr(III) Acetate polymer gels are viscoelastic, that is , their properties are intermediate between those of elastic solids and viscous liquids. For an elastic solid, application of a shear stress, τ_s, causes the solid to deform. Once the stress is removed,

the substance returns back to its original state except when the shear exceeds a certain limit (called yield stress). Generally, the elastic nature dominates in the early times, while the viscous nature becomes more prominent later in time. Also, studies showed that the gel's intrinsic permeability to water decreases with increased polymer concentration.(Vargas-Vasquez et al. 2009)

Jin Liu and Seright studied the difference in gel behavior in rheometers in comparison with gel behavior during gel thrust through fractures.(Liu and Seright 2000)

2.3.4 Gel Performance in Fractures

"Gel syneresis" is used to describe the solvent (water) expulsion from the gel. The primary cause for gel syneresis is the excessive cross-linker concentration in the gel formation. The second main reason for gel syneresis is the effect of temperature. HPAM Cr(III) Acetate gels are not protected against high temperature. At reservoir temperatures higher than 60 ^{o}C(140 ^{o}F) , the gels experience thermal hydrolysis (molecules of water are split apart). This leads to the contraction of the gel due to expulsion of some water from the gel structure. Severe syneresis might reduce the gel volume even up to 90% of the original gel volume. Thus, to prevent gel syneresis, the gel must have a predetermined optimum concentration of Chromium (III) Acetate. Some researchers found that, syneresis begins after 120 hr. for high Chromium Acetate concentration of 16.7 wt.% and polymer concentration of 1 wt.%.(Vargas-Vasquez et al. 2009)

The successful placement of HPAM/Cr(III) Acetate gels requires the knowledge of gelation time and the ultimate gel strength. Oil field operators need the two

parameters to know the time during which the HPAM/Cr(III) Acetate solution is pumpable and the maximum drawdown the gel can sustain. Rheology tests provide accurate gel descriptions, however, these tests lack practicality since they are expensive, time consuming and destructive to the gel network. Another choice is the bottle testing which are practical but provide gel descriptions that lack accuracy. There is no practical test that can provide representative descriptions yet in the oil field industry. The topic is under ongoing research in an attempts to develop practical and accurate characterization of HPAM/Cr(III) Acetate without disrupting the polymer gel network. Till that day, experiments should be conducted to gain better understanding of the HPAM/Cr(III) Acetate reaction and the gelation time.(Vargas-Vasquez et al. 2009)

Seright published a series of papers between 1995 and 2006 investigating the PAM-Cr Carboxylate gels behavior flow through fractured rocks. Most of the work was done using preformed gels.(McCool et al. 2009) In one of the earliest attempts, Seright conducted a series of experiments to study Cr(III)-Acetate-HPAM gels extrusion through fractures and pipes. He supplemented his work with a numerical study to study the optimum placements of preformed gels and water-like gelants. An ideal gel placement, the fracture is plugged far from the wellbore, but remains open near the well. The objective is to reduce the water channeling without affecting the productivity of the well. If the near wellbore is plugged, this will affect the well productivity. See **Fig.2.7.** In vertical fractures that cut multiple zones, gravity should be utilized to place the gel in the lower part of the fracture, reducing water flow from the lower zones while leaving the upper segment open to oil flow. (The placement specifications mentioned earlier are

not necessary for injection wells). The amount of gel that leaks-off from the fracture face is critical to the productivity/injectivity of the well. The distance of gelant leak-off into the formation will be greater for high viscosity gels. During the experiments, Seright found that Cr(III)-Acetate-HPAM exhibited shear-thinning behavior with low flow rates, that is, the gel resistance to flow decreased with increased flow rates. In contrary, at high flow rates, the pressure gradient was almost independent of the injection rate. This was usually observed in fluid injection after placement of preformed gels. In extremely small width fracture, the gel dehydrated during thrust which reduced the rate of propagation. He concluded his work with comparison of the performance of preformed gels vs. water-like viscosity gels. For preformed gels, the degree of gel penetration is insensitive to the fracture length ratio (the length of a less-conductive fracture / length of the most-conductive fracture in the system). For water-like gels, however, the penetration decreased radically with increased fracture length ratio. From that, Seright recommended the use of preformed gels for fracture length ratios below 2. The dehydration behavior can aid in controlling the gel placement by minimizing the degree of gel penetration (the distance of gel penetration into a given fracture pathway / the distance of penetration for the most-conductive fracture pathway between an injector-producer pair).(Seright 1997)

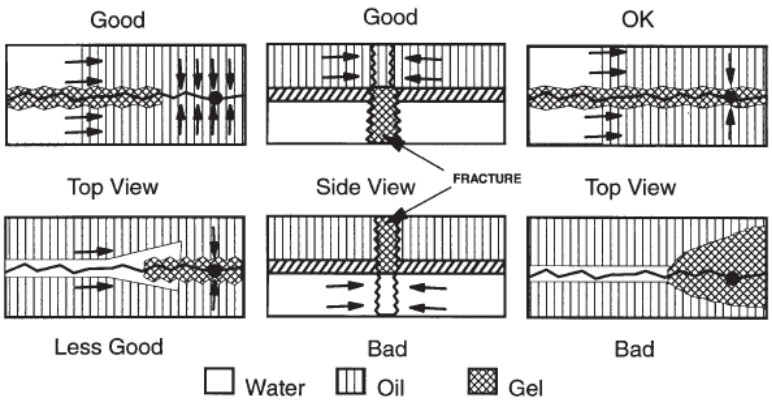

Fig.2.7 – Idealized Placement Locations for Gels in Fractures

To continue his previous work, Seright (Seright 1999a, 1999b, 2001) performed a series of experiments using HPAM-Cr(III) Acetate gels to illustrate gel dehydration during extrusion through fractures. Several issues were addressed: gel extrusion at different pressure gradients, gel behavior in wide fractures, water flow after gel placement and effluent compositions after gel breakthrough. For all of the experiments gel was allowed to age for 24 h, five times the gelation time, before injecting the gel into the cores. The gel was noted to show dehydration when subjected to pressure against the porous medium. The gel concentrates when water leaks-off from the gel, one of the driving forces to that is pressure difference between the fracture and the adjacent porous rock. The work confirmed that gel dehydration becomes more pronounced at lower fracture conductivities. The dehydration resulted in a delay of the gel propagation by a factor between 20 and 40 for fractures conductivities between 1 and 242 darcy-ft. It was also found that during the water injection after gel placement, the fracture was not

completely healed but the fracture conductivity was reduced significantly. The highest practical injection rate should be used to maximize gel penetration through fractures. However, in wide fractures where the dehydration is limited, lower injection rates are desired to form more rigid gels less likely to washout. Furthermore, the effect of molecular weight on the performance of the gel was studied. Gels made with high molecular weight polymers showed two advantages over those made with low molecular weight ones: lower cost and deeper penetration. Simple models were proposed that account for many of the experimental observations. Additionally, Seright proposed equations relating pressure gradient to fracture conductivity, fracture width, and fracture permeability suitable for fractures with widths , wf , between 0.006 and 0.4 inches:

$dp/dl = 0.02(w_f)^{-2}$ .....(2.3)

$dp/dl = 550(K_f\, w_f)^{-2/3}$ .....(2.4)

where:

dp/dl : pressure gradients in psi/ft

w_f : fracture width in inches

k_f: fracture permeability *in* Darcy's

The pressure gradient was found to be insensitive to fluid velocity. Therefore, minimum pressure gradient required for gel extrusion can be represented by the eqs.:

$dp/dl = C_a\, \mu_w / K_f$ .....(2.5)

Where:

Ca : constant

μ_w :viscosity of water in cp

k_f: fracture permeability *in* Darcys

At any point in the fracture, the gel permeability to water, k_{gel}, was empirically related to the average gel composition by the equation:

$$K_{gel} = 0.00011 + 1.0\,(C/C_o)^{-2} \quad \text{.....(2.6)}$$

Where:

K_{gel}: the gel permeability to water, md

C = produced gel concentration, g/m^3

C_o =injected gel concentration, g/m^3

Wilton and Asghari (Wilton and Asghari 2007) conducted experimental studies to investigate two new mechanisms for improved gel placement: Cr (III) Acetate preflush and overload. In order to achieve the condition of gel stability without leak-off, Chromium diffusion into the matrix must get minimized. In the first set of experiments, Berea sandstone slabs were cut and were flooded with Chromium (III) Acetate solution. In the second set of experiments, gelant with higher concentration of Cr (III) Acetate was injected into the fractured system to check whether the diffused portion of Cr (III) Acetate will affect the gel strength or not. Both of the proposed techniques showed great results in opposing the effect of leak-off. It was recommended that at least a pre-flush distance of 1 cm is required for gel performance enhancement. For gel overload, as the Chromium concentration increases, the pressure resistance increased. Also, the residual resistance factor increased (a measure of gel strength and effectiveness) as the Chromium aged. However, the behavior of gel resistance increase was less noticeable at low flow rates. In comparison, the pre-flush approach showed more consistent pressure

response and permeability reduction due to the fact this technique allows better gel/rock contact. In the overload approach, the gel near the fracture face gets lower in Chromium concentration compared to the rest of the gel. Therefore, the gel is expected to be slightly weaker at the rock-gel interface.

Seright published a series of papers between 1995 and 2006 investigating the behavior of PAM – Cr(III) Carboxylate gels flow in fractured systems. Most of his work was conducted using preformed gels owing to the fact that injection time is usually greater than the gelation time. McCool *et al* tried to extend the previous work done on this topic done by Seright and other researchers. They used a 1,031-ft-long tubing was used to simulate the fracture and in-line mixed gels were injected. The main objective of the work was to investigate the shearing effects on the behavior of gels. The others concluded that preformed gels experience great flow resistance at the entrance where the gel is partially damaged. In contrary, in-line (in-situ) gels flow resistance increases with time and produces more structured gel than preformed gels. Additionally, shearing induces syneresis even if the shearing took place after the gel was formed without undergoing syneresis. (McCool et al. 2009)

Sydansk and Southwell made a comprehensive literature review of the application of Chromium cross-linked PAM gels in the oil industry. They addressed the applications in conformance control, sweep improvement, water-shutoff treatments and the gel technology's development. The supplemented the review with presenting and discussing some field applications. They concluded with discussing and suggesting

screening parameters and engineering practices for good candidate reservoirs for conformance control treatment. (Sydansk and Southwell 2000)

2.4 Experimental Studies

Martin and Kovarik have reported some of the earliest experimental investigations (1987 and 1988) of using gels for conformance control for CO_2 EOR applications. They conducted various vial tests, core tests and flow visualization studies using test conditions matching some west Texas reservoirs: 1500 psi, 105 ^{o}F and 1200 psi. They examined various gel systems: Xanthan Gum cross-linked with Pfizer X-LINK 1000, Phenolic gel (FLOPERM 325), Vinyl gel (FLOPERM 465), PAM Cyanagel cross-linked with 100 with Cr (VI) and PAM/OCL. To assess the effectiveness of the gel, the permeability pre-gel was compared to the one after the gel application. All of the tested gels, however, sowed weak performance when CO_2 or water was injected. Some of the gels were good in the beginning but later on, the gel did sustain the long term injection. Relatively, the Phenolic gel (FLOPERM 325) and the Vinyl gel (FLOPERM 465) were more successful in reducing the CO_2 permeability.(Martin and Kovarik 1987; Martin et al. 1988)

M. Raje *et al* reported experimental studies on two novel gel systems: a biopolymer termed KUSP1and SMRF (sulfomethylated resorcinol and formaldehyde). Gels were allowed to form in-situ and CO_2 was injected at supercritical condition. KUSP1 systems were injected into the porous medium in two ways: CO_2 injection induced KUSP1 in-situ gelation and monoethylphthalate ester aided KUSP1 gelation

after more than 100 hr. at 90°F. The first approach was successful in reducing the permeability to about 85% of the original brine permeability. The later showed even better reduction in permeability reaching 98% of the original. Both of the approaches sustained prolonged brine and CO_2 injection. The SMRF system reduced the permeability from about 700 md to water to less than 1md to CO_2 with the reduction sustaining prolonged CO_2 injection. Although the results were attractive in terms of permeability reduction, the economics and the availability of the tested gel systems is of doubt. In their later work, some of authors used more common gels like the ones base on PAM.(Raje et al. 1996)

Asghari was one of researchers using the KUSP1 and SMRF systems back in 1999. (Raje et al. 1996) In 2004, Asghari *et al* (Asghari and Taabbodi 2004) , conducted a series studies on high and low molecular weight Polyacrylamide gels with Chromium (III) as cross-linker. Also, he introduced Sodium Lactate as an additive to the gel system as a gel stability agent and gelation time delayer. For all the experiments they reported the success of the gel application in the form of residual resistance factors (RRF):

$RRF=K_{absw} /K_{rig}$……………………………………………………………………….(2.7)

Where:

K_{absw}: absolute permeability to brine

K_{rig}: relative permeability to certain phase (brine or oil) after gel treatment

The gelation time, the time needed for a reaction between a polymer and a cross linker to increase the viscosity substantially, was also investigated for the three systems. Viscosity was measured as function of time to compare the gel systems. The high

molecular weight PAM gel was more successful than the low weight one. The high molecular weight PAM gel reduced the permeability to water by more than 1500 times without S_{or}, more than 100 times for water with S_{or} and 1500 times for CO_2 with S_{or}. The low molecular weight reduced the brine CO_2 permeability over 100 times. The presence of sodium lactate in the solution delays the gelation time and increases the RRF to water while it decreases it for CO_2. Although sodium lactate showed better control of gelation time, an advantage of the additive is that makes the gel structure unstable resulting in partial washout during brine injection. In 2007, Asghari (Kuzmichonok and Asghari 2007), tried to investigate the phenomenon of disproportionate permeability reduction (DPR) in carbonate rocks. The gel systems showed higher reduction in permeability to water than to oil. The theory of DPR will be discussed in details.

In 2006, Schechter *et al* investigated the effectiveness of Guar gum with a borate cross linker. The performance of the gel was studied using CT imaging to provide visual feeling of the gel leakoff. In addition, the flood success in the presence of gel was compared to continuous gas injection (CGI) case quantitatively in terms of recovery factors (RF). To avoid excessive leakoff, the gel was allowed to set for 16 hours before injection. Injected water was doped with sodium iodide and potassium iodide to aid in CT images visual clarity. The researchers were able to minimize the gel leakoff significantly.(Chakravarthy et al. 2006)

Schechter utilized again the CT imaging to evaluate the performance of gels. This time, the researchers used PAM- Cr(III) Acetate gels with different consideration. The used concentration showed great performance in increasing the ultimate oil recovery

and improving the sweep efficiency in fractured systems. As expected, the higher concentration gels had better stability and less degradation with time. Further investigation of PAM gels performance using CT imaging is needed, especially in balancing the costs of higher concentration gels with their better performances. (D. S. Schechter 2010)

2.5 Disproportionate Permeability Reduction

The application of gels success in water-shutoff in producers and mobility control treatments in injectors aims at reducing the mobility to unwanted fluids such as water and CO_2 without significantly affecting the oil mobility. The gel application has been associated, both in lab studies and in field application, with a phenomenon called "disproportionate permeability reduction" or DPR. Common polymer gels reduce the permeability to water more than that to oil. This is critical to the attainment of the application.

The question arises: how to utilize this and how to maximize the disproportionate permeability reduction? However, the utilization of this phenomenon especially in unprotected hydrocarbon-productive zones requires a good understanding of the phenomenon, why it occurs and what parameters control it. Several researchers, notably Seright, have studied this phenomenon extensively. Some of the key work will be reviewed and discussed under a group of parameters and models. (Seright 1996, 1999c)

2.5.1 Factors Affecting the Performance of DPR

2.5.1.1 Effects of Capillary Forces and Gel Elasticity

It was found that capillary forces and gel elasticity might contribute to the DPR. When oil droplets extrude through the aqueous gel , there are two competing forces acting opposite to each other; a capillary force is trying to open the channel while a gel forced elastic confining force on the oil droplet is trying to close the channel. Thus, the radius to oil droplet flow will be a function of the balance of these two forces. See **Fig.2.8.** In contrast, when water flows through the same channel, there are no capillary forces trying to open the channel.(Seright 1996)

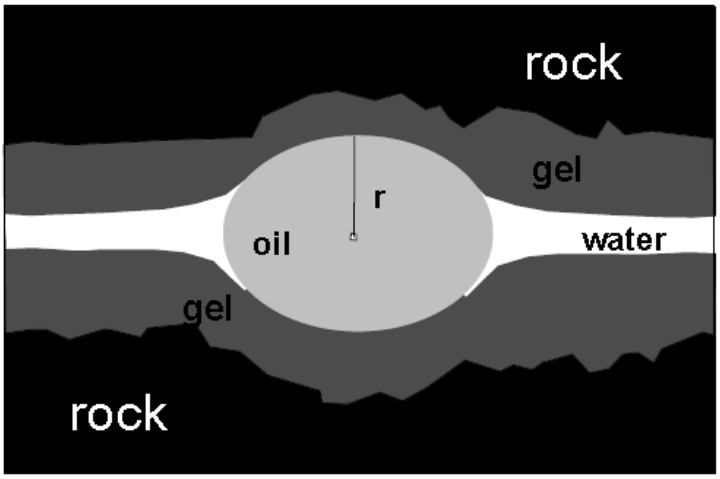

Fig.2.8 – Effect of Capillary Forces and Gel Elasticity on DPR

The capillary pressure across the interface between oil droplets is proportional to the interfacial tension, σ. Thus, using surfactant agents increase the interfacial tension supports the capillary forcing the way through the gel countering the elastic force from the gel. Thus, altering the surface tension affects the radius opening to oil but not to water.

2.5.1.2 Effects of Gel Elasticity

In concept, increasing the gel elasticity results in a larger path around the oil droplet and, thus a higher effective oil permeability. One way to alter that is the introduction of gas as in foam-gel applications; however, this concept was not supported by experimental results. Another theoretical concept is that increasing the system temperature produces more elastic and less rigid gel resulting in more pronounced DPR effect.(Seright 1996)

2.5.1.3 Segregated Oil and Water Pathways

Another possible explanation for DPR is that it might be caused by oil and water has segregated microscopic pathways. The concept is that water based gels follow the water pathways and thus leaving the other pathways open to oil while most of the water pathways get blocked by gel and, thus, reducing permeability water more than that to oil. Similarly, oil based gels thrust through the oil pathways leaving the water pathways intact while blocking the oil pathways.

This theory was tested experimentally and supporting results were observed using oil-based gel reduced the permeability to oil much more than to water. In contrary,

water based gels did not show a similar behavior; injection of oil-based gels at different gel/oil ratios failed to have an impact on the DPR which makes the segregated-pathway theory in doubt. More work is needed to investigate this concept and its effect on disproportionate permeability reduction.(Seright 1996)

2.5.1.4 Effect of Residual Oil Saturation

The theory states that the disproportionate permeability reduction increases with increasing residual nonwetting-phase saturation. Studies supported this, as maintaining higher residual oil saturation in the treated region of an oil zone could significantly reduce the damage to oil productivity.(Seright 1999c)

2.5.1.5 Effects of Rock Permeability and Flow Rate

Experimental results indicate that disproportionate permeability reduction may be more noticeable in high-permeability rock than in low permeability ones. In terms of low rate, it was observed that the reduction in permeability was flow-rate independent for oil, but the reduction in permeability was lower with higher water flow rates. A probable explanation is the hydrophilic, affinity to water, nature of gels.(Seright 1996)

2.5.1.6 Effect of Pressure Drawdown

The studies showed that higher DPR was achieved with increased pressure gradient only up to a certain extent where a permeability reduction disappears. In that case, it is an indication of gel washout by injected fluid. In other words, to a certain extent increasing the pressure gradient reduces the damage to oil productivity without affecting the gel reduction of water permeability.(Seright 1999c)

S. Ganguly *et al* reported studies on the effect of flow rate on DPR by varying the pressure gradient. Also, the role of dehydration on DPR was investigated. The experiments were conducted in Berea sandstone cores with PAM-Cr(III) Acetate gels. (Ganguly et al. 2003) The DPR was expressed in terms of residual resistance factors (RRF) for oil and brine. The residual resistance factors for oil (F_{rro}) and for water (F_{rrw}) are:

$$F_{rro} = \frac{k_o}{k_{og}} \quad \text{.....(2.8)}$$

$$F_{rrw} = \frac{k_w}{k_{wg}} \quad \text{.....(2.9)}$$

Where:

k_{og}: the permeability to oil at endpoint saturations after gel treatment

k_{wg} : the permeability to water at endpoint saturations after gel treatment

k_o: the permeability to oil and water before treatment at interstitial water saturation

k_w : the permeability to water before treatment at residual oil saturation.

The gels experienced dehydration by injection of oil or water, creating a new pore space within the system increased with increasing pressure gradient. The permeabilities to oil and water in increased as pressure gradient increased. It was noted that at lower pressure gradients, permeability to water post gel was reduced much greater than that to oil indicating significant DPR($F_{rro} < F_{rrw}$).Thus, pressure gradient had a greater effect on water permeability than on oil permeability. They concluded that, the effect of pressure gradient on the permeability to oil or water is attributed to the

deformation of the pore structure. Therefore, two reasons cause the larger DPR values at lower pressure gradients: i) the new pore space caused by dehydration has relatively large oil saturations ii) the new pore space is water wet.

2.5.1.7 Effect of Cross-Linkers

K. Ashgari *et al* studied two different cross-linkers with PAM gels and their effect on DPR. The effect of residual oil saturation was also studied by performing experiments with and without residual oil present prior to gel placement. The gels consisted of 7500 ppm of high molecular weight PAM and 300 ppm of one of the two cross-linkers Chromium (III)-Acetate or Chromium (III)-chloride. Both of the systems showed the behavior DPR with and without the presence of S_{or}. However, the performance of Cr(III)-Cl was weaker than its competitor. Thus, the Cr(III)-Ac is preferred in that manner. (Kuzmichonok et al. 2007)

2.5.2 Descriptive Models

The nature of DPR and the ambiguity of the mechanisms of its occurrence urged many researchers to propose descriptive models. Zaitoun *et al*., Nilsson *et al*. and Liang made notable efforts presenting and discussing explanations based on "wall-effect" , "gel-droplet" and "combined-effect" models. Disproportionate permeability reduction can be explained by a "wall-effect" model if the gelant is prepared from the wetting phase and by a "gel-droplet" model if the gelant is prepared from the nonwetting phase. The combined model predicts that DPR increases as the residual nonwetting-phase

saturation increases. (Liang and Seright 2000; Nilsson et al. 1998; Seright 1996; Zaitoun et al. 1998)

2.5.2.1 "Wall-Effect" Model

In 1998 Zaitoun *et al*. proposed suggested their model attributing the DPR to the pore walls. In a strongly water-wet rock, the presence of oil droplet at the center of the pore will reduce the effective width of the channel open to water flow reducing the permeability to water greatly. If oil is to be flooded, however, the restriction does not exist. See **Figure 2.9.** On the other hand, in an oil wet rock, the gel could anchor on the small water-wet portions of the rock surface then spreading over the predominant oil-wet surface shifting the wettability towards water-wet. Then, even in the oil-wet core, the permeability to water will be reduced to a greater extent more than that to oil See **Fig.2.10.** .(Zaitoun et al. 1998)

Zaitoun *et al*. observations were reported for a silane-treated oil-wet sandstone core with adsorbed uncrosslinked polymer gel. Based on that, they the adsorbed polymer layer was responsible for the DPR in both the oil- and water-wet cores. However, in most of the applications, the used polymers are cross-linked gels. Thus, the application of the model to that case is to be investigated. If the model is correct, the DPR should vanish in strongly oil-wet polyethylene cores with no water-wet surface for the polymer molecules to anchor on.(Zaitoun et al. 1998)

Liang and Seright conducted a series of studies to put this model into test. However, for an oil-wet polyethylene core, the water-based gel reduced the permeability to water much more than that to oil in contradiction with the model. Also, the model

could not explain why an oil-based gel reduces the permeability to oil more than that to water in a strongly water-wet rock. Obviously, the oil-based gel will not adhere onto the water-wet surface. In conclusion, the "wall effect" model explains DPR only when the gelant matches the wetting phase.(Liang and Seright 2000)

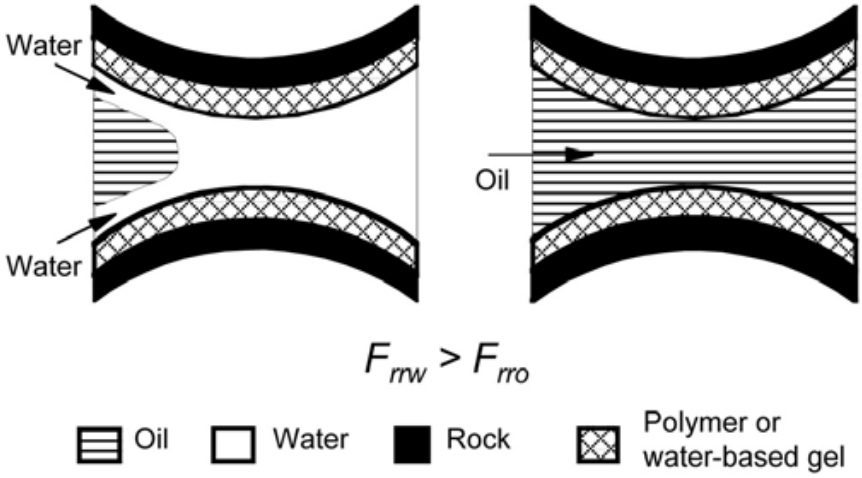

Fig.2.9 – Wall-Effect Model12: Water-Based Gel with Water-Wet Rock

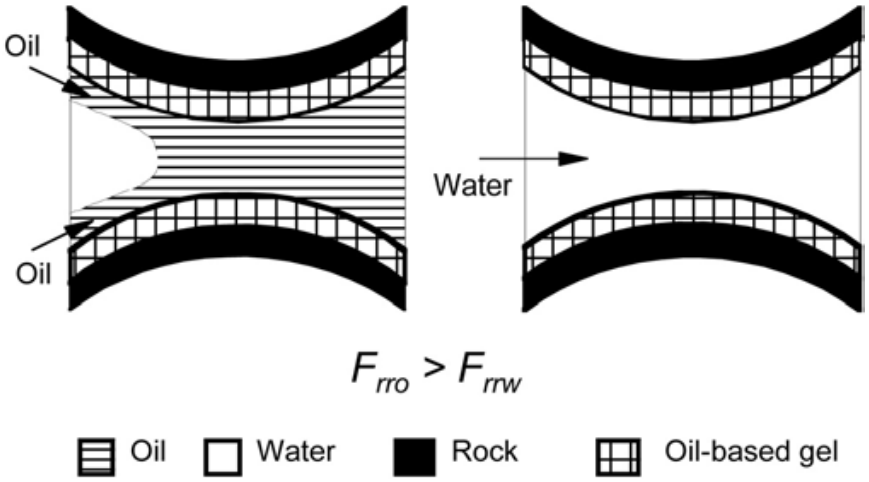

Fig.2.10 – Wall-Effect Model12: Oil-Based Gel with Oil-Wet Rock

2.5.2.2 "Gel-Droplet" Model

Nilsson *et al*. proposed that the mechanism for the DPR is because water and oil flow more easily in some channels than in others. To highlight the difference between the "wall-effect" model and this one, it is important to notice that in "gel-droplet" model, the gel does not adhere to the surface. Instead, the gel flows in the center and it forms in the center causing more restriction to flow of the wetting phase than to the nonwetting phase. (Nilsson et al. 1998)

In an oil-wet core, water flow is restricted only by the thin film of oil on the pore wall while if oil flows in the same pore, the flow is restricted by a residual water droplet. See **Fig.2.11.** This is why the endpoint permeability is always higher for the non-wetting phase than that of the wetting phase. The water-based gel flows in the center of the pore

and when the gel forms it replaces the residual water droplet. **Fig.2.11** shows that if the gel droplet is at the same size of the previous water droplet, the presence of the gel droplet reduces the volume fraction available to water flow. Thus, the gel will reduce the permeability to water without significantly harming the permeability to oil. Of course, if the gel droplet is of different size from the water droplet, the DPR will be different. When the gel droplet is larger, it will reduce the permeability to oil and when it is lower, it will open more flow to water than the residual water drop. Similarly, if the rock is-water wet and the gel is oil-based, the reduction in permeability will be more to oil than to water. See **Fig.2.12.**

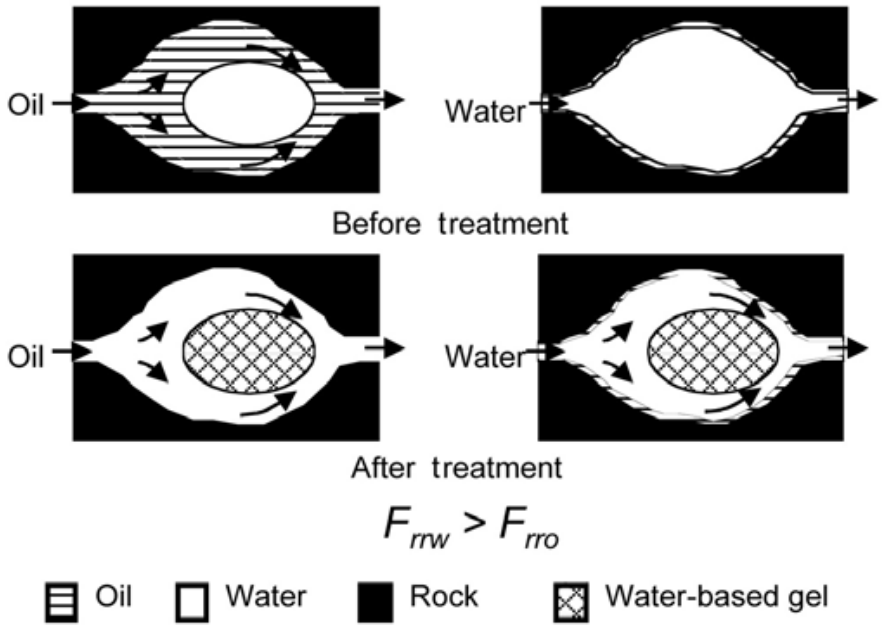

Fig.2.11 – Gel-Droplet Model: Water-Based Gel with Oil-Wet Rock

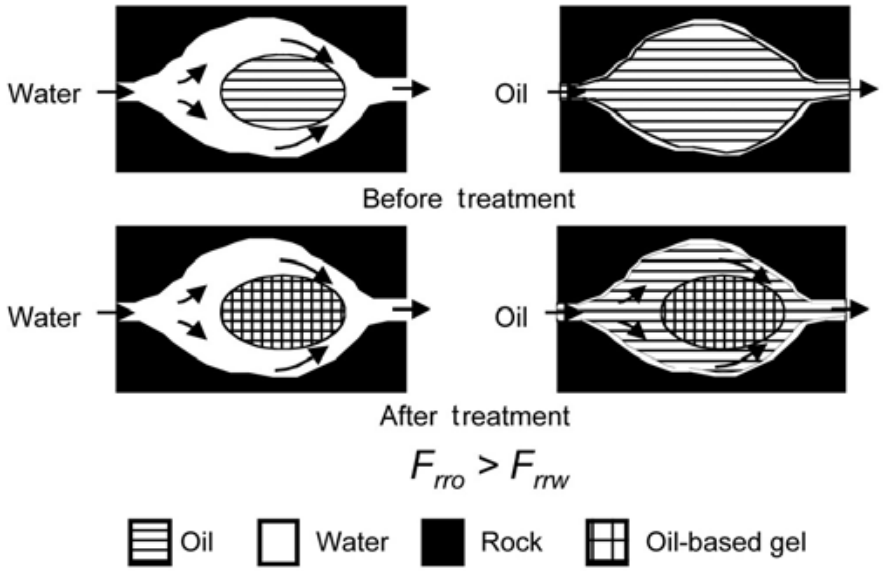

Fig.2.12 – Gel-Droplet Model: Oil-Based Gel with Water-Wet Rock

According to the model, in a water-wet system, a strong water-based gel could completely block the pores by capturing the residual oil droplets. The authors argued that even with syneresis, the gel droplet will still occupy a significant fraction of the pore causing significant permeability reduction to both water and oil. However, in a water-wet system this model could not explain why a water-based gel reduced the permeability to water much more than that to oil. Similarly, it cannot explain why an oil-based gel reduced the permeability to oil more than that to water in an oil-wet system.

2.5.2.3 The Combined Model

In review, the DPR can be explained using the wall-effect model only if the gelant is prepared from or matches the wetting phase. On the other hand, the gel-droplet

model explains the disproportionate permeability reduction when the gelant is prepared from or the nonwetting phase. In a combined model, the individual models apply for the fitting circumstances. Particularly, the wall-effect model applies for water-based gels in water-wet cores and for oil- based gels in oil-wet cores. The droplet model applies for water-based gels in oil-wet cores and for oil-based gels in water-wet cores. In a water-wet core, the disproportionate permeability reduction increases with increased residual oil saturation. (Liang and Seright 2000)

2.5.2.4 Modified "Wall-Effect" Model

The wall-effect model proposed by Zaitoun *et al*. could be modified so that it satisfactory explains the observations. In a modified wall-effect model, in a strongly water-wet system, the adsorbed layer on the pore walls after treatment can either be a polymer or a water-based gel. See **Fig.2.13.** The presence of residual oil droplets at the center of the pores in a strongly water-wet system will reduce the water flow during a waterflood. Therefore, for a given thickness of a gel layer, the permeability reduction for water during water flooding is greater than for oil during oilflooding. Similarly, for a strongly oil-wet system, oil-based gel could form a gel layer on the pore walls. See **Fig.2.14.**(Liang and Seright 2000)

In the presence of residual water droplets at the center of the pores, this reduces the effective width of the oil flow. Therefore, for a given thickness of layer of the oil-based gel, the reduction in permeability for oil during oilflooding is greater than that for water during waterflooding. That is why in an oil-wet system an oil-based gel reduced the permeability to oil more than that to water.

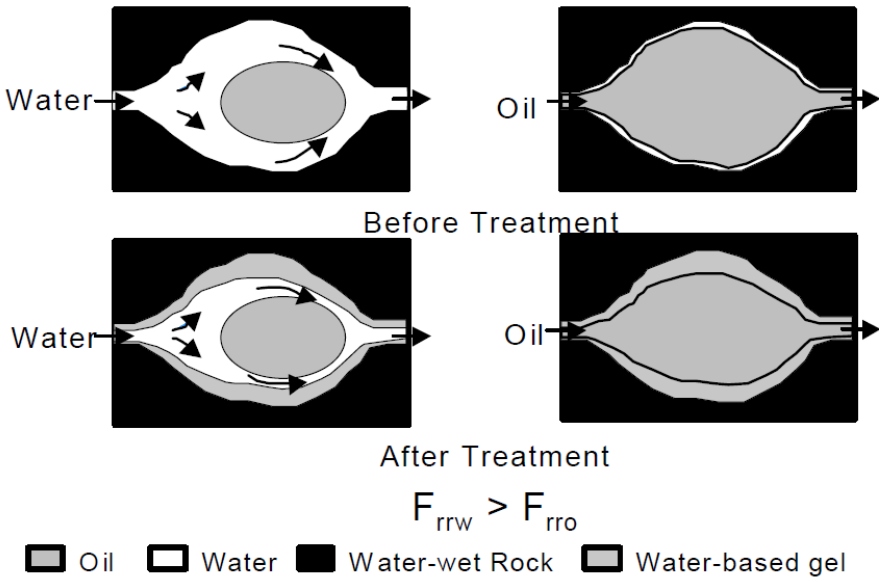

Fig.2.13 – Modified Wall-Effect Model For Water-wet Rock

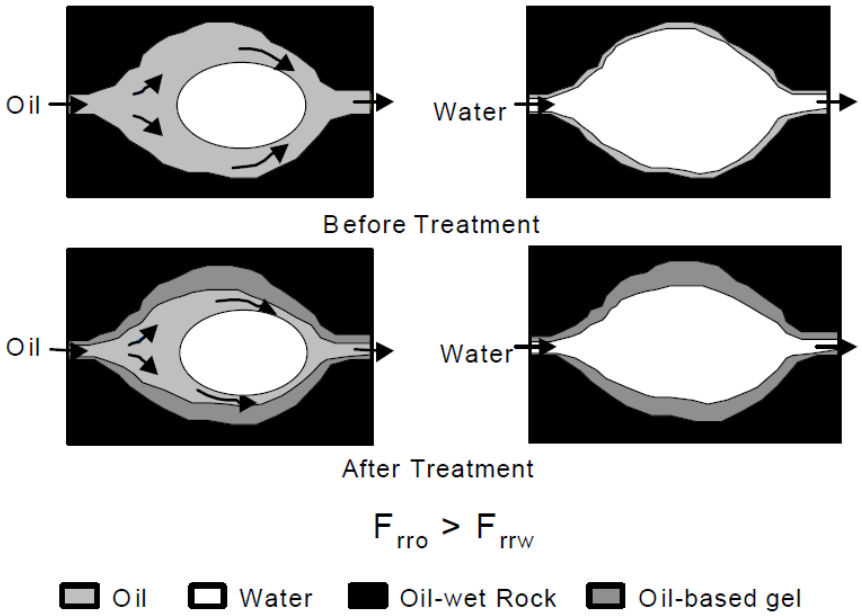

Fig.2.14 – Modified Wall-Effect Model For Oil-wet Core

R. S. Seright *et al* ran a series of studies using X-ray CT imaging to investigate the phenomenon of DPR in strongly water-wet Berea sandstone and in an oil-wet polyethylene core of similar distributions of pore sizes. Three-dimensional images were constructed to study the oil and water imbibition and drainage pathways and fluid distributions before and after gel placement. See **Fig.2.15 and 2.16.** The results suggested that in Berea sandstone permeability to water was low because water must flow through gel itself while oil flowing and pressing the gel forced pathways by dehydration leading to high permeability to oil. In Berea cores, gel trapped an effective amount of oil that became immobile during water flow making the water pathways only through the narrow films or through the gel itself. In contrary, oil pathways were open during oil flow. In the polyethylene core, no significant DPR was caused by oil trapping. Instead, oil was flowing through the narrow films and pathways. After the gel was placed in Berea cores, the pores At S_{or} had higher oil saturations than at S_{or} before gel placement. This is an indication of the oil trapping restricting the flow to water. The authors suggested that a reduction in the gel volume was caused by a dehydration mechanism rather than a gel ripping mechanism. The last finding contradicts with what other researchers suggested. (Seright et al. 2001; Seright et al. 2006)

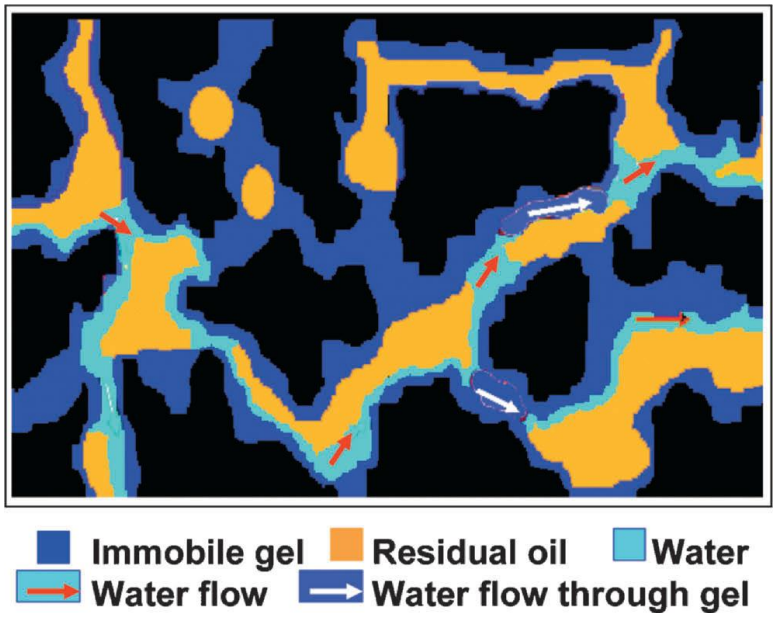

Fig.2.15 – Water Flow Following Oil Injection after Gel Placement in Water-Wet Berea

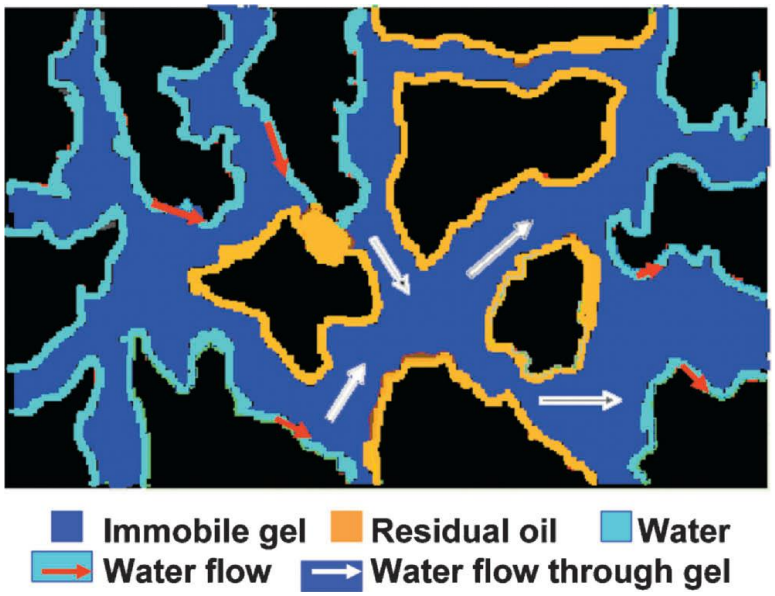

Fig.2.16 – Water Flow Following Oil Injection after Gel Placement In Oil-Wet Polyethylene

2.5.3 "Clean Up" Behavior

Because gel reduce permeability to water more than that to oil , in field application, an unfavorable behavior occurs with high mobility ratio in oil zones when wells are put back to production post gel treatments. The permeability values need some time to stabilize. This behavior is termed "cleanup time".

Seright studied this behavior and its change with various cycles of oil and water injection. See **Fig.2.17.** Two gel systems were utilized a pore-filling Cr(III)-Acetate-HPAM gel and for a weak adsorbing polymer. Mobility ratio model was used to estimate the cleanup time. It was found that the cleanup time was similar for radial versus linear flow. The time increased, of course, with increased distance of gel penetration while it decreased with pressure drawdown increase. It will take a longer time to achieve the cleanup with higher values of k_w at S_{or} , but it was insensitive to the values of *ko* at S_{wr}. Although k_o at S_{wr} *had* no effect on the cleanup time, it affected how much of the original was recovered. In comparison of the two gels, after treatment with Cr(III)-Acetate-HPAM gel, water permeability stabilized for over six months while for adsorbed polymer, permeability to water increased steadily over time due to erosion. (Seright 2006a)

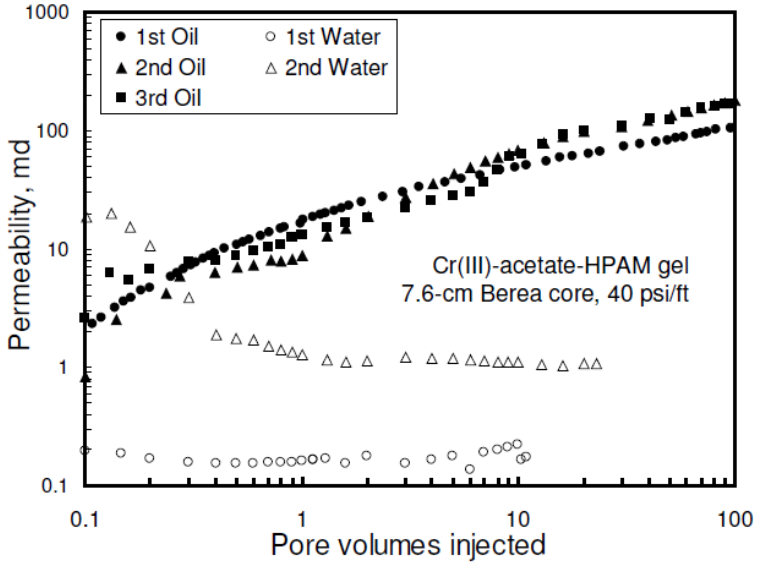

Fig.2.17 – Permeability to Oil and Water after Gel Placement in a Berea Core

Gel treatments have always been considered for gel treatments of fracture or channel. R.S. Seright took an extra step investigating the utilization of disproportionate permeability reduction (DPR) to reduce excess water production from unfractured wells (i.e., radial flow into porous rock).He focused on estimating the time needed for "clean-up". Various challenges, however, limit the application of DPR. Most notably is the variable performance. When applied in field, the performance varies greatly due to changes in in reservoir conditions. Secondly, the F_{rro}(residual resistance factor to oil) must be less than 2 for radial flow application. **Fig.2.18** shows the equivalent resistance that fluid must flow to cross the gel and enter the fracture. As shown in the figure, productivity loss in radial flow is much more sensitive to residual resistance factors (RRF) than to radius of gel penetration. The authors claim that they were successful in

finding different gel formulation where when gels can be dehydrated with time, water residual resistance factors reached greater than 2,000 and to oil of 2 or less. The previous conclusion enlightens the road towards a probable application in unfractured production wells. (Seright 2006b, 2009)

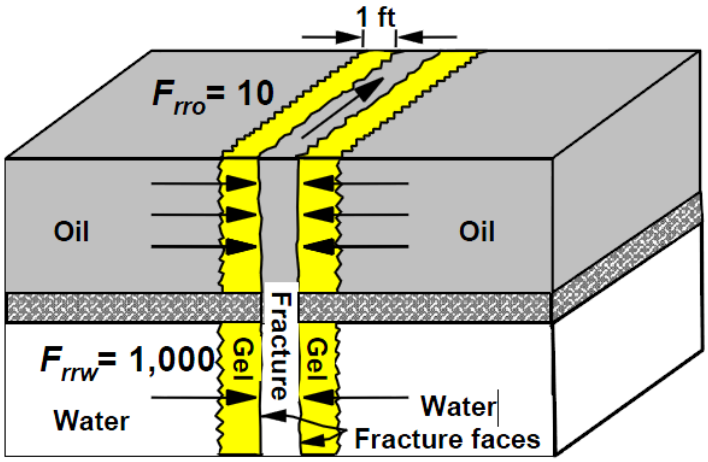

Fig.2.18 – Gel Restricting Water Entry into a Fracture

A model was suggested to estimate permeability to water post gel placement.

k_{gel} = 0.125 / C……..….(2.10)

Where:

k_{gel}: permeability of the gel to water k_{gel} in md

C: polymer concentration in %

Another model was proposed for cleanup time estimation assuming that the recovery of oil productivity is dominated by the intrinsic permeability of the gel to water:

$k_o = k_w + B\,(PV)^n$……..…….(2.11)

Where:

PV = pore volumes of fluid injected

n = pore volume exponent

B = fitting parameter

2.6 Field Cases

The increased oil production and decreased water production made the gel treatments of high attractiveness. Economic success rates for injection well treatments showed high are around 85%. However, the key towards a successful application involves the consideration of choosing the right injection wells, right chemicals and balancing the sizing economically and technically. The chemical concentration of the gel, for instance, must provide both complete plugging of channels and having appropriate gelation time. (Smith 1999)

The evaluation process should start with a qualitative decision whether the field is good candidate for gel treatment or not. Then, the design should get more specific investigating what type of gel to be used, what concentrations of gels and cross-linkers, how fast should the gel form and how much gel should be injected to achieve economical feasible successful treatment.

Determining the proper gel treatment size is difficulty. Injection well treatments, as in CO_2 EOR applications, are usually easier and more successful compared to their counterpart's production wells. It is to be emphasized also that injection wells require higher volumes because the objective is not only to plug the channels around the wellbore but to extend that deep in the targeted zones to achieve the successful sweep. If the treatment is not large enough, the injected water or CO_2 will move around the gel and flow back in the channel. However, the economics plays an opposite role; while gel treatments of small channels are economic; this becomes a more difficult issue as the channels size increase. The question remains: what is the minimum gel volume that will be effective? Different strategies have been suggested to answer this question; the strategies fall under two different approaches: volume strategies and distance strategies. The distance strategy suggests that the gel treatment should advance a certain distance away from the well to a distance reaching 50 ft. It is suggested that this approach is used when the vertical crossflow is limited. On the other hand, the size strategy suggests the required volume is that estimated to fill a portion of the channel volume from injector to producer. The volume is estimated as a percent of moveable pore volume in the channel (MPV).Different approaches have been suggested to quantify the channel volume.(Smith 1999)

$$MPV = 1 - S_{or} - S_{wi} \quad \text{.....(2.12)}$$

Where:

MPV:moveable pore volume

S_{or}:residual oil saturation

S_{wi}:irreducible water saturation

In addition to the qualitative issues associated with the gels, further risk considerations are required to ensure success. Common risk factors include: plugging the injection well and decreased oil production as result of decreased water injection. Also, the gel design should be done appropriately to avoid polymer production which might be of severe impact on the separation process.

Woods *et al* presented one of the earliest successful gel treatments for Lick Creek Field in Arkansas that 17 API oil. The successful application was preceded by two failed attempts. The first attempt was to utilize alternating CO_2 and water (WAG) was did not solve the channeling problem. The second pilot was flooding anionic polyacrylamide, but it was successful for only a few cycles. The successful treatment was composed of single stage injection of a low viscosity monomer solution with organic cross-linker. The gel was allowed to form in-situ. The treatment was performed on two wells that showed good results in improving the sweep efficiency resulting in higher oil production and higher injection pressure. The treatment paid out in 1 ½ months. (Woods et al. 1986)

Hild and Wackowski reported the results of PAM-Cr(III) Acetate gel treatments in improving sweep of the CO_2 flood at Rangely Weber Sand Unit located in northwestern Colorado. An amount of 10,000 bbl of gel was deployed for 44 injection wells treatment. The project showed encouraging results resulting in an incremental oil recovery of 21 bbls/day. Water production was reduced by 98 bbls/day and incremental gas was slightly higher at 98 mcfpd. The low gas increase was attributed to an improvement in reservoir gas retention because CO_2 injection was increased

significantly. The economic analysis of the project showed a payout period of 8 months and a rate of return of 365%.(Hild and Wackowski 1999)

Karaoguz *et al* and Topguder reported several field applications of Cr(III) Acetate cross-linked PAM gels in Bati Raman field for water shutoff and conformance improvement. Bati Raman field in southeastern Turkey is a naturally fractured carbonate reservoir with heavy-oil (12-15 API).The field suffered from the heterogeneities and the unfavorable mobility ratios between injected CO_2 and the heavy oil. Injected volumes for injection wells were 6,500 to 11,000 bbls/well. The economic studies indicated that relatively large volumes of gels are required, thus, the gel was designed to be a flowing gel (low concentration of moderately high molecular weight polymer).The wells showed increase in injection pressure indicating the reduction in the injectivity. In one of the cases, an offset producer experienced fluid level changes consistent with reduction in pressure transmission lowering with time. This behavior is an evidence of the success in plugging the fractures during the treatment. The improved sweep efficiency resulted in 12% incremental oil recovery which paid out in 12 months. (Karaoguz et al. 2007; Topguder 2010)

CHAPTER III

EXPERIMENTAL SETUP AND CONDITIONS

The experimental setup consists of the coreflood system and the visualization system i.e. the CT scanner. The instrumental setup is briefly discussed and details are presented about the used chemicals and core samples.

3.1 Instruments Setup

Throughout the experiments, CO_2 will be flooded at supercritical conditions (89 ^{o}F and 1070 psi). Also, a minimum miscibility pressure value is to be attained to initiate the state of dynamic miscibility. Thus, control over the pressure and temperature is needed. The tubings and fittings are made of stainless steel provided by Swagelok® designed to withstand high pressure and temperature. **Fig 3.1** shows a schematic of the experimental coreflood setup.

In summary, the experimental setup is composed of the following components: the injection system, the core holder, the production system, the temperature control system and the CT scanner.

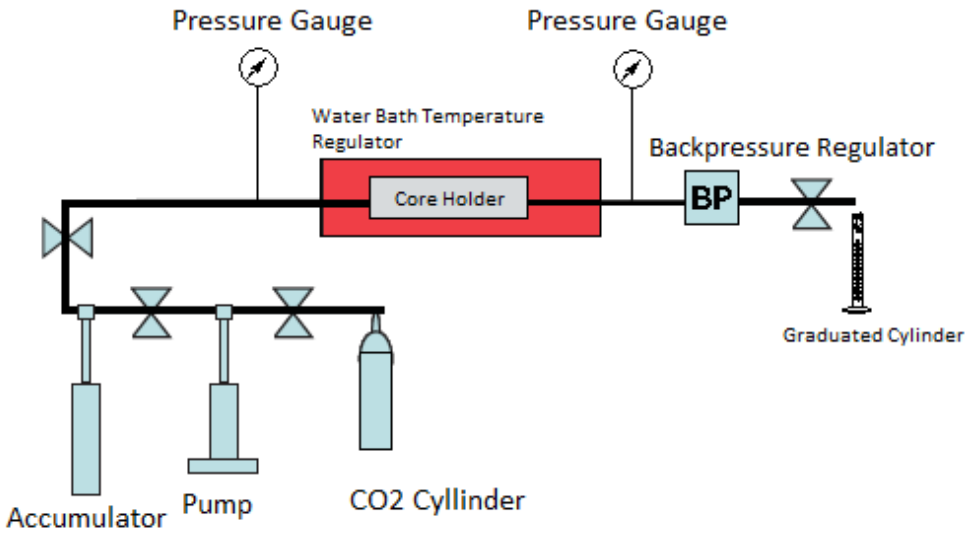

Fig.3.1 – Schematic of Instrument Setup

3.1.1 Injection System

The injection system consists of an accumulator and a pump. The positive displacement ISCO® 5000 D syringe pump is shown in **Fig 3.2.** The pimp is used the transfer fluids at the desired rate or pressure. The accumulator, shown in **Fig.3.3**, is used to pressurize the CO_2 and for brine, oil or gel during floods. The pump is equipped with a programmable controller to run either at constant flow rate or a constant pressure. The pump injects water at the bottom of the accumulator pushing the floating piston up resulting in pressurizing the CO_2 or pushing the liquids out of the accumulator from an

outlet at the top of the accumulator. The accumulator outlet is connected to the coreflood cell through tubing.

Fig.3.2 – ISCO® Pump

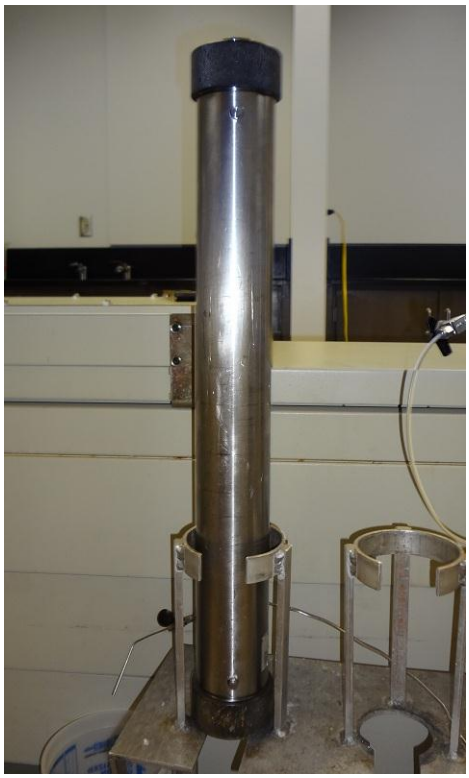

Fig.3.3 – Fluids Accumulator

3.1.2 Coreflood Cell

The coreflood cell is a TEMCO® aluminum core-holder. See **Fig.3.4.** The coreholder has three ports: one connected to the accumulator, the second is connected the production line and the third serves to provide overburden pressure. The inlet and outlet ports are in contact with the core while the third one is isolated from the core by a sleeve. A Grainger® hydraulic hand pump injects hydraulic fluid around the sleeve into

the sleeve – inner wall annulus to create overburden pressure. The sleeve is made of Viton® to withstand high pressure. See **Fig.3.5.**

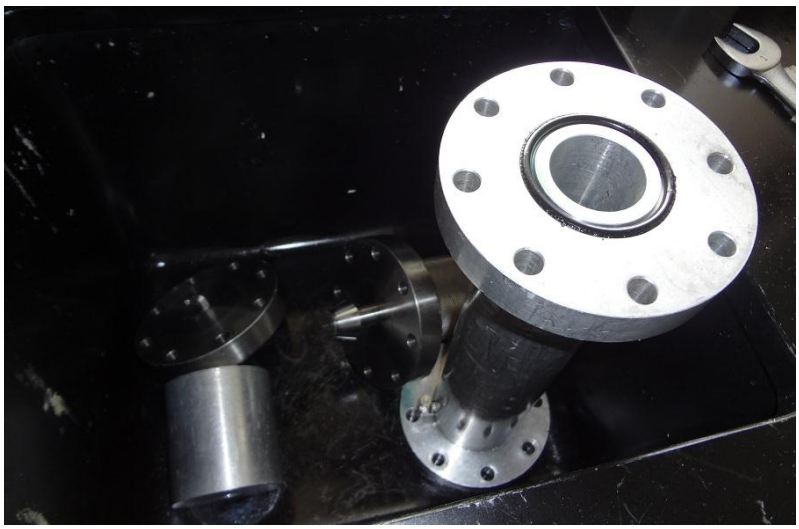

Fig.3.4 – TEMCO® Coreflood Cell

Fig.3.5 – Grainger® Hydraulic Hand Pump

3.1.3 Production System

The outlet of the coreholder is connected to a backpressure regulator to ensure that the pressure inside the core holder is higher than the minimum pressure required for both miscibility and supercritical condition. The backpressure regulator is followed by a Swagelok® needle valve that is closed during saturation process.

3.1.4 Temperature Control System

The core holder is placed in water bath cylinder with inlet and outlet ports. A water heater warms the water up to a desired predetermined temperature. Connecting the two, a water pump withdraws the warm water from the heater reservoir and injects it into the bath cylinder while the outlet port drains the water inside the cylinder. The warm water is circulated for enough time before CO_2 injection to ensure establishing the heat inside the coreholder.

3.1.5 X-Ray CT Scanner

The water bath cylinder, including the core holder, is placed under the CT scanning area. The CT is scanner is a fourth generation Universal systems HD 350-E system. See **Fig.3.6.** The scanner obtains cross-sectional images starting at the injection end of the core moving at a constant interval towards the production end. Images are then recombined using ImageJ® software for both qualitative and quantitative analysis.

The images show fluids distribution inside the core, fluid saturations, porosity and can also be reconstructed for flow visualization.

Fig.3.6 – HD 350-E CT Scanner

3.1.6 Data Acquisition System

Two Omega® digital pressure gauges are fixed one at the coreholder inlet and one at the outlet. The pressure can be read real time to monitor the pressure drop across the system. The pressure is also monitored to avoid pressure in the system approaching that of the confining pressure.

3.2 Core Samples

All the core samples used for the studies are medium to high permeability Indiana limestone provided by Kocurek® Industries, Inc. See **Fig.3.7.** The cores are cut in 1 inch diameter and 5 inch length. The average brine permeability is around 70 md.

Fig.3.7 – Indiana Limestone Core

3.3 Chemicals

The HPAM gel and the Cr(III) Acetate crosslinker were purchased from Sigma-Aldrich®. In addition, Sodium Lactate was used for some experiments and was provided by the same source. The oil used was refined Soltrol oil from Chevron Phillips.

A common gel system is the Xanthan Gum/trivalent chrome; xanthan belongs to the family of Polysaccharides. The system has been applied in field applications for about three decades. Xanthan gels are typically formed by the ionic bonding of the trivalent Chrome molecules on the Xanthan molecules. See **Fig.3.8.** The environmental issues cost and availability considerations make this gel system amongst the most popular ones. (Avery et al. 1986)

A characteristic of this gel system is the shear thinning behavior; when subjected to shear, the gel gets lower in viscosity. Therefore, Xanthan gels are typically formed in on the surface and injected into the desired formation. Another characteristic of the gel is that it might either swell or synerese. Swelling occurs when the gel contacts with excess brine over a long period of time; swelling can lower the gel strength and cause the gel to breakdown. Syneresis, however, describes the separation of the solvent from the gel as gel shrinks in size; this can cause the gel to loose volume and possibly leaving more room for flow of other fluids. The previous two characteristics can cause the gel to gain/loose volume up to 70% of the original size.(Avery et al. 1986; Gales et al. 1994)

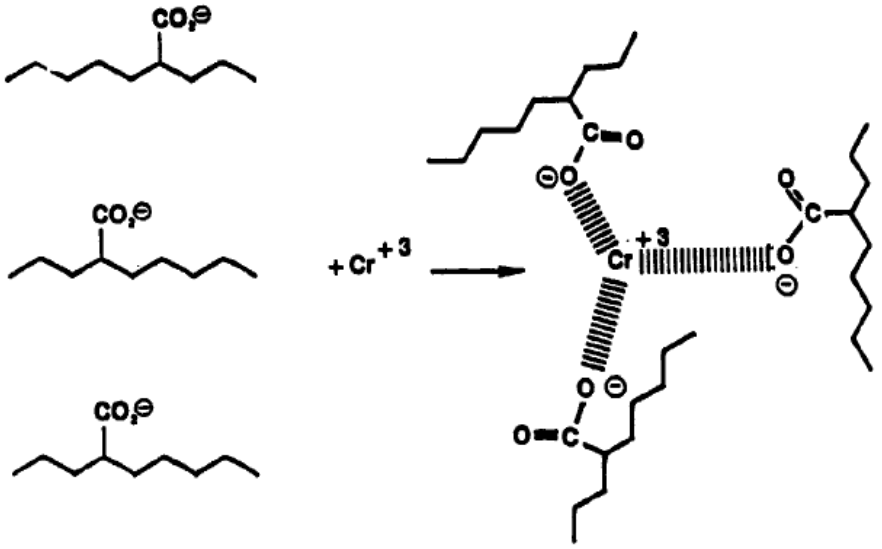

Fig.3.8 – Xanthan/Cr (III) Ionic Bonding

Dopants were added to enhance the CT images contrasts between different phases. For that, 1-iodohexadecane was added to the oil phase in 10% by weight. For the gel, 6% by weight of KI was added to the aqueous solution. Both of the chemicals were purchased from Sigma-Aldrich®.

3.4 CT Data Processing

To evaluate the success of the CO_2 floods, two quantitative parameters can be obtained using CT imaging: recovery factor and saturation distribution. During floods the CT values inside the core change with time but two CT numbers remain unchanged independent of the reflected X-ray energy and can be fixed and used in calculations of

porosity and phase saturation. The Hounsfield number, N_{ct}, is a dimensionless quantity. **Table 3.1** lists CT numbers for some common materials. (F. Mees 2003)

Table 3.1 – CT Number of Common Materials(Jarrell 2002)

Material	CT	Density(kg/m^3)
Air	-1000	1.82
Water	0	1000
Quartz	1589	2190
Berea Sandstone	1608	2120
Indiana Limestone	1531	2220
Alumina	2478	2820

For vacuum or air:

N_{ct} =-1000

And for water:

N_{ct} =0

Then, porosity is calculated as:

$$\emptyset = \frac{CT_{wr} - CT_{Dry}}{CT_{Water} - CT_{Air}} \quad \text{.....(3.1)}$$

For a rock saturated with oil and water, the water and CO_2 saturation are calculated as:

$$S_w = \frac{CT_X - CT_{or}}{CT_{wr} - CT_{or}} \quad \text{.....(3.2)}$$

And

$$S_{CO2} = \frac{CT_X - CT_{or}}{CT_{CO2Sat} - CT_{or}} \quad \text{.....(3.3)}$$

CT_{or} can be obtained by linear interpolation between dry core and water saturated core as:

$$CT_{or} = CT_{Dry} + \frac{CT_{Oil} - CT_{Air}}{CT_{Water} - CT_{Air}}(CT_{wr} - CT_{Dry}) \quad \text{.....(3.4)}$$

Where:

CT_{wr}: CT number of 100% water saturated core inside the coreholder

CT_{or}: CT number of 100% oil saturated core inside the coreholder

CT_{CO2Sat}: CT number of 100% CO_2 saturated core inside the coreholder

CT_{Dry}: CT number of dry core inside the coreholder

CT_{Water}: CT number of water =0

CT_{Air}: CT number of water =-1000

CT_{Oil}: CT number of Oil

CT_{Mat}: CT number of the matrix content

3.5 Experimental Procedure

A standardized procedure and conditions are applied to all experiments. The experimental temperature is 120 ^{o}F(49 ^{o}C) and the overburden pressure is 2,000 psig(13.79 M Pa).The key experimental steps are as follows:

1. Core is heated overnight in an oven to remove all residual saturation liquids.
2. Weight of the dry core is measured. Then, the core is CT scanned at a confining pressure to determine CT_{dry}.

3. The core is saturated with brine in the vacuum chamber until complete water saturation is ensured.
4. The wet core is weighted and CT scanned at a confining pressure to determine CT_{wr}.
5. The core is flooded with water at steady state flow to measure the base water permeability using Darcy law.
6. The core is heated again and evacuated.
7. The dry core is placed in the coreholder and flooded with CO_2 until full saturation is reached.
8. The core CT scanned under 100% CO_2 saturation to get $CT_{100\%CO2}$.
9. The core is flooded with oil until the saturation is ensured.
10. The backpressure regulator at the outlet is fully closed to allow the pressure to build up in the core holder. (Overburden pressure is at least 300 psi higher than the pressure inside the rubber sleeve).
11. The oil injection is stopped once the desired pressure is reached.
12. The oil saturated core is scanned to get $CT_{or.}$
13. Gels are injected into the fracture and allowed to age for the desired time. The healed core is CT scanned.
14. CO_2 is injected at a pressure higher than that in the coreholder.
15. The core is CT scanned at different injected volumes and times. Pressure, injected volume and recovery data are recorded.

- For a fractured core: step 2 is repeated after fracturing the core.
- Gels are prepared and allowed to reach the desired gelation status (preformed or in-situ).
- After the gel is injected, it is left for the desired time before proceeding with the experiment. If the gel is to form in-situ, it's left in the coreholder for 24 hrs.
- For a fractured core: the porosity calculated using CT_{dry} and CT_{wr} will correspond to the (matrix +fracture) porosity and not the matrix porosity alone.
- For VWAG experiments, step 12 will be followed by three cycles with each of them scanned: viscosified water – CO_2 Injection – viscosified water.

CHAPTER IV

EXPERIMENTAL RESULTS AND DISCUSSION

The laboratory studies from the coreflood experiments are discussed in the following sections. The core flood experiments are preceded by basic rock, oil, water and CO_2 properties used in the studies under the specified conditions. The CT images will be utilized both for real-time quantitative and qualitative evaluation of the used core samples and the coreflood results and findings. The technique will follow numerical quantitative analysis with average CT number taken over every slice of image; qualitative visualization will utilize coloring the CT images as a function of CT number distribution throughout the slices and the core.

The experiments are divided into three sets : the first set discusses the ideal condition as observed in unfractured Limestone core with CGI (continuous gas injection) in comparison with a two experiments with fractured Limestone cores :one with CGI and the other with water as the injection fluid. The latter two attempt to answer the question whether CGI or WF (waterflood) recover more in untreated fractured reservoirs. The second set introduces application of cross-linked gels treatments to fractured cores prior to CO_2 CGI injections. The third set discusses the feasibility of viscosified waters as displacing fluid chased/ or not with CGI of CO_2 in fractured cores.

Most of the experiments will follow the standard procedure stated earlier; however, some specifics will be different from one experiment to another that would be stated in each individual experiment discussion section.

4.1 Rock Samples Evaluation

All of the cores used in the studies are Indiana Limestone cut into 1" diameter x 5" length. The rocks are moderate in heterogeneity with slight variations from one core to another. The rocks have brine permeability of 70-80 md. See **Fig.4.1.** To evaluate the recovery data properly, the cores are tested for porosity distribution. The goal is to quantify the correct pore volume of each core and verify the viability of using CT imaging for quantitative analysis of porosity and fluids distribution during corefloods. The CT obtained porosity is compared with weight difference obtained porosity. In other words, porosity will be obtained using:

1) CT number difference between dry core and brine saturated core.
2) Core weight difference between dry core and brine saturated core.

Fig.4.1 – Indiana Limestone Core

The dry Indiana Limestone cores were prepared first by heating in the oven for two days. The heating temperature was adjusted to reach the minimum temperature required to evaporate the residual liquids up to a temperature of 100 ^{o}C (220 ^{o}F).The dry cores were then weighed and CT scanned. After the cores got scanned and weighed, they were immersed in a desiccator filled with brine and a vacuum pump was applied to ensure complete saturation of the effective pore space with brine. Each core was placed in the desiccator for a minimum of 10 pump working hours. The cores were then weighed and scanned again.

The following images were processed using a color spectrum from 1700 to 2200 as shown below; different colors with different in-between transitions are used to facilitate visualization. **Fig.4.2** shows the color spectrum and the corresponding color to the CT numbers.

Fig.4.2 – Color Spectrum (CT number 1700~2200)

The following images **Fig.4.3 and 4.4** are for a sample core comparison of dry Indiana Limestone and brine saturated Indiana Limestone core (sample AH-6):

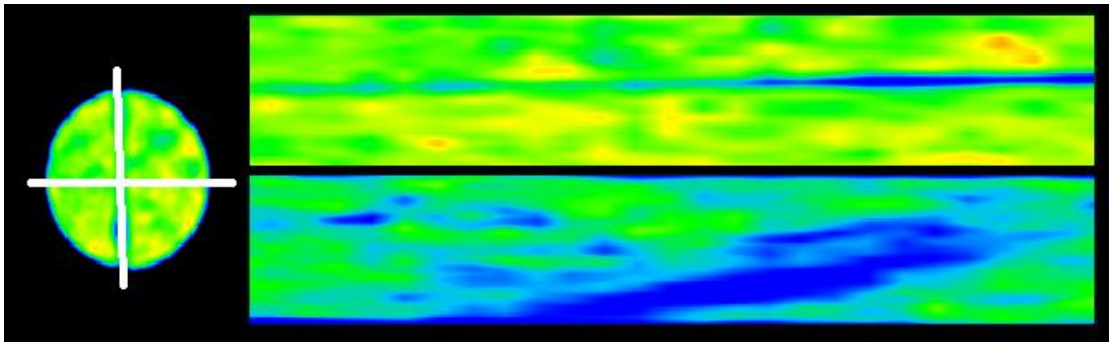

Fig.4.3 – CT Image of Dry Indiana Limestone Core

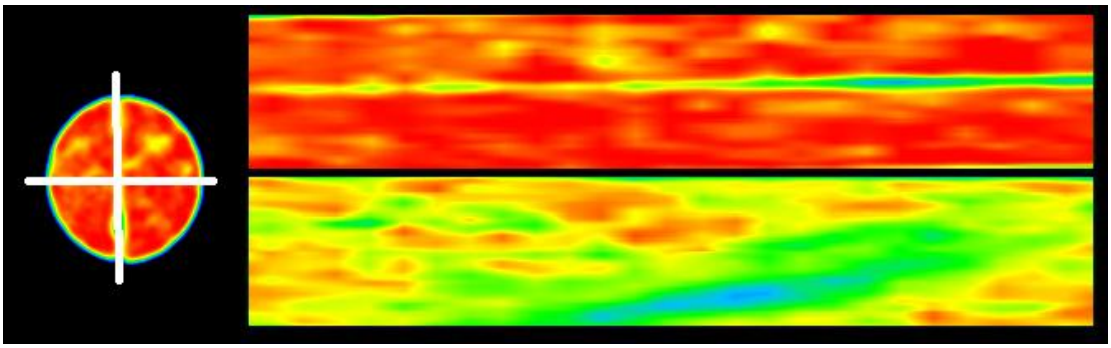

Fig.4.4 – CT Image of Brine Saturated Indiana Limestone Core

The upper slab corresponds to the horizontal cross-section and the lower one corresponds to the vertical cross section through the fracture. The images show darker color (more towards the red) for higher CT numbers corresponding to the water (CT number=0) and shows lighter color (more towards the blue) for lower CT numbers corresponding to the air (CT number=-1000). The images show the lower slab having much lighter color than the upper one. This corresponds to the lower CT number in the fracture plane compared to the pore space.

Note: The fluid flow direction is from right (inlet) to left (outlet).

The upper slab corresponds to the horizontal cross-section and the lower one corresponds to the vertical cross section through the fracture. This will be consistent for all of the CT images following throughout this thesis.

Fig.4.5. shows the average CT number of the dry and the wet core at every slice. The dotted line shows the porosity at each slice calculated from the average CT numbers. Using the CT numbers, the average porosity for the sample core was 15.8% compared to a value of 14.2% obtained from the weight difference approach. The difference in the estimated porosity corresponds to an approximate pore volume of 0.2 cc. The low effect validates the application of CT imaging for quantitative analysis for the coreflood experiments.

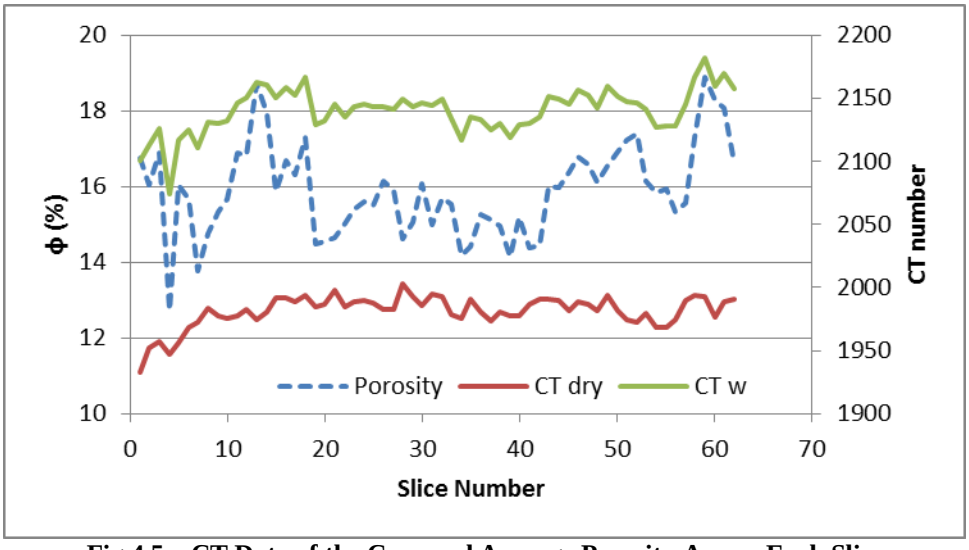

Fig.4.5 – CT Data of the Core and Average Porosity Across Each Slice

The porosity and pore volume measurements for the used core samples are listed in **Table 4.1** below:

Table 4.1 – Porosity and Pore Volume Measurements for Used Samples

Core No.	Effective Porosity (%)	Pore Volume(cc)
AH1	13.97	8.99
AH2	13.88	8.93
AH3	14.43	9.29
AH4	14.45	9.30
AH5	14.71	9.47
AH6	14.22	9.15
AH7	13.92	8.96
AH8	14.19	9.13
AH9	14.42	9.28
AH10	16.03	10.32
AH11	17.09	11.00
AH12	14.17	9.12
AH13	14.46	9.31
AH14	15.49	9.97
AH15	15.89	10.23
Average	14.75	9.50

4.2 Fluids Properties under Experimental Conditions

Table 4.2 shows the main properties for the used Soltrol 130 oil.

Table 4.2 – Soltrol 130 Oil Properties

Grade	Soltrol 130
Supplier	Chevron Phillips Chemical Company
Initial boiling point°C	181
10% °C	184
90% °C	200
Dry point °C	208
Flash point °C	61
Density @ 15.6°C(g/cc)	0.76
Density @ 60 F(lb./gal)	6.34
Specific Gravity	0.7635
Isoparaffin content wt.%	99+
Aromatics content ppm	70
Aniline point °C	86.7
Molecular Weight (g/mole)	163

The experiments were designed to be run under supercritical conditions of CO_2. The supercritical condition is reached at conditions exceeding 1072 psi and 89 ^{o}F. Another important parameter to be estimated is the MMP (minimal miscible pressure) to ensure that the CO_2 supercritical fluid will flow above the MMP. The MMP is commonly estimated using slim-tube tests. However, due to limited time and data, a quick estimation using Cronquist correlation (Equation 2.4) was used according to the following equation:

$$MMP = 15.988T^{(0.744206+0.0011038MwC5+)} \quad \text{.....(1.7)}$$

T = Temperature in ^{o}F (Experimental condition 120 °F)

MwC5+ = Molecular weight of pentanes and heavier fractions in the oil (*Soltrol*-13 oil has a maximum Mw of 163)

Using the above correlation the MMP is determined to be 1335 psi. All of the experiments were run at much higher pressure and temperature to ensure reaching the supercritical CO_2 state and the MMP. The experiments were run at a temperature of 120 ^oF, 1700 psi CO_2 injection pressure and a constant overburden pressure at 2,000 psi. **Table 4.3** shows details of basic CO_2 properties at selected conditions. The typical properties will be around 0.45 cp and 0.58 to 0.63 g/cc compared to 1.02 g/cc for the used brine.

Table 4.3 – CO_2 properties at Selected Conditions (Jarrell 2002)

Temperature ^{o} F	Pressure PSIA	Density LB/CF	Density gm./cc	Viscosity cp
120	1600	32.94	0.5277	0.03958
120	1700	36.53	0.5851	0.04499
120	1800	39.05	0.6255	0.04936
130	1600	26.62	0.4264	0.03196
130	1700	30.60	0.4902	0.03648
130	1800	33.94	0.5436	0.04094
140	1600	22.47	0.3600	0.02817
140	1700	25.79	0.4130	0.03119
140	1800	29.05	0.4653	0.03466

4.3 Experiments in Unfractured Limestone

To obtain an ideal case set for comparison and evaluation of other cases and scenarios, CO_2 was first injected into unfractured Limestone core. The experiment was designed to ensure that CO_2 enters as supercritical fluid and at pressure above the MMP.

Before the coreflood experiment, the core was first studied for porosity using the weight difference approach as in the typical procedure detailed earlier. The core was left in the oven for two days under temperature higher than 100 ^oC; the core was then weighed and saturated with brine using a vacuum pump. The brine saturated core was then weighed and scanned under the CT scanner; the core was then heated again in the oven. After that, the core was placed under a confining pressure of 2000 psi and under temperature of 70 °F and the dry core was scanned. Then, the oil was injected with outlet valve closed to establish the oil saturation. Five pore volumes of doped oil (about 50 cc) were injected while keeping the outlet valve closed; the core was then left for 6 hours under high pressure. The outlet valve was then opened and five more pore volumes of oil were injected to ensure complete saturation with oil; then the core was CT scanned.

Prior to the CO_2 injection, the water was circulated in the bath around the coreholder for about 30 minutes at a temperature of 120 °F to establish equilibrium state. The CO_2 was then injected at 1700 psi at supercritical conditions.

To qualitatively assess the success of the flood the CT images were colored depending of the CT intensity across the core. **Fig.4.6, 4.7, 4.8 and 4.9** show the coloring spectrum used in the images, a scan of the oil saturated core and a scan after 1 and 3 PVs of CO_2 injection ,respectively.

Fig.4.6 – CT Images Color Spectrum (Exp#1)

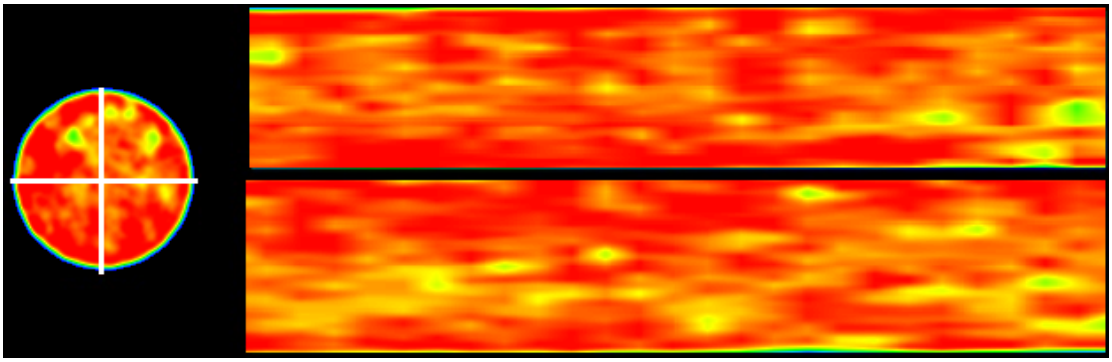

Fig.4.7 – CT Image of Oil Saturated Core (Exp#1)

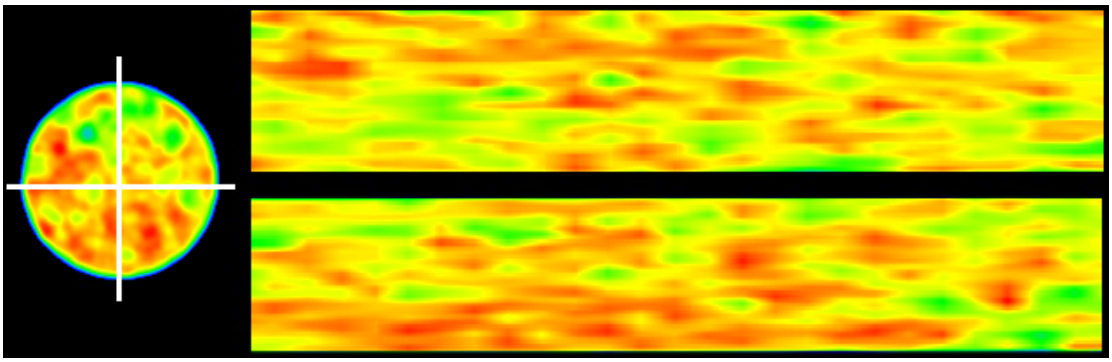

Fig.4.8 – CT Image of Oil Saturated Core after Flooded with 1 PV of CO_2 (Exp#1)

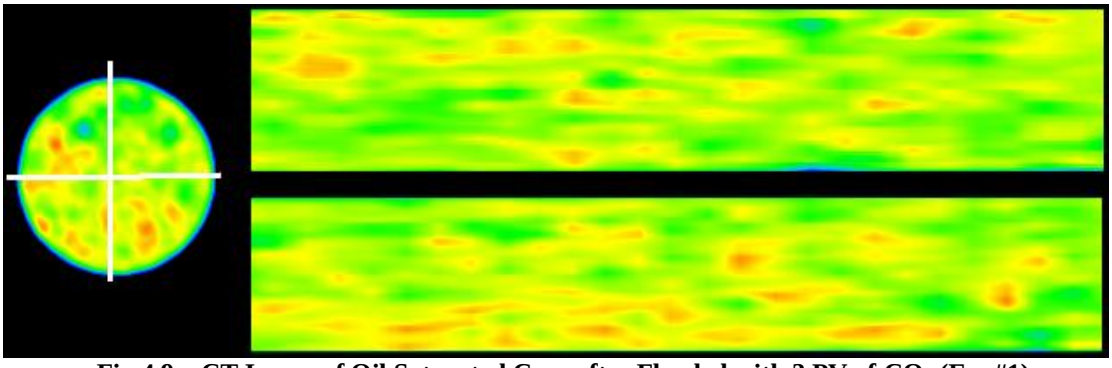

Fig.4.9 – CT Image of Oil Saturated Core after Flooded with 3 PV of CO_2 (Exp#1)

The recovery data are shown as follows:

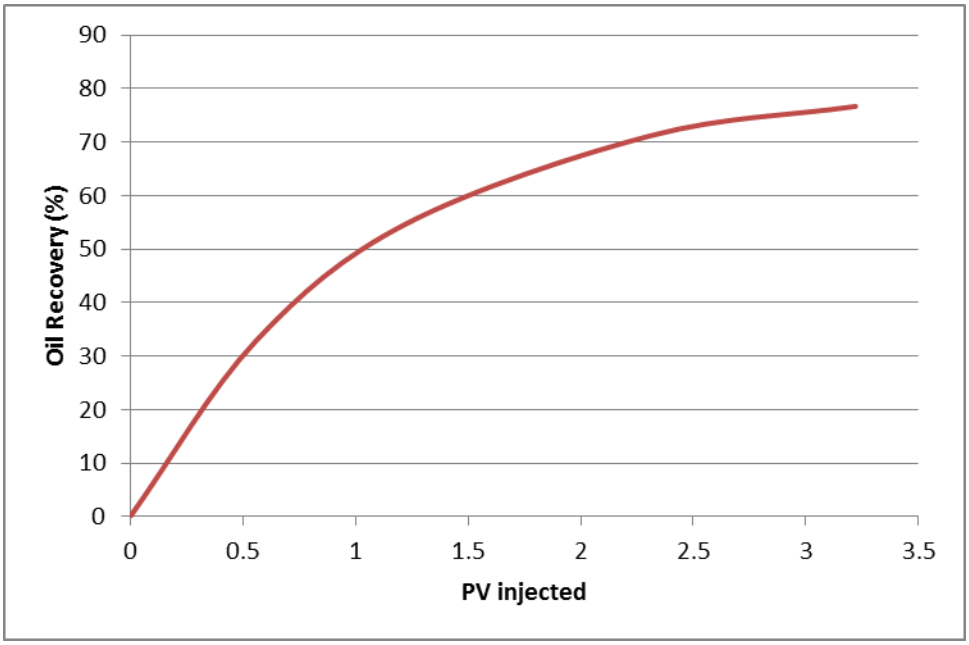

Fig.4.10 – Unfractured Limesone CGI Flood Recovery Curve (Exp#1)

Table 4.4 – Unfractured Limesone CGI Flood Recovery Data (Exp#1)

PV_{inj}	0.56	1.23	2.31	3.22
Rec(%)	32.9	54.8	71.2	76.7

Note: The fluid flow direction is from right (inlet) to left (outlet). The upper slab corresponds to the horizontal cross-section and the lower one corresponds to the vertical cross section through the fracture. This will be consistent for all of the CT images following throughout this thesis.

The OOIP (original oil in place) in the core prior to the injection of the CO_2 was estimated to be 9.13 cc. At the end of the experiment, 7 cc of the oil was recovered accounting for about 76.7% RF (recovery factor) of the OOIP. See **Fig.4.10 and Table 4.4.** The two CT images show fluid distribution across the core; the reddish coloring indicates the higher CT numbers oil while shifting left towards yellow and green shows low CT number indicative of swept areas or presence of vugs. It can be observed from the images that the CO_2 swept the oil to a great extent.

4.4 Experiments in Fractured Limestone

The presence of natural fractures is the extreme case of heterogeneity in reservoirs. The fractures act as a super highway easing water or CO_2 channeling brining a further complication to the CO_2 flooding project design. Two studies were designed to test how much oil can be recovered one with CO_2 or water as injection fluid. The two base experiments will provide an answer to the question whether which is better: CO_2 or water in presence of fractures in addition to being a comparison cases with mobility control treatments in later sections. To mimic natural fractures, the cores were cut in the center as shown in **Fig.4.11.**The frack caused the rock permeability to brine to increase up to 30 times more than the original permeability.

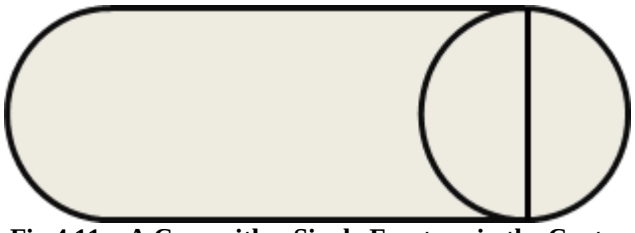

Fig.4.11 – A Core with a Single Fracture in the Center

4.4.1 CGI in Fractured Limestone

To show the impact of the presence of the fracture, a coreflood experiment was conducted with CGI under the same conditions applied in experiment no.1.

Before the coreflood experiment, the core was first studied for porosity using the weight difference approach as in the typical procedure detailed earlier. The core was left in the oven for two days under temperature higher than 100 ^{o}C; the core was then weighed and saturated with brine using a vacuum pump. The brine saturated core was then weighed and scanned under the CT scanner; then the core was cut in the center and heated again in the oven. After that, the fractured core was placed under a confining pressure of 2000 psi and under temperature of 70 °F and the dry core was scanned. Then, the oil was injected with outlet valve closed to establish the oil saturation. Five pore volumes of doped oil (about 50 cc) were injected while keeping the outlet valve closed; the core was then left for 8 hours under high pressure. The outlet valve was then opened and five more pore volumes of oil were injected to ensure complete saturation with oil; then the core was CT scanned.

Prior to the CO_2 injection, the water was circulated in the bath around the coreholder for about 30 minutes at a temperature of 120 °F to establish equilibrium state. The CO_2 was then injected at 1700 psi at supercritical conditions.

To qualitatively assess the success of the flood the CT images were colored depending of the CT intensity across the core. **Fig.4.12 through 4.17** show the coloring spectrum used in the images, a scan of the oil saturated core and a scan after 1 and 3 PVs of CO_2 injection respectively.

Fig.4.12 – CT Images Color Spectrum (Exp#2)

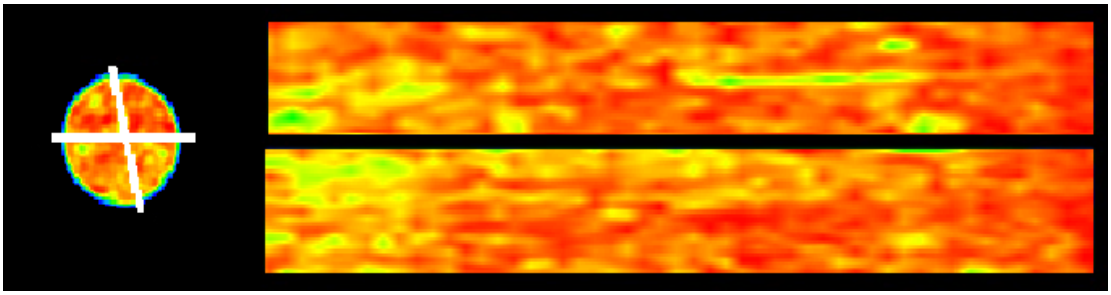

Fig.4.13 – CT Image of Oil Saturated Core (Exp#2)

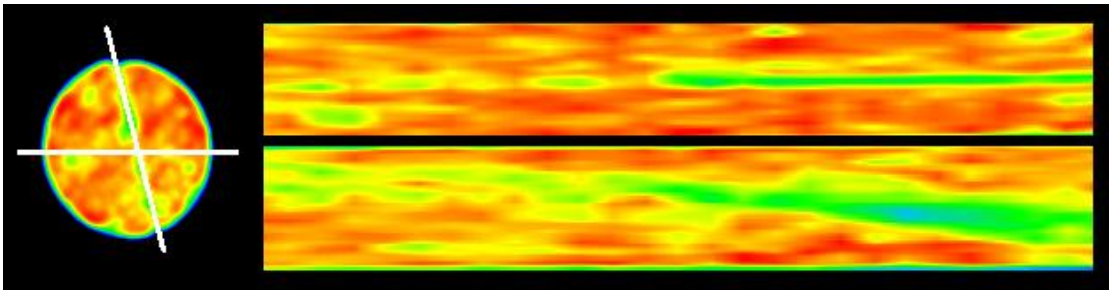

Fig.4.14 – CT Image of Oil Saturated Core after Flooded with 1 PV of CO_2 (Exp#2)

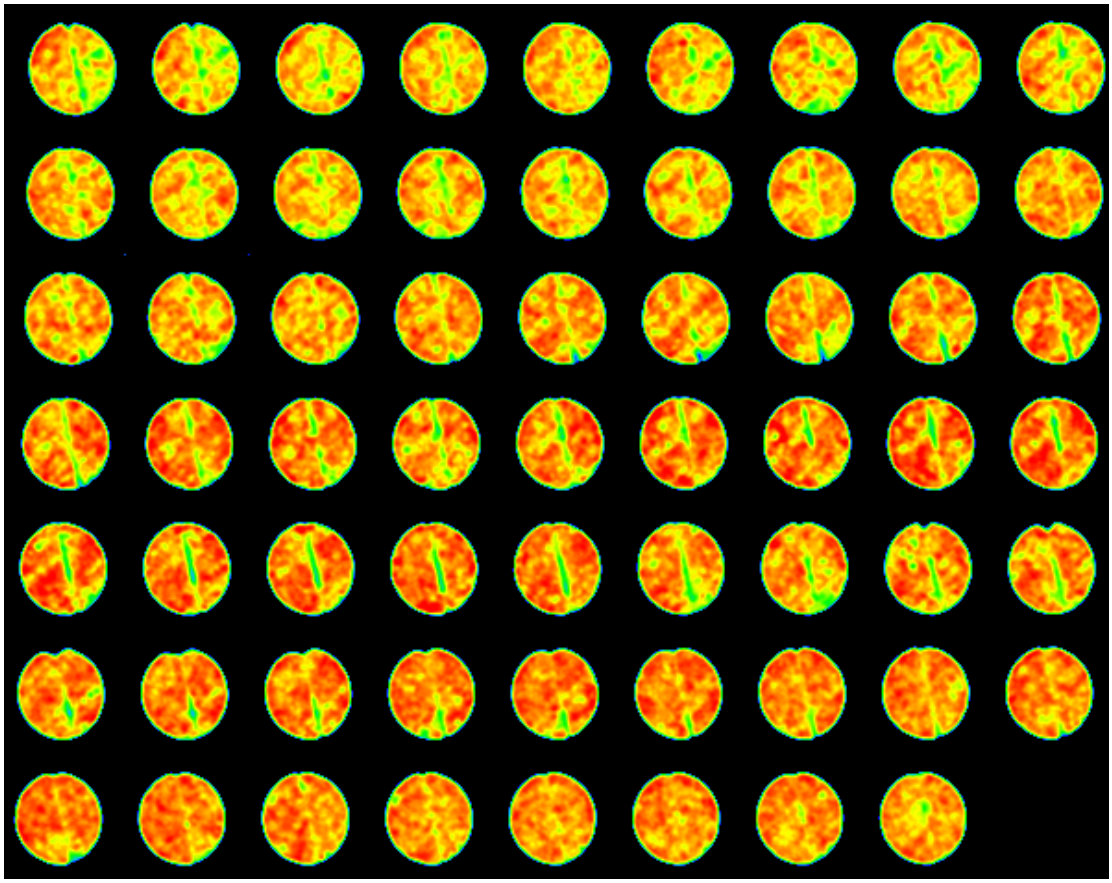

Fig.4.15 – Vertical Slice CT Images of 1PV CO_2 Flooded Core (Exp#2)

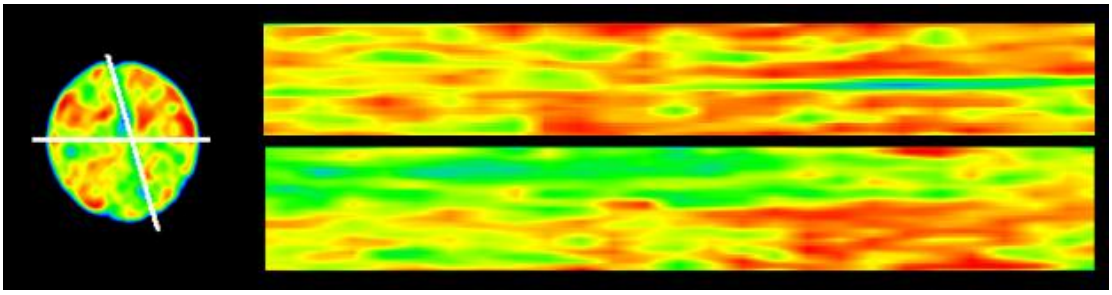

Fig.4.16 – CT Image of Oil Saturated Core after Flooded with 3 PV of CO_2 (Exp#2)

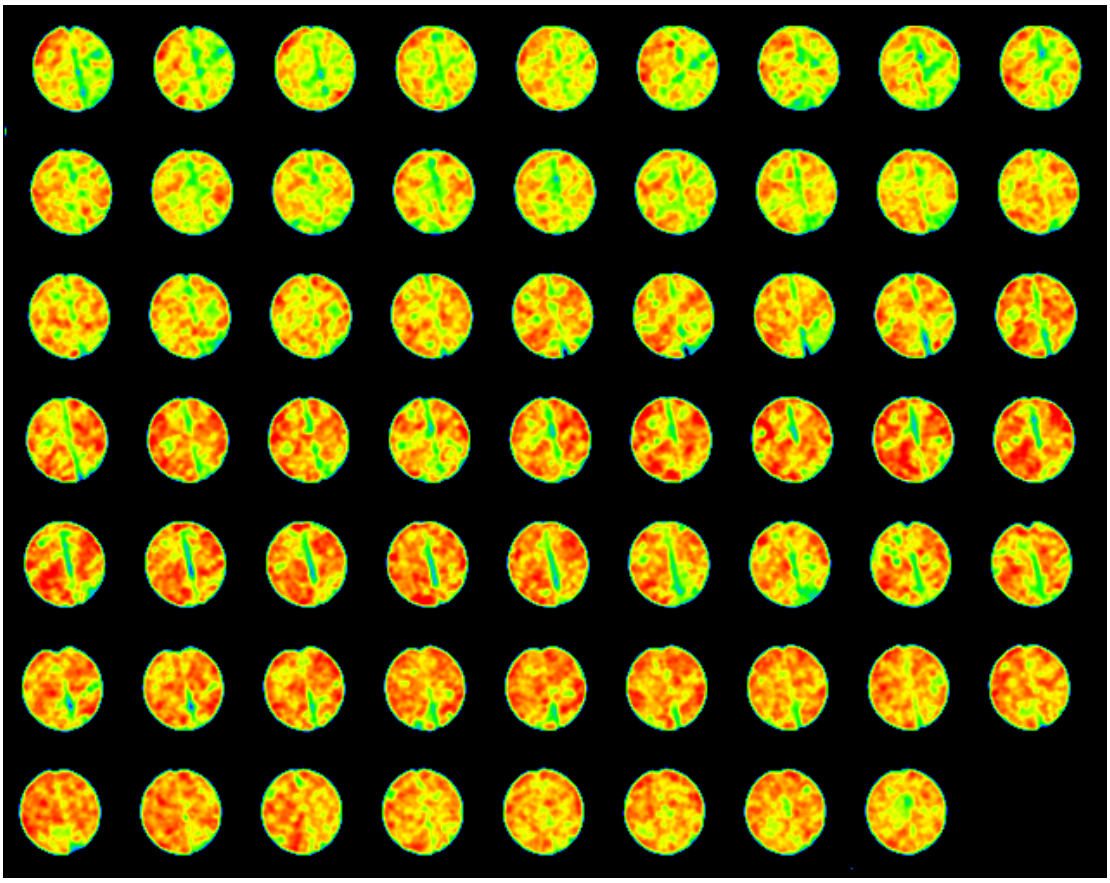

Fig.4.17 – Vertical Slice CT Images of 3PV CO_2 Flooded Core (Exp#2)

Note: the vertical slice images are lined horizontally , a row by row from top to bottom with the first image being the inlet and last image being the outlet.

The two CT images show fluid distribution across the core; the reddish coloring indicates the higher CT numbers oil while shifting left towards yellow and green shows low CT number indicative of the fracture, vugs or swept areas. The CT images show that CT intensity changes were much less significant compared to the unfractured core

indicating less efficient sweep and ultimate oil recovery. The upper slab in the oil saturated or after the flood CT image shows a horizontal cross-section intersecting the fracture plane. The image shows an interesting observation, the fracture is relatively wider towards the injection end which explains the darker CT color around the wider portion of the frack. This suggests that darker areas were less swept affected by the fracture. The wider segment provided a conductive path while when the fracture narrowed, some CO_2 was forced to diffuse through the porous medium extracting more oil.

The recovery data are shown as follows:

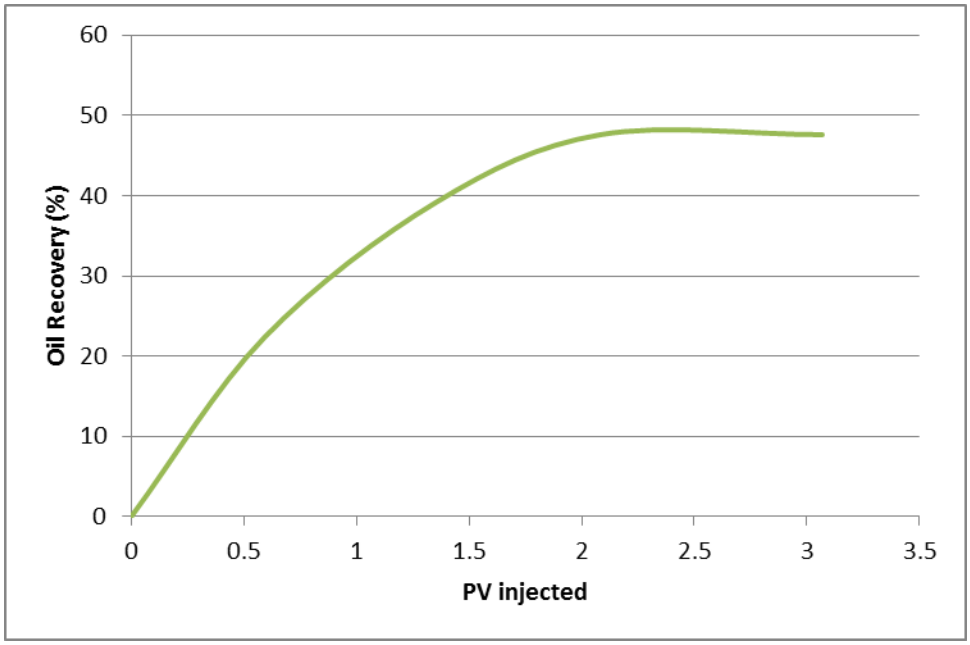

Fig.4.18 – Fractured Limesone CGI Flood Recovery Curve (Exp#2)

Table 4.5 – Fractured Limesone CGI Flood Recovery Data (Exp#2)

PV_{inj}	0.59	1.35	2.08	3.07
Rec(%)	22.4	39.2	47.6	47.6

The OOIP (original oil in place) in the core prior to the injection of the CO_2 was estimated to be 8.93 cc. At the end of the experiment, about 4.3 cc of the oil was recovered accounting for about 47.6% RF of the OOIP. See **Fig.4.18 and Table 4.5.**

4.4.2 Waterflood in Fractured Limestone

To show the impact of the presence of the fracture, the same coreflood experiment was repeated with water as the injected fluid. The purpose was to see whether, the, less viscous and consequently with better mobility, water will recover more oil than the CO_2 in fractured systems under the same conditions applied in experiment no.2.

The experimental procedure had some changes from the previous experiment. Before the coreflood experiment, the core was first studied for porosity using the weight difference approach as in the typical procedure detailed earlier. The core was left in the oven for two days under temperature higher than 100 ^{o}C; the core was then weighed and saturated with brine using a vacuum pump. The brine saturated core was then weighed and scanned under the CT scanner; then the core was cut in the center and heated again in the oven. After that, the fractured core was placed under a confining pressure of 2000

psi and under temperature of 70 °F and the dry core was scanned. Then, the oil was injected with outlet valve closed to establish the oil saturation. Five pore volumes of doped oil (about 50 cc) were injected while keeping the outlet valve closed; the core was then left for 8 hours under high pressure. The outlet valve was then opened and five more pore volumes of oil were injected to ensure complete saturation with oil; then the core was CT scanned. The water was then injected to the core at 2 cc/min and the recovery data was recorded.

To qualitatively assess the success of the flood the CT images were colored depending of the CT intensity across the core. **Fig.4.19, 4.20, 4.21 and 4.22** show the coloring spectrum used in these images, a scan of the oil saturated core , a scan after 1 PV and a scan after 3 PV of water injection respectively. For this experiment, the oil was not doped and the resulting CT number was lower for oil than the denser water with 0.76 g/cc compared to 1.02 g/cc. Therefore, the color coloring spectrum was flipped with a narrower range because the CT readings were very close to each other.

Fig.4.19 – CT Images Color Spectrum (Exp#3)

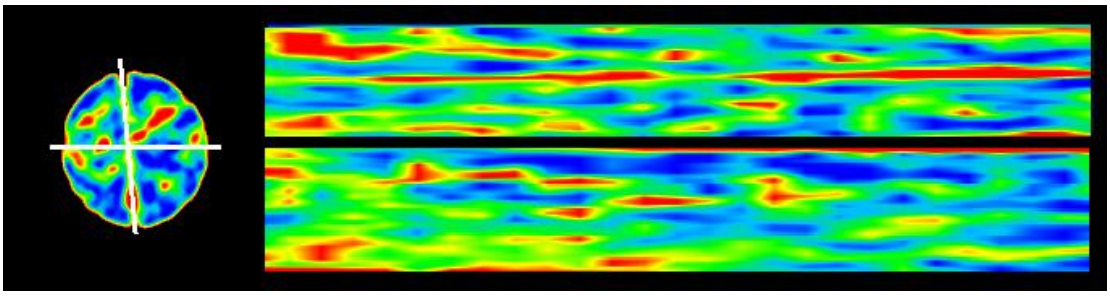

Fig.4.20 – CT Image of Oil Saturated Core (Exp#3)

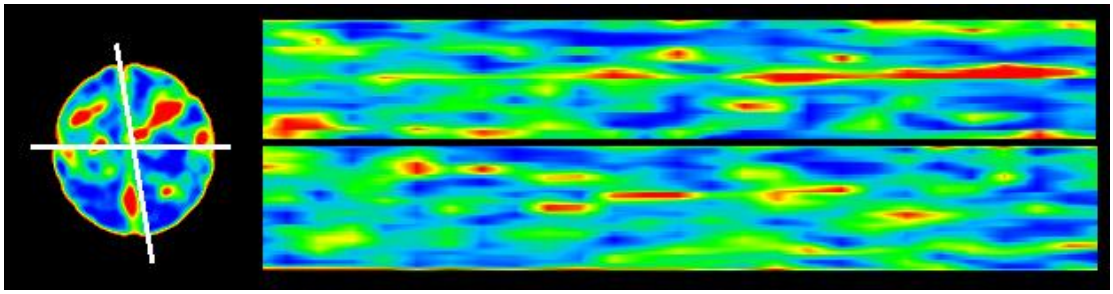

Fig.4.21 – CT Image of Oil Saturated Core after 1PV of Waterflood (Exp#3)

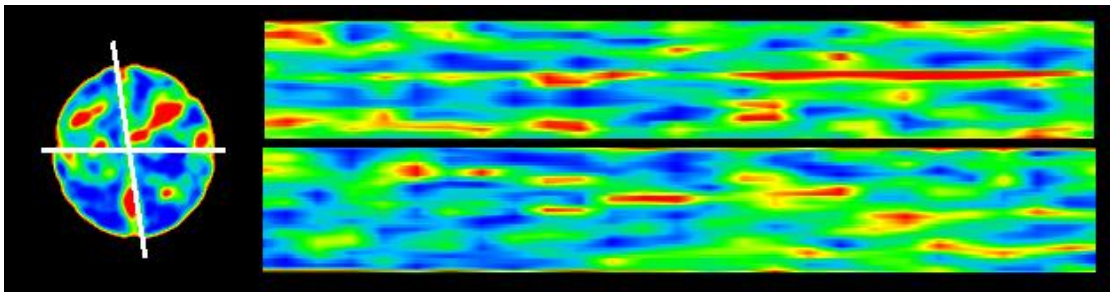

Fig.4.22 – CT Image of Oil Saturated Core after 3PV of Waterflood (Exp#3)

The CT images show fluid distribution across the core; the greenish coloring shows the water while shifting towards yellow and red is indicative of the fracture, vugs or oil. The CT images show that CT intensity changes were much less significant compared to the unfractured core indicating less efficient sweep and ultimate oil

recovery. Comparing the three images , the coloring changes in a way less visible than the older experiments due to poorer sweep and closer CT numbers of the two fluids oil and water. The upper slab in the oil saturated or after the flood CT image shows a horizontal cross-section intersecting the fracture plane. The image shows an interesting observation, the fracture is more visible in the first image with the core saturated with oil. The later images show then the CT number through fracture area increases especially closer to the production outlet. This suggests two things: 1) the fracture is slightly wider towards the inlet thus having lower CT number 2) more of the denser water and oil resided in the fracture compared to the first image. The image coloring changes also suggest that the second portion of the core was swept slightly better than the first one affected by the fracture. The wider segment provided a conductive path while when the fracture narrowed, some water was forced to diffuse through the porous medium extracting more oil.

The OOIP (original oil in place) in the core prior to the injection of the CO_2 was estimated to be 9.15 cc. At the end of the experiment, about 3.5 cc of the oil was recovered accounting for about 38.3% RF of the OOIP. See **Table 4.6.**

Table 4.6 – Fractured Limesone Water Flood Recovery Data (Exp#3)

PV_{inj}	0.52	1.10	2.04	3.08
Rec(%)	21.9	32.8	38.3	38.3

Fig.4.23 shows the recovery curves of the first three base cases experiments. Although, the CGI case resulted in better recovery than the WF one, it is still far from the ideal recovery efficiency. This issue will be discussed in an attempt towards solutions in fractured systems. In our case, the CGI having higher recovery than the WF indicates that efficiency was more dominant than the presence of the fracture. This, off course, will be different with fractures having different aperture and conductivity.

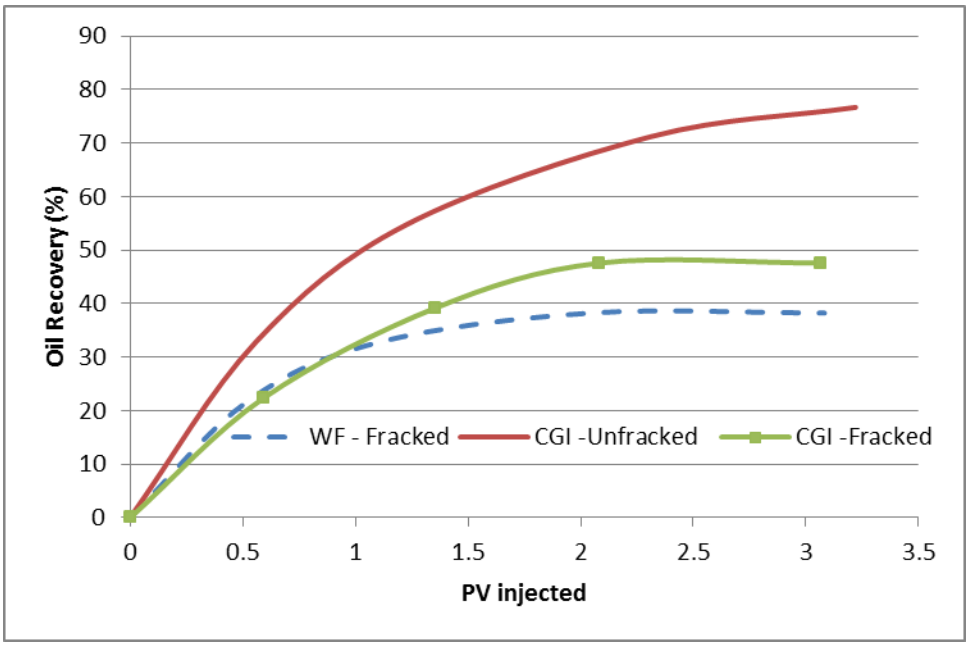

Fig.4.23 – Base Limesone Core Flood Recovery Curves (Exp#1, 2 and 3)

4.5 Experiments in Fractured Limestone Using Cross-linked Gels for Conformance Control

The previous experiments highlighted the impact of the presence of fractures on ultimate oil recovery. The recovery was inefficient especially with fractures with higher conductivity. The most common solutions to heterogeneities and fractures are:

1. Foam applications.
2. CO_2 viscosifying polymers.
3. Placement of cross-linked gels.
4. Water alternating gas (WAGs)

We decided to test the latter two because they are more direct solutions and easier to control and evaluate for success or failure. In fact, application of cross-linked gels is considered to be the most aggressive mobility control approach. In our research for proper chemical systems, the most common systems were:

1. HPAM gel cross-linked with Cr(III)Ac.
2. Xanthan gum.
3. Guar gum with Borate crosslinker.

The HPAM – Cr(III)Ac system was chosen due to several reasons : availability, price, chemical properties and reported successful applications. Most of the applications reported in the literature have been applied in water shutoff treatments in production gels. The objective of the study is to evaluate the possibility and feasibility of application with CO_2 EOR processes.

The WAG studies will be coupled with viscosified waters to assess its attractiveness compared to direct gel treatments followed by CGI. For that purpose, two chemical systems were tested: HPAM and Xanthan.

For all of the following experiments, the cores were cut in the center in the same manner described earlier. The experimental results proved the success of gel application compared untreated cores. It is assumed that the viscous gels will flow only through the super highway fractures and not through the matrix. This assumption was tested and will be discussed next.

Gel application success is typically described in terms of gel strength. The gel strength is function of many parameters; the main factors are polymer concentration, crosslinker concentration and temperature. The polymer and crosslinker concentration will be varied throughout the experiments while maintain the other factors consistent. (Seright 1997; Seright et al. 2011)

4.5.1 3000 PPM Gel Application

The first experiment utilized 3,000 ppm HPAM polymer cross-linked with 300 ppm of Cr(III)Ac (with 6 wt.% KI dopant).At the time of gel injection, the gel was characterized to be “runny fluid”.

Before the coreflood experiment, the core was first studied for porosity using the weight difference approach as in the typical procedure detailed earlier. The core was left in the oven for two days under temperature higher than 100 ^{o}C; the core was then weighed and saturated with brine using a vacuum pump. The brine saturated core was

then weighed and scanned under the CT scanner; then the core was cut in the center and heated again in the oven. In the meanwhile, the gel ingredients were mixed together using a magnetic stirrer until the mixture got homogenous; the gel was allowed to stir for about 8 hours. The gel was then allowed to reside for 12 hours. After that, the fractured core was placed under a confining pressure of 2000 psi and under temperature of 70 °F and the dry core was scanned. Then, the oil was injected with outlet valve closed to establish the oil saturation. Five pore volumes of doped oil (about 50 cc) were injected while keeping the outlet valve closed; the core was then left for 8 hours under high pressure. The outlet valve was then opened and five more pore volumes of oil were injected to ensure complete saturation with oil; then the core was CT scanned. Then, 30 cc of preformed gel were injected at injection pressure of around 100 psi; the outlet valve was left open for the gel to exit and not flow back inside the core. The system was then left intact for the gel to strengthen.

Prior to the CO_2 injection, a CT scan was taken to evaluate the gel placement. Afterwards, warm water was circulated in the bath around the coreholder for about 30 minutes at a temperature of 120 °F to establish equilibrium state. The CO_2 was then injected at 1700 psi at supercritical conditions. The recovery data were recorded and several CT scans were taken.

To qualitatively assess the success of the gel treatment and the flood the CT images were colored depending of the CT intensity across the core. **Fig.4.24 through 4.33** show the coloring spectrum used in the images, scans of the oil saturated core and scans after 3 PV of CO_2 injection respectively.

For this experiment, the difference in CT intensity between the doped oil (0.76 g/cc) and the supercritical CO_2 (0.58 g/cc) facilitated the view and the evaluation of the success of the flood. The gel with higher density and enhanced CT reading with KI dopant was viewed with higher CT reading. Therefore, the coloring spectrum was chosen in way covering the CT numbers with the darkest reddish coloring indicates the presence of oil while the lighter coloring, shifting towards yellow and green indicates the unswept areas or the fracture or vugs.

Fig.4.24 – CT Images Color Spectrum (Exp#4)

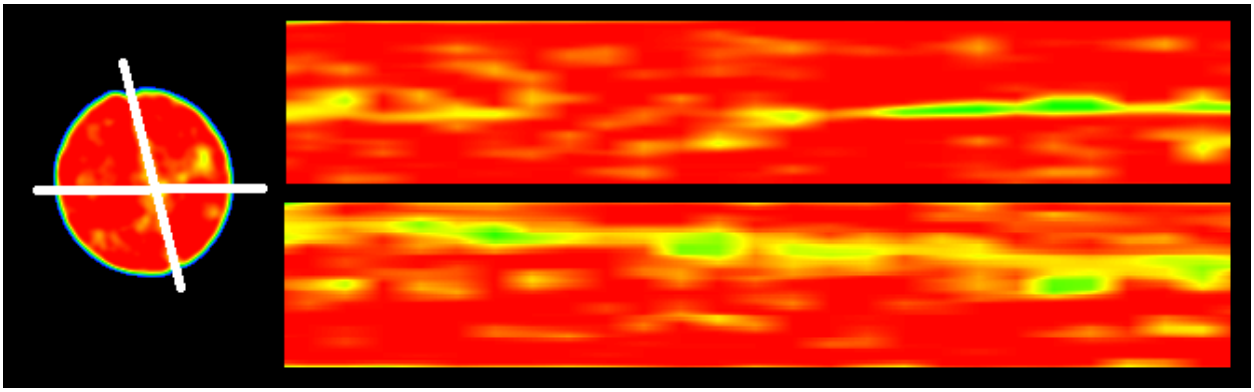

Fig.4.25 – CT Image of Oil Saturated Core (Exp#4)

Fig.4.26 – Vertical Slice CT Images of Oil Saturated Core (Exp#4)

The oil saturated images show that the core was saturated with oil to a great extent. The whole image was colored with red except the fracture area colored with yellow. Some of the spots show slightly lighter colors indicating the presence of small vugs or relatively larger pores. If this is true, these spots would be swept better than others.

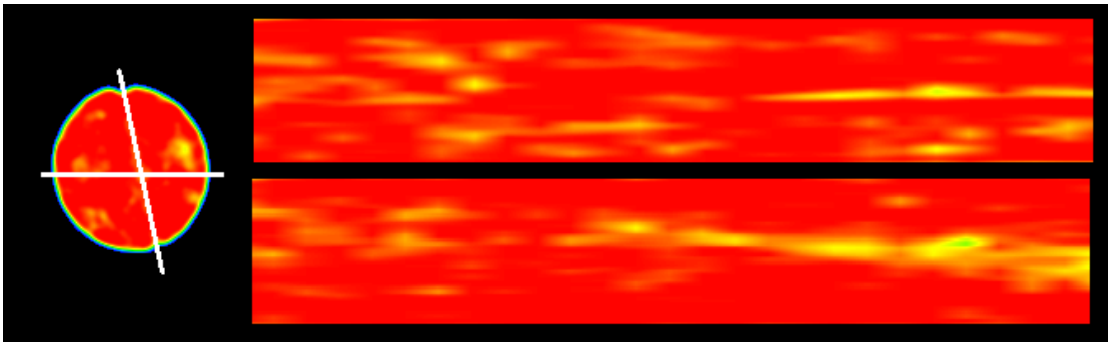

Fig.4.27 – CT Image of Oil Saturated Core after Gel Treatment (Exp#4)

Fig.4.28 – Vertical Slice CT Images of Oil Saturated Core after Gel Treatment (Exp#4)

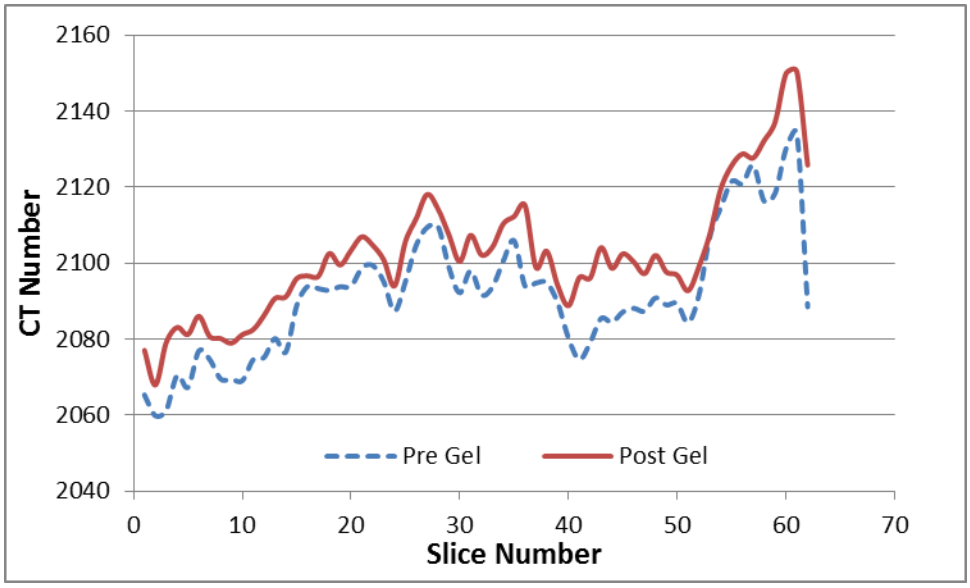

Fig.4.29 – CT Intensity Before and After Gel Treatment (Exp#4)

After the gel placement, the gel with higher density and CT value darkened the colors. The vertical slab which passes through the fracture plane shows that the some yellow areas remained the same after the placement of the gel while some spots got reddish in color indicating the successful placement in some areas and not in the others. The horizontal cross-section image confirms the same conclusion; the relatively wider segment portion of the fracture remained yellow in color. Moreover, the horizontal cross section also shows that the areas directly around the fracture got darker in color which suggests that some of the gel "leaked off" into the matrix. Confirming these observations requires direct gel strength and stability evaluation with the coreflood and assessing the recovery efficiency and the recovered liquids.

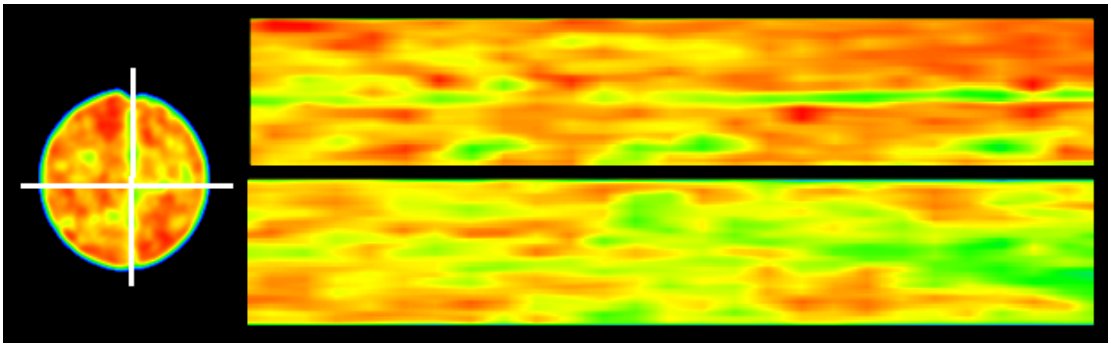

Fig.4.30 – CT Image of Oil Saturated Core Flooded With 1PV of CO_2 (Exp#4)

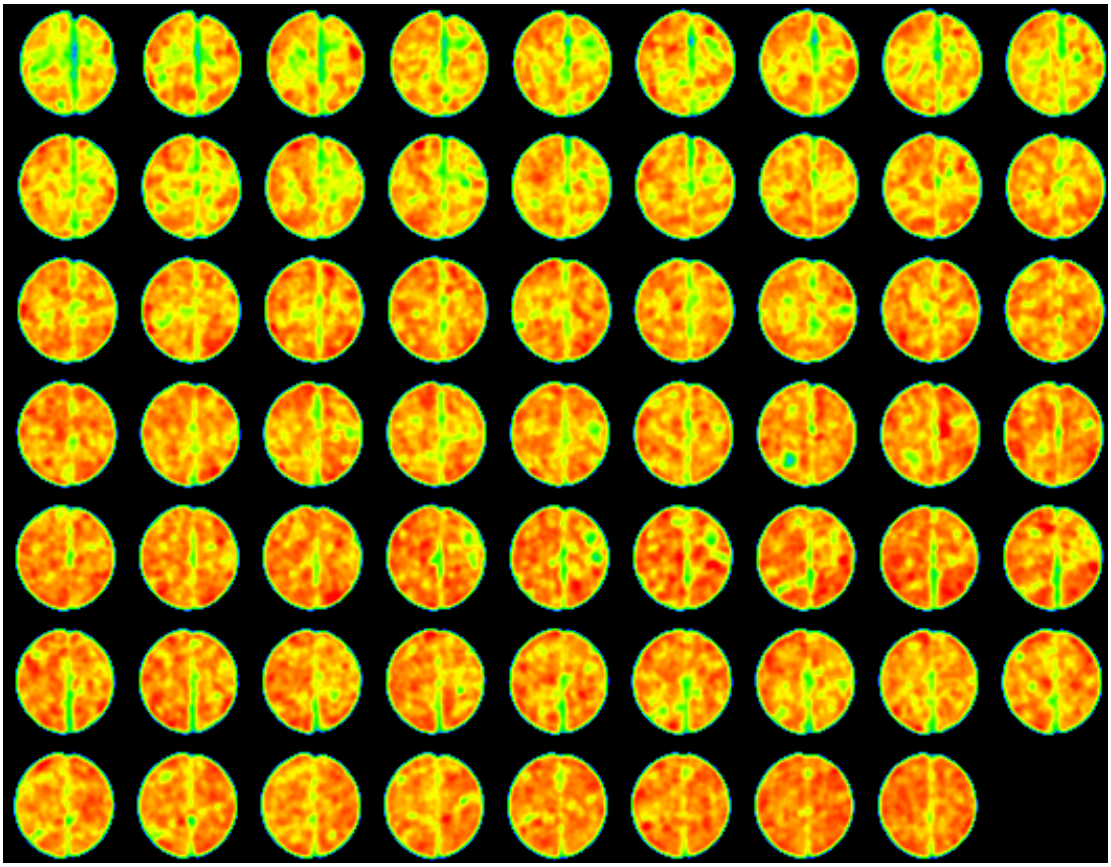

Fig.4.31 – Vertical Slice CT Images of Oil Saturated Core Flooded With 1PV of CO_2 (Exp#4)

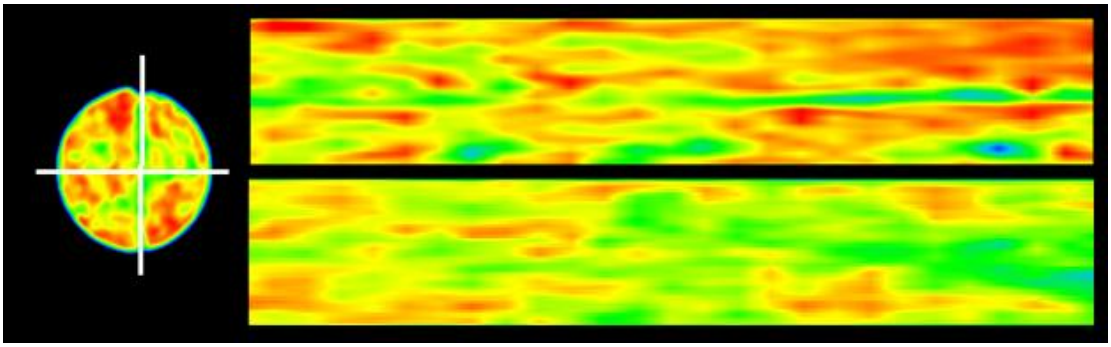

Fig.4.32 – CT Image of Oil Saturated Core Flooded With 3PV of CO_2 (Exp#4)

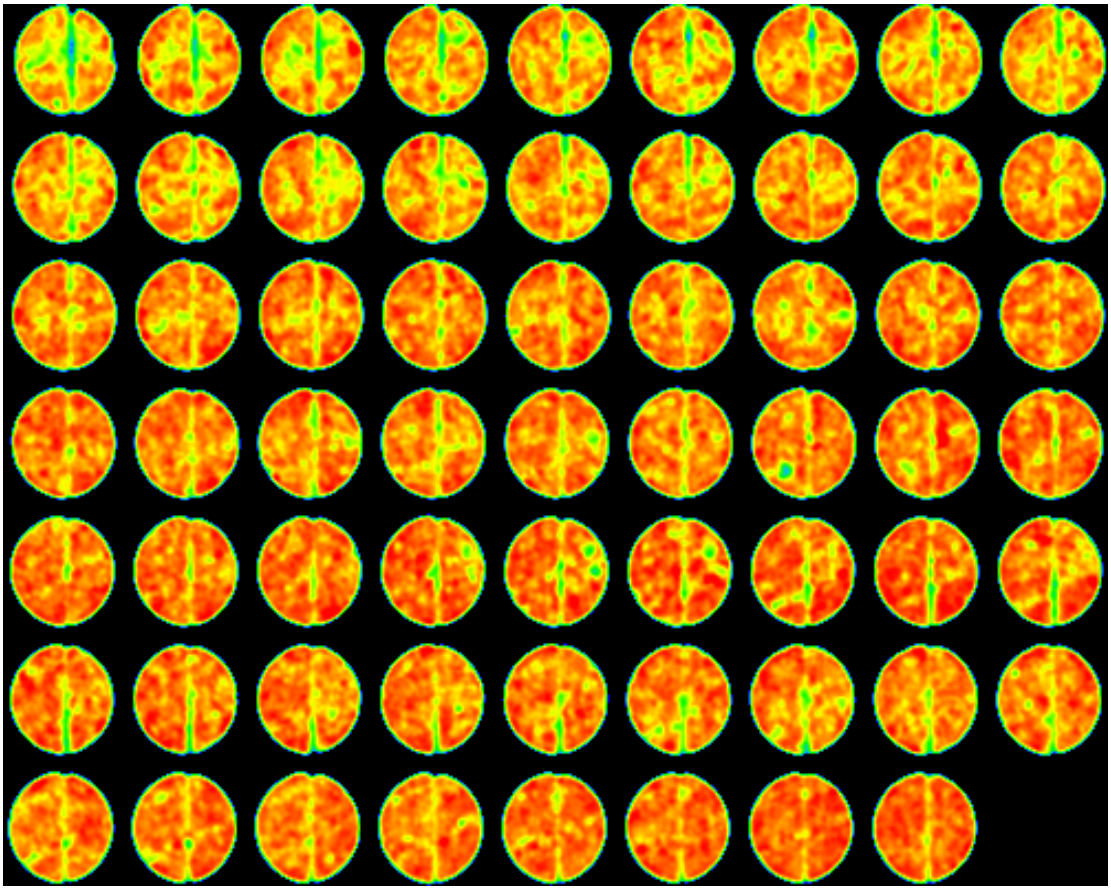

Fig.4.33 – Vertical Slice CT Images of Oil Saturated Core Flooded With 3PV of CO_2 (Exp#4)

The coreflood was carried out with the CO_2 entering at 1,700 psi and 120 ^oF. The CO_2 breakthrough occurred before injecting the first PV. The horizontal slab shows that the fracture area got colored in light green with CT numbers even less than pre-gel image; this confirms that the gel did not remain in place. Some of the gel was produced with the first PV of CO_2. Small spots of the core remained the same after the coreflood having dark red color. Most of the rock was flushed in inefficient way; some portions were flushed relatively better than others due to the heterogeneity of the core. As time progressed more CO_2 diffused into the matrix pushing more oil out.

It was assumed that the preformed cross-linked gel would not enter the matrix region; however the CT images showed a contradicting finding. Ideal gel placement will place the gel only in the fracture and that gel would remain the fracture plugging it against low viscosity CO_2. The gel was not strong enough and it flowed with the produced oil and some of it leaked off into the matrix. Only a small portion acted in hindering the flow of CO_2 forcing it to flow the matrix.

The recovery data are shown as follows:

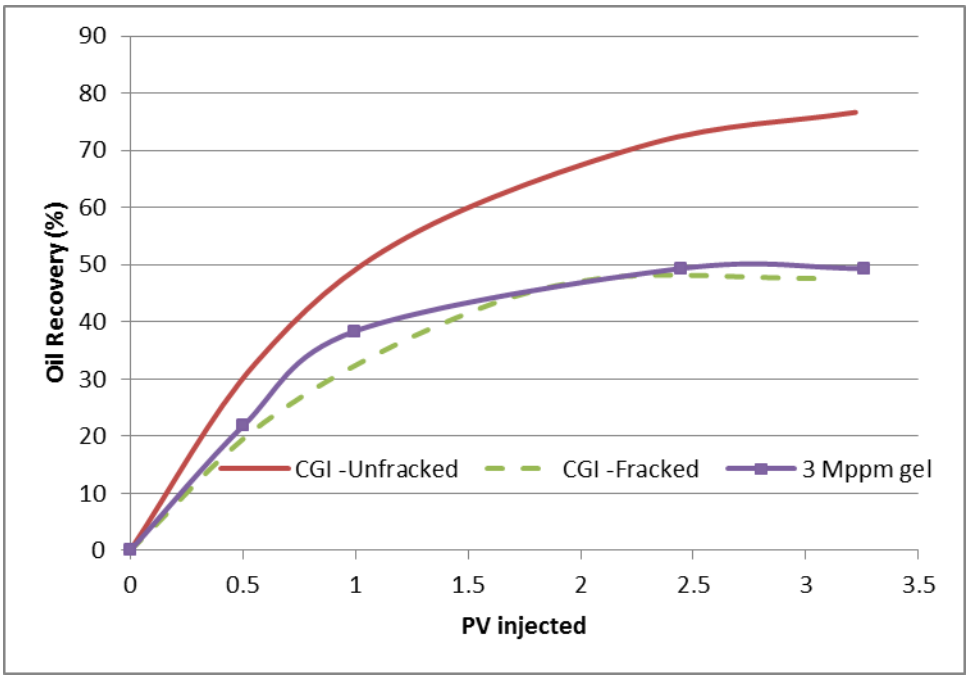

Fig.4.34 – 3,000 PPM Gel – Fractured Limesone CGI Flood Recovery Curve (Exp#4)

Table 4.7 – 3,000 PPM Gel – Fractured Limesone CGI Flood Recovery Data (Exp#4)

PV_{inj}	0.50	1.00	2.45	3.26
Rec(%)	21.9	38.4	49.3	49.3

The OOIP in the core prior to the injection of the CO_2 was estimated to be 9.12 cc. At the end of the experiment, about 4.5 cc of the oil was recovered accounting for about 49.3% RF of the OOIP. See **Fig.4.34 and Table 4.7.** In comparison with the previous results the gel application resulted in an incremental recovery of 2% only compared to the CGI without gel treatment. The treatment is far from perfect and one of things that need to be tweaked was the gel concentration. In the next experiments, the gel concentration will be increased to avoid gel breakdown and leak-off during CO_2

flooding. Success in achieving this goal will reflect the recovery data and can be evaluated qualitatively with the CT images.

4.5.2 7,500 PPM Gel Application

In the previous study to control CO_2 mobility in the fracture, low concentration 3000 ppm HPAM gel was tested. The application resulted in incremental recovery compared to the untreated core. The incremental recovery was not satisfactory. The gel exhibited leakoff and breakdown resulting in fraction of the gel produced with the recovered oil. The study was expanded with using 7,500 ppm HPAM gel cross-linked with 750 ppm of Cr(III)Ac (with 6 wt.% KI dopant). The gel performance was evaluated both quantitatively and qualitatively using the recovery data and CT imaging technique. At the time of gel injection, the gel was characterized to be "thick fluid".

Before the coreflood experiment, the core was first studied for porosity using the weight difference approach as in the typical procedure detailed earlier. The core was left in the oven for two days under temperature higher than 100 ^{o}C; the core was then weighed and saturated with brine using a vacuum pump. The brine saturated core was then weighed and scanned under the CT scanner; then the core was cut in the center and heated again in the oven. In the meanwhile, the gel ingredients were mixed together using a magnetic stirrer until the mixture got homogenous; the gel was allowed to stir for about 8 hours. The gel was then allowed to reside for 12 hours. After that, the fractured core was placed under a confining pressure of 2000 psi and under temperature of 70 °F and the dry core was scanned. Then, the oil was injected with outlet valve closed to

establish the oil saturation. Five pore volumes of doped oil (about 50 cc) were injected while keeping the outlet valve closed; the core was then left for 8 hours under high pressure. The outlet valve was then opened and five more pore volumes of oil were injected to ensure complete saturation with oil; then the core was CT scanned. Then, 30 cc of preformed gel were injected at injection pressure of around 100 psi; the outlet valve was left open for the gel to exit and not flow back inside the core. The system was then left intact for the gel to strengthen.

Prior to the CO_2 injection, a CT scan was taken to evaluate the gel placement. Afterwards, warm water was circulated in the bath around the coreholder for about 30 minutes at a temperature of 120 °F to establish equilibrium state. The CO_2 was then injected at 1700 psi at supercritical conditions. The recovery data were recorded and several CT scans were taken.

To qualitatively assess the success of the gel treatment and the flood the CT images were colored depending of the CT intensity across the core. **Fig.4.35 through 4.44** show the coloring spectrum used in the images, scans of the oil saturated core and scans after 1 and 3 PV of CO_2 injection respectively.

For this experiment, the difference in CT intensity between the doped oil (0.76 g/cc) and the supercritical CO_2 (0.58 g/cc) eased the view and the evaluation of the success of the flood. The gel with higher density and enhanced CT reading with KI dopant was viewed with higher CT reading. Therefore, the coloring spectrum was chosen in way covering the CT numbers with the darkest reddish coloring indicates the

presence of oil while the lighter coloring, shifting towards yellow and green indicates the unswept areas or the fracture or vugs.

Fig.4.35 – CT Images Color Spectrum (Exp#5)

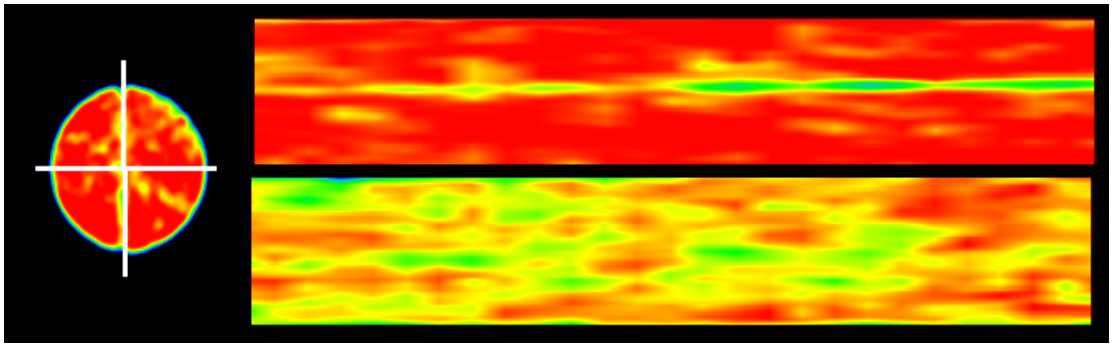

Fig.4.36 – CT Image of Oil Saturated Core (Exp#5)

Fig.4.37 – Vertical Slice CT Images of Oil Saturated Core (Exp#5)

The oil saturated images show that the core was saturated with oil to a great extent. The whole image was colored with red while the fracture area colored with yellow. Some of the spots had a dark yellow color having intermediate intensity between that of the fracture and the color observed otherwise in the matrix. These light colored spots indicate the presence of non-connected pores, small vugs or relatively larger pores. If this is true, these spots would be swept better than others.

The upper slab corresponding to the horizontal cross-section intersecting the fracture plane shows that the fracture has relatively uniform area and width. The lower slab, vertical cross-section, running across the fracture shows yellow color almost everywhere across the plane. The low CT numbers confirm the right positioned cross-section that will aid in evaluating the success degree of gel placement afterwards.

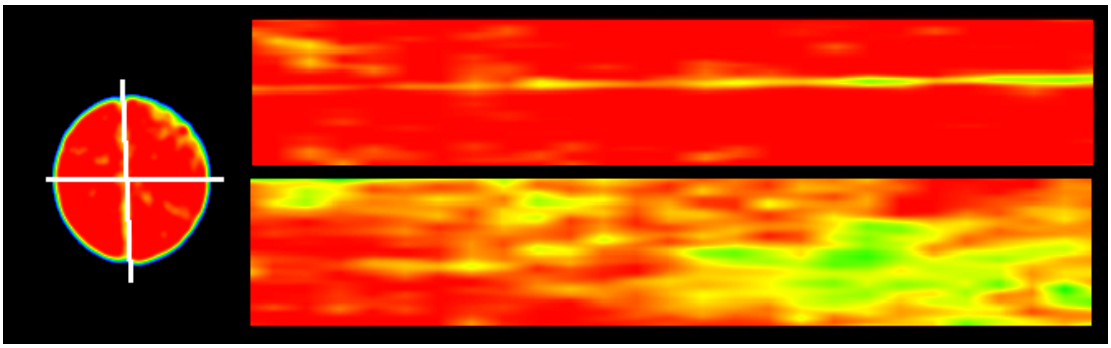

Fig.4.38 – CT Image of Oil Saturated Core after Gel Treatment (Exp#5)

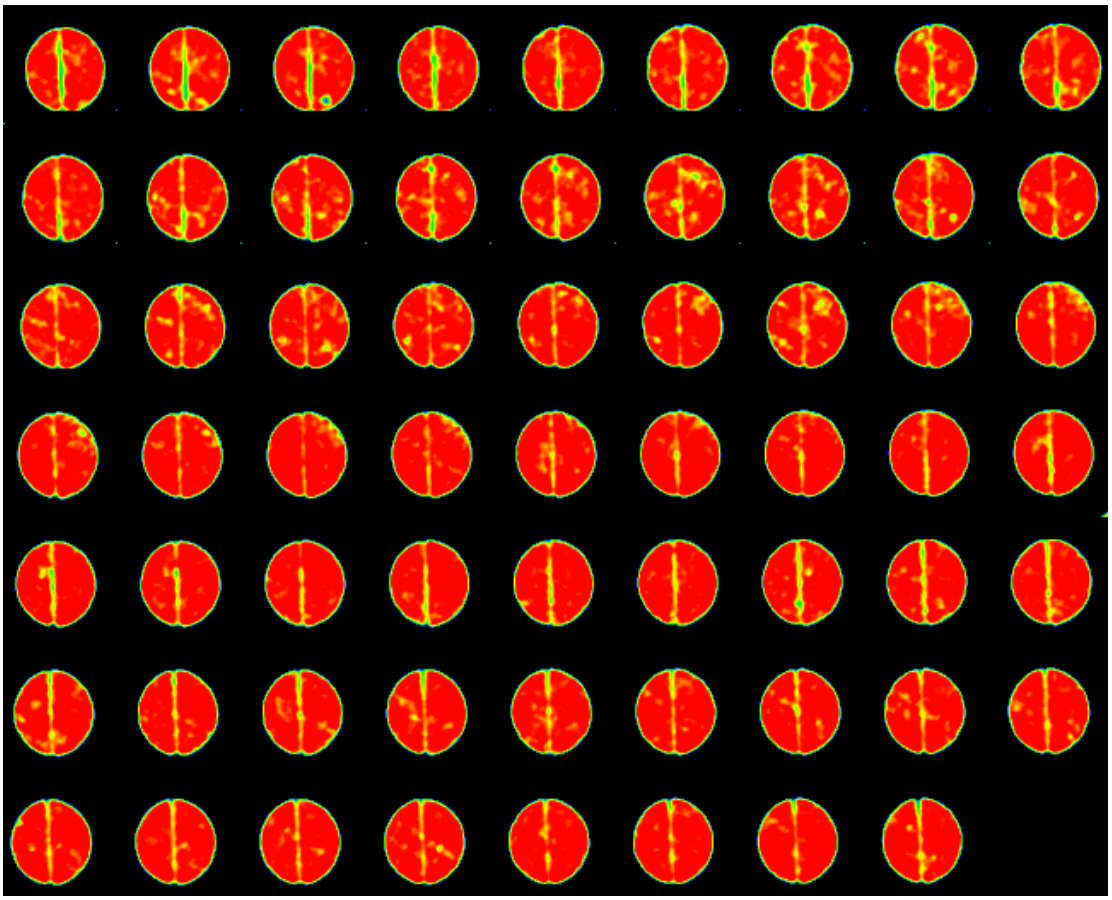

Fig.4.39 – Vertical Slice CT Images of Oil Saturated Core after Gel Treatment (Exp#5)

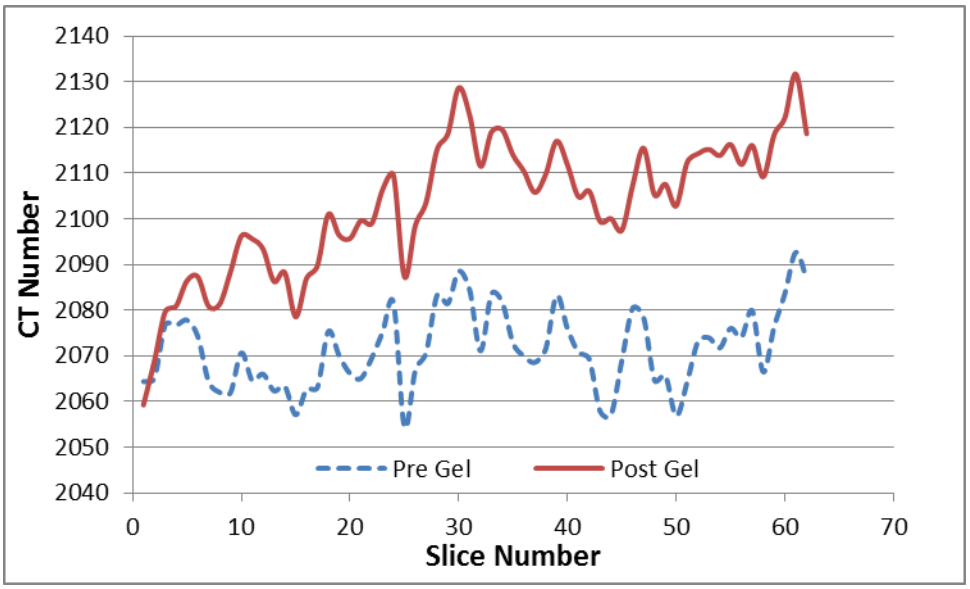

Fig.4.40 – CT Intensity Before and After Gel Treatment (Exp#5)

After the gel placement, the gel with higher density and CT value darkened the colors. The horizontal cross-section shows that the fracture remained yellow in color. However, a quick look shows that small spots around the fracture changed their color suggesting that a certain degree of leakoff. It is assumed based on the visual evaluation of the images that the leakoff is limited. The vertical slab passing through the fracture plane shows that the most of the yellow areas changed into red after the placement of the gel; the color shift acts as an indication of the successful placement of the gel. Confirming these observations requires direct gel strength and stability evaluation with the coreflood and assessing the recovery efficiency and the recovered liquids.

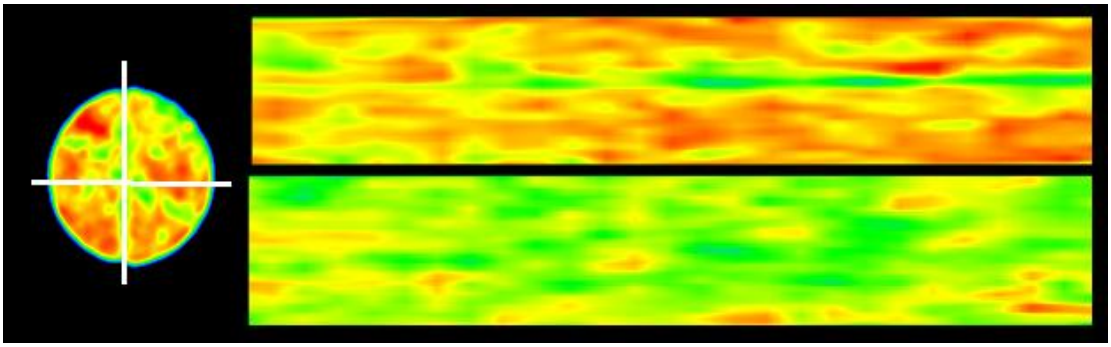

Fig.4.41– CT Image of Oil Saturated Core Flooded With 1PV of CO_2 (Exp#5)

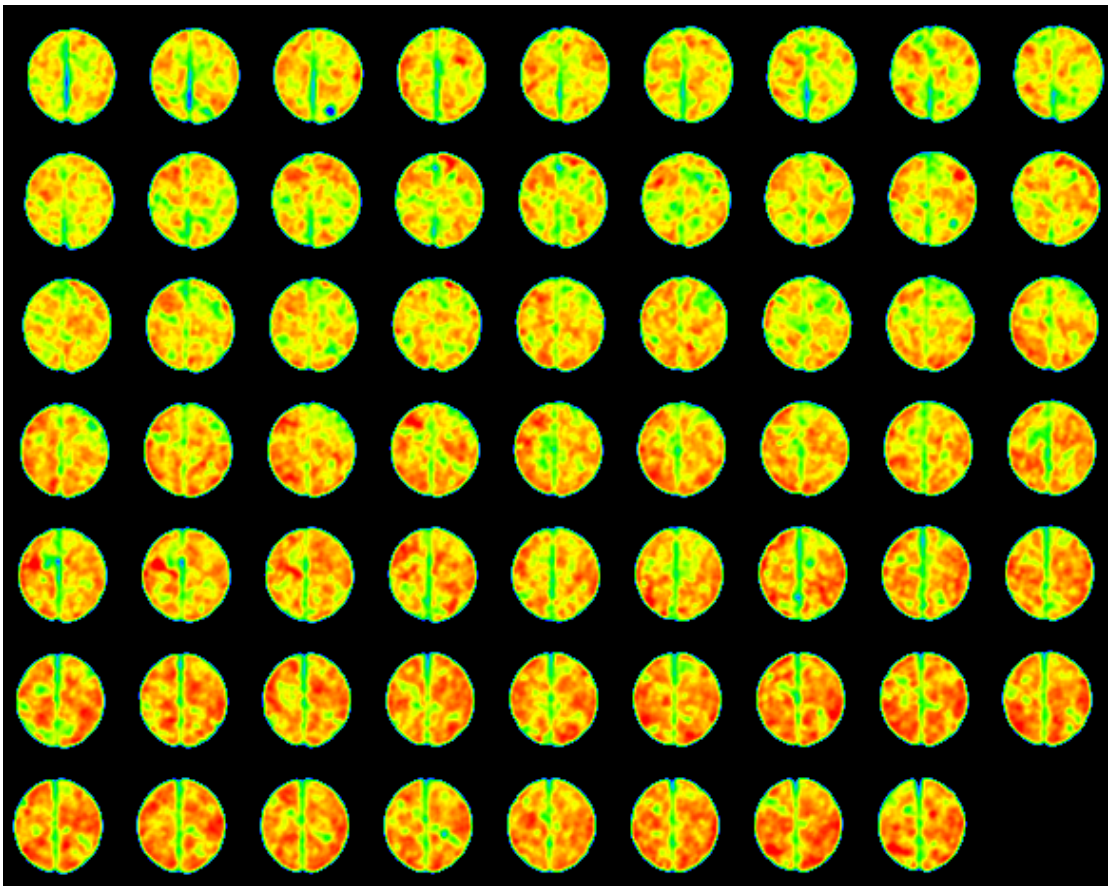

Fig.4.42 – Vertical Slice CT Images of Oil Saturated Core Flooded With 1PV of CO_2 (Exp#5)

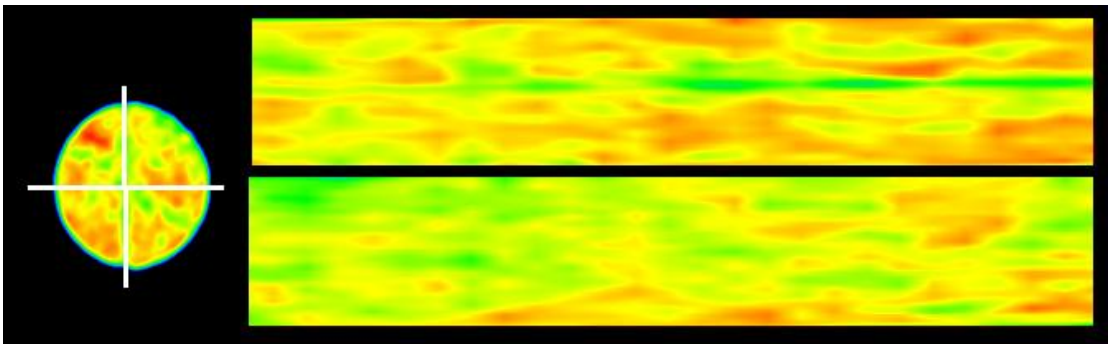

Fig.4.43 – CT Image of Oil Saturated Core Flooded With 3PV of CO_2 (Exp#5)

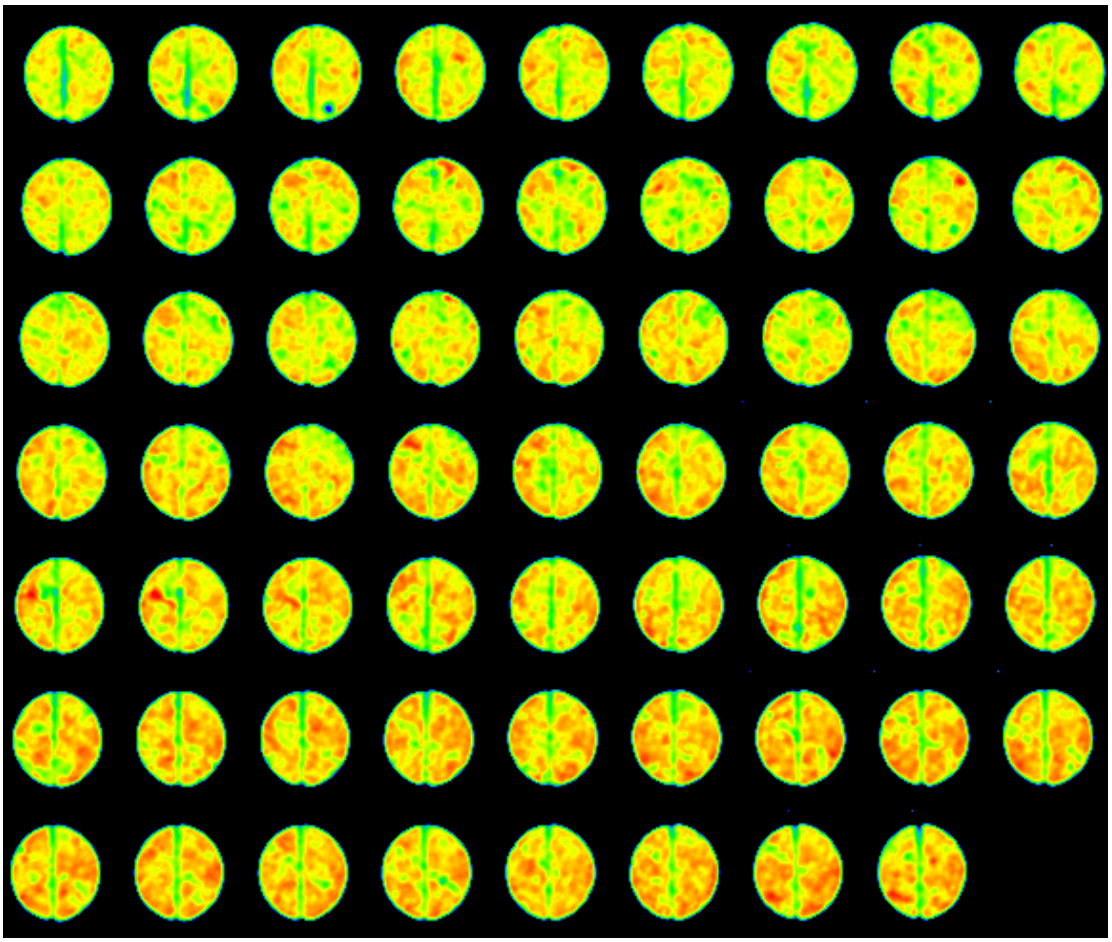

Fig.4.44 – Vertical Slice CT Images of Oil Saturated Core Flooded With 3PV of CO_2 (Exp#5)

The coreflood was carried out with the CO_2 entering at 1,700 psi and 120 ^{o}F. The CO_2 breakthrough was successfully delayed with minimal gel produced with the recovered oil. The horizontal slab shows that the fracture area got colored in green-yellow with CT intensity comparable to that of pre-gel image; this confirms that the gel remained in the fracture to a good extent. Low amount of the gel was produced with the first PV of CO_2. Small spots of the core remained the same after the coreflood having

dark red color while others got flushed greatly. Most of the rock was flushed in acceptable efficiency; some portions were flushed relatively better than others due to the heterogeneity of the core.

Ideal gel placement will place the gel only in the fracture and that gel would remain the fracture plugging it against low viscosity CO_2. The gel was strong and it small amount flowed with the produced oil and some of it appears to have leaked off into the matrix. A big fraction of the injected gel contributed to the mobility control hindering the flow of CO_2 forcing it to flow the matrix.

The recovery data are shown as follows:

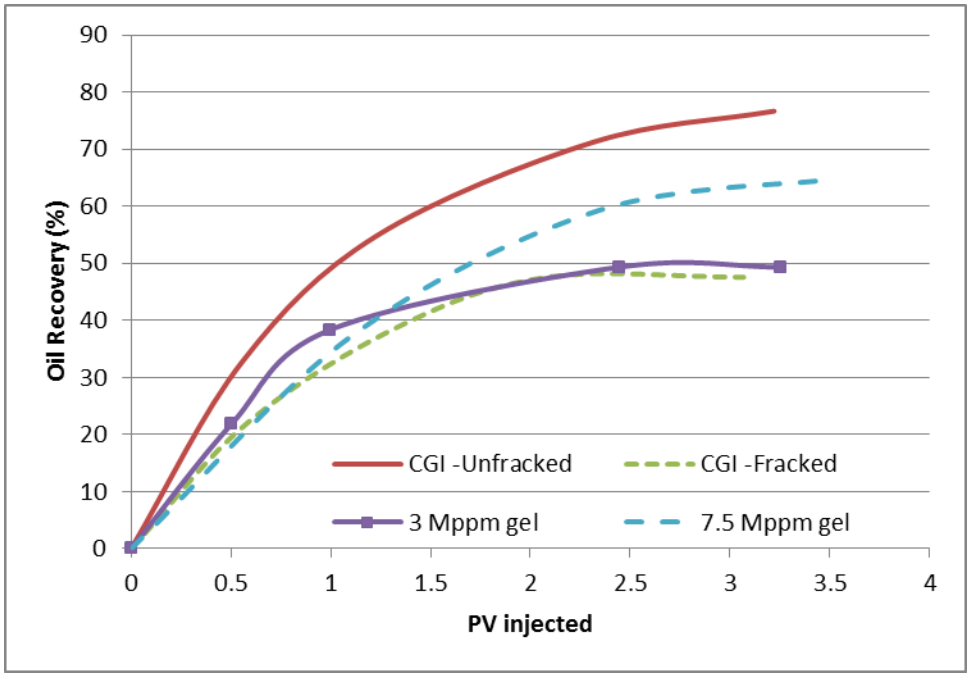

Fig.4.45 – 7,500 PPM Gel – Fractured Limesone CGI Flood Recovery Curve (Exp#5)

Table 4.8 – 7,500 PPM Gel – Fractured Limesone CGI Flood Recovery Data (Exp#5)

PV_{inj}	1.12	2.34	3.48
Rec(%)	37.7	59.2	64.6

The OOIP in the core prior to the injection of the CO_2 was estimated to be 9.29 cc. At the end of the experiment, about 6 cc of the oil was recovered accounting for about 64.6% RF of the OOIP. See **Fig.4.45 and Table 4.8.** In comparison with the previous results the 7,500 ppm gel application resulted in an incremental recovery of 17% compared to the CGI without gel treatment and 15% more oil than the failed gel treatment with concentration of 3,000 ppm. The treatment is still less than ideal and more improvements could be added to the current treatment. In the next experiment, the gel concentration will be increased one more time in an attempt to have lower degree of leak-off and mobility control enhancement during CO_2 flooding. Success in achieving this goal will reflect the recovery data and can be evaluated qualitatively with the CT images.

4.5.3 10,000 PPM Gel Application

In the previous study to control CO_2 mobility in the fracture, moderate concentration 7,500 ppm HPAM gel was tested. The application resulted in incremental recovery compared to the untreated core and compared to the one treated with low concentration 3,000 ppm HPAM gel. The incremental recovery satisfactory but there

was still some room for improvement. The gel exhibited limited leak off and breakdown resulting in small fraction of the gel produced with the recovered oil. The study was expanded with using 10,000 ppm HPAM gel cross-linked with 1,000 ppm of Cr(III)Ac (with 6 wt.% KI dopant). The gel performance was evaluated both quantitatively and qualitatively using the recovery data and CT imaging technique. At the time of gel injection, the gel was characterized to be "very thick fluid".

Before the coreflood experiment, the core was first studied for porosity using the weight difference approach as in the typical procedure detailed earlier. The core was left in the oven for two days under temperature higher than 100 ^{o}C; the core was then weighed and saturated with brine using a vacuum pump. The brine saturated core was then weighed and scanned under the CT scanner; then the core was cut in the center and heated again in the oven. In the meanwhile, the gel ingredients were mixed together using a magnetic stirrer until the mixture got homogenous; the gel was allowed to stir for about 8 hours. The gel was then allowed to reside for 12 hours. After that, the fractured core was placed under a confining pressure of 2000 psi and under temperature of 70 °F and the dry core was scanned. Then, the oil was injected with outlet valve closed to establish the oil saturation. Five pore volumes of doped oil (about 50 cc) were injected while keeping the outlet valve closed; the core was then left for 8 hours under high pressure. The outlet valve was then opened and five more pore volumes of oil were injected to ensure complete saturation with oil; then the core was CT scanned. Then, 30 cc of preformed gel were injected at injection pressure of around 100 psi; the outlet

valve was left open for the gel to exit and not flow back inside the core. The system was then left intact for the gel to strengthen.

Prior to the CO_2 injection, a CT scan was taken to evaluate the gel placement. Afterwards, warm water was circulated in the bath around the coreholder for about 30 minutes at a temperature of 120 °F to establish equilibrium state. The CO_2 was then injected at 1700 psi at supercritical conditions. The recovery data were recorded and several CT scans were taken.

To qualitatively assess the success of the gel treatment and the flood the CT images were colored depending of the CT intensity across the core. **Fig.4.46 through 4.58** show the coloring spectrum used in the images, scans of the CO_2 saturated core, oil saturated core and scans after 1 and 3 PV of CO_2 injection respectively.

For this experiment, the difference in CT intensity between the doped oil (0.76 g/cc) and the supercritical CO_2 (0.58 g/cc) eased the view and the evaluation of the success of the flood. The gel with higher density and enhanced CT reading with KI dopant was viewed with higher CT reading. Therefore, the coloring spectrum was chosen in way covering the CT numbers with the darkest reddish coloring indicates the presence of oil while the lighter coloring, shifting towards yellow and green indicates the unswept areas or the fracture or vugs.

Fig.4.46 – CT Images Color Spectrum (Exp#6)

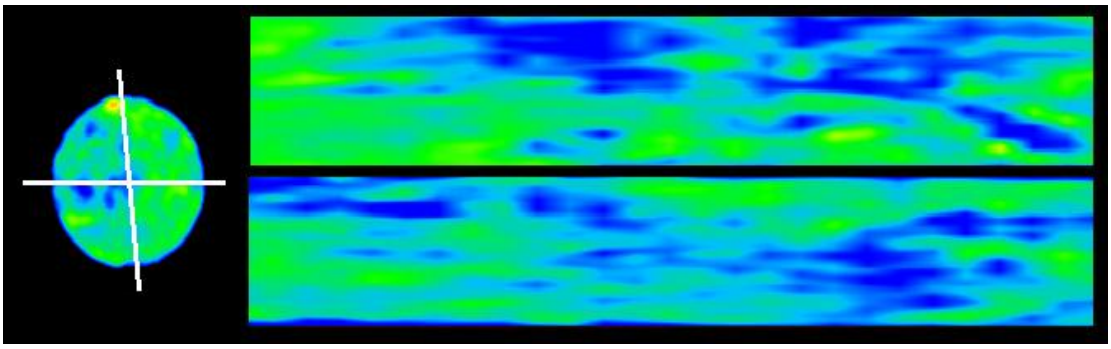

Fig.4.47 – CT Image of CO_2 Saturated Core (Exp#6)

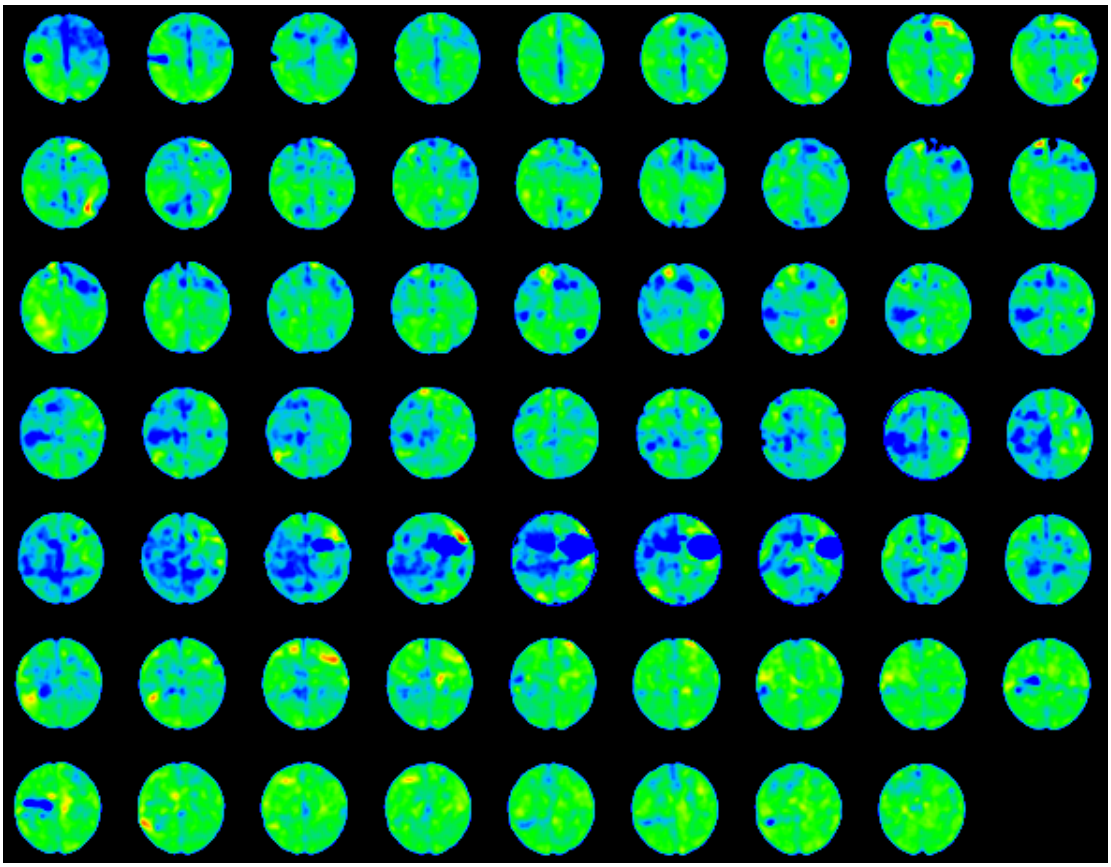

Fig.4.48 – Vertical Slice CT Images of CO_2Saturated Core (Exp#6)

CO_2 has low density and CT value. The CO_2 saturated images show very low CT intensity. Most of the image is colored with dark green with some spots reaching dark blue. Some of the spots had a dark yellow or reddish yellow indicating high density region or dead pores. If this is true, these spots would not be affected that much by the oil saturation or the flood process.

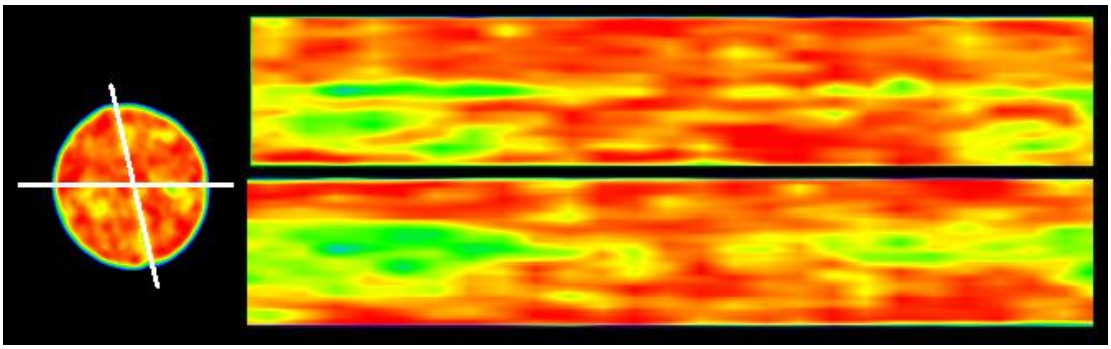

Fig.4.49 – CT Image of Oil Saturated Core (Exp#6)

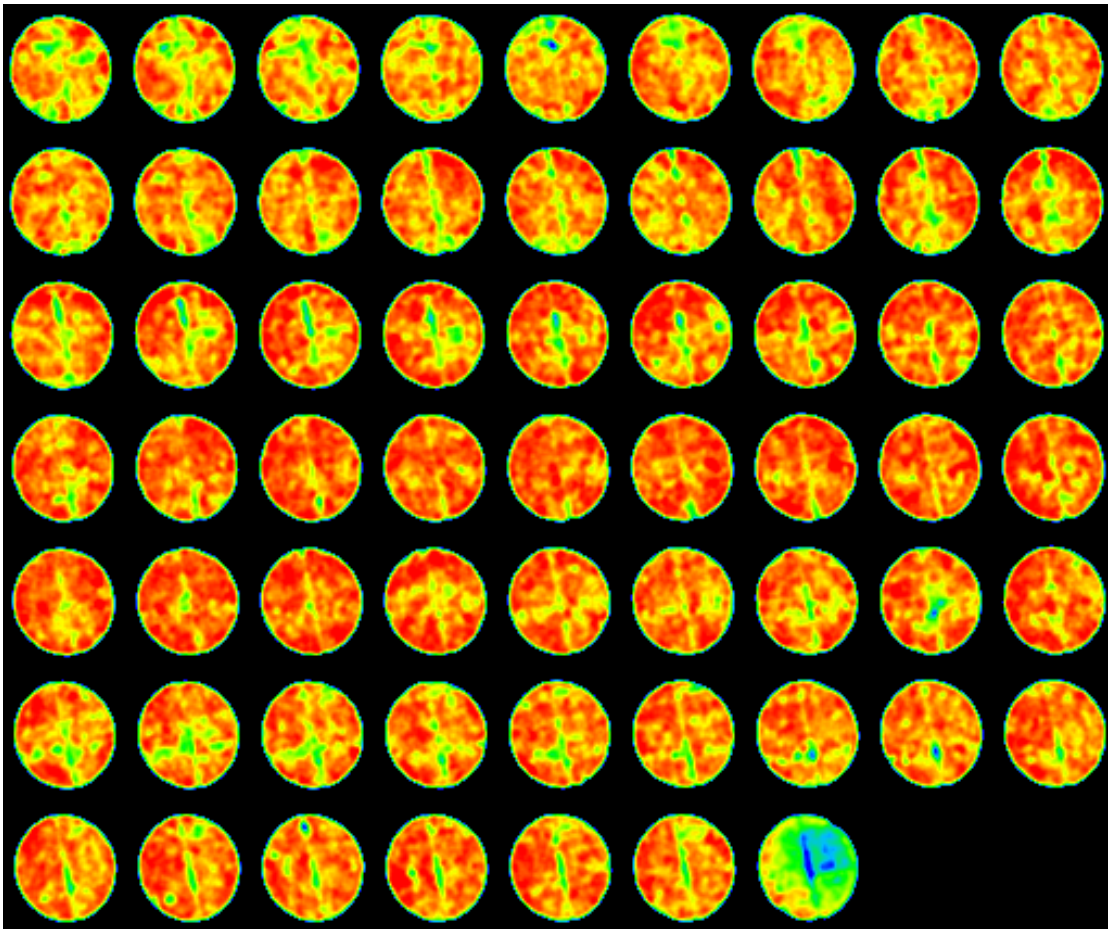

Fig.4.50 – Vertical Slice CT Images of Oil Saturated Core (Exp#6)

The oil saturated images show that the core was saturated with oil to a great extent. The whole image was colored with red while the fracture area colored with yellow to dark green. Some of the spots had a dark yellow color having intensity close to that that of the fracture. Some spots continued to have dark green-blue color. These variations in the colors of the matrix show the heterogeneity of this core indicating the

presence of some vugs or non-uniform pores. If this is true, these spots would be swept better than others.

The upper slab, corresponding to the horizontal cross-section and intersecting the fracture plane, suggest that the fracture have a rough surface that fluctuates in width. The lower slab, vertical cross-section, running across the fracture shows dark green color (shift to left on the color spectrum bar) and yellowish red coloring across the plane. The low CT numbers confirm the plane was positioned that it intersected the fracture and some parts of the matrix. This cross-section will aid in evaluating the success degree of gel placement afterwards.

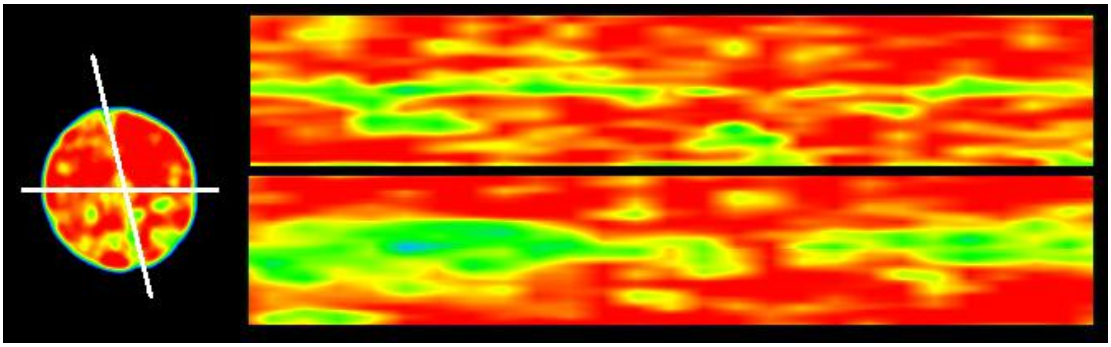

Fig.4.51 – CT Image of Oil Saturated Core after Gel Treatment (Exp#6)

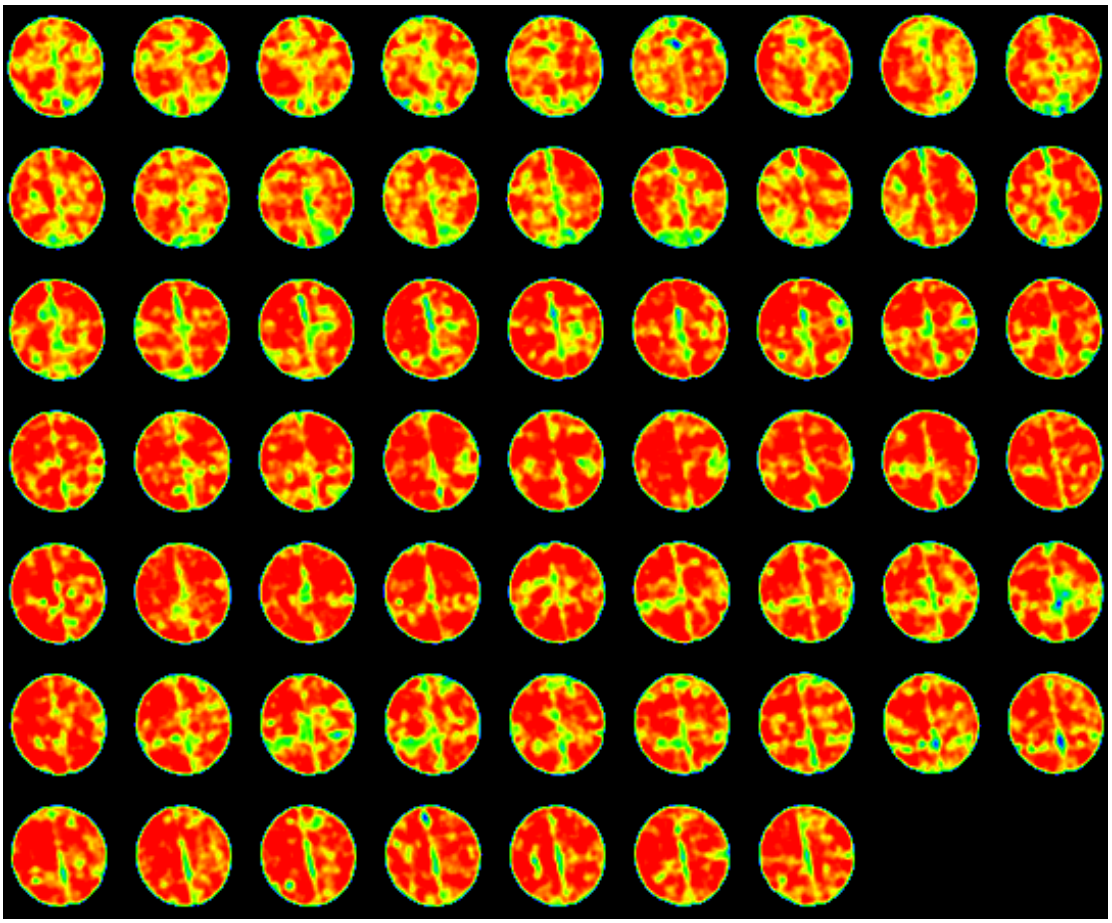

Fig.4.52 – Vertical Slice CT Images of Oil Saturated Core after Gel Treatment (Exp#6)

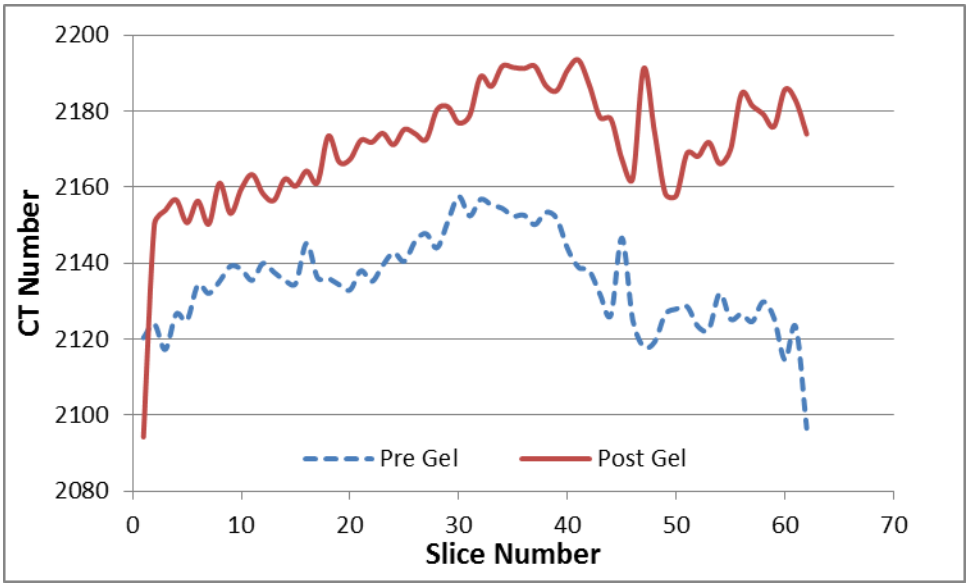

Fig.4.53 – CT Intensity Before and After Gel Treatment (Exp#6)

After the gel placement, the gel with higher density and CT value darkened the colors. The horizontal cross-section shows that the fracture changed color slightly shifting towards higher CT intensity. However, the image shows that small spots around the fracture barely changed their color suggesting that a very limited degree of leakoff. It is assumed based on the visual evaluation of the images that the leakoff is very low. The vertical slab passing through the fracture plane shows that the most of the blue areas changed into dark green and the reddish areas got darker after the placement of the gel; the color shift due to CT intensity increase acts as an indication of the successful placement of the gel. Confirming these observations requires direct gel strength and stability evaluation with the coreflood and assessing the recovery efficiency and the recovered liquids. Two scans were taken at different times during the waterflood to take a deeper look at the flood behavior.

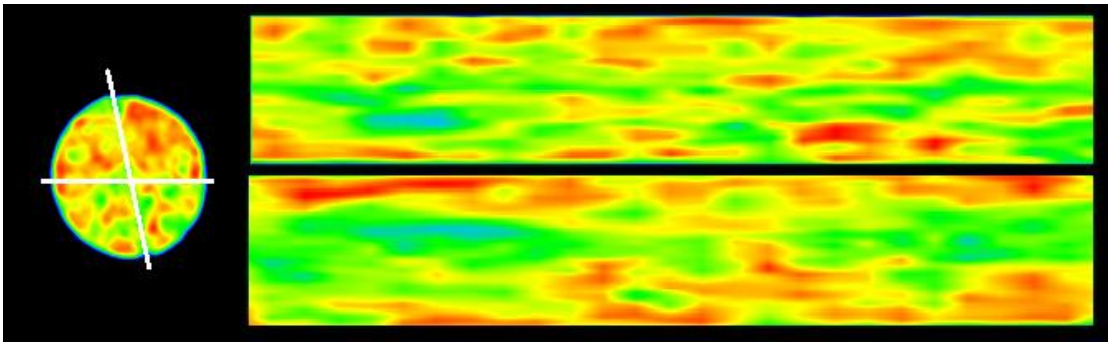

Fig.4.54 – CT Image of Oil Saturated Core Flooded With 1PV of CO_2 (Exp#6)

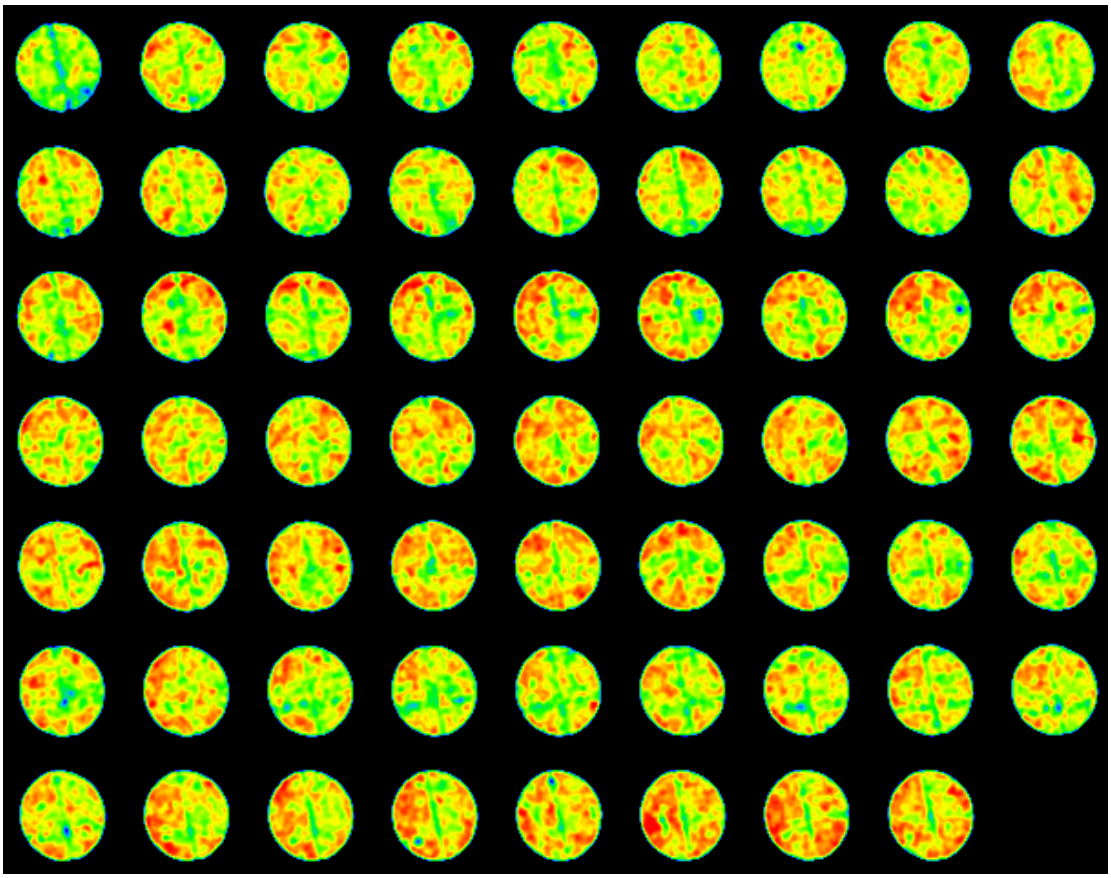

Fig.4.55 – Vertical Slice CT Images of Oil Saturated Core Flooded With 1PV of CO_2 (Exp#6)

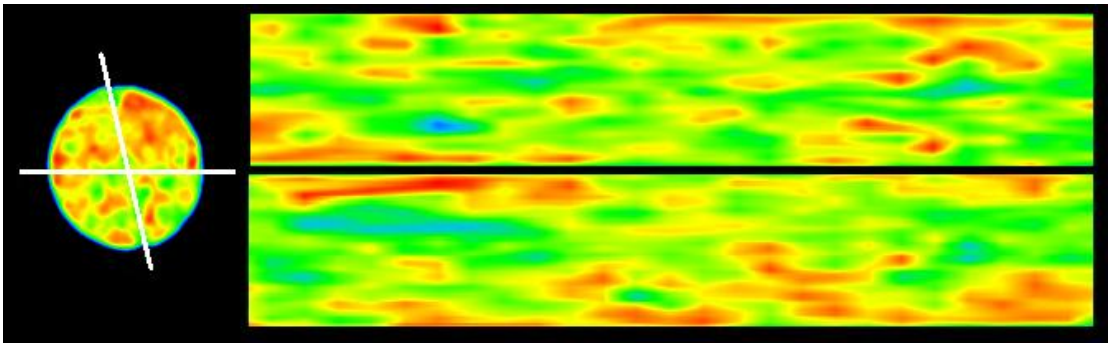

Fig.4.56 – CT Image of Oil Saturated Core Flooded With 3PV of CO_2 (Exp#6)

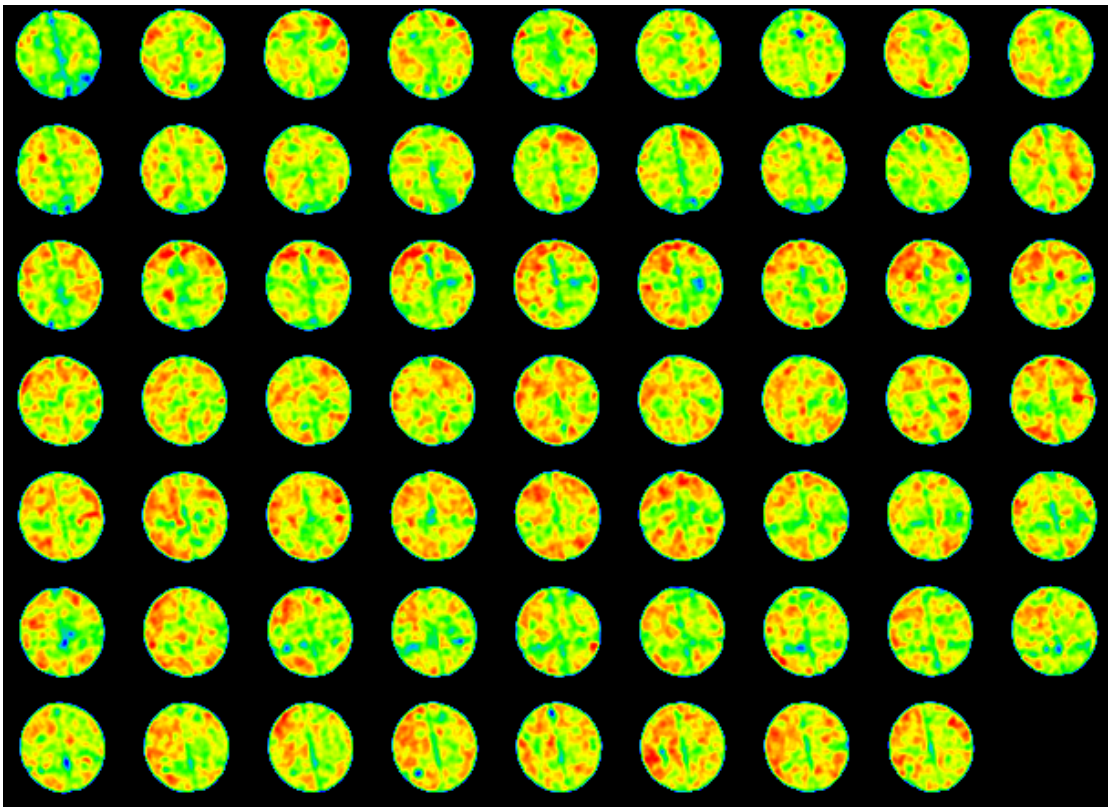

Fig.4.57 – Vertical Slice CT Images of Oil Saturated Core Flooded With 3PV of CO_2 (Exp#6)

The coreflood was carried out with the CO_2 entering at 1,700 psi and 120 ^{o}F. The CO_2 breakthrough was successfully delayed with minimal gel produced with the recovered oil. The horizontal slab shows that the fracture area got colored in green-yellow with CT intensity comparable to that of pre-gel image; this confirms that the gel remained in the fracture to a good extent. Low amount of the gel was produced with the first PV of CO_2. Small spots of the core remained the same after the coreflood having dark red color while others got flushed greatly reaching dark green – blue color close to

that of CO_2 saturated core. Most of the rock was flushed in efficiently; some portions were flushed relatively better than others due to the heterogeneity of the core.

Ideal gel placement will place the gel only in the fracture and that gel would remain the fracture plugging it against low viscosity CO_2. The gel was very strong and it small amount flowed with the produced oil and minimal amount appears to have leaked off into the matrix. A big fraction of the injected gel contributed to the mobility control hindering the flow of CO_2 forcing it to flow the matrix. The spots in the core those were red in the CO_2 saturated core CT image remained the same during the oil saturation and the flood process indicating some dead small pores.

In comparison between **Fig.4.54 and 4.55 vs. Fig.4.56 and 4.57**, the effect of the last PV of CO_2 is highlighted. The image shows that more incremental recovery was achieved with this PV of CO_2.This is observed by noticing that some spots experienced color shifting from red to yellow, yellow to green and slight ones shifting from green to blue.

The recovery data are shown as follows:

Table 4.9 – 10,000 PPM Gel – Fractured Limesone CGI Flood Recovery Data (Exp#6)

PV_{inj}	0.68	1.34	2.18	3.38
Rec(%)	21.4	45.6	64.3	69.7

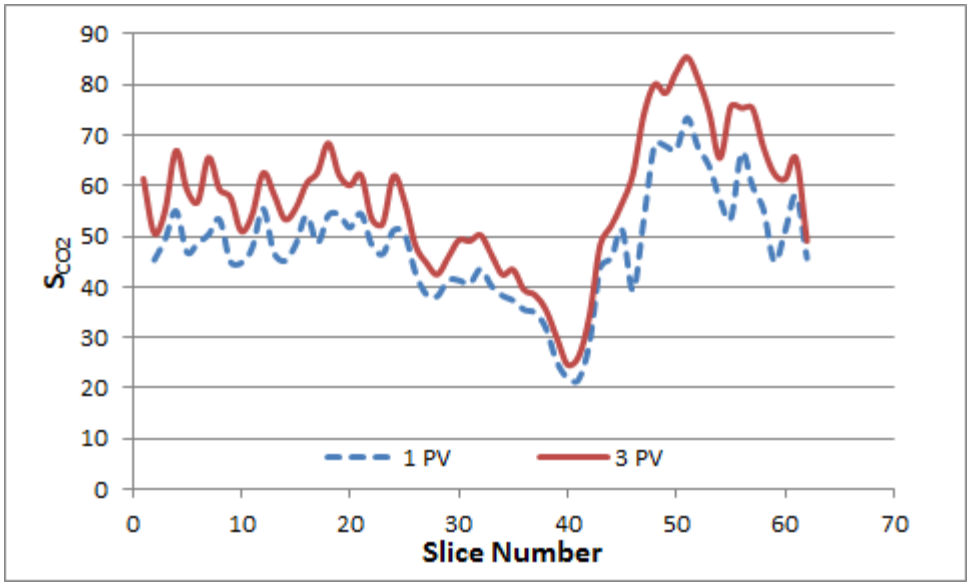

Fig.4.58 – 10,000 PPM Gel – CO_2 Saturation Across The Core (Exp#6)

CT data was processed to estimate CO_2 saturation changes between the two scans. **Fig.4.58** shows the CO_2 profile across the core. As with the CT intensity, the CO_2 saturation was unevenly distributed across the core. The CO_2 saturation was lower in the middle part were through the previous CT images we noticed that the fracture was slightly narrower than the rest of the core. This observation aids us in noticing the contribution of the fracture opening to the overall CO_2 saturation across the slice attained from the CT intensity data.

The OOIP in the core prior to the injection of the CO_2 was estimated to be 9.3 cc. At the end of the experiment, about 6.5 cc of the oil was recovered accounting for about 70% RF of the OOIP. See **Fig.4.59 and Table 4.9.**

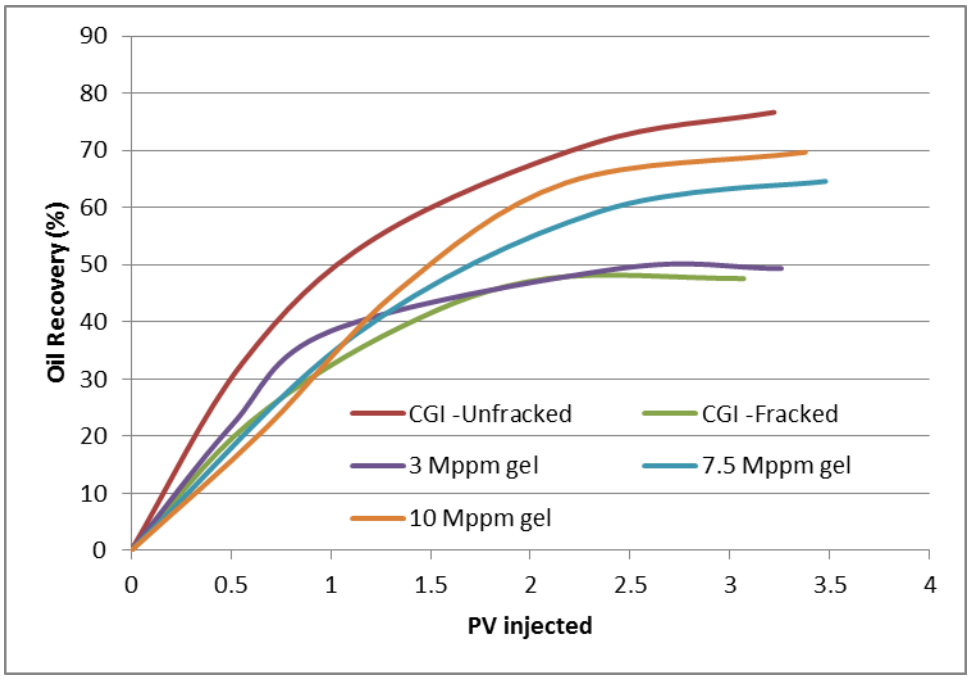

Fig.4.59 – 10,000 PPM Gel – Fractured Limesone CGI Flood Recovery Curve (Exp#6)

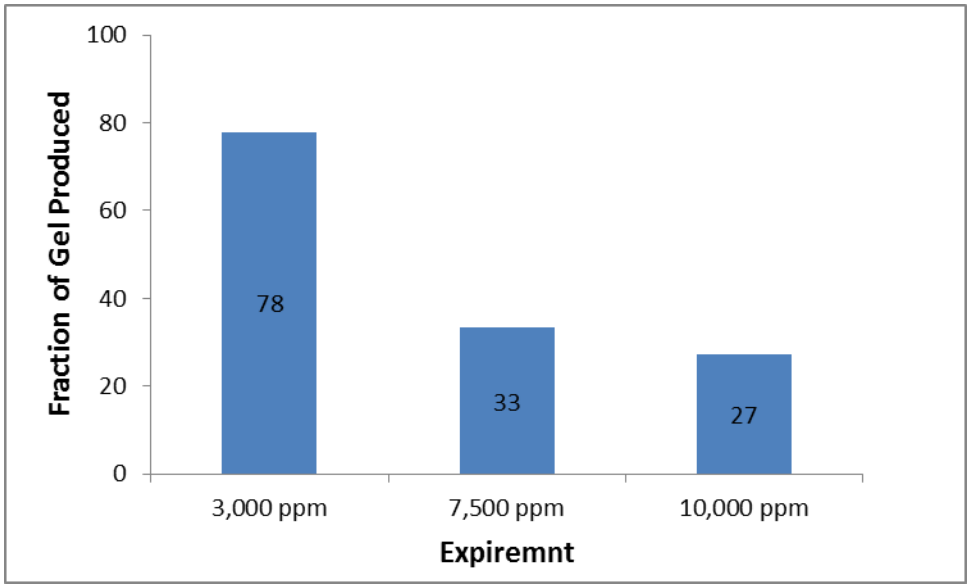

Fig.4.60 – Fraction of Gel Produced Ultimatily Produced

In comparison with the previous results, the 10,000 ppm gel application resulted in an incremental recovery of 22% compared to the CGI without gel treatment and 20% more oil than the failed gel treatment with concentration of 3,000 ppm. The difference between the 7,500 ppm gel and the 10,000 ppm gel is about 5% in terms of ultimate recovery. It is difficult to attribute that 5% to the gel alone and not considering the effect of the core itself. However, the lower degree of leakoff observed using the CT images and the lower amount of gel produced during the experiment assures that that the 10,000 ppm gel is more stable and resistant against CO_2 floods. The treatment gave satisfying results with 7% only less recovery than the ideal unfractured core. **Fig.4.60** shows the amount of gel produced as percentage of the gel resided i.e. lost to the core during placement. The change in gel composition lowered the gel production to 27-33% for the 7,500 and 10,000 ppm respectively to more than 78% with the low concentration 3,000 ppm gel. The percentage of gel produced gives a direct indication of how resistant the gel is to injected fluid which directly affects the overall oil recovery. The difference between the 7,500 and 10,000 ppm was again not as significant as these two compared to the 3,000 ppm case. In the next stage of experiment, different approach will be tested with the HPAM polymer in addition to Xanthan to viscosify the water alternating with gas.

4.6 Experiments in Fractured Limestone Using Viscosified Water Alternating Gas (VWAG)

In the previous experiments, cross-linked gels were tested for conformance control effectiveness. The results were encouraging showing high recovery factors with successful treatments. Another approach employs the use of alternating cycles of water and CO_2.To avoid excessive CO_2 breakthrough through the fractures or higher permeability areas, a cheaper and more viscous water is used to hinder the advance of CO_2 flood front. Water and CO_2 are injected in cycles of small pore volumes (5% or less) until the desired amount of gas is injected. The alternating cycles of CO_2 and water combine the microscopic efficiency of CO_2 in extracting oil with the macroscopic sweep efficiency of the water.(Chakravarthy et al. 2006)

The WAG approach has been studied extensively in the literature. Another tweak that can be added to the WAG is to viscosify the water with polymers. The goal is to increase the water viscosity to an extent delaying the CO_2 breakthrough without having the viscosity too high that the water acts like a gel with very low mobility. Previous attempts were conducted adding amounts of polymers without cross-linking agents. Excessive amounts of viscosified water diffused into the matrix leaving the fractures open to CO_2 flow. The recovery efficiency was thus harmed. (Chakravarthy et al. 2006)

In this set of experiments we decided to evaluate the effectiveness of WAGs coupled with viscosifying the chase water. In order to minimize the leakoff to the matrix, small amounts of cross-linkers will be added to the viscosified water to thicken the water so that it remains in the permeable channels and fractures decelerating the advance of the

CO_2 to the best possible degree. Four preliminary tests were designed using two chemicals: PAM and Xanthan gum polymers. Each polymer was tested for the same concentration with two different cross-linker concentrations.

For all of the following experiments, the cores were cut in the center in the same manner described earlier. The experimental results showed incremental recovery of WAG application compared to plain CGI or waterflood. The performance was even better with lower degree of leakoff. It is assumed that the viscous water will flow more through the super highway fractures than through the matrix. This assumption was tested and will be discussed next. The procedure for all the experiments was the same; one pore volume of viscosified water was first injected to heal the fracture chased by one pore volume of CGI of CO_2 to see how much oil will be recovered due to the CO_2 only after sweeping the rock with viscosified water; at last, one pore volume of viscosified water was injected to assess the feasibility of additional pore volumes of injection fluids.

4.6.1 PAM Viscosified Water Alternating Gas (VWAG) Conc#1

The first experiment utilized 3,000 ppm HPAM polymer cross-linked with 50 ppm of Cr(III)Ac (with 6 wt.% KI dopant).At the time of viscosified water injection, the fluid was characterized to be "very runny fluid".

Before the coreflood experiment, the core was first studied for porosity using the weight difference approach as in the typical procedure detailed earlier. The core was left in the oven for two days under temperature higher than 100 ^{o}C; the core was then weighed and saturated with brine using a vacuum pump. The brine saturated core was

then weighed and scanned under the CT scanner; then the core was cut in the center and heated again in the oven. In the meanwhile, the viscosified water ingredients were mixed together using a magnetic stirrer until the mixture got homogenous; the mixture was allowed to stir for about 8 hours. After that, the fractured core was placed under a confining pressure of 2000 psi and under temperature of 70 °F and the dry core was scanned. Then, the oil was injected with outlet valve closed to establish the oil saturation. Five pore volumes of doped oil (about 50 cc) were injected while keeping the outlet valve closed; the core was then left for 8 hours under high pressure. The outlet valve was then opened and five more pore volumes of oil were injected to ensure complete saturation with oil; then the core was CT scanned.

Warm water was circulated in the bath around the coreholder for about 30 minutes at a temperature of 120 °F to establish equilibrium state. Prior to any injection, a CT scan was taken to evaluate the injected fluids performance. After that, one pore volume of viscosified water was injected at injection pressure of around 100 psi. The CO_2 was then injected at 1700 psi at supercritical conditions. A third pore volume of viscosified water was injected at injection pressure of 100 psi. The recovery data were recorded and several CT scans were taken.

To qualitatively assess the success of the flood, the CT images were colored depending of the CT intensity across the core. **Fig.4.61 through 4.69** shows the coloring spectrum used in the images scans of the oil saturated core and different CT scans during the flood.

For this experiment, the difference in CT intensity between the doped oil (0.76 g/cc) and the supercritical CO_2 (0.58 g/cc) facilitated the view and the evaluation of the success of the flood. The viscosified water with higher density and enhanced CT reading with KI dopant was seen with higher CT reading. Therefore, the coloring spectrum was chosen in way covering the CT numbers with the darkest reddish coloring indicates the presence of VW and oil while the lighter coloring, shifting towards yellow and green indicates the unswept areas or the fracture or vugs.

Fig.4.61 – CT Images Color Spectrum (Exp#7)

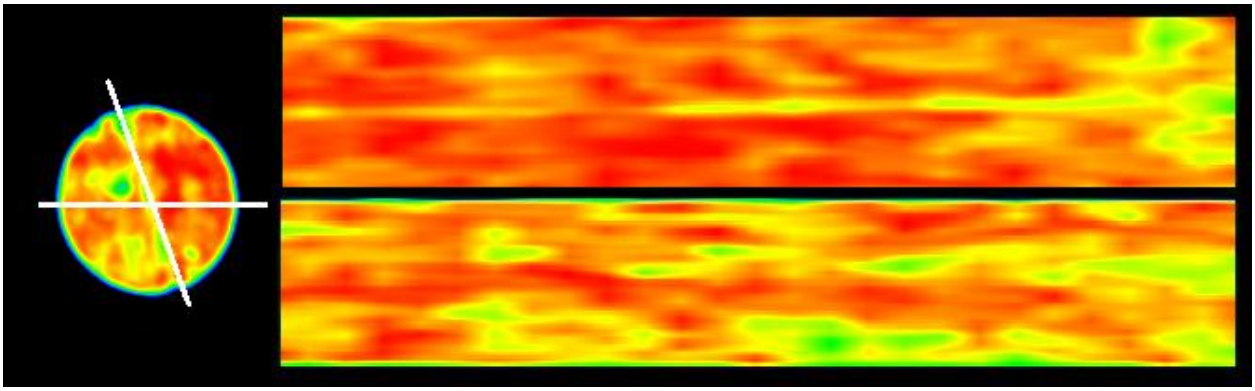

Fig.4.62 – CT Image of Oil Saturated Core (Exp#7)

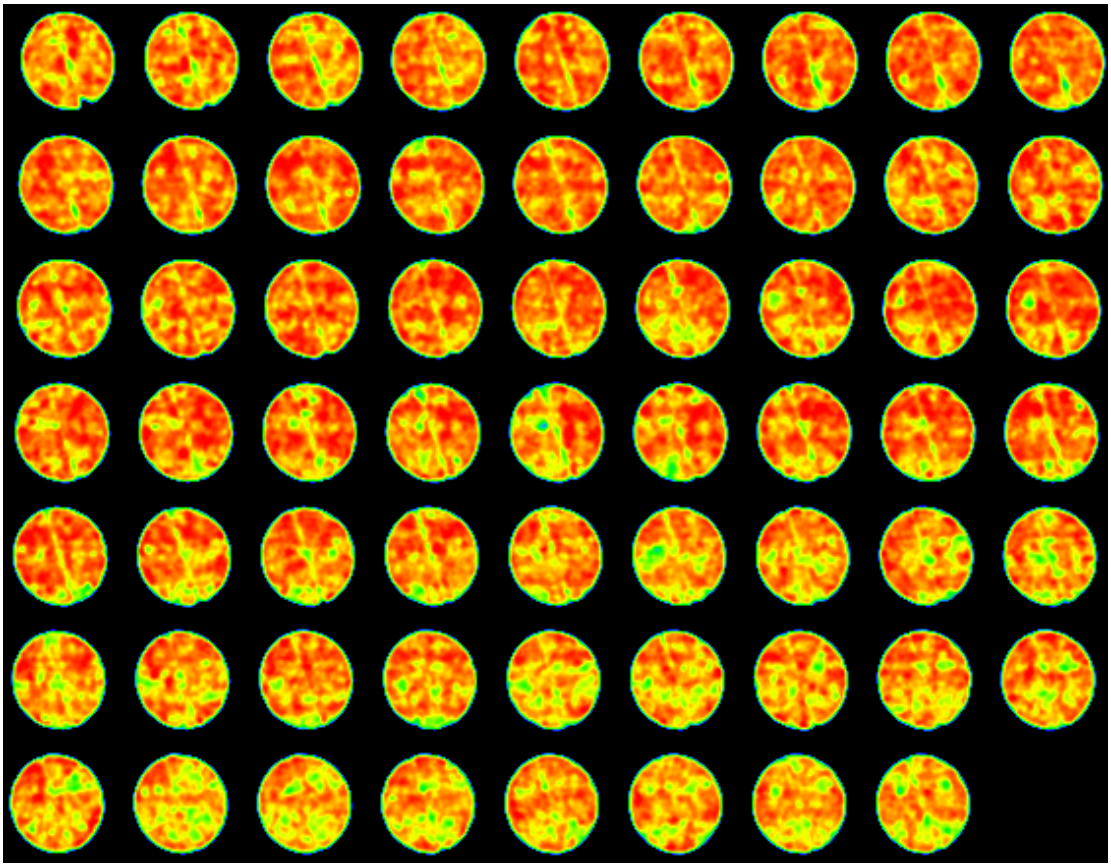

Fig.4.63 – Vertical Slice CT Images of Oil Saturated Core (Exp#7)

The oil saturated core images show that the core was saturated with oil to a great extent. The image was colored with red except the fracture area colored with yellow to light green. Some of the spots show slightly lighter colors indicating the presence of small vugs or relatively larger pores.

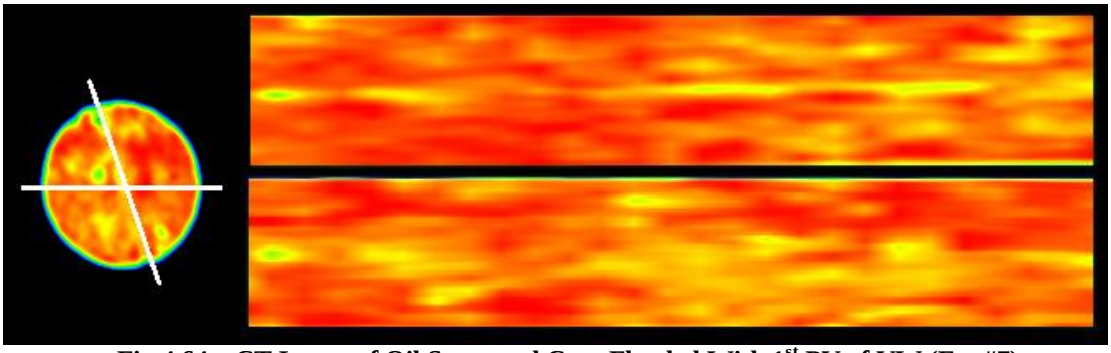

Fig.4.64 – CT Image of Oil Saturated Core Flooded With 1st PV of VW (Exp#7)

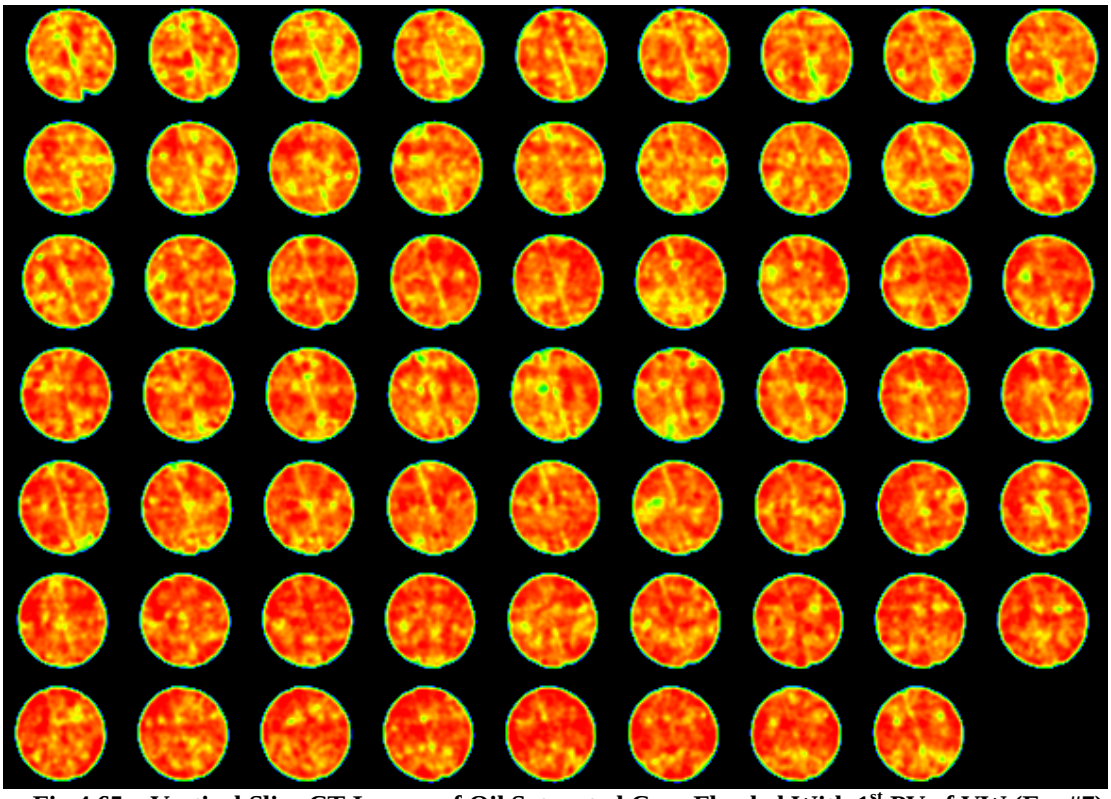

Fig.4.65 – Vertical Slice CT Images of Oil Saturated Core Flooded With 1st PV of VW (Exp#7)

The first PV of viscosified water was injected producing about 22% of the IOIP. After the injection, the VW with higher density and CT value darkened the colors. The vertical slab which passes through the fracture plane shows that the some yellow areas remained the same after the injection while some spots got reddish in color indicating the tendency of the viscous water flow and successful placement in some areas and not in the others. The horizontal cross-section image confirms the same conclusion; the relatively wider segment portion of the fracture remained yellow in color. Moreover, the horizontal cross section also shows that the areas directly around the fracture got darker in color which suggests that some of the VW "leaked off" into the matrix; this was more visible in the areas that were yellow in color prior to the injection of the VW. Confirming these observations requires direct evaluation with the coreflood assessing the recovery efficiency and the recovered liquids.

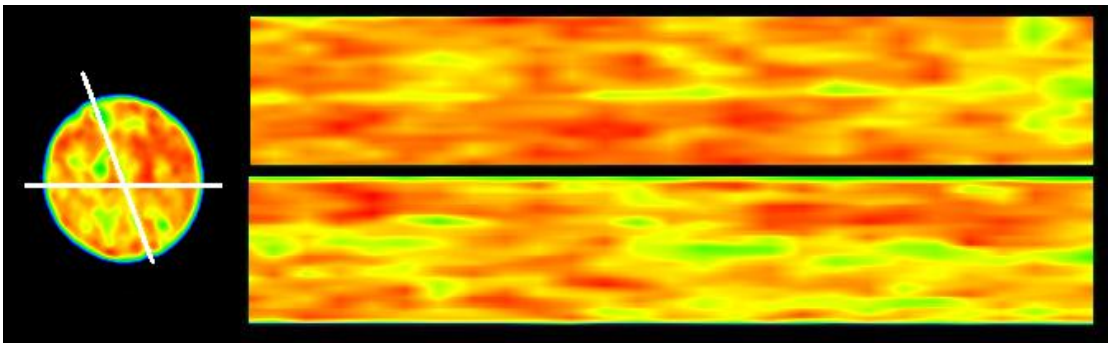

Fig.4.66 – CT Image of Oil Saturated Core Flooded With 1PV of CO_2 (Exp#7)

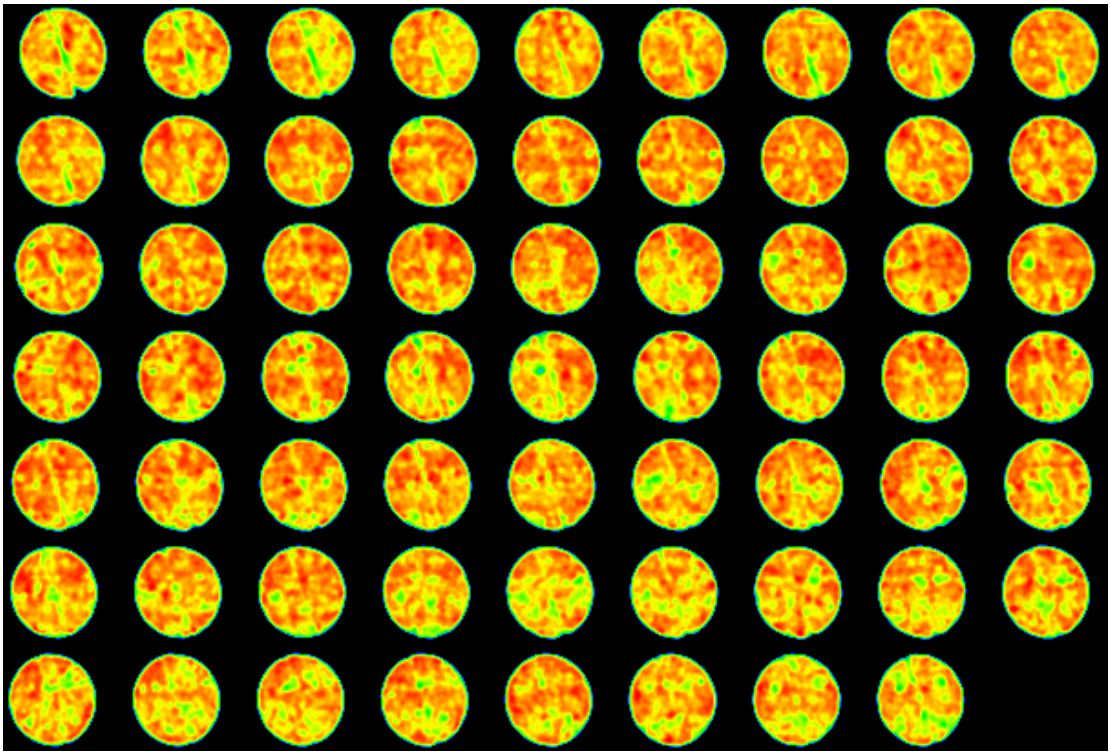

Fig.4.67 – Vertical Slice CT Images of Oil Saturated Core Flooded With 1PV of CO_2 (Exp#7)

Injecting the CO_2 after the first PV of viscosified water produced incremental oil of about 22% elevating the total recovery to about 44% of the IOIP. With the CO_2 having lower CT number , the overall CT images got lighter in color shifting towards light red and yellow. The vertical slab through the fracture plane shows that the area got much lighter in color reaching color intensities close to that prior to the injection of the VW; this observation indicates that some of the viscous water did not remain in the fracture and was produced. The horizontal cross-section image shows that CO_2 diffused into the matrix pushing some oil out of the pores. However, many areas remained

reddish indicating the poor sweep to these areas and that significant amount oil (about 56%) remained untouched.

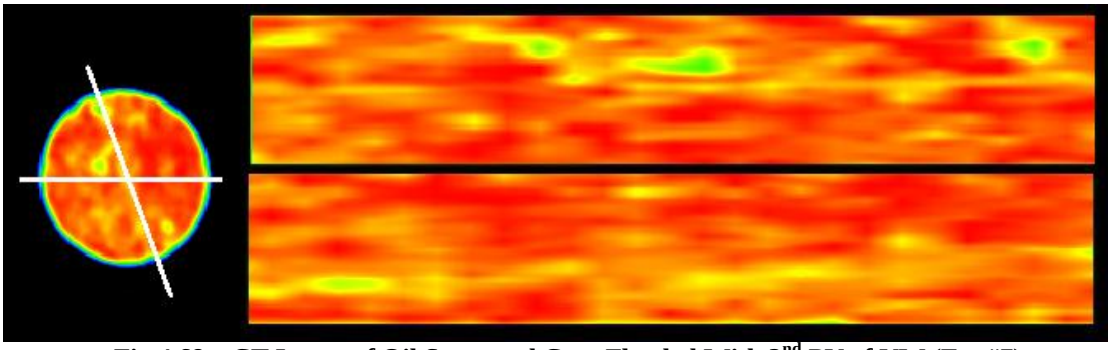

Fig.4.68 – CT Image of Oil Saturated Core Flooded With 2nd PV of VW (Exp#7)

Fig.4.69 – Vertical Slice CT Images of Oil Saturated Core Flooded With 2nd PV of VW (Exp#7)

The coreflood was carried out with the CO_2 entering at 1,700 psi and 120 ^{o}F. The horizontal slab shows that the viscosified water did not remain in place. Small spots of the core remained the same after the coreflood having dark red color. Most of the rock was flushed in inefficient way; some portions were flushed relatively better than others due to the heterogeneity of the core.

It was assumed that the viscosified water would not enter the matrix region; however the CT images showed a contradicting finding. Ideal application will place the

viscosified water in the fracture and that it would remain the fracture plugging it against low viscosity CO_2. The viscosified water was not strong enough and it flowed with the produced oil and some of it leaked off into the matrix. Only a small portion acted in hindering the flow of CO_2 forcing it to flow the matrix.

The recovery data are shown as follows:

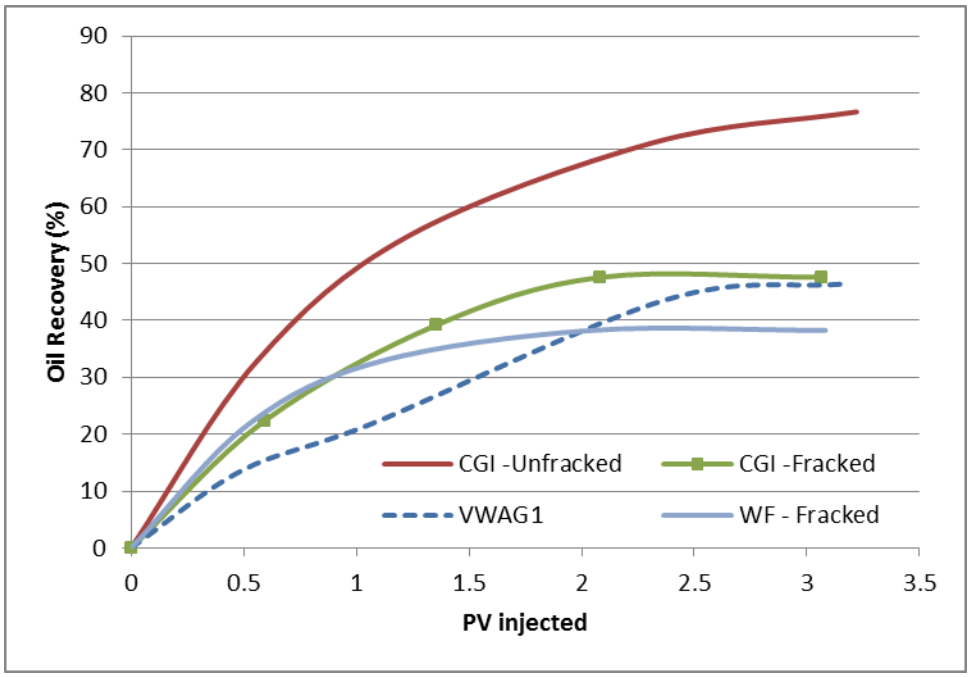

Fig.4.70 – VWAG1 – Fractured Limesone Flood Recovery Curve (Exp#7)

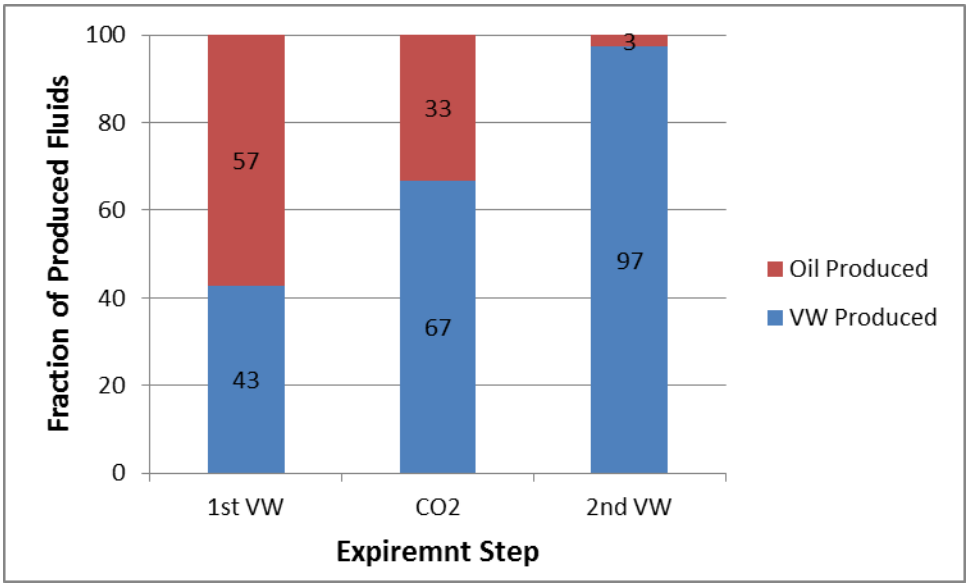

Fig.4.71 – VWAG1 – Fractions of Produced Fluids (Exp#7)

Table 4.10 – VWAG1 – Fractured Limesone Flood Recovery Data (Exp#7)

PV_{inj}	0.49	1.07	2.38	3.18
Rec(%)	13.7	21.9	43.7	46.5

The OOIP in the core prior to the injection of the CO_2 was estimated to be 9.15 cc. At the end of the experiment, about 4.3 cc of the oil was recovered accounting for about 46.5% RF of the OOIP. See **Fig.4.70 and Table 4.10.** **Fig.4.71** shows the fractions of produced fluids with the progress of the experiment. The figure shows that fraction of VW was low in the first stage with significant amount of oil produced and got higher with time as it looks totally unattractive with the third pore volume with only negligible amount oil produced. In comparison with the previous results the VWAG application resulted in an incremental recovery of 8% only compared to the plain water

flood; the recovery was close to that of the CGI in untreated fractured core. The application is far from perfect and one of things that need to be modified was the cross-linker concentration. In the next experiment, the cross-linker concentration will be increased to avoid excessive leak-off during CO_2 flooding. Success in achieving this goal will reflect the recovery data and can be evaluated qualitatively with the CT images.

4.6.2 PAM Viscosified Water Alternating Gas (VWAG) Conc#2

In the previous study to control CO_2 mobility in the fracture, concentration of 3000 ppm HPAM was used to viscosify water alternating with the gas. The application did not show significant increment in total oil recovery compared to the untreated core flooded with CGI. The viscosified water exhibited leakoff and breakdown resulting in significant fraction of the viscosified water produced with the recovered oil. The study was expanded with using the same polymer concentration of 3,000 ppm HPAM gel while doubling the cross-linker concentration (with 6 wt. % KI dopant). The performance was evaluated both quantitatively and qualitatively using the recovery data and CT imaging technique. At the time of viscosified water injection, the fluid was characterized to be "very runny fluid".

Before the coreflood experiment, the core was first studied for porosity using the weight difference approach as in the typical procedure detailed earlier. The core was left in the oven for two days under temperature higher than 100 ^{o}C; the core was then weighed and saturated with brine using a vacuum pump. The brine saturated core was then weighed and scanned under the CT scanner; then the core was cut in the center and

heated again in the oven. In the meanwhile, the viscosified water ingredients were mixed together using a magnetic stirrer until the mixture got homogenous; the mixture was allowed to stir for about 8 hours. After that, the fractured core was placed under a confining pressure of 2000 psi and under temperature of 70 °F and the dry core was scanned. Then, the oil was injected with outlet valve closed to establish the oil saturation. Five pore volumes of doped oil (about 50 cc) were injected while keeping the outlet valve closed; the core was then left for 8 hours under high pressure. The outlet valve was then opened and five more pore volumes of oil were injected to ensure complete saturation with oil; then the core was CT scanned.

Warm water was circulated in the bath around the coreholder for about 30 minutes at a temperature of 120 °F to establish equilibrium state. Prior to any injection, a CT scan was taken to evaluate the injected fluids performance. After that, one pore volume of viscosified water was injected at injection pressure of around 100 psi. The CO_2 was then injected at 1700 psi at supercritical conditions. A third pore volume of viscosified water was injected at injection pressure of 100 psi. The recovery data were recorded and several CT scans were taken.

To qualitatively assess the success of the flood, the CT images were colored depending of the CT intensity across the core. **Fig.4.72 through 4.80** shows the coloring spectrum used in the images scans of the oil saturated core and different CT scans during the flood.

For this experiment, the difference in CT intensity between the doped oil (0.76 g/cc) and the supercritical CO_2 (0.58 g/cc) facilitated the view and the evaluation of the

success of the flood. The viscosified water with higher density and enhanced CT reading with KI dopant was seen with higher CT reading. Therefore, the coloring spectrum was chosen in way covering the CT numbers with the darkest reddish coloring indicates the presence of VW and oil while the lighter coloring, shifting towards yellow and green indicates the unswept areas or the fracture or vugs.

Fig.4.72 – CT Images Color Spectrum (Exp#8)

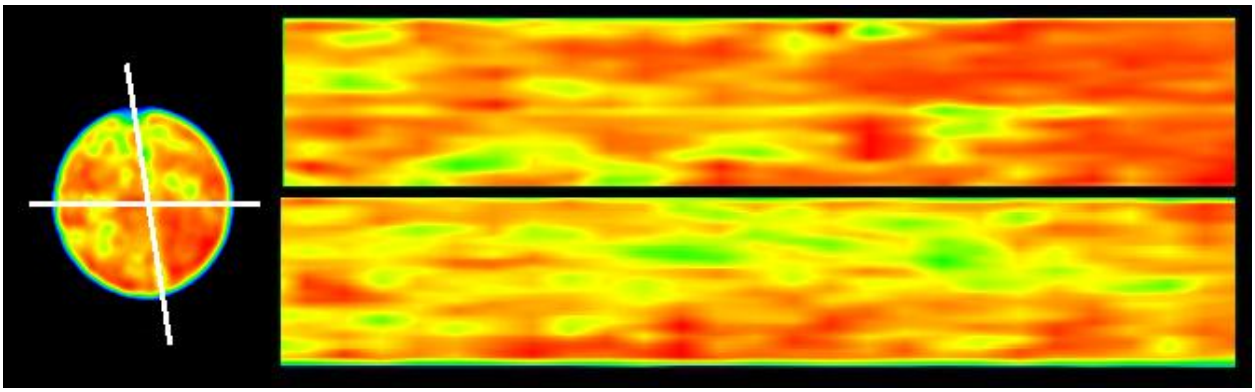

Fig.4.73 – CT Image of Oil Saturated Core (Exp#8)

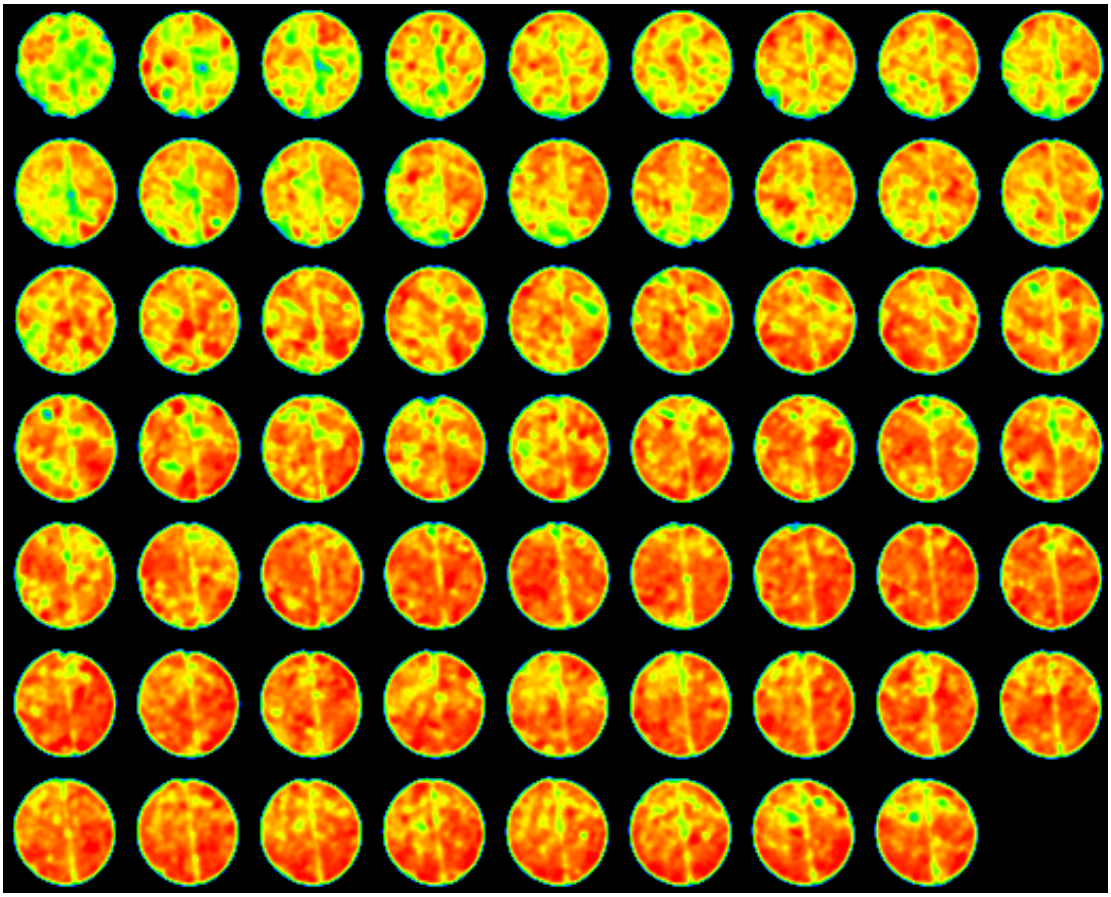

Fig.4.74 – Vertical Slice CT Images of Oil Saturated Core (Exp#8)

The oil saturated core images show that the core was saturated with oil to a great extent. The image was colored with red except the fracture area colored with yellow to light green. Some of the spots show slightly lighter colors indicating the presence of small vugs or relatively larger pores.

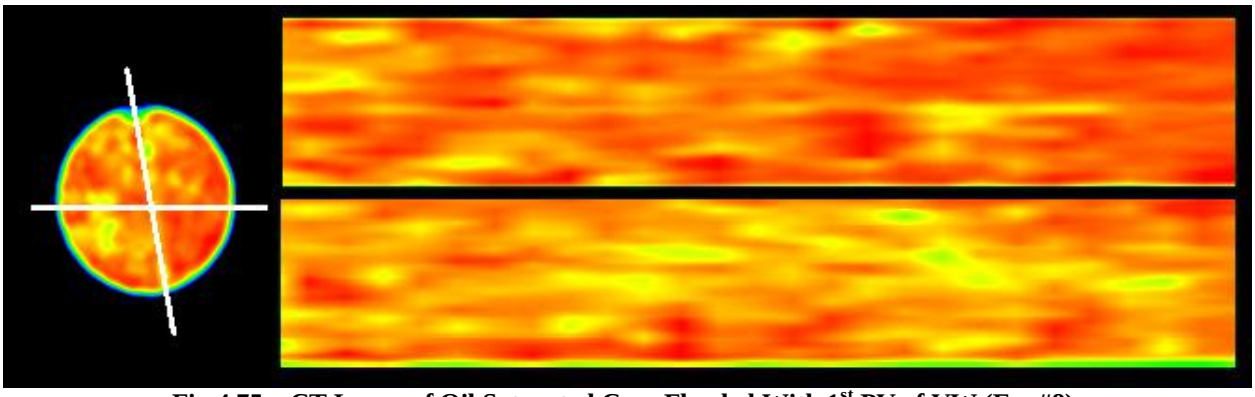

Fig.4.75 – CT Image of Oil Saturated Core Flooded With 1st PV of VW (Exp#8)

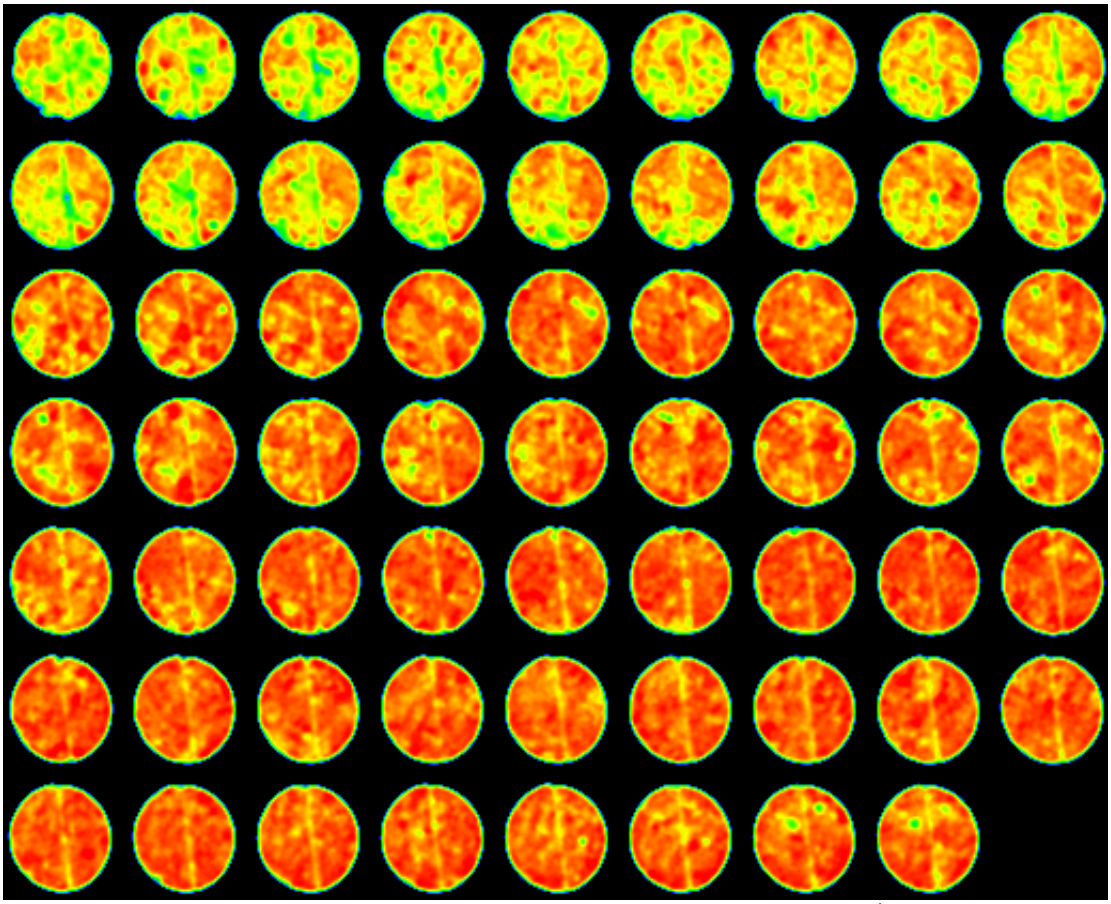

Fig.4.76 – Vertical Slice CT Images of Oil Saturated Core Flooded With 1st PV of VW (Exp#8)

The first PV of viscosified water was injected producing about 25% of the IOIP. After the injection, the VW with higher density and CT value darkened the colors. The vertical slab which passes through the fracture plane shows that visible color shift occurred across the plane turning from green and yellow to dark yellow and reddish indicating the tendency of the viscous water to flow through fracture. The horizontal cross-section image confirms the same conclusion; the relatively wider segment portion of the fracture remained yellow in color. Furthermore, the horizontal cross section also shows that small areas directly around the fracture got darker in color which confirms the success in minimizing the VW "leakoff" into the matrix compared to the first VWAG experiment. Confirming these observations requires direct evaluation with the coreflood assessing the recovery efficiency and the recovered liquids.

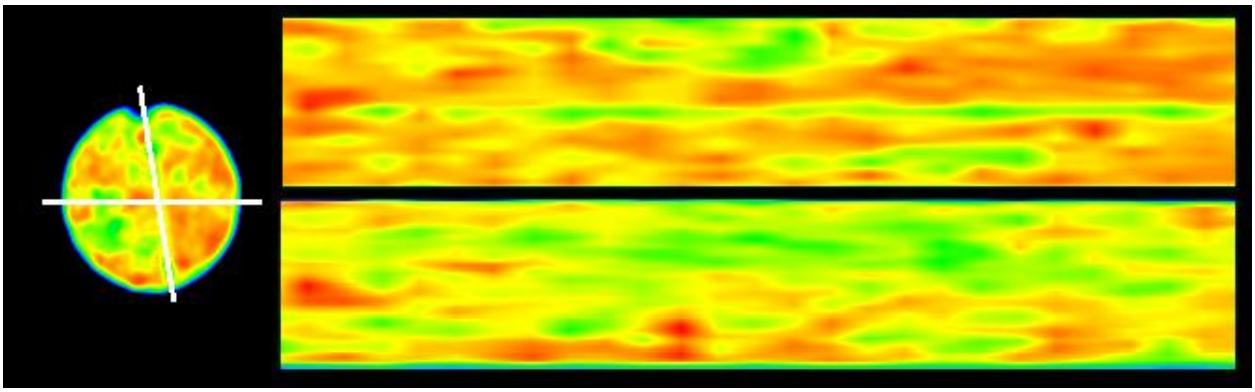

Fig.4.77 – CT Image of Oil Saturated Core Flooded With 1PV of CO_2 (Exp#8)

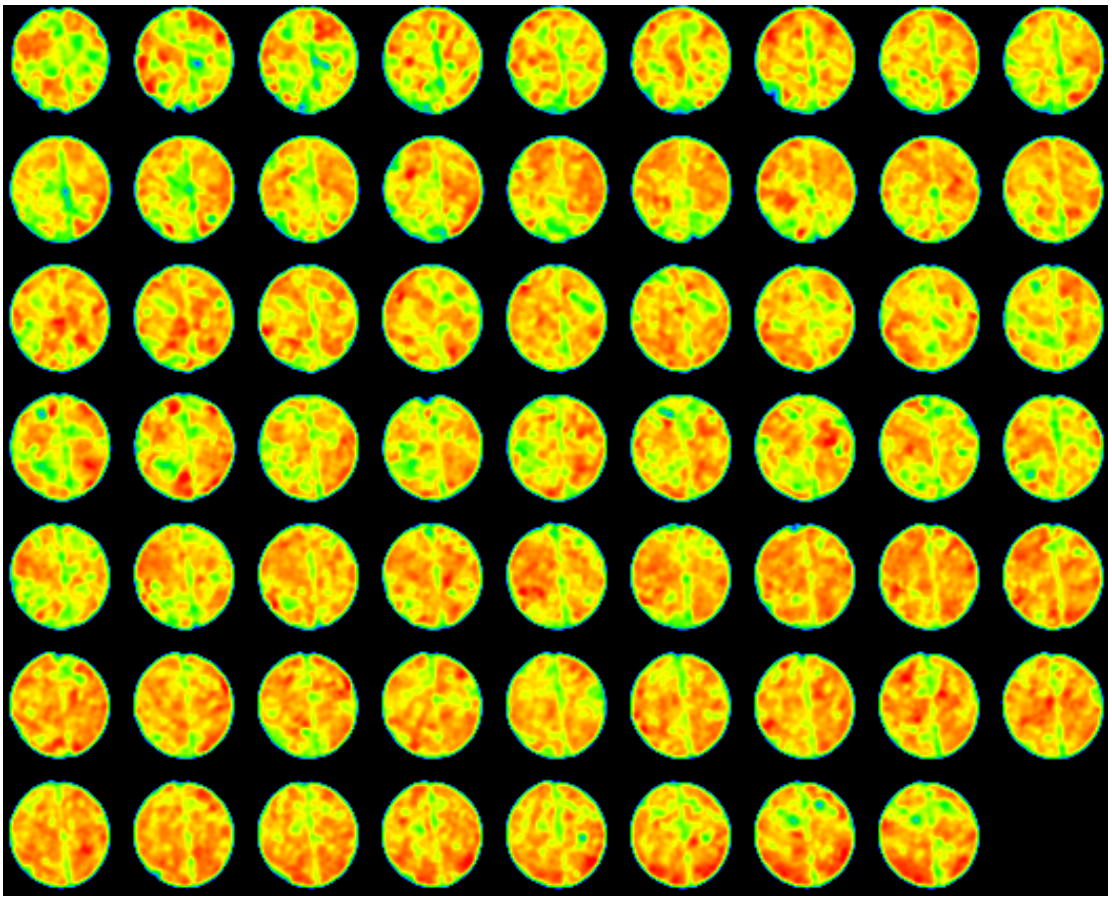

Fig.4.78 – Vertical Slice CT Images of Oil Saturated Core Flooded With 1PV of CO_2 (Exp#8)

Injecting the CO_2 after the first PV of viscosified water produced incremental oil of about 25% elevating the total recovery to about 50% of the IOIP. With the CO_2 having lower CT number , the overall CT images got lighter in color shifting towards light red and yellow. The vertical slab through the fracture plane shows that the area got much lighter in color reaching color intensities close to that prior to the injection of the VW; this observation indicates that some of the viscous water did not remain in the

fracture and was produced. The horizontal cross-section image shows that CO_2 diffused into the matrix pushing some oil out of the pores. However, many areas remained reddish indicating the poor sweep to these areas and that significant amount oil (about 50%) remained intact.

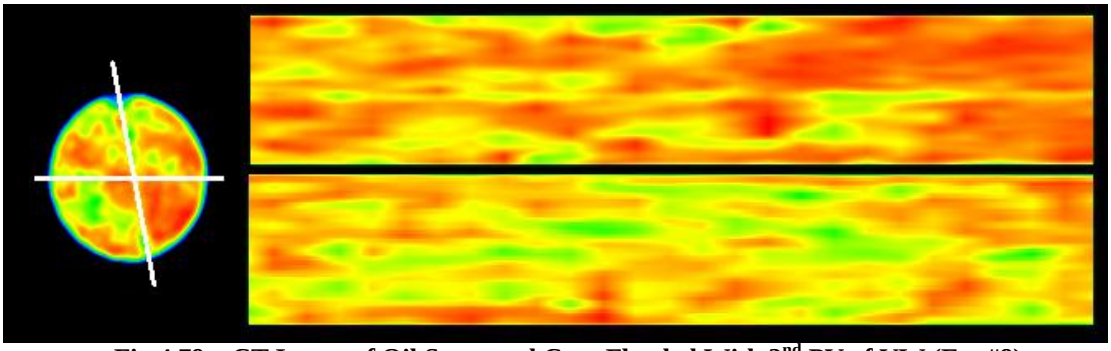

Fig.4.79 – CT Image of Oil Saturated Core Flooded With 2nd PV of VW (Exp#8)

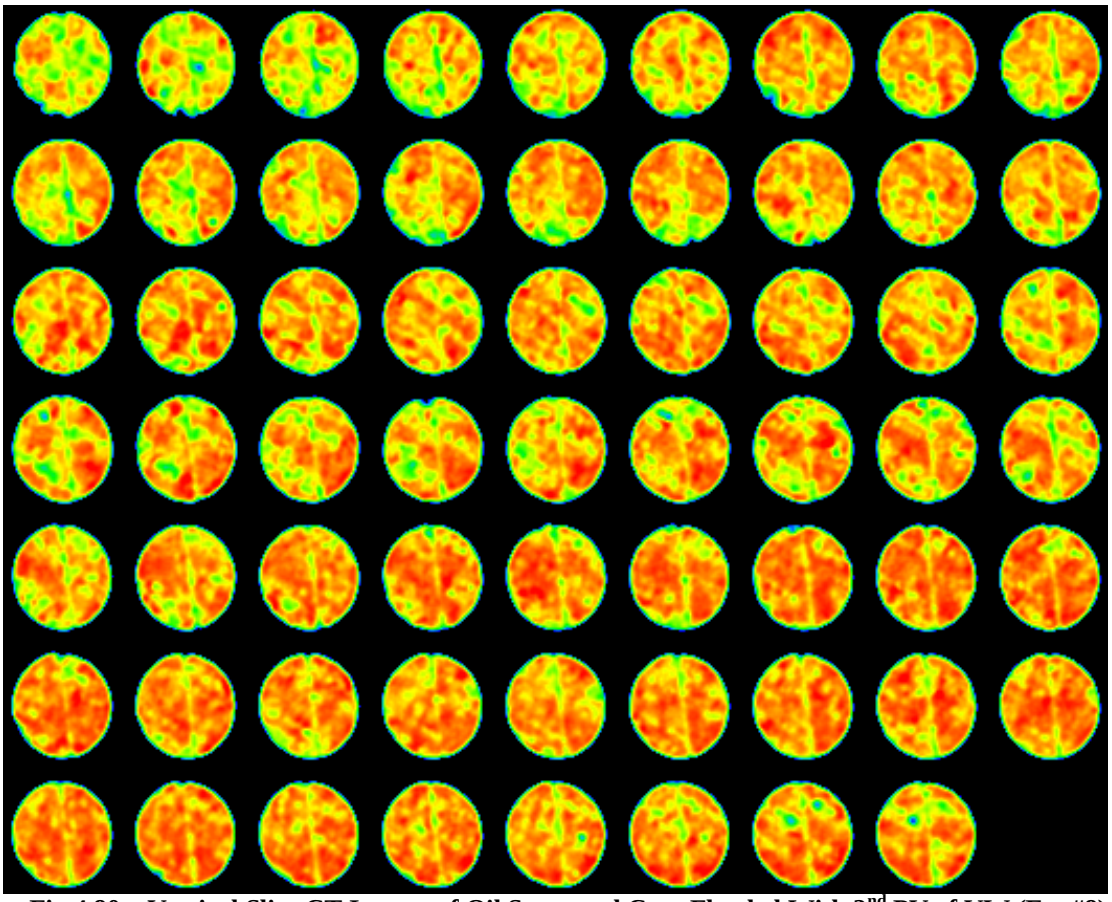

Fig.4.80 – Vertical Slice CT Images of Oil Saturated Core Flooded With 2nd PV of VW (Exp#8)

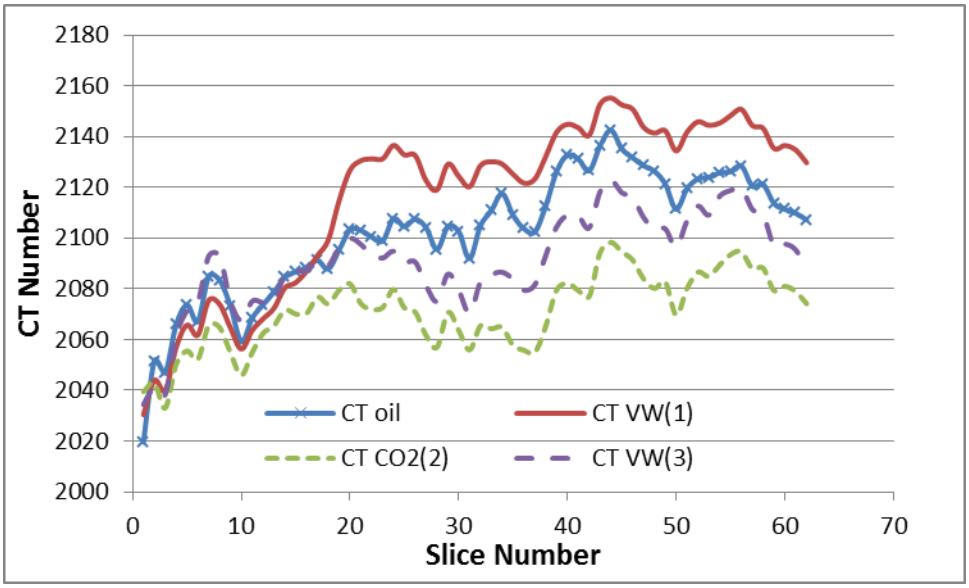

Fig.4.81 – CT Intensity at Different Stages of the Experiment (Exp#8)

Fig.4.81 shows the average CT intensity distribution across the core at different stages of the experiment. The CT intensity was the lowest after the slug of CO_2 was injected while the highest CT intensity was observed directly after the first PV of VW was injected. The CT number of the oil saturated core prior to any injection was higher than the average CT intensity values after the 2nd slug succeeded the CO_2 injection; the lower average CT intensity corresponds to lower density of fluids across the slice. Despite the VW having higher density and higher CT number, this indicates that the VW did not reside in the core to enhance the CT enough. This was confirmed with the production data with significant amounts of VW produced with the oil and not reside in the core.

The coreflood was carried out with the CO_2 entering at 1,700 psi and 120 ^oF. The horizontal slab shows that the viscosified water did not remain in place. Small spots of the core remained the same after the coreflood having dark red color. Most of the rock was flushed in relatively efficient way; some portions were flushed relatively better than others due to the heterogeneity nature of the core.

It was assumed that the viscosified water would not enter the matrix region. Ideal application will place the viscosified water in the fracture and that it would remain the fracture plugging it against low viscosity CO_2. The viscosified water was strong enough compared to the previous experiment resisting the flow of the CO_2 resulting in improving the recovery while some of it leaked off into the matrix or produced with the recovered oil.

The recovery data are shown as follows:

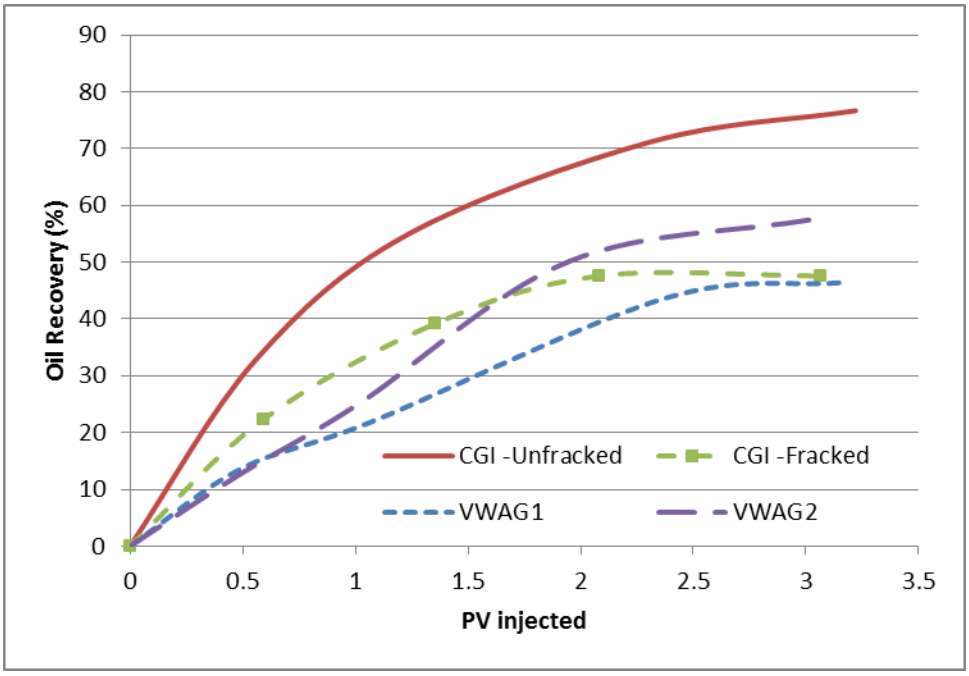

Fig.4.82 – VWAG2 – Fractured Limesone Flood Recovery Curve (Exp#8)

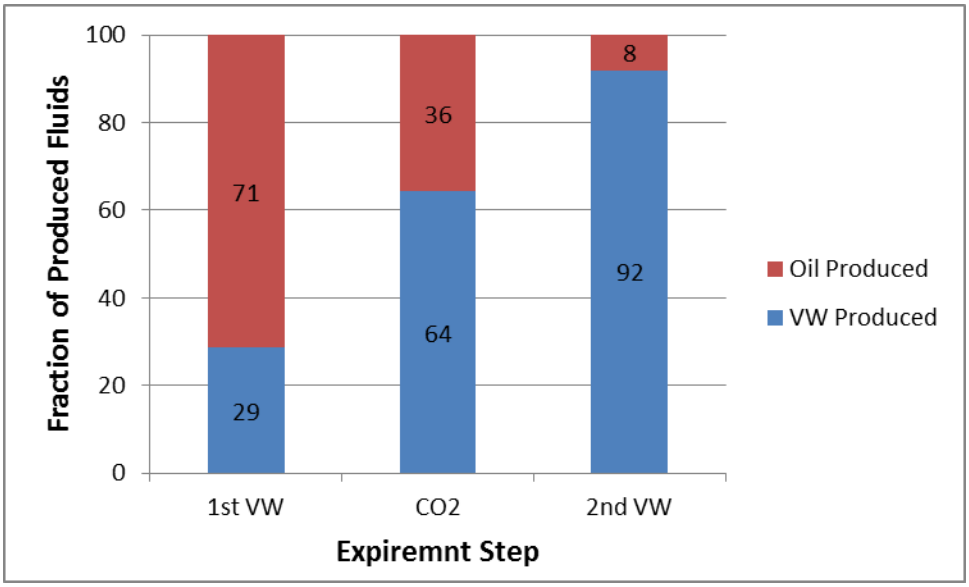

Fig.4.83 – VWAG2 – Fractions of Produced Fluids (Exp#8)

Table 4.11 – VWAG2 – Fractured Limesone Flood Recovery Data (Exp#8)

PV_{inj}	0.48	1.02	1.95	3.05
Rec(%)	12.54	25.07	50.15	57.67

The OOIP in the core prior to the injection of the CO_2 was estimated to be 9.97 cc. At the end of the experiment, about 5.8 cc of the oil was recovered accounting for about 57.7% RF of the OOIP. See **Fig.4.82 and Table 4.11.** **Fig.4.83** shows the fractions of produced fluids with the progress of the experiment. The figure shows that fraction of VW was low in the first stage with 71% of the produced fluids as oil compared to 57% with the first PV from the previous experiment; the amount of oil produced got lower with time as it looks totally unattractive with the third pore volume with only negligible amount oil produced. In comparison with the previous results, the VWAG application resulted in an incremental recovery of about 19% compared to the plain water flood; the recovery was 10% more than that of the CGI in untreated fractured core. The performance was improved significantly with doubling the cross-linker concentration. In the next experiments, Xanthan gum will be tested for the same purpose following the same approach and experimental condition. The objective is to compare the performance of the two polymers in terms of leak-off and recovery efficiency using the recovery data and the CT images.

4.6.3 Xanthan Viscosified Water Alternating Gas (VWAG) Conc#1

In the previous study to control CO_2 mobility in the fracture, concentration of 3000 ppm HPAM was used to viscosify the water alternating with the gas. The low cross-linker concentration did not show significant increment in total oil recovery compared to the untreated core flooded with CGI. However, when the cross-linker concentration was doubled, the overall performance varied noticeably recovering 10% more oil than the CGI case. In both cases, the viscosified water exhibited some degree of leakoff with more significant behavior with the lower concentration case. A decision was made to expand the study using Xanthan Gum to evaluate if this cheaper and more environmental friendly polymer can be used for the same purpose of study. The performance was evaluated both quantitatively and qualitatively using the recovery data and CT imaging technique. The first experiment utilized 3,000 ppm Xanthan polymer cross-linked with 50 ppm of Cr(III)Ac (with 6 wt.% KI dopant). At the time of viscosified water injection, the fluid was characterized to be "very runny fluid".

Before the coreflood experiment, the core was first studied for porosity using the weight difference approach as in the typical procedure detailed earlier. The core was left in the oven for two days under temperature higher than 100 ^{o}C; the core was then weighed and saturated with brine using a vacuum pump. The brine saturated core was then weighed and scanned under the CT scanner; then the core was cut in the center and heated again in the oven. In the meanwhile, the viscosified water ingredients were mixed together using a magnetic stirrer until the mixture got homogenous; the mixture was allowed to stir for about 8 hours. After that, the fractured core was placed under a

confining pressure of 2000 psi and under temperature of 70 °F and the dry core was scanned. Then, the oil was injected with outlet valve closed to establish the oil saturation. Five pore volumes of doped oil (about 50 cc) were injected while keeping the outlet valve closed; the core was then left for 8 hours under high pressure. The outlet valve was then opened and five more pore volumes of oil were injected to ensure complete saturation with oil; then the core was CT scanned.

Warm water was circulated in the bath around the coreholder for about 30 minutes at a temperature of 120 °F to establish equilibrium state. Prior to any injection, a CT scan was taken to evaluate the injected fluids performance. After that, one pore volume of viscosified water was injected at injection pressure of around 100 psi. The CO_2 was then injected at 1700 psi at supercritical conditions. A third pore volume of viscosified water was injected at injection pressure of 100 psi. The recovery data were recorded and several CT scans were taken.

To qualitatively assess the success of the flood, the CT images were colored depending of the CT intensity across the core. **Fig.4.84 through 4.92** shows the coloring spectrum used in the images scans of the oil saturated core and different CT scans during the flood.

For this experiment, the difference in CT intensity between the doped oil (0.76 g/cc) and the supercritical CO_2 (0.58 g/cc) facilitated the view and the evaluation of the success of the flood. The viscosified water with higher density and enhanced CT reading with KI dopant was seen with higher CT reading. Therefore, the coloring spectrum was chosen in way covering the CT numbers with the darkest reddish coloring indicates the

presence of VW and oil while the lighter coloring, shifting towards yellow and green indicates the unswept areas or the fracture or vugs.

Fig.4.84 – CT Images Color Spectrum (Exp#9)

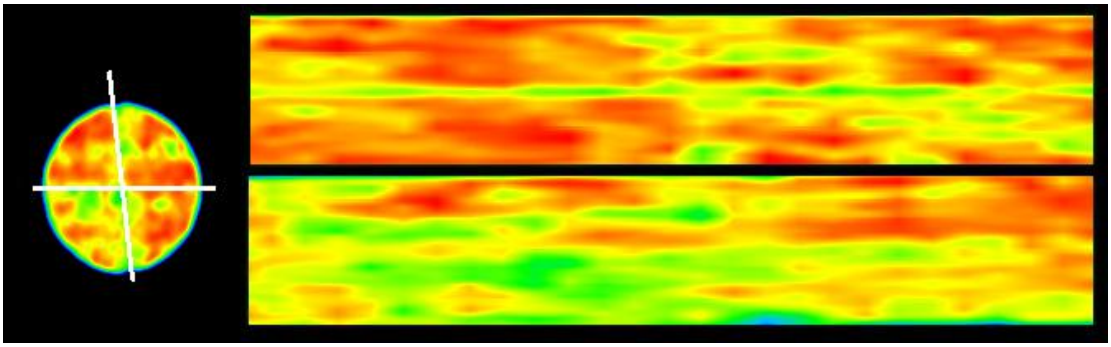

Fig.4.85 – CT Image of Oil Saturated Core (Exp#9)

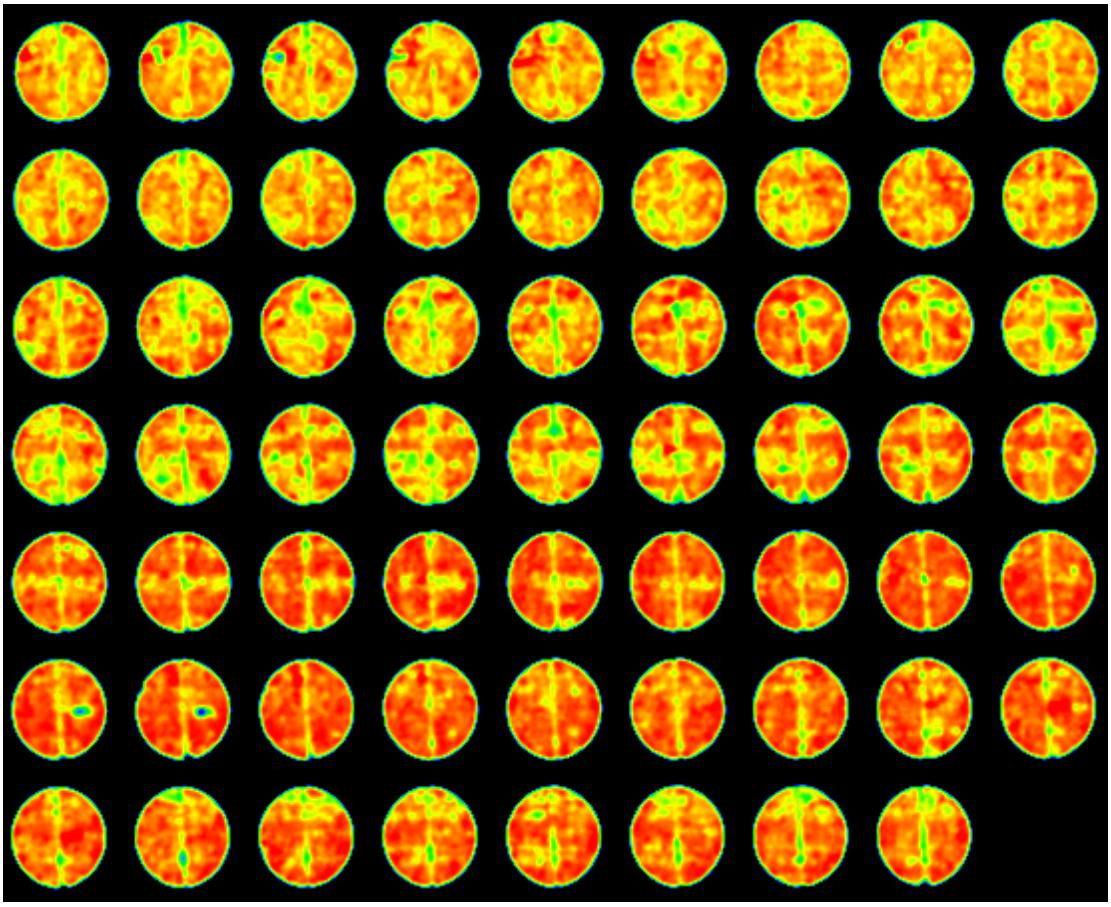

Fig.4.86 – Vertical Slice CT Images of Oil Saturated Core (Exp#9)

The oil saturated core images show that the core was saturated with oil to a great extent. The image was colored with red except the fracture area colored with yellow to light green. Some of the spots show slightly lighter colors indicating the presence of small vugs or relatively larger pores.

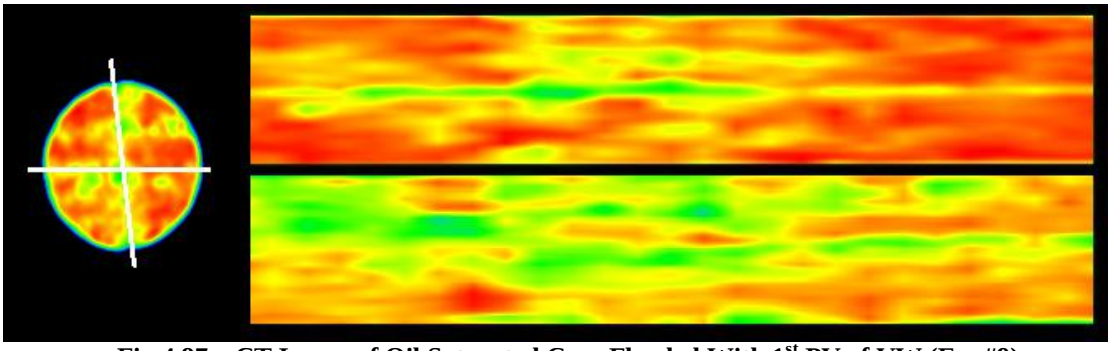

Fig.4.87 – CT Image of Oil Saturated Core Flooded With 1st PV of VW (Exp#9)

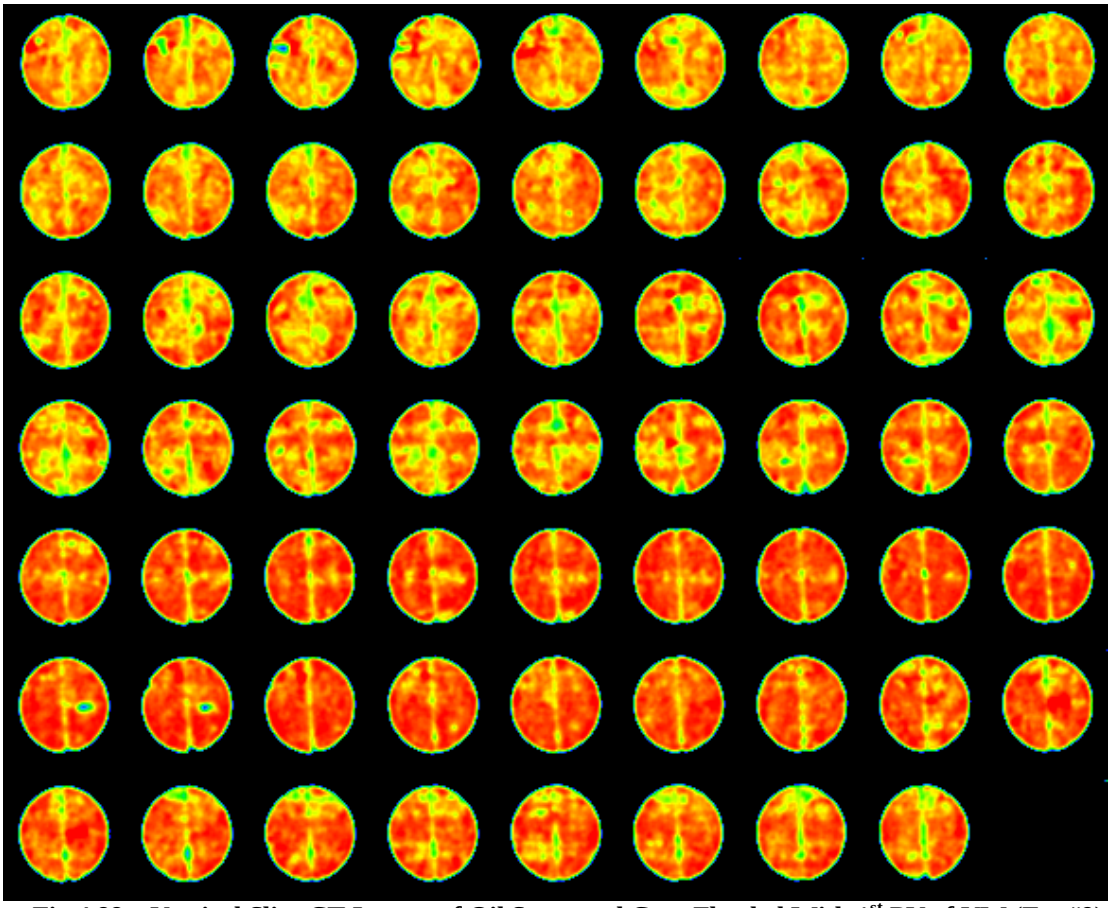

Fig.4.88 – Vertical Slice CT Images of Oil Saturated Core Flooded With 1st PV of VW (Exp#9)

The first PV of viscosified water was injected producing about 24% of the IOIP. After the injection, the VW with higher density and CT value darkened the colors. The vertical slab which passes through the fracture plane shows that visible color shift occurred across the plane turning from green and yellow to dark yellow and reddish indicating the tendency of the viscous water to flow through fracture. The horizontal cross-section image confirms the same conclusion; the relatively wider segment portion of the fracture remained green to yellow in color. Furthermore, the horizontal cross section also shows that small areas around the fracture got darker in color which indicating some degree of "leakoff" into the matrix more than that of the second PAM VWAG experiment. Confirming these observations requires direct evaluation with the coreflood assessing the recovery efficiency and the recovered liquids.

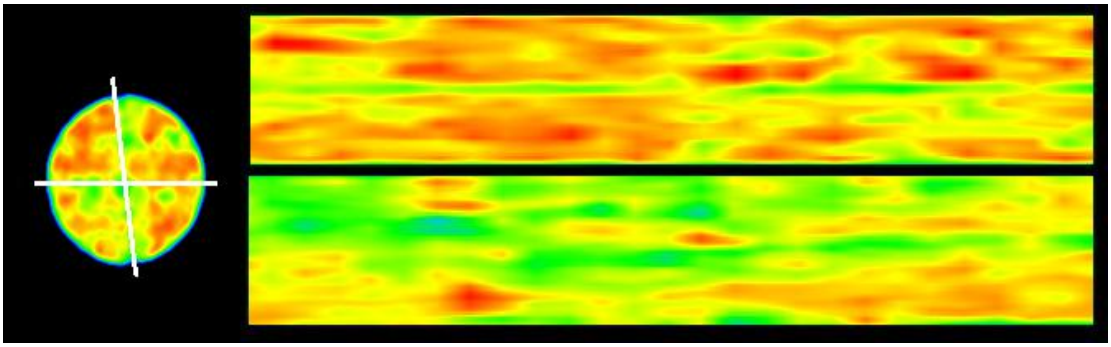

Fig.4.89 – CT Image of Oil Saturated Core Flooded With 1PV of CO_2 (Exp#9)

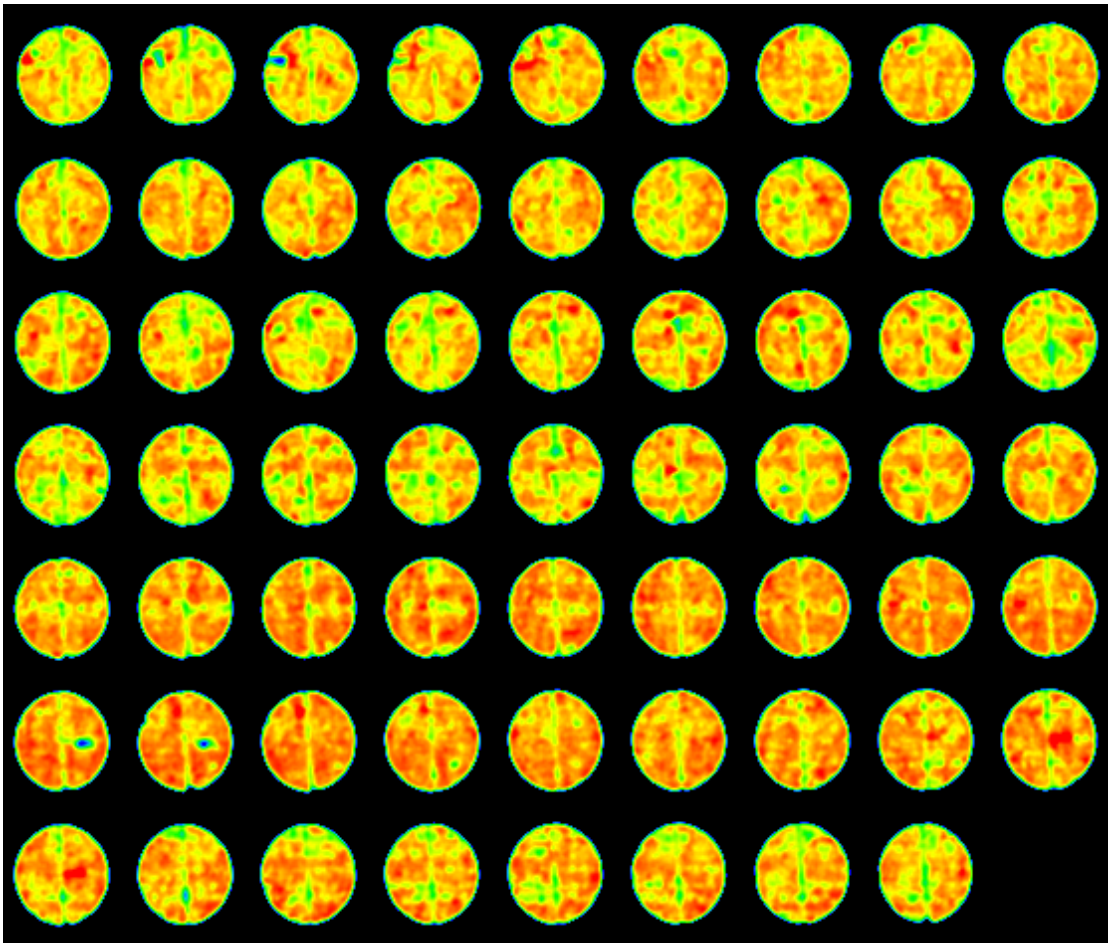

Fig.4.90 – Vertical Slice CT Images of Oil Saturated Core Flooded With 1PV of CO_2 (Exp#9)

Injecting the CO_2 after the first PV of viscosified water produced incremental oil of about 15% elevating the total recovery to about 39% of the IOIP compared to a step recovery of 25% and cumulative recovery of 50% with the second PAM VWAG. With the CO_2 having lower CT number , the overall CT images got lighter in color shifting towards light red and yellow. The vertical slab through the fracture plane shows that the area got much lighter in color reaching color intensities lighter than that prior to the

injection of the VW; this observation indicates that some of the viscous water did not remain in the fracture and was produced. The green color in the fracture also confirms that some degree of the VW remained there; otherwise the color would have shifted more towards blue. The horizontal cross-section image shows that CO_2 diffused into the matrix pushing some oil out of the pores. However, many areas remained reddish indicating the poor sweep to these areas and that significant amount oil (about 60%) remained intact.

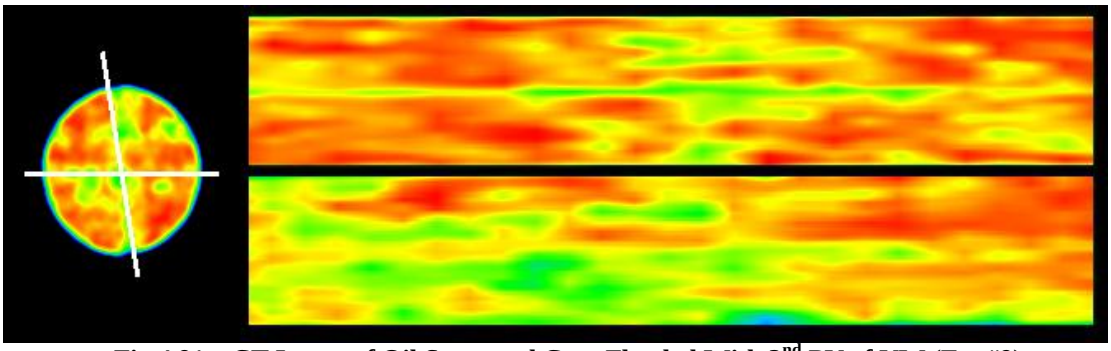

Fig.4.91 – CT Image of Oil Saturated Core Flooded With 2nd PV of VW (Exp#9)

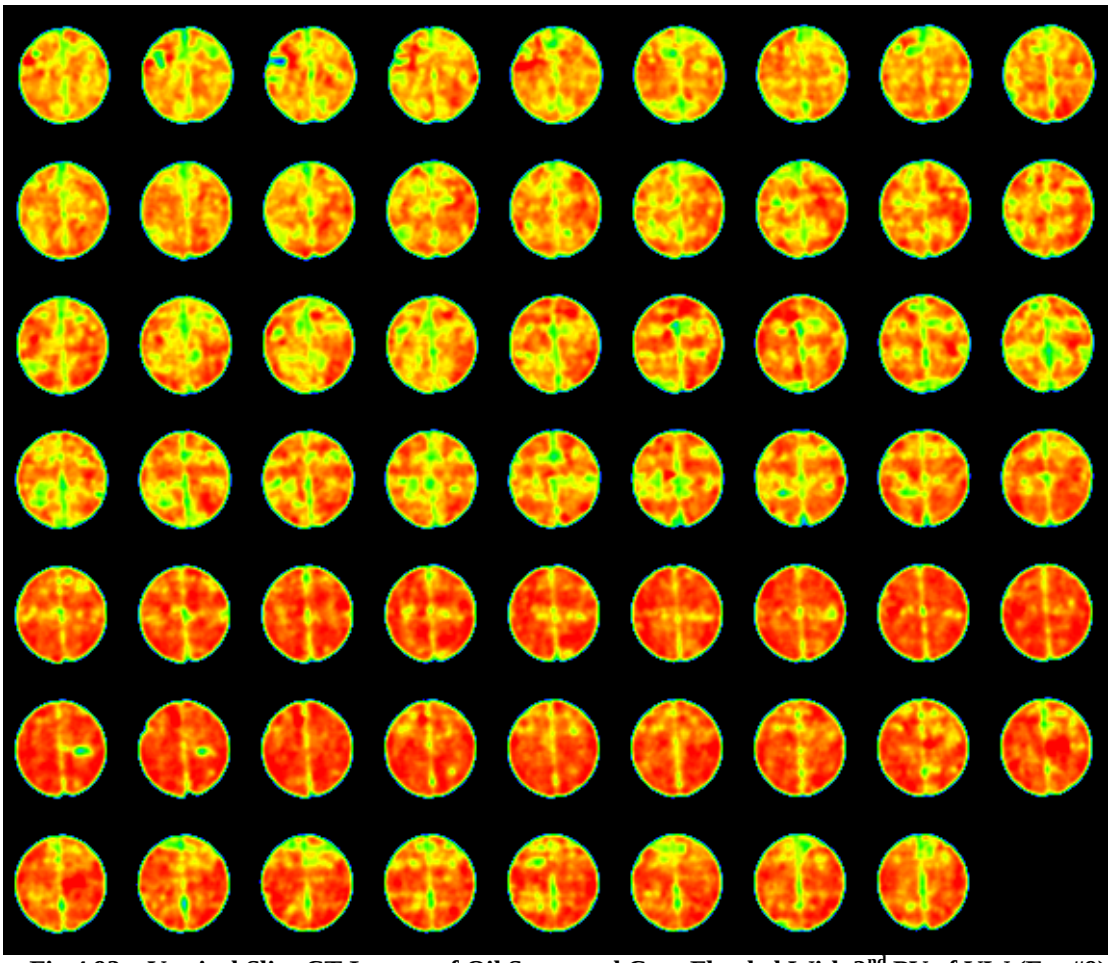

Fig.4.92 – Vertical Slice CT Images of Oil Saturated Core Flooded With 2nd PV of VW (Exp#9)

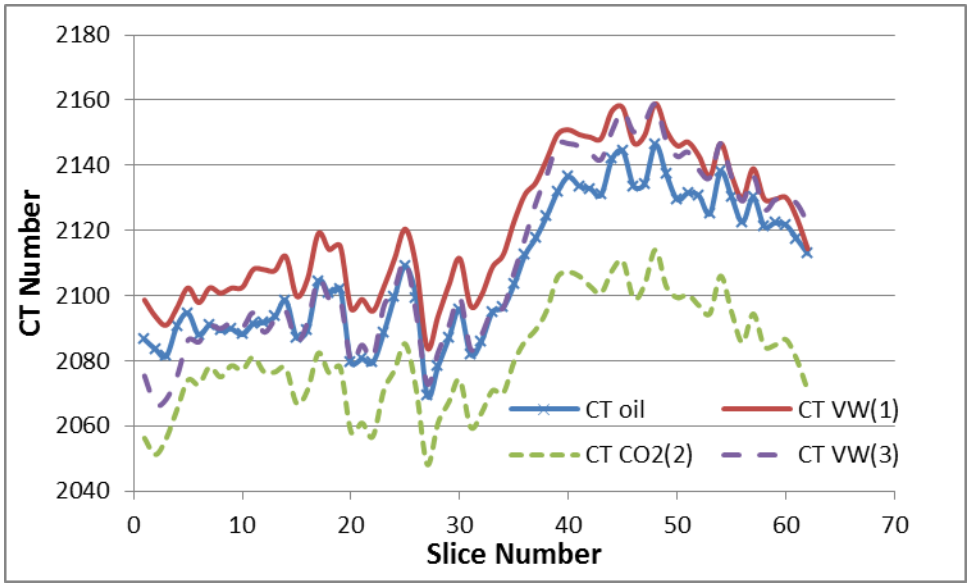

Fig.4.93 – CT Intensity at Different Stages of the Experiment (Exp#9)

Fig.4.93 shows the average CT intensity distribution across the core at different stages of the experiment. The CT intensity was the lowest after the slug of CO_2 was injected while the highest CT intensity was observed directly after the first PV of VW was injected. The CT number of the oil saturated core (CT_{oil}) prior to any injection was higher than the average CT intensity values after the 2nd slug of VW succeeded the CO_2 injection ($CT_{vw(3)}$) in some parts of the core and lower in other parts; mostly , the CT_{oil} was slightly less than $CT_{vw(3)}$; the lower average CT intensity corresponds to lower density of fluids across the slice. Since the VW has higher density and higher CT number, this indicates that the VW resided in the core barely enough to enhance the CT.

This was confirmed with the production data with some amounts of VW produced with the oil and not reside in the core.

The coreflood was carried out with the CO_2 entering at 1,700 psi and 120 ^oF. The horizontal slab shows that the viscosified water did not remain in place. Small spots of the core remained the same after the coreflood having dark red color. Most of the rock was flushed in inefficient way; some portions were flushed relatively better than others due to the heterogeneity nature of the core.

Ideal application will have the viscosified water placed in the fracture and remain there obstructing the flow of the low viscosity CO_2. The viscosified water was not strong enough to sustain the flow and enhance the flood efficiency significantly; most of it has either been produced or leaked off into the matrix.

The recovery data are shown as follows:

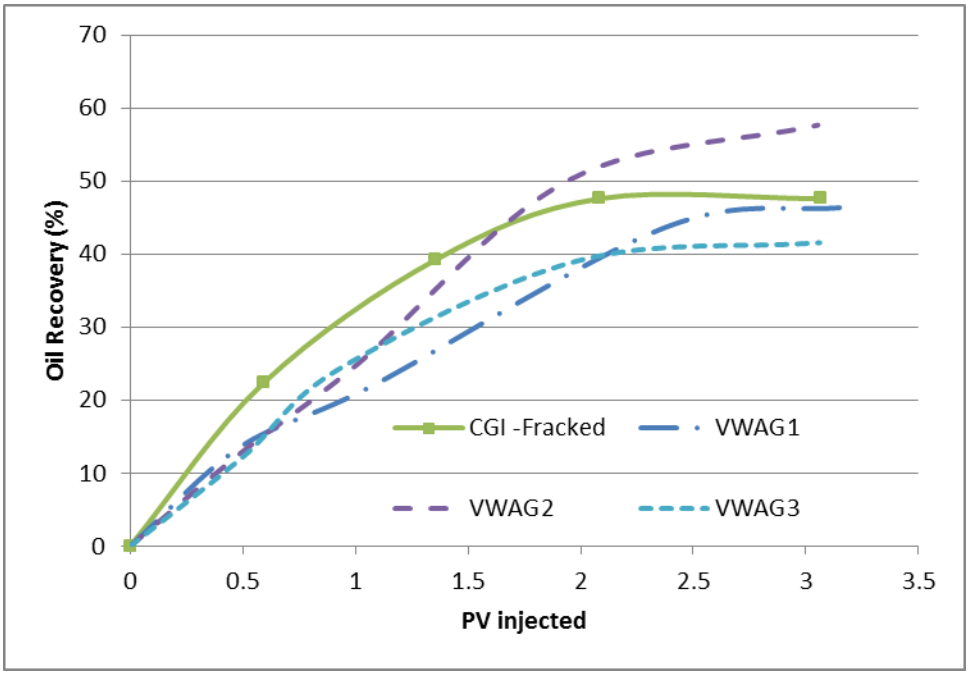

Fig.4.94 – VWAG3 – Fractured Limesone Flood Recovery Curve (Exp#9)

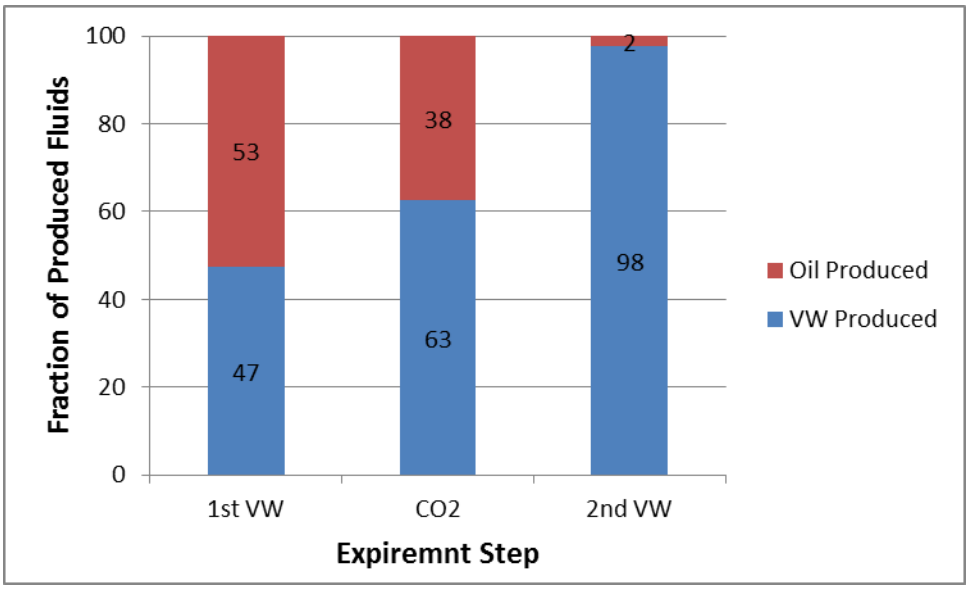

Fig.4.95 – VWAG3 – Fractions of Produced Fluids (Exp#9)

Table 4.12 – VWAG3 – Fractured Limesone Flood Recovery Data (Exp#9)

PV_{inj}	0.50	0.94	1.99	3.06
Rec(%)	12.22	24.44	39.11	41.55

The OOIP in the core prior to the injection of the CO_2 was estimated to be 10.23 cc. At the end of the experiment, about 4.3 cc of the oil was recovered accounting for about 41.6% RF of the OOIP. See **Fig.4.94 and Table 4.12.** **Fig.4.95** shows the fractions of produced fluids with the progress of the experiment. The figure shows that fraction of VW was high even in the first stage with 53% of the produced fluids as oil compared to 71% with the first PV from the previous experiment; the amount of oil produced got lower with time and looks total waste with the third pore volume with only negligible amount oil produced. In comparison with the previous results the VWAG application resulted in an incremental recovery of 3% only compared to the plain water flood; the recovery was 6% less than that of the CGI in untreated fractured core flooded with 3 PVs of CO_2. The performance was the least attractive compared to the previous two VWAG experiments. In the next experiment, the cross-linker concentration will be increased to avoid the excessive leak-off and the low resistance to CO_2 flow. Success in achieving this goal will reflect the recovery data and can be evaluated qualitatively with the CT images.

4.6.4 Xanthan Viscosified Water Alternating Gas (VWAG) Conc#2

In the previous experiment, concentration of 3000 ppm Xanthan was used to viscosify the water alternating with the gas. The low concentration VW showed high degree of leakoff and failed to obstruct the advance of the CO_2.In fact, the performance of the Xanthan mixture performed less than the low crosslinker concentration with PAM. The study was expanded doubling the cross-liner concentration with Xanthan Gum to

see how much improvement will result from tweaking that parameter. The performance was evaluated both quantitatively and qualitatively using the recovery data and CT imaging technique. The experiment utilized 3,000 ppm Xanthan polymer cross-linked with 100 ppm of Cr(III)Ac (with 6 wt.% KI dopant). At the time of viscosified water injection, the fluid was characterized to be "very runny fluid".

Before the coreflood experiment, the core was first studied for porosity using the weight difference approach as in the typical procedure detailed earlier. The core was left in the oven for two days under temperature higher than 100 ^{o}C; the core was then weighed and saturated with brine using a vacuum pump. The brine saturated core was then weighed and scanned under the CT scanner; then the core was cut in the center and heated again in the oven. In the meanwhile, the viscosified water ingredients were mixed together using a magnetic stirrer until the mixture got homogenous; the mixture was allowed to stir for about 8 hours. After that, the fractured core was placed under a confining pressure of 2000 psi and under temperature of 70 °F and the dry core was scanned. Then, the oil was injected with outlet valve closed to establish the oil saturation. Five pore volumes of doped oil (about 50 cc) were injected while keeping the outlet valve closed; the core was then left for 8 hours under high pressure. The outlet valve was then opened and five more pore volumes of oil were injected to ensure complete saturation with oil; then the core was CT scanned.

Warm water was circulated in the bath around the coreholder for about 30 minutes at a temperature of 120 °F to establish equilibrium state. Prior to any injection, a CT scan was taken to evaluate the injected fluids performance. After that, one pore

volume of viscosified water was injected at injection pressure of around 100 psi. The CO_2 was then injected at 1700 psi at supercritical conditions. A third pore volume of viscosified water was injected at injection pressure of 100 psi. The recovery data were recorded and several CT scans were taken.

To qualitatively assess the success of the flood, the CT images were colored depending of the CT intensity across the core. **Fig.4.96 through 4.104** shows the coloring spectrum used in the images scans of the oil saturated core and different CT scans during the flood.

For this experiment, the difference in CT intensity between the doped oil (0.76 g/cc) and the supercritical CO_2 (0.58 g/cc) facilitated the view and the evaluation of the success of the flood. The viscosified water with higher density and enhanced CT reading with KI dopant was seen with higher CT reading. Therefore, the coloring spectrum was chosen in way covering the CT numbers with the darkest reddish coloring indicates the presence of VW and oil while the lighter coloring, shifting towards yellow and green indicates the unswept areas or the fracture or vugs.

Fig.4.96 – CT Images Color Spectrum (Exp#10)

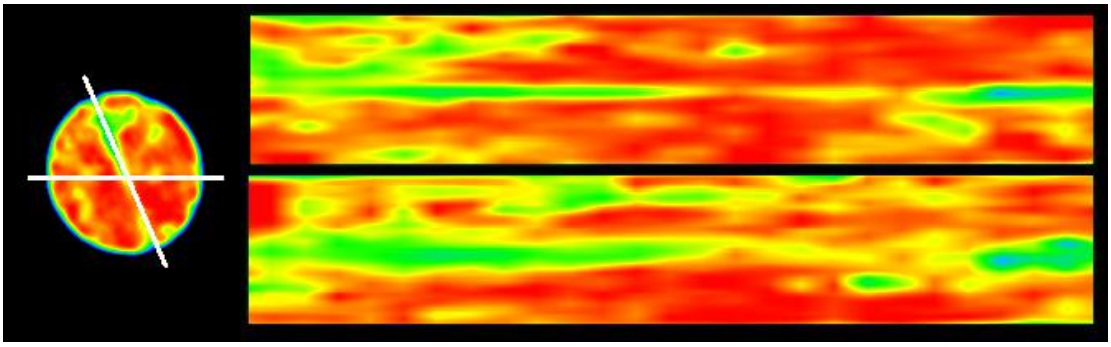

Fig.4.97 – CT Image of Oil Saturated Core (Exp#10)

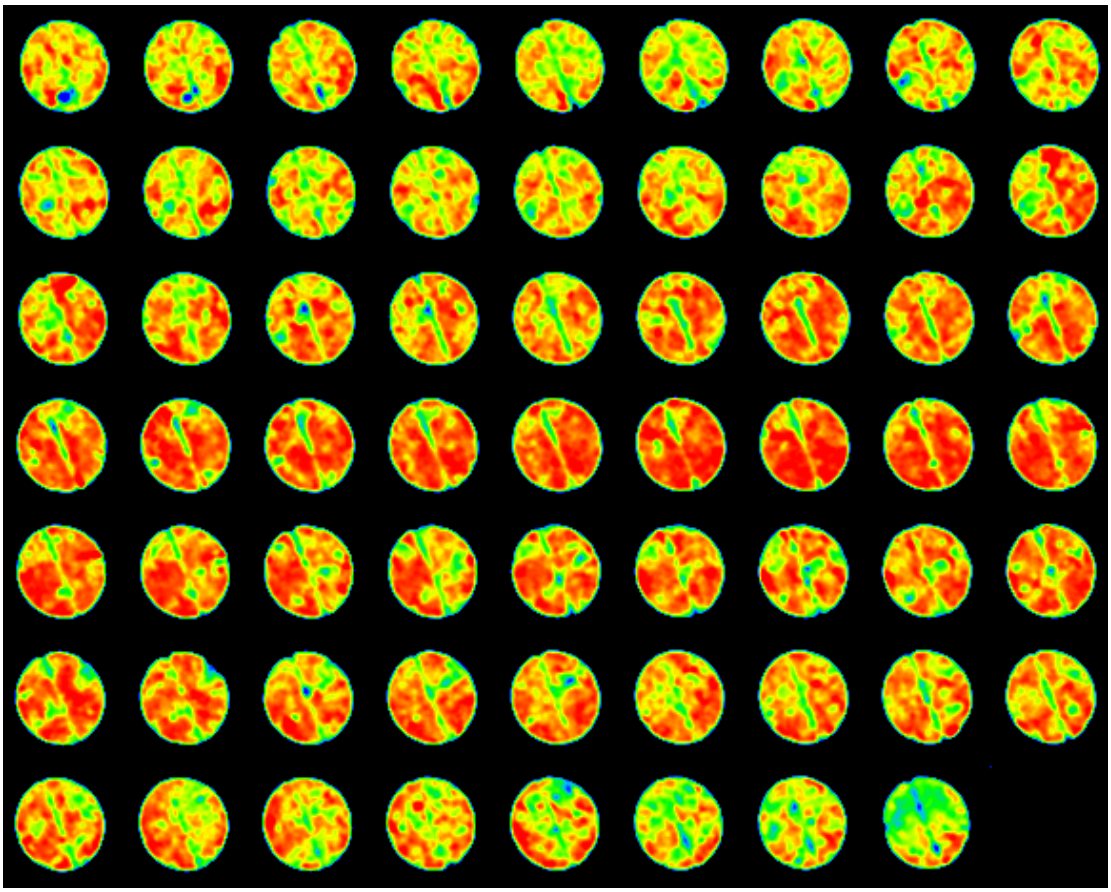

Fig.4.98 – Vertical Slice CT Images of Oil Saturated Core (Exp#10)

The oil saturated core images show that the core was saturated with oil to a great extent. The image was colored with red except the fracture area and small spots around it. Some of the spots show slightly lighter colors indicating the presence of small vugs or relatively larger pores, i.e. lower density. The image also shows that the fracture is relatively narrower in the middle compared to the rest of the fracture plane.

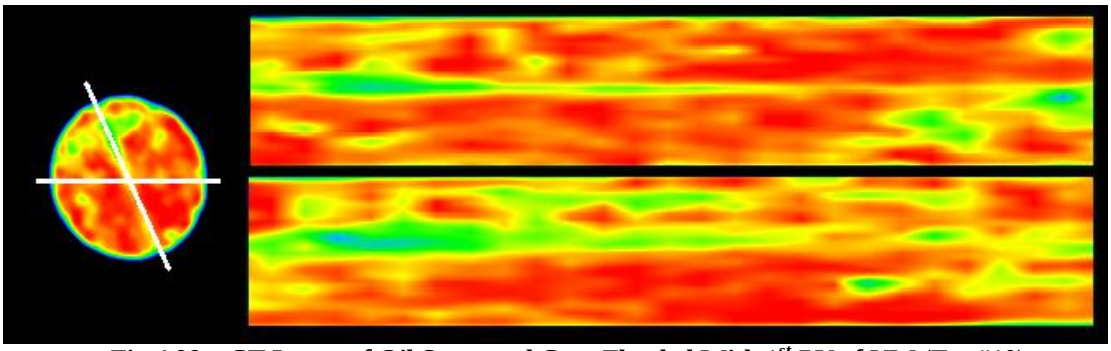

Fig.4.99 – CT Image of Oil Saturated Core Flooded With 1st PV of VW (Exp#10)

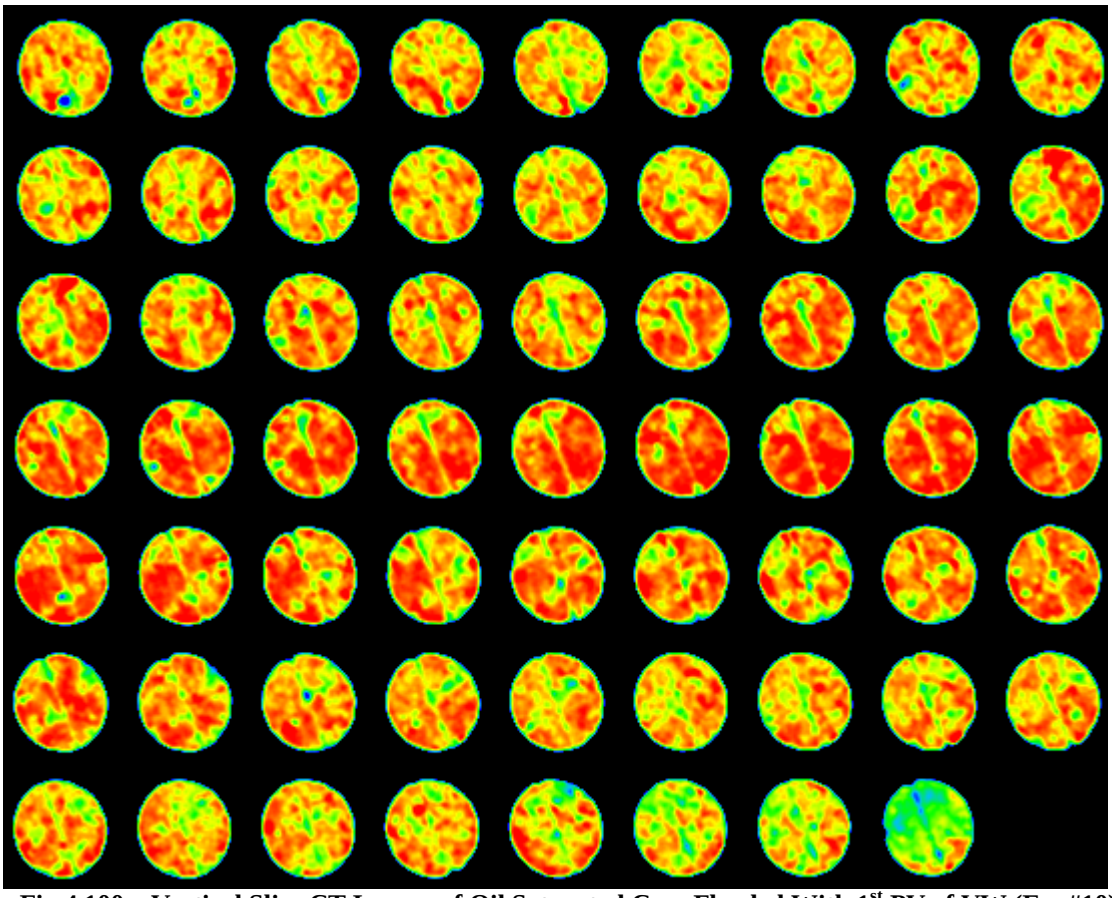

Fig.4.100 – Vertical Slice CT Images of Oil Saturated Core Flooded With 1st PV of VW (Exp#10)

The first PV of viscosified water was injected producing about 25% of the IOIP. After the injection, the VW with higher density and CT value darkened the colors. The vertical slab passing through the fracture plane shows that some color shift occurred across the plane turning some areas from green and light yellow to dark yellow and reddish showing the tendency of the viscous water to flow through fracture. The horizontal cross-section image confirms the same conclusion; the relatively wider

segment portion of the fracture remained green in color while the narrower segment got yellow. Furthermore, the horizontal cross section also shows that limited areas around the fracture got darker in color indicating low degree of "leakoff" into the matrix much less than that observed in the first Xanthan VWAG experiment. Confirming these observations requires direct evaluation with the coreflood assessing the recovery efficiency and the recovered liquids.

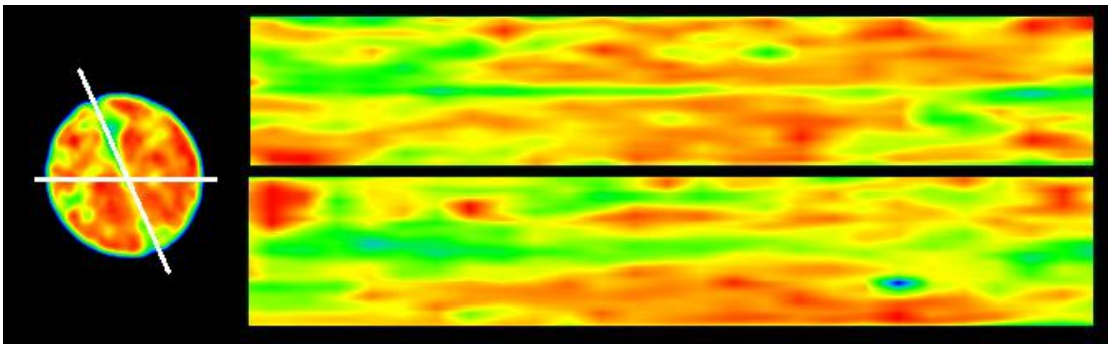

Fig.4.101 – CT Image of Oil Saturated Core Flooded With 1PV of CO_2 (Exp#10)

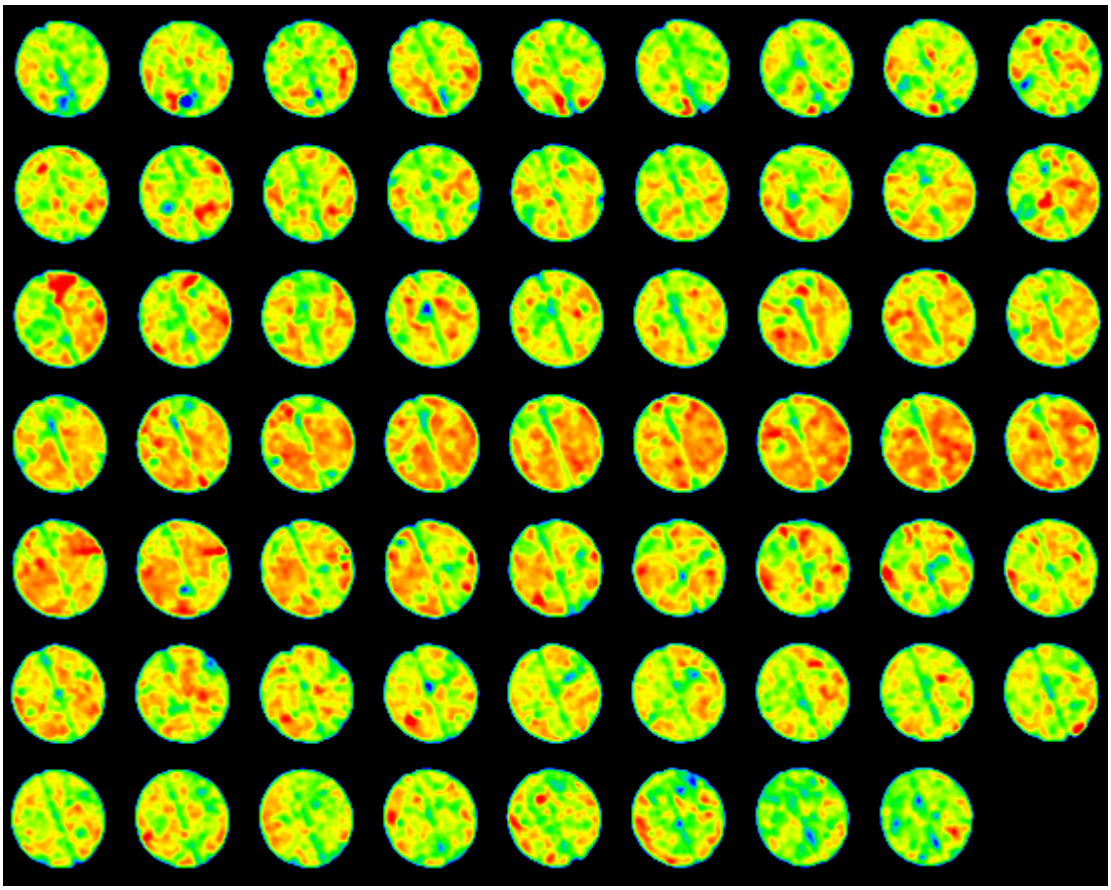

Fig.4.102 – Vertical Slice CT Images of Oil Saturated Core Flooded With 1PV of CO_2 (Exp#9)

Injecting the CO_2 after the first PV of viscosified water produced incremental oil of about 20.5% elevating the total recovery to about 45.5% of the IOIP compared to a step recovery of 24% and cumulative recovery of 39% with the first Xanthan VWAG. With the CO_2 having lower CT number , the overall CT images got lighter in color shifting towards light yellow and green; some spots ,however, continued to have reddish color but lighter than before. The previous observation suggests that some areas got

swept greatly (green) while some areas were barely touched (light red) and that significant amount oil (about 54.5%) remained intact. The vertical slab through the fracture plane shows that the area got lighter in color reaching color intensities close to that before the injection of the VW; this observation indicates that some of the viscous water did not remain in the fracture and was produced. The yellow color in the fracture also confirms that some degree of the VW remained there; otherwise the color would have shifted more towards dark green and blue.

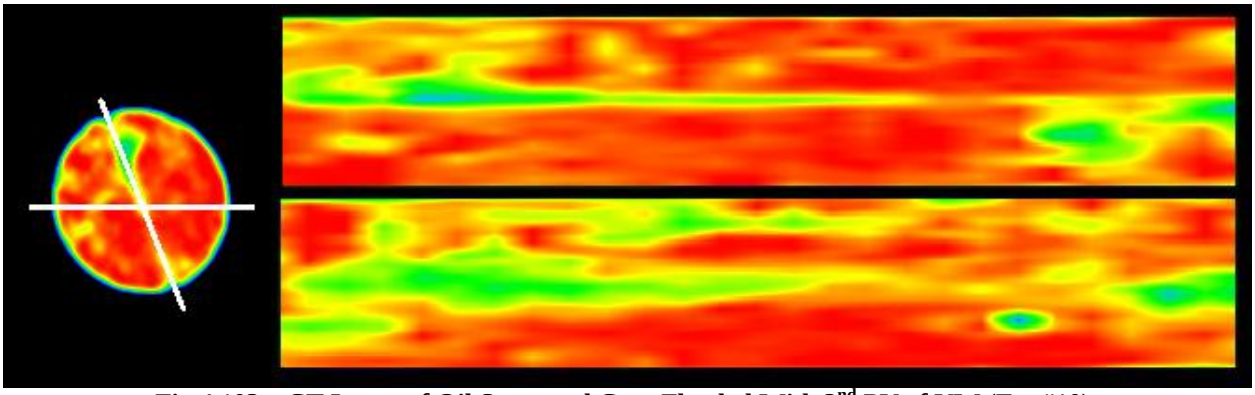

Fig.4.103 – CT Image of Oil Saturated Core Flooded With 2nd PV of VW (Exp#10)

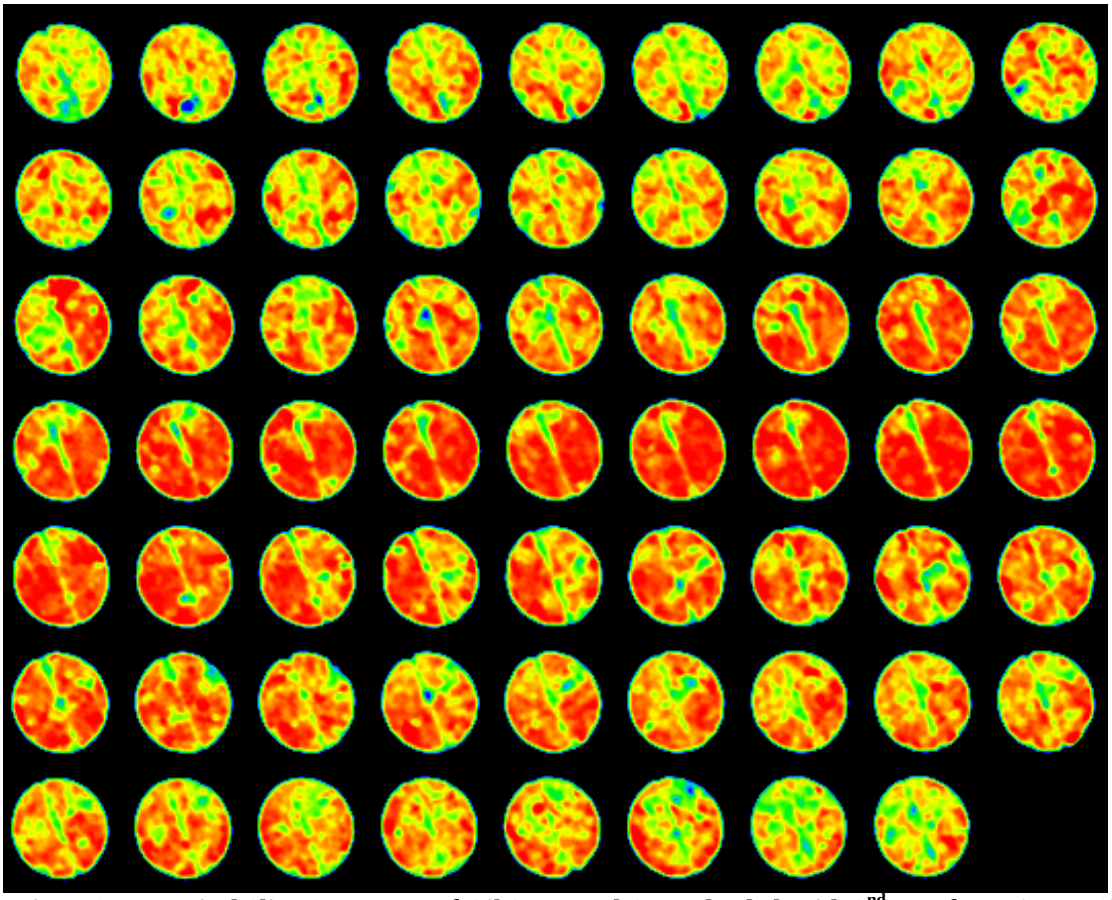

Fig.4.104 – Vertical Slice CT Images of Oil Saturated Core Flooded With 2nd PV of VW (Exp#10)

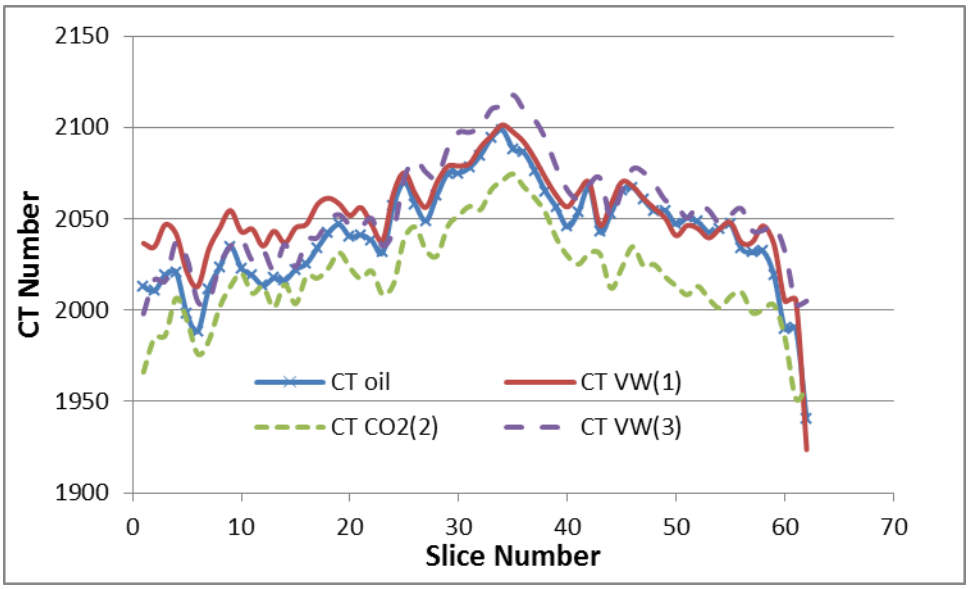

Fig.4.105 – CT Intensity at Different Stages of the Experiment (Exp#10)

Fig.4.105 shows the average CT intensity distribution across the core at different stages of the experiment. The CT intensity was the lowest after the slug of CO_2 was injected. Interestingly; the CT intensity directly after the first PV of VW was injected was not the highest; the CT intensity after the first and the second slugs of VW were close to each other. The lower average CT intensity corresponds to lower density of fluids across the slice. This suggests that second injected slug of the VW compensated for the CT intensity lost due to the produced oil confirming that some amount of the VW resided in the fracture. The CT number of the oil saturated core prior to any injection was less than the average CT intensity values after the 1^{st} and 2^{nd} VW slugs.

The coreflood was carried out with the CO_2 entering at 1,700 psi and 120 ^{o}F. The horizontal slab shows that the viscosified water remained in place to some extent. Small spots of the core remained the same after the coreflood having red color. Most of the rock was flushed in relatively efficient way; some portions were flushed relatively better than others due to the heterogeneity nature of the core.

Ideal application will place the viscosified water in the fracture and that it would remain the fracture plugging it against low viscosity CO_2. The viscosified water was strong enough compared to the previous experiment resisting the flow of the CO_2 resulting in improving the recovery while some of it leaked off into the matrix.

The recovery data are shown as follows:

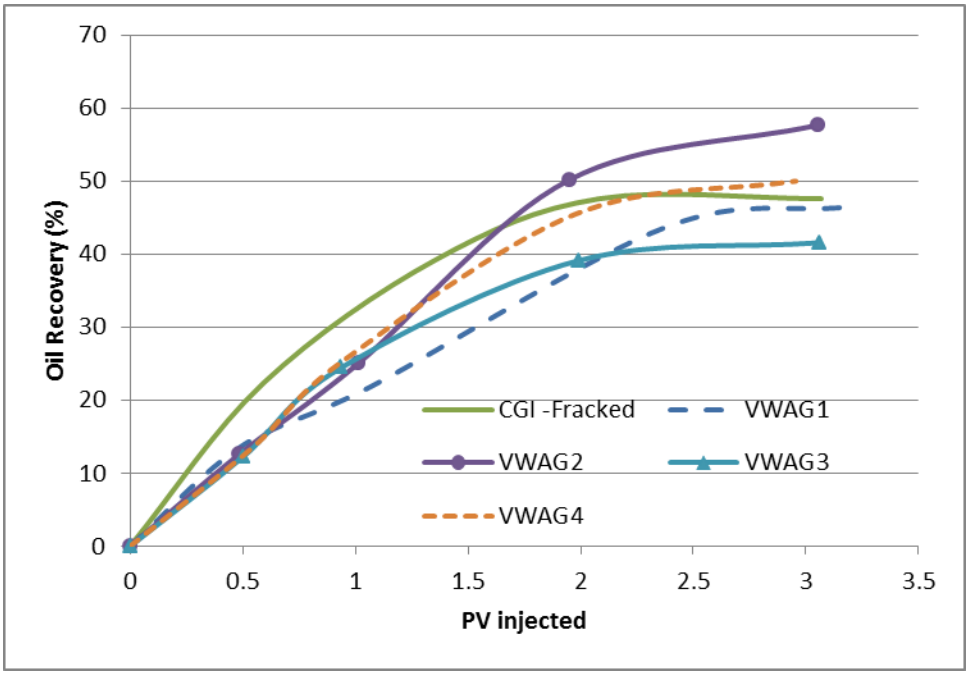

Fig.4.106 – VWAG4 – Fractured Limesone Flood Recovery Curve (Exp#10)

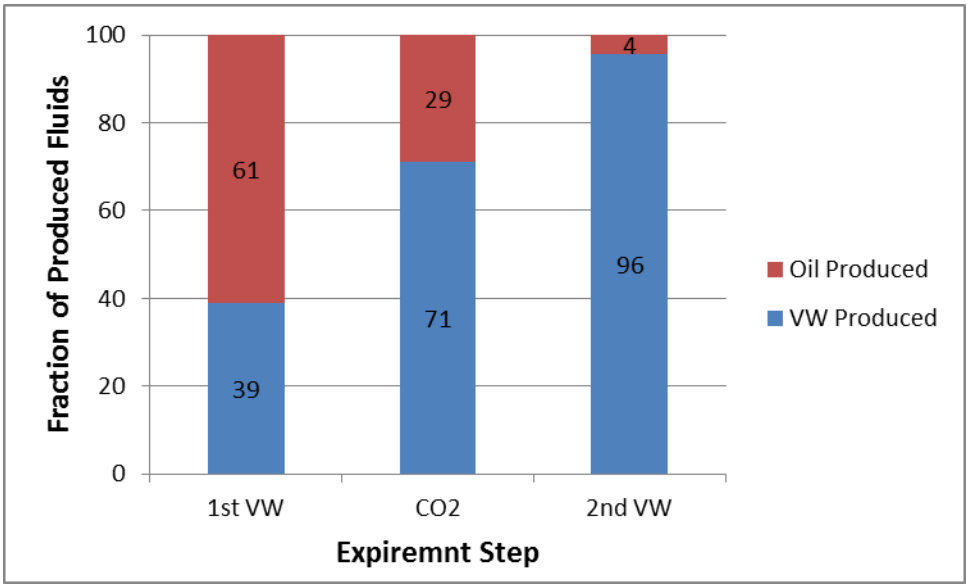

Fig.4.107 – VWAG4 – Fractions of Produced Fluids (Exp#10)

Table 4.13 – VWAG4 – Fractured Limesone Flood Recovery Data (Exp#10)

PV_{inj}	0.55	0.93	1.97	2.96
Rec(%)	13.64	25.00	45.45	50.00

The OOIP in the core prior to the injection of the CO_2 was estimated to be 11 cc. At the end of the experiment, about 5.5 cc of the oil was recovered accounting for about 50% RF of the OOIP. See **Fig.4.106 and Table 4.13. Fig.4.107** shows the fractions of produced fluids with the progress of the experiment. The figure shows that fraction of VW in the first stage was 61% of the produced fluids as oil compared to 53% with the first PV from the previous Xanthan VWAG experiment; the amount of oil produced got lower with time as it looks totally unattractive with the third pore volume with only negligible amount oil produced.

In comparison with the previous results the application resulted in an incremental recovery of 11.7% compared to the plain water flood; the recovery was 2.4% only more than that of the CGI in untreated fractured core. The performance was improved significantly with doubling the cross-linker concentration. However, the increment in recovery over CGI was not satisfactory. The overall performance of PAM was better than Xanthan for the same concentrations with lower degree of leakoff and 5-6% more oil recovered. The higher concentration of Xanthan performed closer to the lower concentration PAM in terms of leakoff and ultimate recovery, 46.5% vs. 50% respectively. The higher concentration PAM recovered 7-10% more than the other two. It is important to emphasize that the polymer type had significant impact on the final recovery. More importantly, however, the degree of crosslinking plays more effective role in enhancing the performance of viscosified water. Analyzing the production fluids data, it was found that 90-95% of the produced oil was recovered with the first two slugs: VW and CO_2; about 70-75% of the produced VW was produced with the third

slug VW. In future studies, the cross-linker and polymer concentration shall be studied more for effects on leak-off and ultimate recovery enhancement over CO_2 CGI flooding in untreated fractured rocks.

4.7 Comparison and Discussion of Experimental Results

The previous experiments started with three base experiments to evaluate the performance of CO_2 floods in fractured rocks in comparison with unfractured rocks. The performance waterflood was also studied to highlight the difference in effectiveness of oil recovery between the two injection fluids and the impact of their physical properties in the presence of fractures. The later research investigated two CO_2 mobility control techniques: gel treatments and viscosified water-alternating-gas (VWAG).

The main goal of the application of EOR methods such as CO_2 and the introduction of chemicals into the reservoir in different approaches is to maximize the ultimate oil recovery in efficient and economical way. The common parameter available for comparison and qualitative evaluation of all presented experiments is the ultimate oil recovery. Other parameters can be comparative for every category by itself. **Fig.4.108** shows the recovery curves of all experiments in terms of oil recovery% vs. PV injected; **table 4.14** arranges the recovery results tabulated to facilitate the comparison of recoveries against injected pore volumes of 0.5, 1, 2 and 3. For the base and gel application experiments, all the injected pore volumes were CO_2.The first and third pore volumes in VWAG experiments were viscosified water while the second pore volume was CO_2.

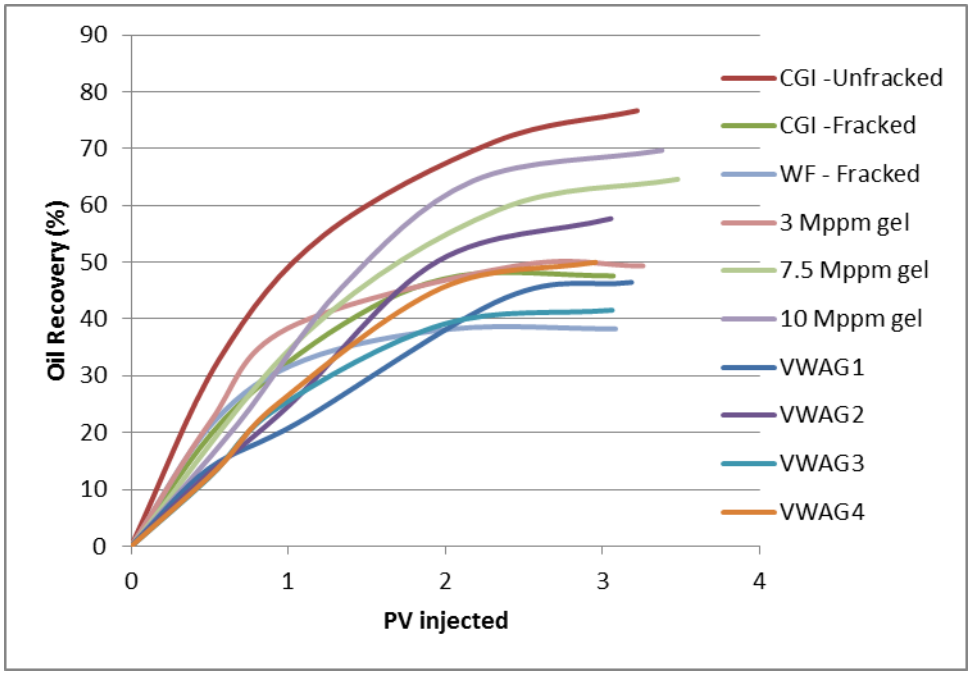

Fig.4.108 – Expiremntal Recovery Curves

Table 4.14 – Expiremntal Recovery Data

Experiment	≈ 0.5 PV	≈ 1 PV	≈ 2 PV	≈ 3 PV	2 /3 PV	2-1 PV	3-2 PV
WF – Fracked	21.9	32.8	38.3	38.3	100	5.5	0
CGI –Unfracked	32.9	54.8	71.2	76.7	92.9	16.4	5.5
CGI –Fracked	22.4	39.2	47.6	47.6	100	8.4	0
3 Mppm gel	21.9	38.4	49.3	49.3	100	11.0	0
7.5 Mppm gel	-	37.7	59.2	64.6	91.7	21.5	5.4
10 Mppm gel	21.4	45.6	64.3	69.7	92.3	18.8	5.4
VWAG1	13.7	21.9	43.7	46.5	94.1	21.9	2.7
VWAG2	12.54	25.07	50.15	57.67	87.0	25.1	7.5
VWAG3	12.22	24.44	39.11	41.55	94.1	14.7	2.4
VWAG4	13.64	25.00	45.45	50.00	90.9	20.5	4.5

After injecting the first pore volume, the highest recovery (after the unfractured core ideal case) was obtained with the 10,000 ppm treatment with about 45.6%; it is highlighted also that the first slug of viscosified water recovers less than an equivalent slug of CO_2 with 22-25% vs.39-45% respectively. The first PV injected after the gel treatment resulted in higher recovery than the other scenarios; the recovery after the gels was 38-45% in comparison with 39% with plain CGI and 22-25% with the VW. In addition, with the first injected PV, the effect on recovery of the gel concentration or the viscosified water composition was not clear as the difference in recoveries was narrow.

The second injected PV again highlighted the superiority of gel application resulting in recovery of 49-64% as opposed to 47% with CGI and 40-50% with VWAG. The second pore volume injected in three of the VWAG experiments, CO_2, did not compensate for the effect of doubled the amount of CO_2 with CGI in untreated core with 40-45% against 47%; the only exception was the 2nd PAM VWAG experiment that recovered 50% with the second injected PV; the waterflood case recovered the least with 38% after the second injected PV. The second PV added incremental oil of 11-20% for the gel experiments, 15-25% for the VWAG experiments and 8% for CGI case.

The ultimate recovery was again the highest with the successful gel treatments (7,500-10,000 ppm) with 64-70% compared to 47% with the neat CGI. Thus, the incremental recovery after the effective gel treatments was 17-22% more than the CGI in fractured rock case; the failed case resulted in ultimate recovery of 49%, thus, 2% only more than the untreated core with CGI. The viscosified water performance varied from 41-46% with the failed attempts (1st PAM and 1st Xanthan) and 50-58% with the other

two (2^{nd} PAM and 2^{nd} Xanthan);the second PAM VWAG test (VWAG2) added 10% more oil than the CGI while the second Xanthan (VWAG4) added 2.4% only more oil. The third PV of waterflood added no incremental recovery; the ultimate recovery was 38% only. About 87-94% of the recovered oil was recovered with the first and second PV excluding the third one. The third PV added incremental oil of 5.4% for the two gel experiments (7,500-10,000 ppm), 2.5-7.5% for the VWAG experiments and 5.5% for CGI case.

To emphasize the differences in sweep efficiency and gel performance on CT images, **Fig.4.109 through 4.128** have been duplicated from previous studies with arrows indicating where the CO_2 has reached in the fracture and circles around sample areas where CO_2 with prominent diversion has occurred. The first images (Exp#1) are from CGI in unfractured rock. Images from (Exp#2) show the performance of CGI in untreated fractured core. The last images (Exp#1) are from the 10,000 ppm gel treatment experiment followed by CGI injection.

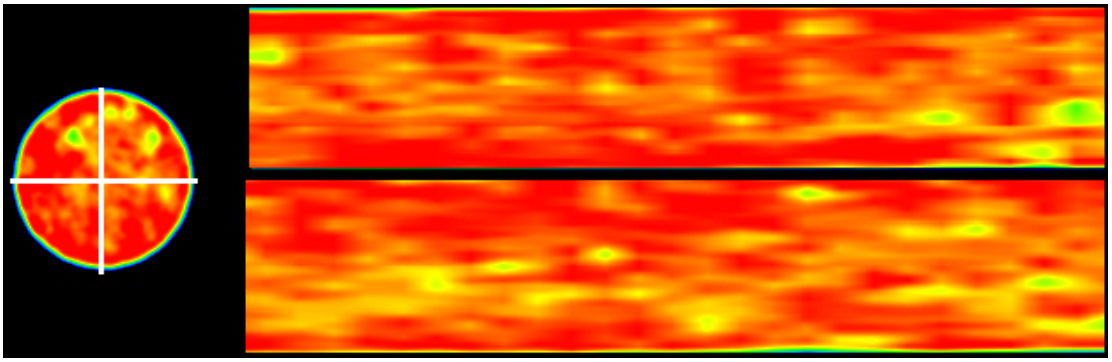

Fig.4.109 – CT Image of Oil Saturated Core (CGI)

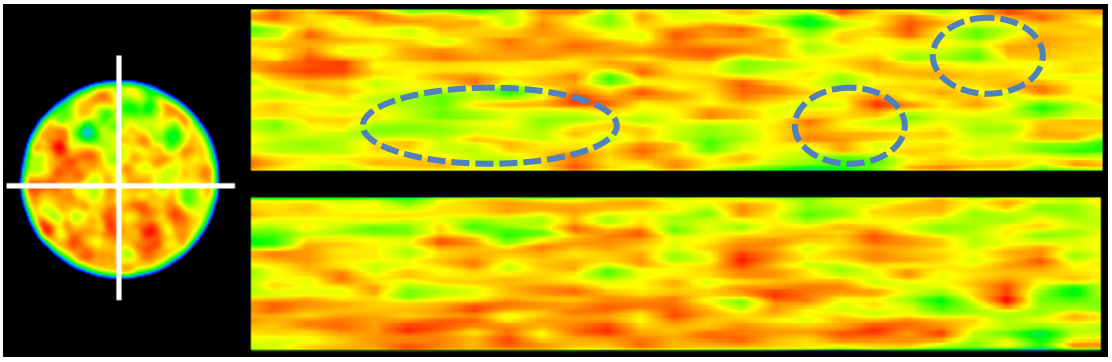

Fig.4.110 – CT Image of Oil Saturated Core after Flooded with 1 PV of CO_2 (CGI)

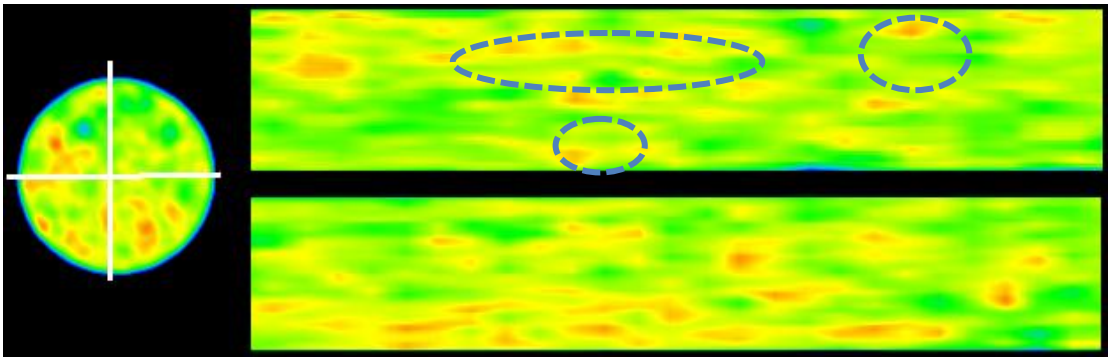

Fig.4.111 – CT Image of Oil Saturated Core after Flooded with 3 PV of CO_2 (CGI)

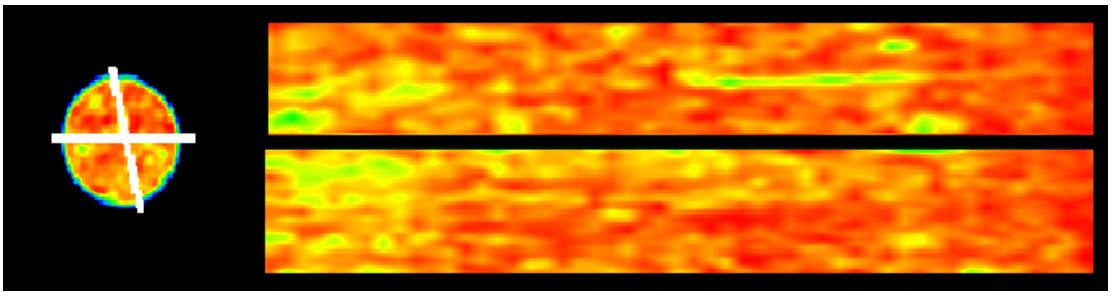

Fig.4.112 – CT Image of Oil Saturated Core (CGI-Fracked)

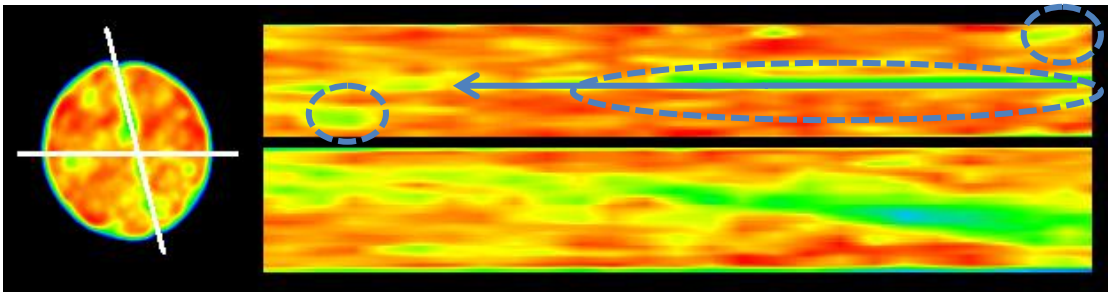

Fig.4.113 – CT Image of Oil Saturated Core after Flooded with 1 PV of CO_2 (CGI-Fracked)

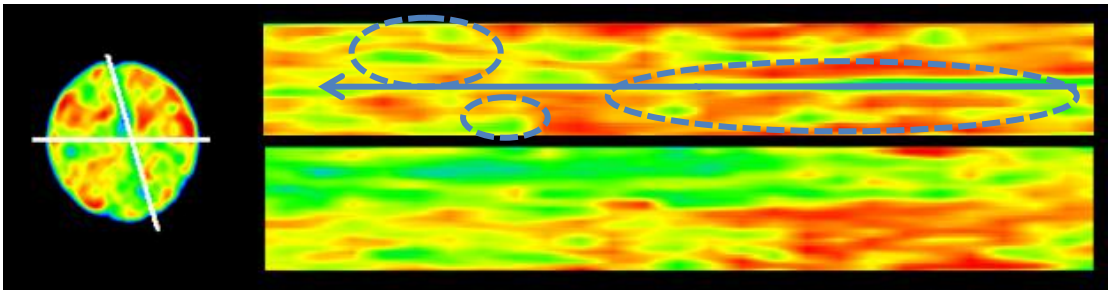

Fig.4.114 – CT Image of Oil Saturated Core after Flooded with 3 PV of CO_2 (CGI-Fracked)

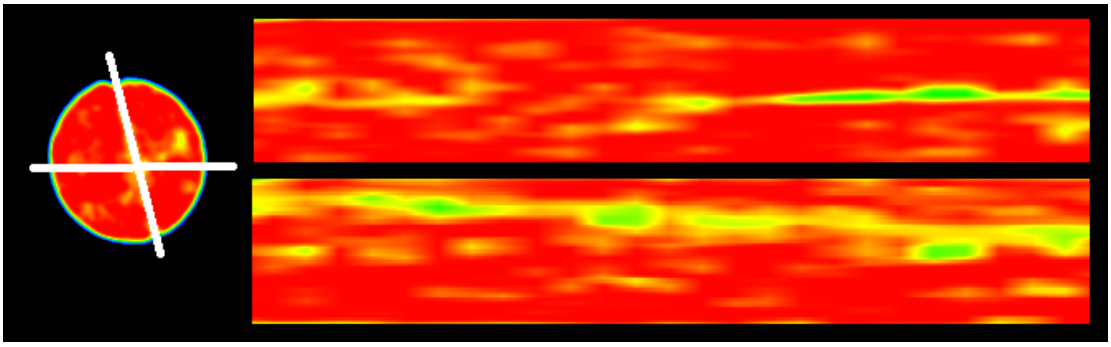

Fig.4.115 – CT Image of Oil Saturated Core (3,000 ppm)

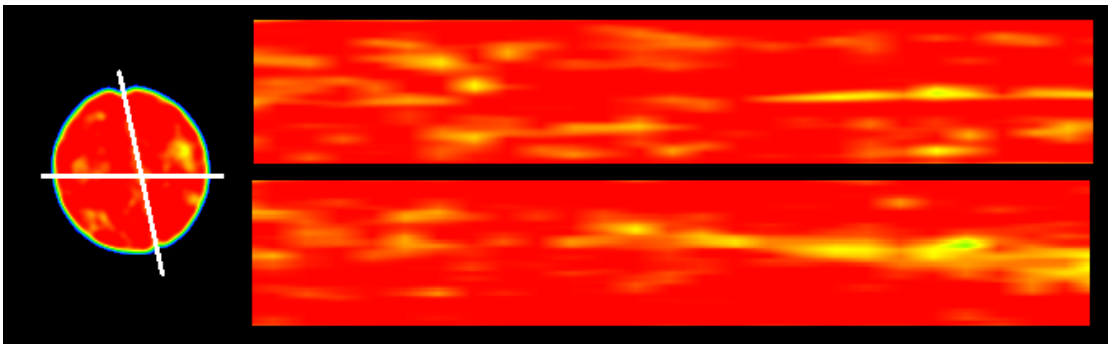

Fig.4.116 – CT Image of Oil Saturated Core after Gel Treatment (3,000 ppm)

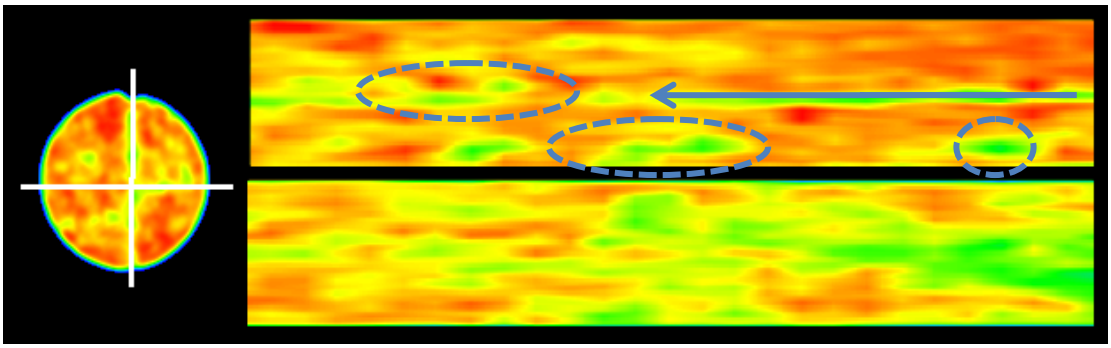

Fig.4.117 – CT Image of Oil Saturated Core Flooded With 1PV of CO_2 (3,000 ppm)

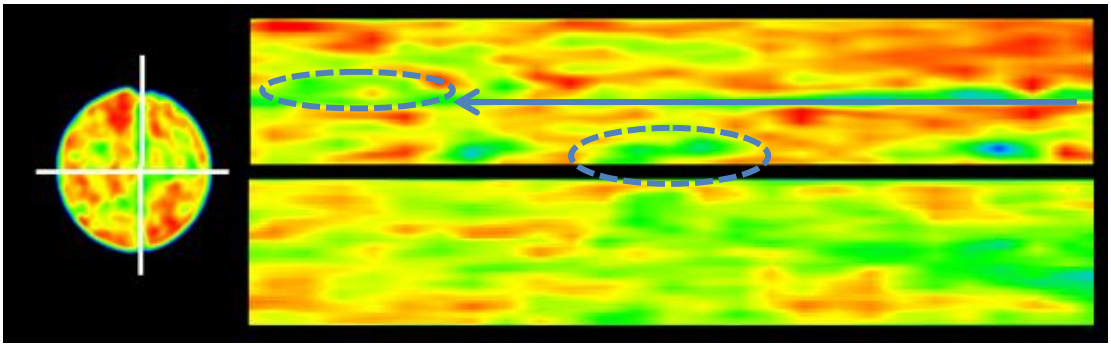

Fig.4.118 – CT Image of Oil Saturated Core Flooded With 3PV of CO_2 (3,000 ppm)

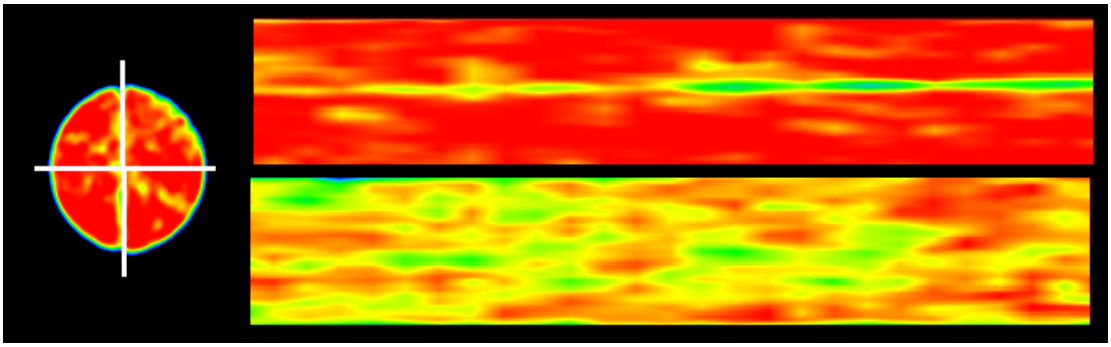

Fig.4.119 – CT Image of Oil Saturated Core (7,500 ppm)

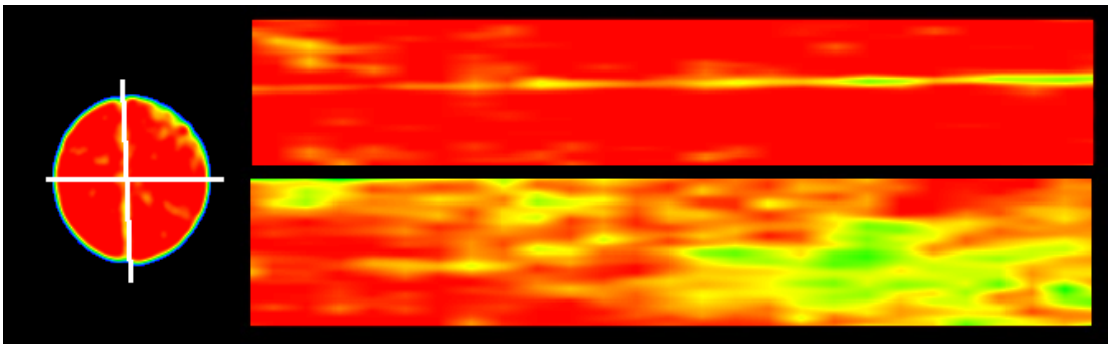

Fig.4.120 – CT Image of Oil Saturated Core after Gel Treatment (7,500 ppm)

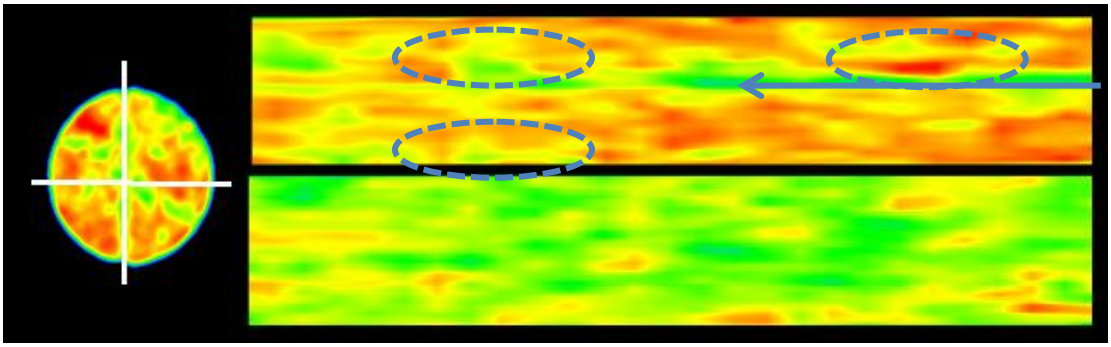

Fig.4.121 – CT Image of Oil Saturated Core Flooded With 1PV of CO_2 (7,500 ppm)

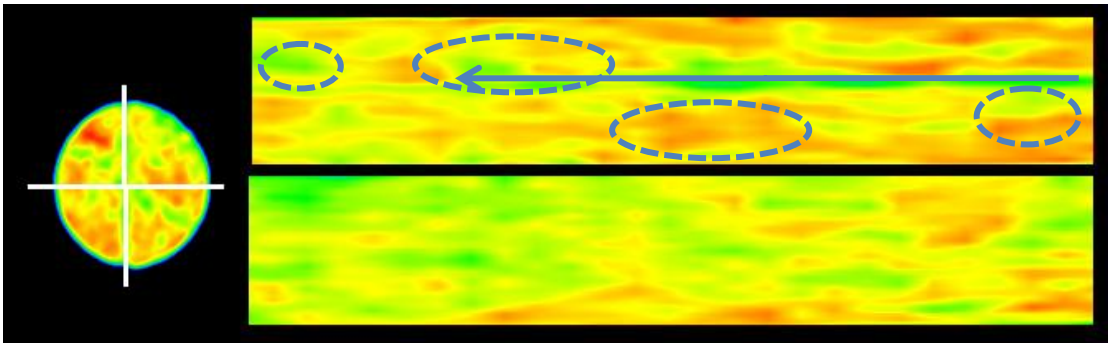

Fig.4.122 – CT Image of Oil Saturated Core Flooded With 3PV of CO_2 (7,500 ppm)

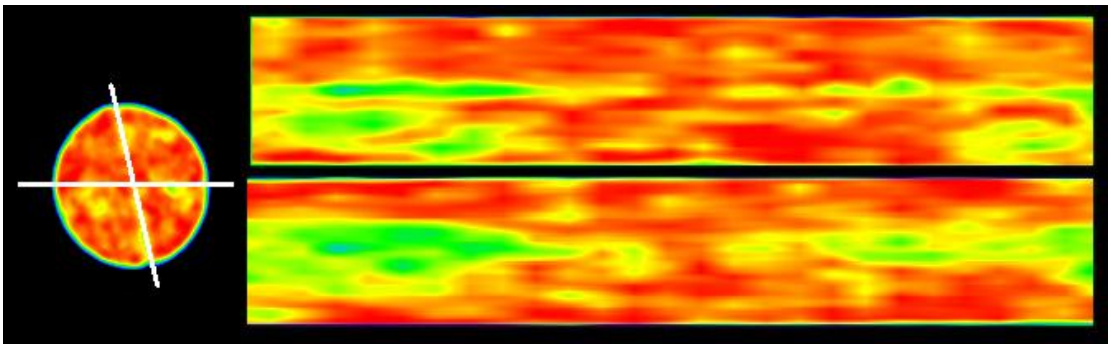

Fig.4.123 – CT Image of Oil Saturated Core (10,000 ppm)

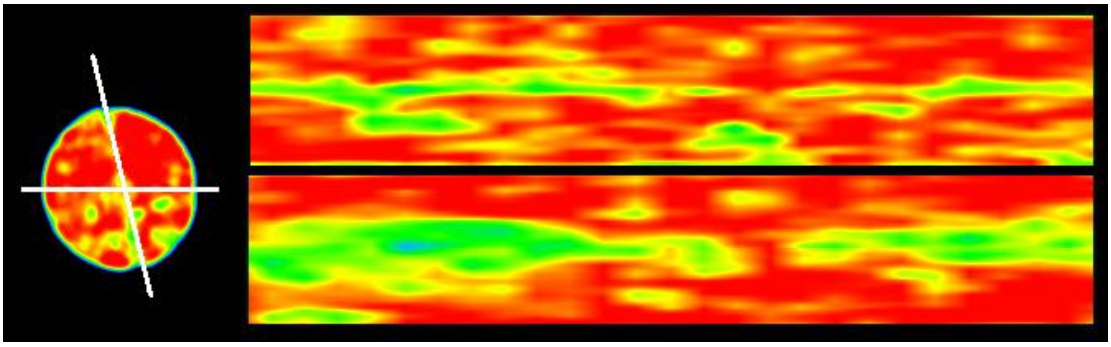

Fig.4.124 – CT Image of Oil Saturated Core after Gel Treatment (10,000 ppm)

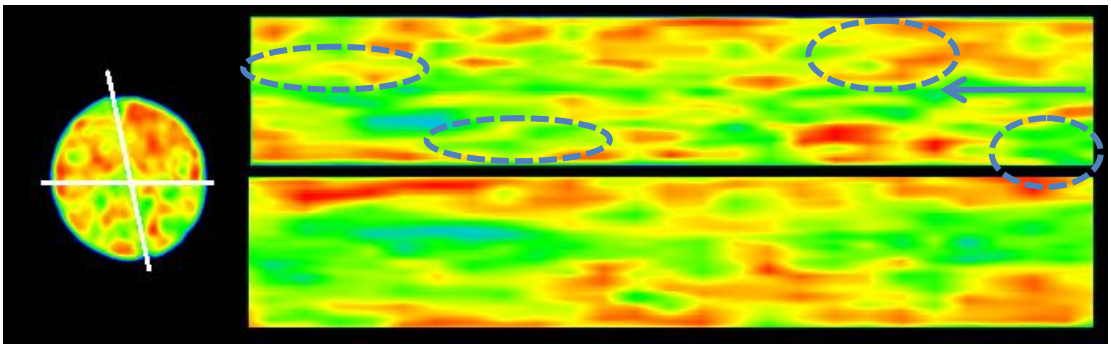

Fig.4.125 – CT Image of Oil Saturated Core Flooded With 1PV of CO_2 (10,000 ppm)

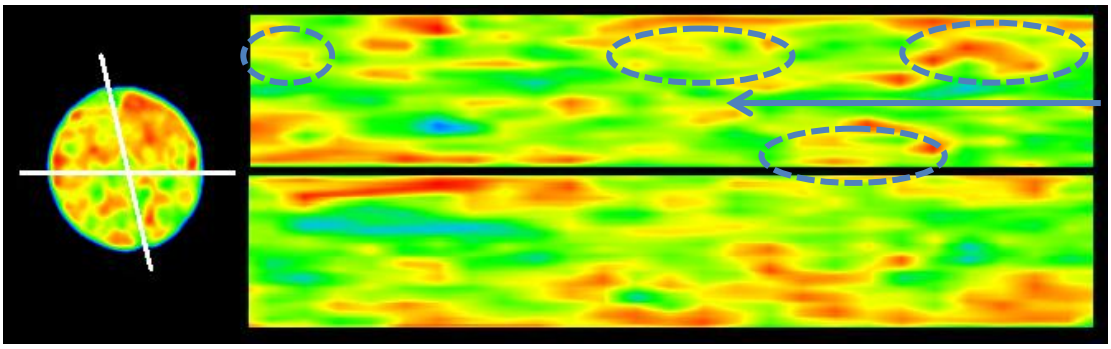

Fig.4.126– CT Image of Oil Saturated Core Flooded With 3PV of CO_2 (10,000 ppm)

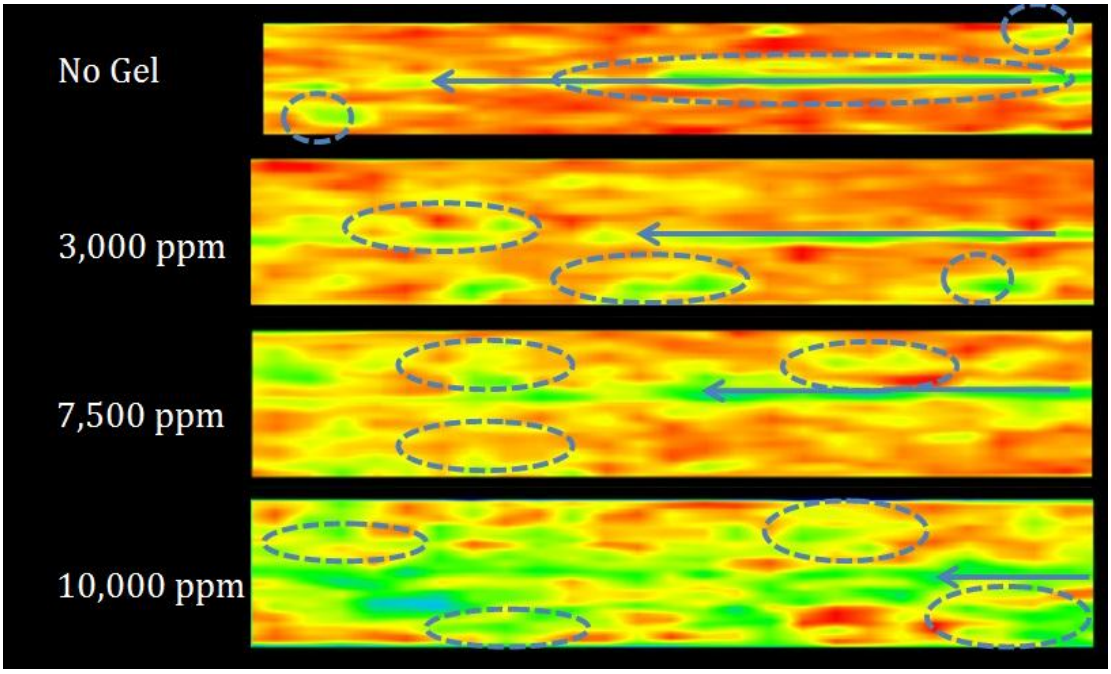

Fig.4.127 – Comparison of Sweep and Gel Performance After 1PV of CO_2

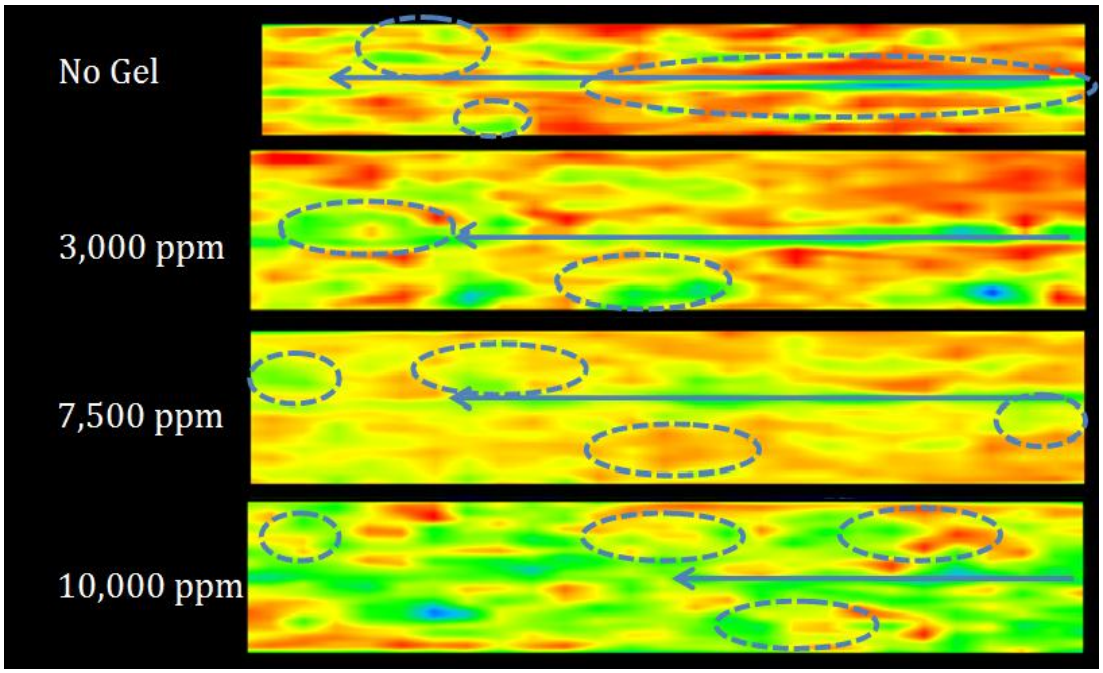

Fig.4.128 – Comparison of Sweep and Gel Performance After 3PV of CO_2

CHAPTER V

CONCLUSIONS AND RECOMMENDATIONS

5.1 Conclusions

Based on the experimental results and utilizing the quantitative recovery data and the qualitative CT images, the following conclusions can be stated:

1. Even with the viscosified water having high viscosity and more uniform overall conformance than the neat CO_2 alone especially in fractures, the extraction effectiveness of the first PV of CO_2 in fractured cores was more dominant than the viscosity effect; the first PV of CO_2 in the CGI experiment recovered 39.2% versus 22-25% of the oil recovered by equivalent volume of VW.
2. The difference in performance of different concentration of treatment gels and viscosified water composition is less clear in the beginning of CO_2 floods. More CO_2 volumes injected disclose the strength of the gel or the resistance of the viscosified water against CO_2.
3. After the easy oil gets extracted by the injection fluids, the differences in sweep between different experiments and modes gets clearer as the challenge becomes to force the CO_2 to sweep areas barely or untouched by CO_2 in normal floods with no chemical treatment.
4. The second PV added incremental oil of 11-20% for the gel experiments, 15-25% for the VWAG experiments and 8% for CGI case. The higher increment caused

by the 2nd slug in VWAG compared to gel application is attributed to the nature of the CO_2 itself; the higher increment of the 2nd slug over the first slug does not mean higher ultimate recovery.

5. Even if the rocks are flooded with water or viscosified water, the chasing CO_2 will help in extracting residual oil increasing the overall recovery.
6. Gel treatments were more successful than the tested VWAGs in extracting more. The aggressive approach of injecting high viscosity fluids to plug permeable channels or fractures proved to be effective. The ultimate recovery was the highest with the gel treatments (7,500-10,000 ppm) with 64-70% compared to 47% with the neat CGI. Thus, the incremental recovery was 17-22% more than the CGI in fractured rock case.
7. The viscosified water performance varied from 41-46% with the failed attempts (1st PAM and 1st Xanthan) and 50-58% with the other two (2nd PAM and 2nd Xanthan);the second PAM VWAG test (VWAG2) added 10% more oil than the CGI while the second Xanthan (VWAG4) added 2.4% only more oil.
8. VWAG application proved to be highly sensitive to the degree of cross-linking. In both Xanthan and PAM tests, doubling the cross-linker concentration resulted in additional 10% oil recovery.
9. Comparison of the successful gel treatments (7,500-10,000 ppm) and the successful VWAGs (2nd PAM and 2nd Xanthan) suggests that the CO_2 physical properties are more dominant than the effect of the fracture in limited conductivity/narrow fractures.

10. In relatively narrower segments of the fracture, CO_2 diffuses into the matrix and the fracture appears to be with no significant effect on the CO_2 advance. On the other hand, conductive segments provide super highways for CO_2 flow keeping the adjacent matrix oil relatively intact.
11. The heterogeneity nature of the cores is not function of the fractures or channels only. Differences in pore throats distribution cause variation in sweep efficiency across the rocks.
12. PAM proved to be generally more effective than Xanthan in hindering the advance of the flow and sustaining the erosion by CO_2 floods.
13. The second PV added incremental oil of 11-20% for the gel experiments, 15-25% for the VWAG experiments and 8% for CGI case. On the other hand, the third PV added incremental oil of 5.4% for the two gel experiments (7,500-10,000 ppm), 2.5-7.5% for the VWAG experiments and 5.5% for CGI case.
14. About 87-94% of the recovered oil was recovered with the first and second PV excluding the third one. Thus, care should be taken in design aspects to inject the optimum amounts of CO_2 producing maximum possible oil without excessive injection or recycling of injected fluids harming the economics.
15. All CO_2 injection modes recovered more oil than the WF. After certain pore volume, no more oil was produced. The third PV of waterflood added no incremental recovery; the ultimate recovery was 38% only while the CGI in untreated core added around 10% more oil. The increment with gel treatment reached as high as 30% with the 10,000 ppm gel treatment. The high difference

in recovery is attributed to the physical properties of the CO_2 and the interaction with the oil.

5.2 Recommendations

1. Larger core samples should be used to minimize the discrepancy between experiments and to further ease recovery data gathering and analysis. Larger cores aid in better visualization of CO_2 interaction with oil and the effect on heterogeneities, gravity and viscous forces.
2. Better volumetric control over CO_2 injections at higher pressure supercritical conditions.
3. Cores with larger diameter will facilitate gel leak-off studies under the CT scanner. Question is raised whether CT intensity can be used to correlate with gel strength.

NOMENCLATURE

bbl	barrel (5.615 cubic foot)
Cr (III) Ac	Chromium Acetate
CC	Cubic Centimeter
CGI	Continuous Gas Injection
CO_2	Carbon Dioxide
EOR	Enhanced Oil Recovery
FCM	First Contact Miscibility
HPAM	Hydrolyzed Polyacrylamide
mcfpd	Mega Cubic Foot Per Day
MCM	Multiple Contact Miscibility
md	Millidarcy
MMP	Minimum Miscibility Pressure
OOIP	Original Oil In Place
ppm	Parts Per Million
PV	Pore Volume
RF	Recovery Factor
VW	Viscosified Water
WAG	Water Alternating Gas
WF	Waterflood
ϕ	Porosity

REFERENCES

Aleidan, A. and Mamora, D. 2011. Comparative Study of Oil Recovery During Miscible Co2 Injection in Carbonate Cores and Slimtube. Paper presented at the SPE Saudi Arabia section Young Professionals Technical Symposium, Dhahran, Saudi Arabia. Society of Petroleum Engineers SPE-155411-MS. DOI: 10.2118/155411-ms.

Asghari, K. and Taabbodi, L. 2004. Laboratory Investigation of Indepth Gel Placement for Carbon Dioxide Flooding in Carbonate Porous Media. Paper presented at the SPE Annual Technical Conference and Exhibition, Houston, Texas. Society of Petroleum Engineers 00090633. DOI: 10.2118/90633-ms.

Avery, M.R., Burkholder, L.A., and Gruenenfelder, M.A. 1986. Use of Crosslinked Xanthan Gels in Actual Profile Modification Field Projects. Paper presented at the International Meeting on Petroleum Engineering, Beijing, China. 1986 Copyright 1986, Society of Petroleum Engineers 00014114. DOI: 10.2118/14114-ms.

Bae, J.H. 1995. Viscosified Co2 Process: Chemical Transport and Other Issues. Paper presented at the SPE International Symposium on Oilfield Chemistry, San Antonio, Texas. Copyright 1995, Society of Petroleum Engineers Inc. 00028950. DOI: 10.2118/28950-ms.

Bae, J.H. and Irani, C.A. 1993. A Laboratory Investigation of Viscosified Co2 Process. *SPE Advanced Technology Series* **1** (1): 166-171. DOI: 10.2118/20467-pa

Bataweel, M.A., Nasr-El-Din, H.A., and Schechter, D.S. 2011. Fluid Flow Characterization of Chemical Eor Flooding: A Computerized Tomography (Ct) Scan Study. Paper presented at the SPE/DGS Saudi Arabia Section Technical Symposium and Exhibition, Al-Khobar, Saudi Arabia. Society of Petroleum Engineers SPE-149066-MS. DOI: 10.2118/149066-ms.

Benham, A.L., Dowden, W.E., and Kunzman, W.J. 1960. *Miscible Fluid Displacement - Prediction of Miscibility* Original edition. ISBN.

Chakravarthy, D., Muralidharan, V., Putra, E. et al. 2006. Mitigating Oil Bypassed in Fractured Cores During Co2 Flooding Using Wag and Polymer Gel Injections. Paper presented at the SPE/DOE Symposium on Improved Oil Recovery, Tulsa, Oklahoma, USA. Society of Petroleum Engineers SPE-97228-MS. DOI: 10.2118/97228-ms.

CHEMWIKI. Kinetic Vs Thermodynamic Stability. http://chemwiki.ucdavis.edu/Physical_Chemistry/Chemical_Equilibrium/Kinetically_vs_Thermodynamically_Stable.

D. S. Schechter, S.C. 2010. Improve Co2 Flood Efficiency Using Cross-Linked Gel Conformance Control and Co2 Viscosifier Techniques. Paper presented at the SPE.

DiGiacomo, P.M. and Schramm, C.M. 1983. Mechanism of Polyacrylamide Gel Syneresis Determined by C-13 Nmr. Paper presented at the SPE Oilfield and Geothermal Chemistry Symposium, Denver, Colorado. Copyright 1983, Society of Petroleum Engineers 00011787. DOI: 10.2118/11787-ms.

Du, D.-X., Beni, A.N., Farajzadeh, R. et al. 2008. Effect of Water Solubility on Carbon Dioxide Foam Flow in Porous Media: An X-Ray Computed Tomography Study. *Industrial & Engineering Chemistry Research* **47** (16): 6298-6306. DOI: 10.1021/ie701688j

Eakin, B.E. and Mitch, F.J. 1988. Measurement and Correlation of Miscibility Pressures of Reservoir Oils. Paper presented at the SPE Annual Technical Conference and Exhibition, Houston, Texas. 1988 Copyright 1988, Society of Petroleum Engineers 00018065. DOI: 10.2118/18065-ms.

Emadi, A., Sohrabi, M., Jamiolahmady, M. et al. 2011. Mechanistic Study of Improved Heavy Oil Recovery by Co2-Foam Injection. Paper presented at the SPE Enhanced Oil Recovery Conference, Kuala Lumpur, Malaysia. Society of Petroleum Engineers SPE-143013-MS. DOI: 10.2118/143013-ms.

Emera, M.K. and Lu, J. 2005. Genetic Algorithm (Ga)-Based Correlations Offer More Reliable Prediction of Minimum Miscibility Pressures (Mmp) between the Reservoir Oil and Co2 or Flue Gas. Paper presented at the Canadian International Petroleum Conference, Calgary, Alberta. Petroleum Society of Canada PETSOC-2005-003. DOI: 10.2118/2005-003.

Enick, R.M., Beckman, E.J., Shi, C. et al. 2000. Direct Thickeners for Carbon Dioxide. Paper presented at the SPE/DOE Improved Oil Recovery Symposium, Tulsa, Oklahoma. Copyright 2000, Society of Petroleum Engineers Inc. 00059325. DOI: 10.2118/59325-ms.

Espie, T. 2005. A New Dawn for Co2 Eor. Paper presented at the International Petroleum Technology Conference, Doha, Qatar. International Petroleum Technology Conference IPTC-10935-MS. DOI: 10.2523/10935-ms.

F. Mees, R.S., M. Van Geet and P. Jacobs. 2003. *Applications of X-Ray Computed Tomography in the Geosciences* Geological Society Special Publication Original edition. ISBN.

Firoozabadi, A. and Aziz, K. 1986. Analysis and Correlation of Nitrogen and Lean-Gas Miscibility Pressure(Includes Associated Paper 16463). *SPE Reservoir Engineering* **1** (6): 575-582. DOI: 10.2118/13669-pa

Fjelde, I., Zuta, J., and Duyilemi, O.V. 2008. Oil Recovery from Matrix During Co2-Foam Flooding of Fractured Carbonate Oil Reservoirs. Paper presented at the Europec/EAGE Conference and Exhibition, Rome, Italy. Society of Petroleum Engineers SPE-113880-MS. DOI: 10.2118/113880-ms.

Gales, J.R., Young, T.-S., Willhite, G.P. et al. 1994. Equilibrium Swelling and Syneresis Properties of Xanthan Gum-Cr(Iii) Gels. *SPE Advanced Technology Series* **2** (2): 190-198. DOI: 10.2118/17328-pa

Ganguly, S., Willhite, G.P., Green, D.W. et al. 2003. Effect of Flow Rate on Disproportionate Permeability Reduction. Paper presented at the International Symposium on Oilfield Chemistry, Houston, Texas. Society of Petroleum Engineers 00080205. DOI: 10.2118/80205-ms.

Glaso, O. 1980. Generalized Pressure-Volume-Temperature Correlations. *SPE Journal of Petroleum Technology* **32** (5): 785-795. DOI: 10.2118/8016-pa

Heller, J.P., Dandge, D.K., Card, R.J. et al. 1985. Direct Thickeners for Mobility Control of Co2 Floods. *Society of Petroleum Engineers Journal* **25** (5): 679-686. DOI: 10.2118/11789-pa

Hild, G.P. and Wackowski, R.K. 1999. Reservoir Polymer Gel Treatments to Improve Miscible Co2 Flood. *SPE Reservoir Evaluation & Engineering* **2** (2): 196-204. DOI: 10.2118/56008-pa

Hoek, J.E.v.d., Botermans, W., and Zitha, P.L.J. 2001. Full Blocking Mechanism of Polymer Gels for Water Control. Paper presented at the SPE European Formation Damage Conference, The Hague, Netherlands. Society of Petroleum Engineers 00068982. DOI: 10.2118/68982-ms.

Jarrell, P.M., Charles Fox, Michael Stein & Steven Webb. 2002. *Practical Aspects of Co2 Flooding*. Spe Monograph Series. Richardson, TX: SPE. Original edition. ISBN 978-1-55563-096-6.

Jin, H., McCool, C.S., Willhite, G.P. et al. 2002. Propagation of Chromium(Iii) Acetate Solutions through Dolomite Rock. Paper presented at the SPE/DOE Improved

Oil Recovery Symposium, Tulsa, Oklahoma. Copyright 2002, Society of Petroleum Engineers Inc. 00075159. DOI: 10.2118/75159-ms.

Karaoguz, O.K., Topguder, N.N.S., Lane, R.H. et al. 2007. Improved Sweep in Bati Raman Heavy-Oil Co2 Flood: Bullhead Flowing Gel Treatments Plug Natural Fractures. *SPE Reservoir Evaluation & Engineering* **10** (2): pp. 164-175. DOI: 10.2118/89400-pa

Kuzmichonok, L. and Asghari, K. 2007. Evaluating Polyacrylamide-Cr (Iii) Gel Performance for Conformance Control in Carbonate Porous Medium. Paper presented at the Canadian International Petroleum Conference, Calgary, Alberta. Petroleum Society of Canada PETSOC-2007-122. DOI: 10.2118/2007-122.

Kuzmichonok, L., Asghari, K., and Nakutnyy, P. 2007. Performance of Polyacrylamide-Chromium (Iii) Gel in Carbonate Porous Media: Effect of Source of Crosslinker on Disproportionate Permeability Reduction and Gel Strength. Paper presented at the Canadian International Petroleum Conference, Calgary, Alberta. Petroleum Society of Canada PETSOC-2007-121. DOI: 10.2118/2007-121.

Le, V.Q., Nguyen, Q.P., and Sanders, A. 2008. A Novel Foam Concept with Co2 Dissolved Surfactants. Paper presented at the SPE/DOE Symposium on Improved Oil Recovery, Tulsa, Oklahoma, USA. Society of Petroleum Engineers SPE-113370-MS. DOI: 10.2118/113370-ms.

Liang, J. and Seright, R.S. 2000. Wall-Effect/Gel-Droplet Model of Disproportionate Permeability Reduction. Paper presented at the SPE/DOE Improved Oil Recovery Symposium, Tulsa, Oklahoma. Copyright 2000, Society of Petroleum Engineers Inc. 00059344. DOI: 10.2118/59344-ms.

Liu, J. and Seright, R.S. 2000. Rheology of Gels Used for Conformance Control in Fractures. Paper presented at the SPE/DOE Improved Oil Recovery Symposium, Tulsa, Oklahoma. Copyright 2000, Society of Petroleum Engineers Inc. 00059318. DOI: 10.2118/59318-ms.

Liu, Y., Grigg, R.B., and Bai, B. 2005. Salinity, Ph , and Surfactant Concentration Effects on Co2-Foam. Paper presented at the SPE International Symposium on Oilfield Chemistry, The Woodlands, Texas. 2005,. Society of Petroleum Engineers Inc. 00093095. DOI: 10.2118/93095-ms.

Martin, F.D. and Kovarik, F.S. 1987. Chemical Gels for Diverting Co2: Baseline Experiments. Paper presented at the SPE Annual Technical Conference and Exhibition, Dallas, Texas. 1987 Copyright 1987, Society of Petroleum Engineers 00016728. DOI: 10.2118/16728-ms.

Martin, F.D., Kovarik, F.S., Chang, P.-W. et al. 1988. Gels for Co2 Profile Modification. Paper presented at the SPE Enhanced Oil Recovery Symposium, Tulsa, Oklahoma. 1988 Copyright 1988, Society of Petroleum Engineers 00017330. DOI: 10.2118/17330-ms.

Masalmeh, S.K., Wei, L., and Blom, C.P.A. 2011. Mobility Control for Gas Injection in Heterogeneous Carbonate Reservoirs: Comparison of Foams Versus Polymers. Paper presented at the SPE Middle East Oil and Gas Show and Conference, Manama, Bahrain. Society of Petroleum Engineers SPE-142542-MS. DOI: 10.2118/142542-ms.

McCool, C.S., Li, X., and Wilhite, G.P. 2009. Flow of a Polyacrylamide/Chromium Acetate System in a Long Conduit. *SPE Journal* **14** (1): pp. 54-66. DOI: 10.2118/106059-pa

Natarajan, D., McCool, C.S., Green, D.W. et al. 1998. Control of in-Situ Gelation Time for Hpaam-Chromium Acetate Systems. Paper presented at the SPE/DOE Improved Oil Recovery Symposium, Tulsa, Oklahoma. 1998 Copyright 1998, Society of Petroleum Engineers, Inc. 00039696. DOI: 10.2118/39696-ms.

Nguyen, Q.P., Alexandrov, A.V., Zitha, P.L. et al. 2000. Experimental and Modeling Studies on Foam in Porous Media: A Review. Paper presented at the SPE International Symposium on Formation Damage Control, Lafayette, Louisiana. Copyright 2000, Society of Petroleum Engineers, Inc. 00058799. DOI: 10.2118/58799-ms.

Nilsson, S., Stavland, A., and Jonsbraten, H.C. 1998. Mechanistic Study of Disproportionate Permeability Reduction. Paper presented at the SPE/DOE Improved Oil Recovery Symposium, Tulsa, Oklahoma. 1998 Copyright 1998, Society of Petroleum Engineers, Inc. 00039635. DOI: 10.2118/39635-ms.

Raje, M., Asghari, K., Vossoughi, S. et al. 1996. Gel Systems for Controlling Co2 Mobility in Carbon Dioxide Miscible Flooding. Paper presented at the SPE/DOE Improved Oil Recovery Symposium, Tulsa, Oklahoma. 1996 Copyright 1996, Society of Petroleum Engineers, Inc. 00035379. DOI: 10.2118/35379-ms.

Rogers, J.D. and Grigg, R.B. 2000. A Literature Analysis of the Wag Injectivity Abnormalities in the Co2 Process. Paper presented at the SPE/DOE Improved Oil Recovery Symposium, Tulsa, Oklahoma. Society of Petroleum Engineers 00059329. DOI: 10.2118/59329-ms.

Seright, R.S. 1996. Disproportionate Permeability Reduction. *New Mexico Petroleum Recovery Research Center*.

Seright, R.S. 1997. Use of Preformed Gels for Conformance Control in Fractured Systems. *SPE Production & Operations* **12** (1): 59-65. DOI: 10.2118/35351-pa

Seright, R.S. 1999a. Polymer Gel Dehydration During Extrusion through Fractures. *SPE Production & Operations* **14** (2): 110-116. DOI: 10.2118/56126-pa

Seright, R.S. 1999b. Mechanism for Gel Propagation through Fractures. Paper presented at the SPE Rocky Mountain Regional Meeting, Gillette, Wyoming. 1999,. Society of Petroleum Engineers, Inc. 00055628. DOI: 10.2118/55628-ms.

Seright, R.S. 1999c. Disproportionate Permeability Reduction. *New Mexico Petroleum Recovery Research Center*.

Seright, R.S. 2001. Gel Propagation through Fractures. *SPE Production & Operations* **16** (4): 225-231. DOI: 10.2118/74602-pa

Seright, R.S. 2006a. Cleanup of Oil Zones after a Gel Treatment. *SPE Production & Operations* **21** (2): pp. 237-244. DOI: 10.2118/92772-pa

Seright, R.S. 2006b. Optimizing Disproportionate Permeability Reduction. Paper presented at the SPE/DOE Symposium on Improved Oil Recovery, Tulsa, Oklahoma, USA. Society of Petroleum Engineers SPE-99443-MS. DOI: 10.2118/99443-ms.

Seright, R.S. 2009. Disproportionate Permeability Reduction with Pore-Filling Gels. *SPE Journal* **14** (1): pp. 5-13. DOI: 10.2118/99443-pa

Seright, R.S., Fan, T., Wavrik, K. et al. 2011. New Insights into Polymer Rheology in Porous Media. *SPE Journal* **16** (1): pp. 35-42. DOI: 10.2118/129200-pa

Seright, R.S., Liang, J., Lindquist, W.B. et al. 2001. Characterizing Disproportionate Permeability Reduction Using Synchrotron X-Ray Computed Microtomography. Paper presented at the SPE Annual Technical Conference and Exhibition, New Orleans, Louisiana. Copyright 2001, Society of Petroleum Engineers Inc. 00071508. DOI: 10.2118/71508-ms.

Seright, R.S., Prodanovic, M., and Lindquist, W.B. 2006. X-Ray Computed Microtomography Studies of Fluid Partitioning in Drainage and Imbibition before and after Gel Placement: Disproportionate Permeability Reduction. *SPE Journal* **11** (2): pp. 159-170. DOI: 10.2118/89393-pa

Smith, J.E. 1999. Practical Issues with Field Injection Well Gel Treatments. Paper presented at the SPE Rocky Mountain Regional Meeting, Gillette, Wyoming.

Copyright 1999,Society of Petroleum Engineers, Inc. 00055631. DOI: 10.2118/55631-ms.

Sydansk, R.D. 1989. *Delayed in Situ Crosslinking of Acrylamide Polymers for Oil Recovery Applications in High-Temperature Formations*. Doc. US 4844168; Other: PPN: US 7-153860A United StatesOther: PPN: US 7-153860AWed Feb 06 19:15:21 EST 2008Patent and Trademark Office, Box 9, Washington, DC 20232NOV; NOV-89-083093; EDB-90-006052English, pt.

Sydansk, R.D. and Southwell, G.P. 2000. More Than 12 Years of Experience with a Successful Conformance-Control Polymer Gel Technology. Paper presented at the SPE/AAPG Western Regional Meeting, Long Beach, California. Copyright 2000, Society of Petroleum Engineers Inc. 00062561. DOI: 10.2118/62561-ms.

Terry, R.E., Zaid, A., Angelos, C. et al. 1987. Polymerization in Supercritical Co to Improve Co/Oil Mobility Ratios. Paper presented at the SPE International Symposium on Oilfield Chemistry, San Antonio, Texas. 1987 Copyright 1987 Society of Petroleum Engineers, Inc. 00016270. DOI: 10.2118/16270-ms.

Topguder, N.N.S. 2010. A Review on Utilization of Crosslinked Polymer Gels for Improving Heavy Oil Recovery in Turkey. Paper presented at the SPE EUROPEC/EAGE Annual Conference and Exhibition, Barcelona, Spain. Society of Petroleum Engineers SPE-131267-MS. DOI: 10.2118/131267-ms.

Vargas-Vasquez, S.M. and Romero-Zerón, L.B. 2008. A Review of the Partly Hydrolyzed Polyacrylamide Cr(Iii) Acetate Polymer Gels. *Petroleum Science and Technology* **26** (4): 481-498. DOI: 10.1080/10916460701204594

Vargas-Vasquez, S.M., Romero-Zerón, L.B., and MacMillan, B. 2009. Characterization of Cr(Ii) and Cr(Iii) Acetate Aqueous Solutions Using Uv-Vis Spectrophotometry and 1h Nmr. *Chemical Engineering Communications* **197** (4): 491-505. DOI: 10.1080/00986440903288153

Vasquez, J., Civan, F., Shaw, T.M. et al. 2003. Laboratory Evaluation of High-Temperature Conformance Polymer Systems. Paper presented at the SPE Production and Operations Symposium, Oklahoma City, Oklahoma. Society of Petroleum Engineers 00080904. DOI: 10.2118/80904-ms.

Webinar. 2011. Co2 Eor and the Transition to Carbon Storage. http://www.youtube.com/watch?v=ff94KMSA7cU.

Wellington, S.L. and Vinegar, H.J. 1987. X-Ray Computerized Tomography. *SPE Journal of Petroleum Technology* **39** (8): 885-898. DOI: 10.2118/16983-pa

Wilton, R. and Asghari, K. 2007. Improving Gel Performance in Fractures: Chromium Pre-Flush and Overload. *Journal of Canadian Petroleum Technology* **46** (2). DOI: 10.2118/07-02-04

Withjack, E.M., Devier, C., and Michael, G. 2003. The Role of X-Ray Computed Tomography in Core Analysis. Paper presented at the SPE Western Regional/AAPG Pacific Section Joint Meeting, Long Beach, California. Society of Petroleum Engineers 00083467. DOI: 10.2118/83467-ms.

Woods, P., Schramko, K., Turner, D. et al. 1986. In-Situ Polymerization Controls Co2/Water Channeling at Lick Creek. Paper presented at the SPE Enhanced Oil Recovery Symposium, Tulsa, Oklahoma. 1986 Copyright 1986, Society of Petroleum Engineers 00014958. DOI: 10.2118/14958-ms.

Xu, J., Wlaschin, A., and Enick, R.M. 2003. Thickening Carbon Dioxide with the Fluoroacrylate-Styrene Copolymer. *SPE Journal* **8** (2): 85-91. DOI: 10.2118/84949-pa

Zaitoun, A., Bertin, H., and Lasseux, D. 1998. Two-Phase Flow Property Modifications by Polymer Adsorption. Paper presented at the SPE/DOE Improved Oil Recovery Symposium, Tulsa, Oklahoma. 1998 Copyright 1998, Society of Petroleum Engineers, Inc. 00039631. DOI: 10.2118/39631-ms.

Zuta, J. and Fjelde, I. 2010. Transport of Co2-Foaming Agents During Co2-Foam Processes in Fractured Chalk Rock. *SPE Reservoir Evaluation & Engineering* **13** (4): pp. 710-719. DOI: 10.2118/121253-pa